DSPACE

https://dspace.org/

Gas-refractory interactions of basic refractories with sulfur-bearing gases produced in converter furnaces during extraction of Platinum Group Metals in noferrous industry

Fotoyi, Ncuthukazi Ziyanda

2011-05-09
http://hdl.handle.net/10539/9676

Downloaded from a DSpace repository. https://dspace.org/


UNIVERSITY OF THE WITWATERSRAND
SCIENTIA ET LABORE
JOHANNESBURG

Gas-refractory interactions of basic refractories with sulfur-bearing gases produced in converter furnaces during extraction of Platinum Group Metals in non-ferrous industry.

NCUTHUKAZI ZIYANDA FOTOYI

A Dissertation submitted to the Faculty of Engineering and the Built Environment, University of the Witwatersrand, in fulfilment of the requierements of the degree of Masters of Science in Engineering

Johannesburg 2009

DECLARATION

I hereby declare that this dissertation, which I herewith submit for the research qualification

MASTERS of SCIENCE Degree in Metallurgy and Materials Engineering

to the University of WITWATERSRAND, Faculty of Engineering and Built Environment, is, apart from the recognised assistance of my supervisors, my own work and has not previously been submitted by me to another University to obtain a research degree.

_____ on this __19__ day of ___June 2009_____

(Candidate)

DEDICATION

I dedicate this work to my parents, Mr. Mphitizeli Stokwe H. and Mrs. Nobuntu L. M. Fotoyi, for always seeing the best in me and encouraging me to work hard and be the best. Thank you for your unconditional love, I love you very much, you are the best parents I could ever ask for.

ACKNOWLEDGEMENTS

Sincere appreciation is extended to :

Almighty God for giving me the courage, energy and strength to complete the project.

Proffesor Hurman Rauf Eric for his guidance and supervising the work.

Proffesor Lesley Cornish for the motivation and help in editing the work.

My family for their love and great support to go through life's journey. To my parents for the values, principles and respect they have taught me. To my sisters and brother, Thenjiwe, Nozuko, Pumeza, Lwandile, Asanda, and Yanga, and my cousins Ntomboxolo, Pheliswa and Neliswa, I appreciate and love the different characters we have all grown up to be, and in each other we have found friendship, comfort, love, understanding. Thando, thank you for the inspiring colourful drawings, you make my day always!!!

My patner Mr. Zivayi Makunike, thank you for touching my life in ways you may never know. I am happy to have you in my life and thankful for the love, support and the joy you bring.

Mintek for financial support, giving a special thanks to the High Temperature Technology Division for support and availing the laboratories and all the necessary equipment requierd to conduct the work. I would also like to thank the Mineralogy Division and Analytical Science Division for their assisatnce in characterization.

My friends thank you for the wonderful moments we shared, the laughter, the joys and the sorrows, and the memories we created all these years and being there when I needed you.

ABSTRACT

The fundamental reaction mechanisms, when unused chrome-magnesite, magnesite-chrome and magnesite refractories are exposed to sulfur-bearing gas mixtures of SO_2-O_2, SO_2-N_2 and SO_2 at 700°C to 1350°C, were investigated. The investigations comprised chemical analyses, thermodynamic analyses and microstructural examination. The extent of the conversion reactions was measured as a function of temperature and reaction time. Six basic refractories were investigated and characterized using Scanning Electron Microscopy (SEM) and X-ray powder diffraction (XRPD) methods. The microstructural examination indicated that physical changes in the original microstructure of the refractory could possibly influence the reactions with sulfur-bearing gases and the chemical analyses of the product phases confirmed the formation of secondary sulfates within pores, along grain boundaries and cracks. The structural features in the original refractory were determined by technological processes employed during original firing in production. The factors attributed to the principal physical changes of the original microstructure were related to the diffusion processes, which affected the phase distribution, pore size distribution and grain size. The fundamental reactions involved in the pore size distribution and microstructure were attributed to the differential diffusion mechanism of individual components that resulted in the development of magnesia spinels.

The effects on the microstructure demonstrated that the reactions were limited to the grain boundary region due to the product layer formed as the reactions progressed. The chemical product analyses indicated that in the sulfates formed, the sulfation reactions were significantly affected by the equilibrium thermodynamics of the oxygen and sulfur dioxide gas combination in the products of $P_{SO_2} P_{O_2}^{1/2}$. The phase changes led to the dissolution of the refractory components and crystallization of MgO and CaO. This influenced the permeability of the sulfur-bearing gases that reacted to form $MgSO_4$ and $CaSO_4$ found as grain boundary and pore space fillings. Resistance to sulfur-bearing gas infiltration and sulfation in fine-grained direct bonded refractories were found to be better than that of the coarse-grained direct bonded refractories. The decreased sulfation of the fine-grained refractory was related to the restricted diffusion processes due to the stable magnesia spinel phases and retention of the closed pore structure at different temperatures. However, the dissolution and crystallization mechanism described in sulfation, demonstrated that $MgSO_4$, $CaSO_4$, $CaMg_3(SO_4)_3$ and compound mixtures of sulfate, silica, magnesia and sesquioxides (Fe_2O_3, Al_2O_3 and Cr_2O_3) were formed along the grain boundaries.

TABLE OF CONTENTS

CHAPTER 1 : INTRODUCTION **1**

CHAPTER 2 : LITERATURE REVIEW **3**

2.1 Introduction. 3

2.2 The reactions occurring in basic refractories and development of microstructure. 4

2.2.1 Phase relationships between iron oxide and spinel phases in basic refractories. 4

2.2.2 Diffusion processes and microstructure developed in basic refractories. 8

2.3 The interactions of basic refractory components with sulfur-bearing gases. 10

2.3.1 Reactions of sesquioxides components (R_2O_3) with sulfur-bearing gases 10

2.3.2 Reactions of MgO-MgR_2O_4 spinel components with sulfur-bearing gases. 12

2.3.3 Structural changes of basic refractory components in sulfur-bearing gases. 14

2.3.4 Reactions of basic oxides with sulfur-bearing gases. 20

2.4 The thermodynamics and equilibrium involving sulfur-bearing compounds. 23

2.4.1 Reaction equilibrium of sulfur-bearing solids 25

CHAPTER 3 : EXPERIMENTAL PROCEDURES **29**

3.1 Overview 29

3.2 Materials 30

3.2.1 Sample Preparation 32

3.3 Apparatus 32

3.4 Gas Preparation and Flow Regulation 32

3.4.1 Mixing of Gases 33

3.4.1.1 Procedure for O_2 Experiments 37

3.4.1.2 Procedure for SO_2-O_2 Experiments 37

3.4.1.3 Procedure for SO_2-N_2 Experiments 38

3.4.1.4 Procedure for SO_2 Experiments 38

3.5 Furnaces, Reactors and Temperatures 38

3.6 Experimental Procedures 39

3.6.1 O_2 Experiments 39

3.6.2 SO_2-O_2 Experiments 39

3.6.3 SO_2-N_2 Experiments 40

3.6.4 SO_2 Experiments 40

3.7 Metallographic Preparation 40

3.8 Scanning Electron Microscopy 41

3.9 X-Ray Diffraction.....41
3.10 Methods used in Determination of Reaction Products.....42
3.10.1 Conversion Method.....42
3.10.2 Product Determining Methods.....42

CHAPTER 4 : RESULTS.....44
4.1 Microstructural and physical characteristics of basic Refractories.....44
4.2 Microstructural and Physical Characteristics in Oxygen Atmosphere.....53
4.3 Thermodynamic analysis of basic refractories in sulfur-bearing gases.....59
4.3.1 Microstructural changes in high temperature SO_2-N_2 Gas mixtures.....63
4.3.1 Microstructural Changes in high temperature SO_2-O_2 Gas mixtures.....69
4.3.2.....69
4.3.3 Microstructural changes in low temperature SO_2-N_2 gas mixtures.....75
4.3.4 Microstructural changes in low temperature SO_2-O_2 gas mixtures.....80
4.4 Kinetic Effects- basic refractories as absorbents of sulfur-bearing gases. 92
4.5 X-Ray Diffraction Analysis.....103

CHAPTER 5 : DISCUSSIONS.....105
5.1 Introduction.....105
5.2 Microstructural changes in reheated basic refractories.....107
5.2.1 Microstructural changes in oxygen atmospheres.....107
5.2.2 Microstructural changes in sulfur-bearing gases at high temperatures.....112
5.2.3 Thermodynamic considerations of $CaSO_4$ formation at high temperatures...116
5.2.4 Microstructural changes in sulfur-bearing gases at low temperatures.....119
5.2.5 Thermodynamic considerations of $MgSO_4$ formation at low temperatures...123
5.3 Thermodynamic considerations of the sulfur-bearing gases.....127
5.4 Sulfation kinetics of basic refractories in sulfur-bearing gases.....130
5.4.1 Effect of Time. 130
5.4.2 Effect of Refractory Composition.....134
5.4.3 Effect of Temperature.....136
5.4.4 Effect of SO_2/O_2 on Sulfation Reaction.....139

CHAPTER 6 : CONCLUSIONS.....142

REFERENCES:.....144

LIST OF FIGURES

Figure ***Page***

Figure 2.1. Decomposition curves of iron (II) sulfate during heating: (a) in air; (b) in argon atmosphere. 1) temperature record; 2) differential record and 3) loss in mass of specimen (Reference Safiullin, Gitis and Panasenko). 11

Figure 2.2. Decomposition curves of iron (II) sulfate during heating: (a) in air; (b) in oxygen atmosphere (Reference Gallagher, Johnson and Schrey). 12

Figure 2.3. Decomposition curves of iron (II) sulfate during heating in nitrogen atmosphere (Reference Gallagher, Johnson and Schrey). 12

Figure 2.4. Reaction rate constant k_2 of MgO in SO_2-O_2 system between 500°C and 1000°C (Reference Podwórny, Piotrowski and Wojsa)..... 14

Figure 2.5. Predominance area diagram of magnesium, sulfur and oxygen at varying temperatures, and partial pressure of oxygen and sulfur dioxide (reference, Liouw, Tsikiris and Gray). 19

Figure 3.1. Schematic diagram of the apparatus and photograph of the furnace. 35

Figure 3.2. Schematic gas flow chart of the gas systems and furnace 36

Figure 4.1. SEM-BSE micrographs of Magnesite refractory (a) microstructure at high magnification, gray phase = magnesia (periclase P), light-gray phase = silicate (S) and black= pores, and (b) microstructure at high magnification showing subhedral magnesia grains with spheroidized grain boundaries and dihedral contact angles between the grains..... 48

Figure 4.2. SEM-BSE micrograph of unreacted Magnesite-chrome brick 1 showing bright phase= chromite (C1), gray phase = magnesia (periclase P), black= pores. Intragranular precipitate chromites =C2 and precipitate continuous chromites =C4. 49

Figure 4.3: SEM-BSE micrographs of unreacted (a) Chrome-Magnesite A showing bright phase= chromite (C1), gray phase = magnesia (periclase P), light-gray phase = silicate (S), black= pores. Intragranular precipitate chromites =C2 and intergranular precipitate chromites = C3 and C4. (b) Chrome-magnesite D50-C5 showing bright phase= chromite (C1), gray phase = magnesia (periclase P), and black= pores. 50

Figure 4.4. SEM-BSE micrographs of unreacted (a) Magnesite-chrome D60/100 showing gray phase = magnesia (periclase P), intragranular precipitate chromites =C2 and intergranular precipitate, blocky chromites = C3 and continuous chromites C4. (b) Magnesite-chrome brick 2 showing gray phase = magnesia (periclase P), black= pores, light-gray phase = silicate (S) and intragranular precipitate chromites =C2 and intergranular precipitate continuous chromites =C4..... 51

Figure 4.5. EDX spectra of forsterite (a), monticellite (b) and chromite (c) phase showing the elements contained in the minerals. 52

Figure 4.6. SEM-BSE micrographs of (a) Magnesite reacted at 700°C showing uneven texture of magnesia grains with dihedral contact angles. (b) Magnesite reacted at 1350 showing smooth texture of magnesia grains and spheroidization achieved by the magnesia grains at the triple points. The gray phase = magnesia (periclase, P), bright phase = silicate (S) and black= pores. 55

Figure 4.7. SEM-BSE micrographs of (a) Magnesite-chrome D60/100 reacted in O_2 gas at 1350°C, showing distribution of chromite grains and increasing volume of magnesia-chromite spinel at low magnification (b) Magnesite-chrome D60/100 at high magnification, showing angular to subherdal blocky intergranular chromites, continuous intergranular chromites and intragranular chromites. The gray phase = magnesia (periclase P), black= pores, bright phase = intragranular chromites precipitate =C2 and intergranular precipitate chromites = C3 and C4. 56

Figure 4.8. SEM-BSE micrographs of (a) Chrome-magnesite A reacted in O_2 gas at 1350°C, showing development and migration of secondary chromites at low magnification (b) Chrome-magnesite A showing magnesia grain with intragranular secondary chromites along the grain boundaries, cracks and high purity interior. Coarse secondary chromites are shown as bright phase= chromite (C1). The gray phase = magnesia (periclase P), black= pores, within magnesia grains borders the bright phase = intragranular chromites precipitate =C2..... 57

Figure 4.9. SEM-BSE micrographs of (a) Chrome-magnesite D50-C5 reacted in O_2 gas at 1350°C, showing dissolution of primary chromite grains and aggregation of magnesium aluminates spinels. (b) Chrome-magnesite D50-C5 showing intragranular secondary chromite precipitates and intergranular silicates between magnesia-chrome spinels. The gray phase = magnesia (periclase P), light-gray phase = silicate (S), black= pores, bright phase = intragranular chromites precipitate =C2 and intergranular precipitate chromites = C3 and C4.....58

Figure 4.10: Predominance area diagrams for Ca-S-O at 1350°C, and varying partial pressures of oxygen and sulfur dioxide using Kellog and Richardson and Jeffes data. 61

Figure 4.11: Predominance area diagrams for Ca-S-O at 700°C to 1350°C, and varying partial pressures of oxygen and sulfur dioxide using FactSage software programme¯. 61

Figure 4.12: Predominance area diagram of Mg-S-O between 700°C to 1000°C, and varying partial pressures of oxygen and sulfur dioxide, using Kellog's data. 62

Figure 4.13: Predominance area diagrams of Mg-S-O between 700°C to 1350°, and varying partial pressures of oxygen and sulfur dioxide, using FactSage software 62

Figure 4.14. SEM-BSE micrographs of (a) Magnesite reacted in SO_2-N_2 gas mixture at 1350°C, showing formation of calcium sulfate at grain boundaries. (b) Magnesite showing formation of silicate and intragranular porosity. The gray phase = magnesia (periclase P), light-gray phase = silicate (S), black= pores and white phase = $CaSO_4$.....65

Figure 4.15. SEM-BSE micrographs of (a) laboratory magnesium oxide powdered pellets, reacted in SO_2-N_2 gas mixtures at 1350°C, showing formation of magnesia grains with some direct bonding between grains. (b) Refractory powdered pellet of magnesite showing magnesia grains with a skeletal structure. The gray phase = magnesia (periclase P), black= pores.....66

Figure 4.16. SEM-BSE micrograph of a refractory powdered pellet of magnesite-chrome reacted in SO_2-N_2 gas mixtures at 1350°C, showing magnesia-chromite contacts and magnesia spinels. The gray phase = magnesia (periclase P), black= pores, bright phase = chromite and intragranular chromites precipitate =C2. 67

Figure 4.17. SEM-BSE micrographs of (a) Magnesite-chrome D60/100 reacted in SO_2-N_2 gas mixture at 1350, showing gray phase = magnesia (periclase P), light-gray phase = silicate (S), black= pores. Intragranular precipitate chromites =C2 and intergranular precipitate chromites = C3. (b) Chrome-magnesite A showing bright phase= chromite (C1), intragranular chromites precipitate =C2 and intergranular precipitate chromites = C3 and C4, gray phase = magnesia (periclase P), black= pores.....68

Figure 4.18. SEM-BSE micrographs of (a) Chrome-magnesite A reacted in SO_2-O_2 gas mixture at 1350C, showing gray phase = magnesia (periclase P), black= pores. Intragranular precipitate chromites =C2. (b) Chrome-magnesite D50-C5 showing bright phase= chromite (C1) with discontinuous magnesium spinel pockets, gray phase = magnesia (periclase P), black= pores. 72

Figure 4.19. SEM-BSE micrograph of the (a) magnesite reacted in SO_2-O_2 gas mixture at 1350C, showing calcium sulfate forming at the grain boundaries. The gray phase = magnesia (periclase P), black= pores and white phase = $CaSO_4$.....73

Figure 4.20. SEM-BSE micrograph of Magnesite-chrome brick 1 reacted in SO_2-O_2 gas mixture at 1350C, showing bright phase= chromite (C1), intragranular precipitate chromites =C2, gray phase = magnesia (periclase P), black= pores. 73

Figure 4.21. SEM-BSE micrographs of (a) magnesite-chrome D60/100 reacted in SO_2-O_2 gas mixture at 1350C, showing formation of magnesia-chromite solid solutions. The gray phase = magnesia (periclase P), bright phase = chromite (C1), (C1), intragranular precipitate chromites = C2, black= pores. (b) magnesite-chrome brick 2 showing disintegration of chromite grains and dissolution of chromite precipitates. The bright phase= chromite (C1), gray phase = magnesia (periclase P), black= pores.....74

Figure 4.22. SEM-BSE micrographs of (a) magnesite refractory reacted in SO_2-N_2 gas mixture at 700°C, showing magnesium sulfate forming along the grain boundaries. (b) Refractory powdered pellet of magnesite showing heterogeneous reaction of magnesia. The grey phase = magnesium sulfate, light grey phase = magnesia (periclase P), black= pores and bright phase = silicate. 77

Figure 4.23. SEM-BSE micrographs of (a) laboratory magnesium oxide powdered pellet reacted in SO_2-N_2 gas mixtures at 700°C, showing a collective mass of particles of a continuous spongy sulfate

structure. The dark grey phase = magnesium sulfate high in SO_3 concentration, light grey phase = magnesia sulfate, white precipitates = MgO, black= pores. 78

Figure 4.24. SEM-BSE micrographs of (a) Refractory powdered pellet of magnesite-chrome refractory reacted in SO_2-N_2 gas mixtures at 700°C, showing the sulfate phase. The dark grey phase (needles) = calcium magnesium sulfate, black= pores, bright phase = chromite (C1), intragranular precipitate chromites = C2, grey phase = magnesia. 78

Figure 4.25. SEM-BSE micrographs of (a) magnesite-chrome D60/100 reacted in SO_2-N_2 gas mixture at 700°C, showing reaction of magnesia matrix with sulfur-bearing gases. The gray phase = magnesia (periclase P), bright phase = chromite (C1), intragranular precipitate chromites = C2, black= pores. (b) magnesite-chrome D60/100 showing development of sulfate mixtures with secondary spinels along the magnesia spinel grain boundaries. The bright phase= chromite (C1), gray phase = magnesia (periclase P), black= pores. 79

Figure 4.26. SEM-BSE micrographs of (a) magnesite refractory reacted for 14 hours in SO_2-O_2 gas mixture at 700°C. The dark grey porous phase = magnesium sulfate ($MgSO_4$), grey phase = magnesia, bright phase =Silicates (S), (b) magnesite refractory at high magnification, the dark grey phase (needles) = concentrated magnesium sulfate, light grey porous phase= calcium magnesium sulfate ($CaMg_3$ $(SO_4)_4$ and light grey phase =Silicates (S), ... 85

Figure 4.27. SEM-BSE micrographs of magnesite refractory reacted in SO_2-O_2 gas mixture at 700°C where, (a) after 7days, showing chemical reaction with the magnesia grains, The dark grey phase between grains = magnesium sulfate ($MgSO_4$), grey phase = magnesia (P), light grey phase =Silicates (S), (b) shows reaction after 2 weeks, showing crack formation, The dark grey phase along grains (needles) = concentrated magnesium sulfate, dark grey porous phase = magnesium sulfate, light grey porous phase= calcium magnesium sulfate ($CaMg_3$ $(SO_4)_4$ 86

Figure 4.28. SEM-BSE micrographs of chrome-magnesite A refractory reacted in SO_2-O_2 gas mixture at 700°C where, (a) after 7days, showing chemical reaction with the magnesia matrix. The dark gray phase = magnesium sulfate, bright phase = chromite (C1), intragranular precipitate chromites = C2. (b) shows reaction after 2 weeks. The bright phase= chromite (C1), gray phase = magnesia sulfate, grey phase with light precipitates = sulfate mixture with secondary spinels. 87

Figure 4.29. SEM-BSE micrographs of chrome-magnesite D50-C5 reacted in SO_2-O_2 gas mixture at 700°C where, (a) after 14 hrs, showing low gas infiltration and reactions forming at the boundaries, (b) after 7days, showing formation of magnesia spinel solid solutions and high gas infiltration. (c) after 2 weeks, showing elongated sulfate structure and spongy sulfate mixtures with secondary spinels. 88

Figure 4.30. SEM-BSE micrographs of magnesite-chrome D60/100 reacted in SO_2-O_2 gas mixture at 700°C, (a) after 14hrs, and showing low gas infiltration reactions forming at the pores. (b) Shows dissolution of spinels, dark gray phase = magnesium sulfate, bright phase = chromite (C1), intragranular precipitate chromites = C2. (c) after 2 weeks, dark grey porous phase = magnesium sulfate, chromite forming large grains (C1), and light grey phase= silicate (S). 89

Figure 4.31. SEM-BSE micrographs of magnesite-chrome brick 2 reacted in SO_2-O_2 gas mixture at 700°C, (a) after 7days, showing reaction of magnesia matrix with gases forming sulfates. The disintegrated dark gray phase = magnesia sulfate, bright phase = chromite (C1), intragranular precipitate chromites = C2, black= pores, (b) after 2 weeks, showing dissolution of magnesia-chromite spinels and crack formation, development of sulfate mixtures with secondary spinels along the magnesia spinel grain boundaries. The bright phase= chromite (C1), gray phase = magnesia sulfate, grey phase with light precipitates = sulfate mixture with secondary spinels, and black = pores. 90

Figure 4.32. SEM-BSE micrographs of magnesite-chrome brick 1 reacted in SO_2-O_2 gas mixture at 700°C where, (a) after 7days, showing crack formation and dissolution of spinels. (b) after 2 weeks, showing disintegration and sulfation $MgFe_2O_4$ spinels. 91

Figure 4.33. Effect of time on sulfation conversions of MgO in basic refractories in SO_2-O_2 mixture at 700°C. 94

Figure 4.34. Total sulfur (wt %) in basic refractories as a function of time in SO_2-O_2 mixture at 700°C. 94

Figure 4.35. Chrome-magnesite A conversion fractions in SO_2-O_2 gas mixtures at different temperatures as a function of time. 95

Figure 4.36. Chrome-magnesite D50-C5 conversion fractions in SO_2-O_2 gas mixtures at different temperatures as a function of time. 95

Figure 4.37. Magnesite conversion fractions in SO_2-O_2 gas mixtures at different temperatures as a function of time. 96

Figure 4.38. Magnesite-chrome D60/100 conversion fractions in SO_2-O_2 gas mixtures at different temperatures as a function of time. 96

Figure 4.39. Magnesite-chrome brick 2 conversion fractions in SO_2-O_2 gas mixtures at different temperatures as a function of time. 97

Figure 4.40. Magnesite-chrome brick 1 conversion fractions in SO_2-O_2 gas mixtures at different temperatures as a function of time. 97

Figure 4.41. Comparison of conversion fractions of basic refractories in SO_2-N_2 gas mixtures at 800°C as a function of time. 98

Figure 4.42. Comparison of conversion fractions of basic refractories in SO_2-N_2 gas mixtures at 1000°C as the function time. 98

Figure 4.43. Comparison of conversion fractions of basic refractories in SO_2 gas atmosphere at 800°C as the function time. 99

Figure 4.44. Comparison of conversion fractions of basic refractories in SO_2 gas atmosphere at 1000°C as the function time. 99

Figure 4.45: The weight gain after 7 days of reaction as a function of the reciprocal absolute temperature at 1atm of SO_2-O_2 gas mixture. 101

Figure 4.46: Sulfate (wt %) added after 7 days of reaction as a function of temperature at 1atm of SO_2-O_2 gas mixture 101

Figure 4.47: The weight gain after 7 days of reaction as a function of the reciprocal absolute temperature at 1atm of SO_2-N_2 gas mixture. 102

Figure 4.48: Sulfate (wt %) added after 7 days of reaction as a function of temperature at 1atm of SO_2-N_2 gas mixture. 102

Figure 5.1. The schematic illustration of Ca_3SiO_5, showing [SiO_4] tetrahedral in dark grey. The Ca, O and Si atoms are presented by the rounded spheres in dark grey, light grey and black, respectively. (Reference: Mori *et al.*). 113

Figure 5.2. The schematic illustration of $CaSO_4$ crystal structure (a), and $CaSO_4$ lattice showing the [SO_4^{2-}] tetrahedra in light grey and dark grey Ca^{2+} cations in-between (Reference, Hasi, Pierre and Raghunathan¯). 114

LIST OF TABLES

Table ***Page***

Table 2.3. Comparison of free energy data 27

Table 2.4: Calculated free energy data of sulphur-bearing gases at different temperatures. 27

Table 2.5: Free Energy Data for Decomposition of Sulfates 28

Table 2.6: Comparison of Free Energy Data for Formation of Sulfates 28

Table 2.7: Comparison of Free Energy Data for Formation of Sulfates 28

Table 3.1. Chemical compositions and properties of refractory materials 30

Table 3.2. Materials. 31

Table 3.3. Gas Specification as provided by the manufacturer. 31

Table 4.1. Compositions of the forsterite, monticellite and chromite minerals. 47

Table 4.2. Sulfate phases found after reaction of the different refractories in SO_2-O_2 and SO_2-N_2 atmospheres. ... 104

Table 5.1. The calculated values for equilibrium O_2 partial pressures at different temperatures 118

Table 5.2. The calculated values for O_2 equilibrium partial pressures in dissociation. H_2O to H_2 and O_2 118

Table 5.3. Equilibrium partial pressures in sulfation reactions. 126

Table 5.4. Standard Gibbs-free energies and equilibrium constants for SO_3 formation in different sulfur-bearing gas mixtures. 129

CHAPTER 1
INTRODUCTION

This project was called the Gas-Refractory Interaction and was based at Mintek. The aim was to develop and understand the mechanisms of reactions taking place between unused basic refractories of magnesite, chrome-magnesite and magnesite-chrome and sulfur-bearing gases produced in converter furnaces during recovery of non-ferrous metals. Refractories are known as a primary material: they resist physical wear, high temperatures and corrosion by chemical agents that may lead to fusion, erosion and creep, and they should do so without losing their structural characteristics. The microstructural evolution and the reactions occurring in basic refractories at different temperatures have been examined, and the diffusion phenomenon is the main processes occurring with refractory components[1–7]. Smelting and converting are industrial processes that involve oxidation reactions and phase relationships in the gas-slag-matte systems, and are carried out in opened reactor furnaces[8–10]. The main purpose of the processes is to remove iron and sulfur from the furnace matte, in an attempt to extract the metal, in reactions conducted between 1200°C up to 1600°C [11–12].

Investigations to understand the oxidation reactions and phase relationships have been reported in the literature, where considerable attention for reaction mechanisms has been given to the interaction of the refractories with basic slags and molten mattes[13 – 20]. There are little data provided on the chemical processes and physical chemistry involved on the interaction of the various gases formed in smelting and converting processes with the basic refractories. The interaction of basic slags, molten mattes and their effect on the refractory properties is beyond the scope of this research; the focus is mainly on the interaction of sulfur-bearing gases and the basic refractories. In the literature the sulfur dioxide, SO_2, has the highest equilibrium pressures in gases found in the gas phase[21], and corrosion of the refractories in converter furnace has been attributed to the effect of sulfate formed from the interactions with sulfur-bearing gases, particularly in the region of the converter above the matte[22]. This is the freeboard region of the converter where sulfur dioxide, sulfur trioxide and the volatile species are formed. The refractory compatibility with these corrosive sulfur-bearing gases and other volatile species formed by reactions remains a challenge. The phases in gas-slag-matte systems are related to the equilibrium conditions, but the open nature of the reaction conditions and different phases makes it difficult for equilibrium to be achieved in a reacting systems[23–27].

The physicochemical processes involved in these chemical interactions affect the refractory properties and its inherent structural features such as pore size distribution, cracks, which could influence the permeability of the gases, and possibly change the microstructure and decrease the quality of the refractories[28]. The oxidizing conditions result in sulfate formation at high equilibrium temperature, which causes the refractory structure to expand and weaken, while low temperatures allow gases to condense as acid solutions and penetrate the refractory structure[22,29]. The physical factors on the refractory structure have been investigated[30 – 38], and the reaction phenomenon was explained by the greater affinity of the oxides, MgO and CaO comprised as refractory components, for sulfur dioxide at smelting and converting temperatures[21,37]. Different models have been applied to explain the $SO_x(g)$ (for x = 2 or 3) uptake of the individual oxide carbonates by adsorption or absorption and conclusions were drawn based on the kinetic and reaction mechanisms[39 – 43].

The lack of data on the chemical interactions between the basic refractories and these gases were the reason for this research. The aim of the present study was to investigate the interaction of the basic refractories with the sulfur-bearing gases by examining the effects of the gases (SO_2, SO_3 and O_2) on the refractory chemistry (pure basic oxides and blended and unblended refractories) and the microstructure (the distribution of the pores, voids and cracks). The compatibility of the basic refractory components with the sulfur-bearing gases were examined, and defined by the reaction mechanisms and changes that occurred in the underlying microstructures. The experiments were formulated such that the reactions represented typical converter furnace conditions that involve mainly SO_2 and O_2, similar to those estimated in non-ferrous industry. The experimental results confirmed the formation of secondary sulfate phases and attributed the changes in microstructure and reaction mechanisms to the important phenomenon of diffusion and sulfur potential of the oxides. The pore size distribution, phase distribution, the grain size distribution developed, played a vital role in the integrity of the refractory and reactions that occurred. The abilities of the different refractories selected to withstand severe conditions were compared. The observations showed how intensely the sulfur-bearing gases reacted with the basic refractories of magnesite, chrome-magnesite and magnesite-chrome and how these could contribute to the degradation of the material during service.

CHAPTER 2
LITERATURE REVIEW

2.1 Introduction.

Refractories are a family of ceramics capable of maintaining good chemical, thermal, and physical features at high temperatures[44–47]. Industries that line their furnaces with these essential basic refractory materials accept the corrosion of the refractory due to the corrosive and erosive environments present during service. Different refractories under different conditions behave differently when reacted with the gases and the mechanism product formed that may lead to corrosion have been suggested as a combination of technological factors during production, service conditions, chemical processes, and material handling. The basic refractories used in the non-ferrous industry are mainly chrome-magnesite and magnesia-chrome refractories[44–47] and these are the standard refractory materials used for lining of reactor furnaces such as Peirce Smith converters. The refractoriness of the material is its ability to withstand extreme conditions without failure and there are no specific selection criteria that one can resort to in choosing a refractory. The choice of a particular refractory considers the properties needed from a refractory and the price.

These basic refractories are formed from dead burned natural magnesia and chromite minerals[44], which upon heating, contain magnesia (MgO), chromite grains ((Mg, Fe) $(Cr, Al)_2 O_4$) and silicate phases in varying compositions. The chrome-magnesite usually contains 15-35 wt % Cr_2O_3 and 42-50 wt % MgO, and can withstand corrosive slags and gases and have high refractoriness[44]. Magnesite-chrome refractories contain about 60% MgO and 8-18% Cr_2O_3, and are highly resistant to basic slags and have better spalling resistance than chrome-magnesite[44]. The silicates are found within the grain boundaries and the composition ranges from 3 to 10 wt% SiO_4, but low percentages are obtained for pure compounds. The phase constituents of the components involved could be determined at different temperatures using binary, ternary, and quaternary phase relationship diagrams[48-52]. The corrosive environments brought about by chemical, thermal, and mechanical effects are important factors when selecting a refractory for a particular application[47]. The physical characteristics and refractory properties are determined by phase distribution, grain size, and pore size distribution in the structure developed.

2.2 The reactions occurring in basic refractories and development of microstructure.

The reactions occurring between chromitite and magnesia minerals in basic refractories are complex[48–49]. Therefore, it is impractical to create a system that includes all the components and reactions involved without making assumptions about the behavior of some of components in the reactions. The developed phase distribution, pore structure and the resulting microstructures from the reactions of magnesite (or periclase, MgO) and chromitite are determined by the crystal structure and the crystallographic behaviour of the different components[53].

2.2.1 Phase relationships between iron oxide and spinel phases in basic refractories.

The fundamental factors of oxidation-reduction and solution-precipitation relationships occurring during reaction in basic refractories has been attributed to the behaviour of iron oxides[1–7,46–51]. Studies[46–51,53,54] on phase composition of magnesia-chromite mixtures have unanimously agreed that diffusion reactions were initiated primarily by oxidation and diffusion of iron oxide contained in chromite grains into the magnesia grains. The changes that occur during reaction of magnesia-chromite mixtures resulted in non-stoichiometric compounds (defect structures)[48–50]. White[53] described the nature of defects in crystals structures of non-stoicheometric compounds and the thermodynamic rationale for their existence. Based on the structural characteristics observed the behaviour of the phases was suggested to be determined by several factors such as temperature, pore size distribution, grain size in reactions conducted by heating different spinel mixtures and/or reheating of the spinel mixtures. A diffusion phenomenon has been suggested to be the main reaction process. The phase distribution of Fe, Cr, Al, Mg, Ca and Si between the minerals, the composition, type of phases, pores size distribution, grain size and diffusion processes at the specific heating temperatures determine new phase formations[47].

Lovell[46–47], Richards and White[48] and Woodhouse and White[49–50], investigated the phase relationships of iron oxide containing spinels and other spinel mixtures, and established phase diagrams that described the behaviour of the different minerals at different temperatures. In the Fe-Mg-Cr-O systems considered in the studies[49], the phase equilibrium diagram indicated that Fe_2O_3 dissociation resulted in a complete series of spinel phases of Fe_3O_4, $FeCr_2O_4$, $MgCr_2O_4$ and $MgFe_2O_4$. In general, the composition mixtures in the raw chromitite mineral containing spinels and magnesia mixtures are described by:

$$(Mg^{2+}, Fe^{2+})\,(Fe^{3+}, Cr^{3+}, Al^{3+})_3O_4 \qquad (2.1)$$

$$(Mg^{2+}, Fe^{3+})_2SiO_4 \qquad (2.2)$$

Richards and White[48] and Woodhouse and White[49] investigated the behaviour of iron oxides (Fe_2O_3, Fe_3O_4, and FeO) and their mixtures with MgO, Cr_2O_3 and Al_2O_3 at different temperatures and atmospheric conditions. The equilibrium data collected for the dissociation of iron oxides suggested that oxidation state of Fe_2O_3 (from Fe^{2+} to Fe^{3+}) changed in oxidizing or reducing conditions. From the dissociation data, the formations of phases were determined and indicated to have occurred through ionic-controlled diffusion processes. The dissociation temperatures decreased with the increasing content of MgO in Fe_2O_3 systems but found to be higher for Fe_2O_3 heated alone[48]. Dissociation continued progressively with changes in the O/Fe ratio and the non-stoicheometric product of magnesiowustite (MgO·FeO) formed at high temperatures. The observed differences in other sesquioxide mixtures was that in the Fe_2O_3-MgO mixtures, $MgFe_2O_4$ spinel existed even before dissociation began, at 700°C for MgO content above 50 wt%. On cooling, the transformation was completely reversed with re-absorption of oxygen by the iron oxides. Harbach and Ford[54] confirmed the findings, and indicated that in oxygen atmospheres, the dissociation temperatures were increased.

In sesquioxide mixtures of Cr_2O_3 and Al_2O_3 with Fe_2O_3[48–49,54–55] similar changes occurred progressively with increasing temperatures and complete series of solid solutions formed. The dissociation temperatures of Fe_2O_3 increased considerably with increasing Cr_2O_3 and Al_2O_3 content[48–50], but suggested partial solubility between Fe_2O_3 and Al_2O_3 affected dissociation at low temperatures. The studies[48] suggested that the dissolution of Fe_2O_3 resulted in lower free energy and dissociation temperatures. The extent of transformation temperatures, the rate of transformation of the sesquioxides phases (R_2O_3 where R = Al, Cr, or Fe), dependent on the chrome, magnesium and alumina compositions. The non-stoicheometric compounds were thus described by the hetero-valent ions ($3R^{2+}$ or $2R^{3+}$) that occupy the lattice of the defected structures in oxidation-reduction reactions[53]. Rigby[4] described this mechanism of diffusion using a phenomenon of crystal chemistry in which the spinels assumed two types of structures, the normal type spinel and the inverse type. The type of crystallographic sites occupied by the divalent metal ion present in the system were such that in the normal type they occupied tetrahedral site, whereas in the inverse type they occupied the octahedral sites, with the trivalent atoms occupying both octahedral and tetrahedral sites. Therefore, dissociation of Fe_2O_3 at different temperatures resulted in new phase.

Brindley and Schaefer[55] discussed the changes in the O/Fe ratio in magnesiowustite ($MgO \cdot FeO$) and magnesioferrite ($MgFe_2O_4$) spinel structures, and showed the structural changes in oxidizing and reducing atmospheres. The studies agreed with Rigby[4] in that the spinels occurred by changes in the crystal lattices, and the mechanism of reaction suggested involved redistribution of the diffusing cations in the crystallographic sites of the reacting oxides. The diffusion was balanced by an addition of one or more oxygen anion, and was associated with volume increases in the structure[55] as two different types of spinels react rather than a reaction between the same groups[4]. Homer and Richardson[56] suggested diffusion processes involved migration of cations through an oxygen lattice by bulk diffusion moving as a front through MgO and unequal diffusion of iron oxide could possibly occur. In the high MgO-low Cr_2O_3 systems dissociation resulted in magnesiowustite $MgO \cdot Fe_2O_3$ formations at high temperatures rather than a magnetite, $MgFe_2O_4$, spinel. The reactions have been described by the homogeneous distribution of Fe^{3+} and Al^{3+} phases and the presence of Cr^{3+} and Mg^{2+} in chromite and magnesia phases at different concentration[48–50] that can be described by:

$$(Mg^{2+})\,(Fe^{3+}, Cr^{3+}, Al^{3+})_3O_4 \qquad (2.3)$$

DeMenezes[5], and Stubican and DeMenezes[57] supported the diffusion phenomon suggested for reaction mechanism proposed by Rigby[4] in basic refractory mixtures, and provided detailed account on oxidation of the iron oxides, dissociation of the spinels and diffusion of the elements in magnesia-chrome refractory mixtures when heated in oxidizing atmosphere. They showed that diffusion of the ionic species within the Fe-Mg-Cr-O systems occurred selectively[5,57], and was determined by the ionic radii, charge of the ions and energy required for formation of cation vacancies. The relative diffusion kinetics were found to be higher for iron oxide , due to reported ionic radii (Ahrens) of the Mg^{2+}, Fe^{2+}, Fe^{3+}, Cr^{3+}, and Al^{3+} species involved in diffusion processes, which were 0.67, 0.74, 0.64, 0.63 and 0.51 respectively.

Structural changes occurred and formation of magnesia spinels enhanced grain growth, in the reaction mechanism attributed to unequal diffusion by Rigby[4] due to slow diffusion kinetics of Mg^{2+} ions, compared to those of iron oxides. This processes occurred by Kirkendall effect, explained by differential diffusion mechanism and this resulted in pore formation and grain growth. Massengale, Mong and Heindl[28] found significant increase permeability when magnesite-chrome refractory mixtures were heated, and this was attributed to the increased pore formation resulting from diffusion processes. Gordon, Merchant and Hollenberg[58] investigated the effects of porosity on grain growth kinetics of high purity magnesium oxide and

magnesiowustite (MgO·FeO), with iron oxide solid solution phases considered as impurities. The structural observations demonstrated that the dissolution of iron oxide in MgO resulted in increased porosity in the diffusion processes relating to the suggestions made in previous studies[55]. In magneisowustite, MgO·FeO, slow diffusion kinetics at low temperatures decreased grain growth kinetics, but at high temperatures, increased grain growth and enhanced pore entrapment. Kapadia and Leipold[59] have correlated the grain-growth mechanism to the cation and anion diffusion processes, which suggested that oxygen anions were faster along the grain boundaries and the composition of the oxygen anions was the limiting factor in grain growth by boundary migration. Rigby, Hutton and Hamilton[3] investigated and elucidated the reactions that occurred in silicate phases, and the proposed diffusion mechanism that suggested that in presence of monticellite ($CaMgSiO_4$) or dicalcium silicate (Ca_2SiO_4) the sesquioxides tended to migrated from chrome grain into the matrix, and silicates formed liquid at low temperatures. However, in forsterite, (Mg_2SiO_4) magnesia migrated into the chrome grains and this increased silicate melting temperatures, due to significant decrease in solubility of spinels into the silicate melts. The phase equilibrium diagrams and phase structure developed from spinel mixture and dicalcium silicate by El-Shahat and White[51], agreed with Rigby *et al.*[3]. The melting temperature of the silicate found to increase with increasing Al_2O_3 and Cr_2O_3 in the silicate melt, relating to Richards and White[48] and Woodhouse and White[49] studies.

In other studies,[60 - 66] diffusion in silicates has been described as the mechanism affected by the size of the diffusing ions and the volume changes that occur in the structure in an anion-controlled or cation-controlled process. Hofmann and Magaritz[63], Watson[64] and Marioka[65–66] Medford[62] described cation-controlled process diffusion attributed to diffusion of Ca^{2+} cation and changes occurring in the lattice parameters and structure. The proposed mechanism was that the amount and distribution of free volume in the silicate structure controlled diffusion of Ca 2+ cations in silicates, rather than the vacancy concentration, i.e. presence of empty sites and free vacancies enhanced a jump of a cation from one equilibrium position to the next. This type of diffusion corresponded to a structure-sensitive process and the amount of free and distribution of free volume controlled the mechanism instead of the vacant site mechanism. Ricker and Osborn[67] attributed the changes in amounts and distribution of free volume to the diffusion and substitution of Ca^{2+} by Mg^{2+} suggested to occur in silicates.

2.2.2 Diffusion processes and microstructure developed in basic refractories.

Studies[48–52] of Fe_2O_3-MgO systems and other mixtures have showed that oxidation-reduction and solution precipitation relationships resulted in different structural features, when heated at different reaction conditions. The microstructure in refractories can described as grains that do not contact, or a network of grains having direct grain-to-grain contacts, with silicate phase interfaces between the grains [1–3,5–6,47,51,55–68] The reactions and diffusion processes that occur have been found to be consistent[6] with those predicted in phase diagrams[48–51]. The changes in microstructures resulting from diffusion processes could possibly be the contributing factors to the decreasing quality of refractory during service[1–3,69]. The microstructures of commercial chrome-magnesite and magnesite chrome refractories have been analyzed using different scanning electron microscopy techniques, and characterized by the structural features (pore size, particles size and grain size), and their composition which was shown as measure of their reflection. The mixtures of magnesia secondary spinel phases, and three silicates namely, forsterite, and monticellite and dicalcium silicate formed in varying compositions formed. The magnesia- spinels formed occurred through diffusion processes and solution precipitation of sesquioxides into magnesia.

Treffner[70] investigated the microstructure of magnesia grains heated at different temperatures, and showed that the diffusion processes resulted in magnesia grains changing their grain orientation. The changes in grain surfaces were attributed to the effects of interfacial energies and minimum interfacial energies obtained for stable phases. Silicates found formed interfaces between the grains, and their composition increased the tendency of liquid formation, and decreased the direct grain to grain contacts. This effect attributed to the silicate wetting behaviour suggesting that interfacial energies in magnesia grain were higher than that of silicates and magnesia. Well-developed grain-to-grain structures achieved in the high purity compounds enhanced the tendency of fine particles to sinter together and lowered interfacial energy[70]. Treffner[71] demonstrated that presence of silicates in basic refractory mixtures influenced the microstructural changes by affecting the microstructure of chromite and the direct bonding between the magnesia spinel phases, and between the magnesia and chromite phases.

Several studies[5–6,51,68] showed that in Cr_2O_3-MgO mixtures the diffusion processes resulted in chromite spinels undergoing microstructural changes and the effect demonstrated direct bonding in of $MgCr_2O_4$ formed, which had varying solution precipitation compositions and different

structures. The structural features showed diffusion of iron oxide in magnesioferrite structures demonstrated as white precipitate structures on the magnesia matrix, while in Cr_2O_3-MgO mixtures and magnesiowustite, the iron oxide often occurred as single spinel solid solution phase. The suggested effects of silicates on the solution precipitations formed and direct bonding between the structures altered the magnesia spinel compositions formed[1–2, 68]. In presences of silicate the differential diffusion mechanism suggested by Hayhurst and Laming[1–2] reported that silicates enhanced the direct bonding, when dissolved sesquioxides from liquid silicate precipitated out as secondary spinels structures. However, Scheerer, Mikami and Tauber[68] and other authors[51,70–71] disagreed with Hayhurst and Laming[1–2] and suggested that development of direct bonding did not require silicates and in fact the silicates reduced the direct bonding thereby forming interfaces between magnesia-magnesia grains and magnesia-chromite grains. The progressive dissolution of spinels resulted in spheroidization of the crystallographic phase boundaries with minimum surface energy as a way of attaining equilibrium[51].

Treffner[71] and Ford, Hayhurst and White[72] suggested that the driving forces on the transformation that occurred in microstructures due to phases tending towards equilibrium were affected by temperature. From microstructures, the silicates were displaced by diffusion and migration from the surface of the chrome grains and this increasing temperature improving the direct bonding. The interfacial energy between chrome spinels and silicates considered was higher than between periclase and chrome spinels. The effect of the developed microstructure on the physical features and properties of the refractory components discussed [71,73–75], have demonstrated that service conditions changed the mineralogical compositions of the original structure thereby enhancing dissolution of refractory components. The nature in which the changes occurred were determined by the different metallurgical environments, in which slagging by solid, liquid and vapor phases produced new formations in microstructures by changing mineralogical compositions[71]. Therefore, producing original structures having stable refractory components by firing at very high temperature could possibly improve physical properties[75–76]. The tendency of the refractories to absorb different constituents from the metallurgical processes during service have been associated with the problems that haven experienced, in which corrosion was the common form of deterioration[69–75].

2.3 The interactions of basic refractory components with sulfur-bearing gases.

The chemical reactions of basic refractories with sulfur-bearing gases and their effect on the microstructure and mineralogy of the refractories have been evaluated and the effects are reported in literature[22,30–38,71,77]. However, the investigations conducted on refractory materials used as linings of furnaces for different metallurgical processes, and had been in service for different periods of time effects. The focused has been on the on the changes in physical properties and few data have been reported on the reaction mechanisms[33–29]. These reaction mechanisms have proven to be important in understanding the behaviour of the different components and diffusion processes that could occur in sulfur-bearing gases. This could possibly help in choosing the proper refractory for a particular application.

2.3.1 Reactions of sesquioxides components (R_2O_3) with sulfur-bearing gases

The equilibrium reactions of sesquioxides sulfates and the thermochemical data from different temperature measurements have been derived[78–79]. Kellogg[79] evaluated and derived thermodynamic data from the gas partial pressures obtained for the decomposition reactions of different sulfates at different temperatures, and ferric, ferrous and aluminum sulfates reactions were determined. The ferric sulfate, $Fe_2(SO_4)_3$, decomposed directly to Fe_2O_3 and SO_3 at decomposition pressures between 520°C and 724°C. Ferrous sulfate, $FeSO_4$, reported was stable under reducing conditions at high temperatures, but no detailed decomposition temperatures were given. Changes due to crystallographic transformation (from α to γ) have been reported for aluminum sulfate decomposition to Al_2O_3 and SO_3 between 572°C and 777°C. Thermal decomposition of $Al_2(SO_4)_3$ had an effect on the thermodynamic properties that involved a metastable phase Al_2O_3 (γ), which converted to a stable Al_2O_3 (α) phase at 827°C.

Podwórny, Piotrowski, and Wojsa[78] evaluated the kinetic studies and mechanisms of gas-solid reactions between MgO-MgR_2O_4 spinels and SO_2-O_2 gas mixtures. The decomposition temperatures determined for aluminum sulfate $Al_2(SO_4)_3$ were between 527°C and 627°C, while the decomposition of ferric sulfate, $Fe_2(SO_4)_3$, occurred between 527°C and 627°C. The results were within the suggested temperature range by Kellogg[79]. The decomposition reactions suggested for sesquioxides sulfates were:

$$Fe_2(SO_4)_3 = Fe_2O_3 + 3SO_3 \qquad (2.4)$$

$$Al_2(SO_4)_3 = Al_2O_3 + 3SO_3 \qquad (2.5)$$

$$Cr_2(SO_4)_3 = Cr_2O_3 + 3SO_3 \qquad (2.6)$$

Safiullin, Gitis and Panasenko[80] and Gallagher, Johnson and Schrey[81] studied the thermochemical conversions of hydrated iron sulfate ($FeSO_4.7H_2O$) to Fe_2O_3, in argon, nitrogen and in oxidizing atmospheres. Reaction mechanisms for the decomposition using thermographic and thermogravimetry technique, illustrated graphs obtained in different atmospheres as shown in Figures 2.1 to 2.3. The studies[80–81]agreed on the decomposition mechanisms, but disagreed on the decomposition temperatures for the reactions. Safiullin *et al.*[80] (Figure 2.1) showed that in oxidizing atmospheres (air) decomposition occurred at 487°C with formation of oxysulfates ($Fe_2O(SO_4)_2$), and Fe_2O_3 formed at high temperature at 760°C. However, in argon atmospheres two oxysulfates components, $Fe_2O(SO_4)_2$ and $Fe_2(SO_4)_3$, formed at 687°C, and both decomposed to Fe_2O_3 at 755°C. These findings corresponded to temperatures obtained for ferric sulfate, $Fe_2(SO_4)_3$, by Kellogg[79]. In Gallagher *et al.*[81] studies the mechanism of reaction in oxidizing atmospheres shown in Figure 2.2 indicated gradual decomposition to Fe_2O_3 occurred between 600°C and 675°C. The findings corresponded with the suggested initial decomposition temperature (600°C) for iron sulfate in studies of Rigby[34], but disagreed with that suggested by Kellogg[79] and Podwórny *et al.*[78] The suggested changes in SO_2 and SO_3 equilibrium pressures possibly due to presence of oxygen affected the decomposition[78–79,81]. In Figure 2.3, decomposition of $Fe_2(SO_4)_3$ to Fe_2O_3 in nitrogen occurred between 675°C to 1000°C. In the results, in oxygen atmosphere conversion of iron (II) to iron (III) occurred before decomposition, whereas in nitrogen these occurred simultaneously.

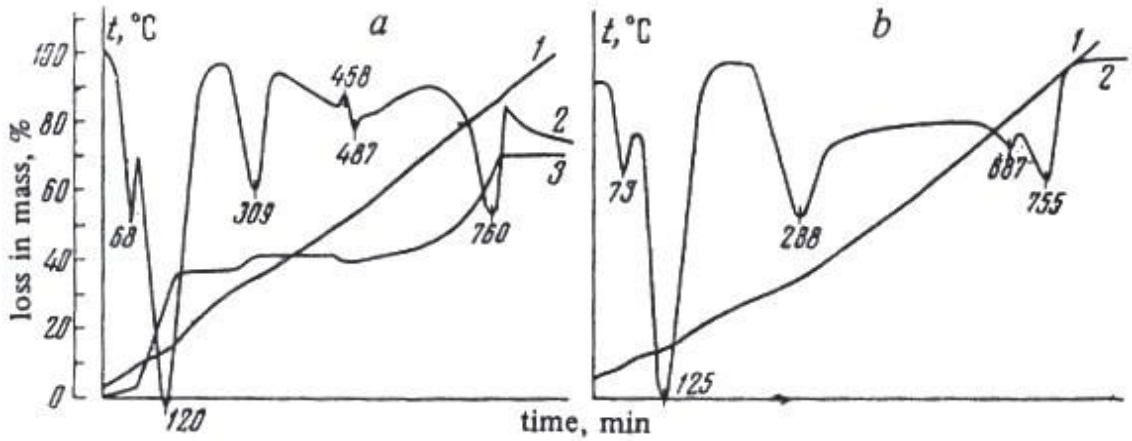


Figure 2.1. Decomposition curves of iron (II) sulfate during heating: (a) in air; (b) in argon atmosphere. 1) temperature record; 2) differential record and 3) loss in mass of specimen (Reference Safiullin, Gitis and Panasenko[80]).

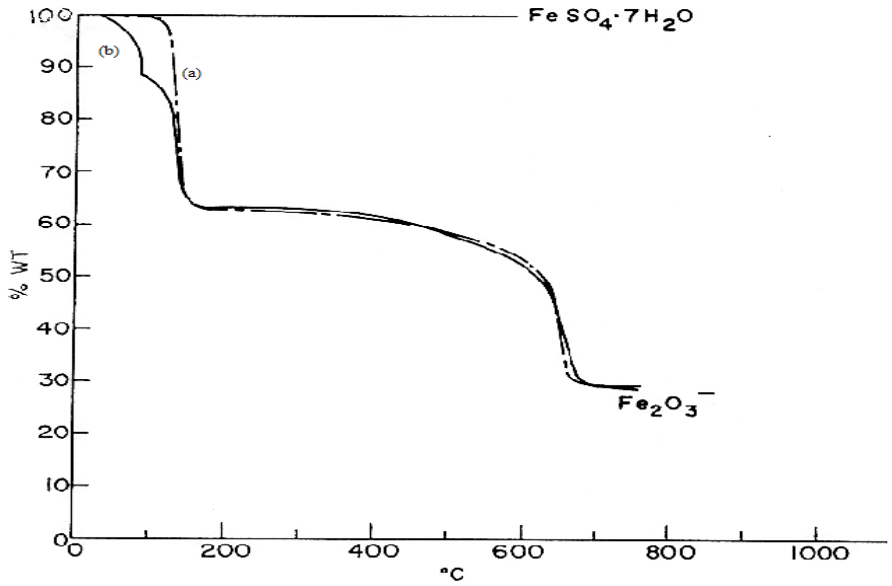


Figure 2.2. Decomposition curves of iron (II) sulfate during heating: (a) in air; (b) in oxygen atmosphere (Reference Gallagher, Johnson and Schrey[81]).

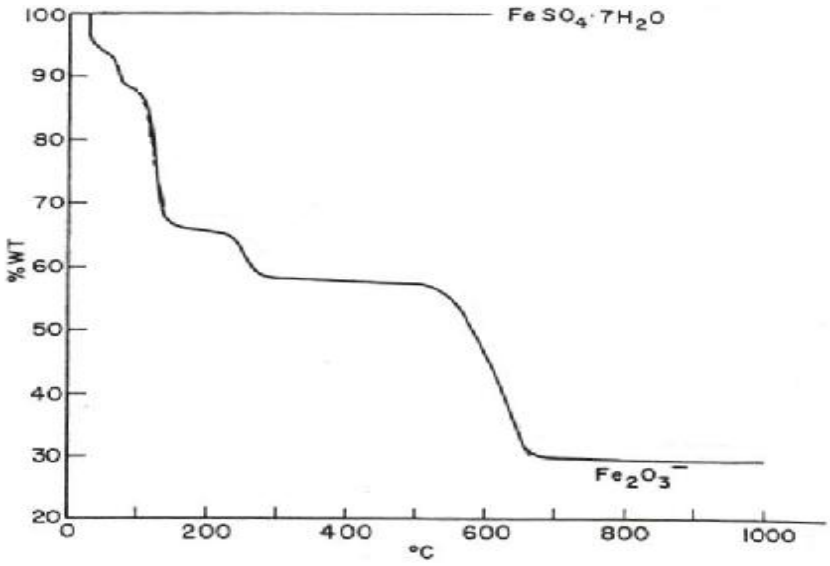


Figure 2.3. Decomposition curves of iron (II) sulfate during heating in nitrogen atmosphere (Reference Gallagher, Johnson and Schrey[81]).

2.3.2 Reactions of MgO-MgR_2O_4 spinel components with sulfur-bearing gases.

Rigby[34] and Trojer[36] suggested that in basic refractories exposed to sulfur-bearing gases, sulfation occurred through dissolutions of magnesia spinel, and MgO formed $MgSO_4$, while iron sulfates possibly occurred below 600°C. The findings supported the reactions shown in Figure 2.2 and 2.2 for iron sulfate[81]. Podwórny *et al.*[78] indicated that different magnesia spinels prepared from sulfate solutions and ammonium carbonates that had been dried, grounded and

heated to 1200°C, formed sulfates in reactions conducted in SO_2-air atmosphere between 550°C and 1000°C. The reaction mechanisms expected using standard free enthalpies were:

$$2SO_2 + O_2 = 2SO_3 \quad (2.7)$$

$$MgO + SO_3 = MgSO_4 \quad (2.8)$$

$$MgCr_2O_4 + SO_3 = MgSO_4 + Cr_2O_3 \quad (2.9)$$

$$MgCr_2O_4 + 4SO_3 = MgSO_4 + Cr_2(SO_4)_3 \quad (2.10)$$

$$MgFe_2O_4 + SO_3 = MgSO_4 + Fe_2O_3 \quad (2.11)$$

$$MgFe_2O_4 + 4SO_3 = MgSO_4 + Fe_2 (SO_4)_3 \quad (2.12)$$

$$MgAl_2O_4 + SO_3 = MgSO_4 + Al_2O_3 \quad (2.13)$$

$$MgAl_2O_4 + 4SO_3 = MgSO_4 + Al_2(SO_4)_3 \quad (2.14)$$

The phase analyses conducted showed that reactions resulted in $MgSO_4$ and different oxides, through reaction Equations 2.8, 2.9, 2.11 and 2.13. Decomposition temperatures for different sulfates were determined, and $MgSO_4$ found decomposed gradually from 927°C to 1027°C, and liberated SO_3 pressures of 5.592×10^{-2} atm were obtained at 1027°C in SO_2-O_2 gas mixtures used in the study. Rigby[34] suggested that $MgSO_4$ formed from $MgFe_2O_4$ in basic refractories started to decompose at 750°C, which are temperatures lower than that obtained for synthetic spinels by Podwórny *et al.*[78]. The reaction equilibrium indicated for the gases suggested that partial pressures decreased with increasing temperature. The kinetic studies demonstrated varying reaction rates for the different spinels that increased with temperature from 500°C to 800°C, and decreased at 1000°C. The suggested shrinking core model proposed[78] proved to be inappropriate in explaining the kinetics of reactions for the magnesia spinel reacted, due to non-linear relationships observed. The non-linear relationship was attributed to changes in spinel structures suggested to occur due to iron oxide dissociation influenced by $Mg^{2+}(Al, Fe, Cr)^{3+}{}_2\ O_4$ changes to $(Mg, Fe)^{2+}(Al, Cr)^{3+}{}_2\ O_4$, as discussed in previous studies[5–7,48–50,54–57]. The changes resulted in lattice transformation and defected structural components formed, and the maximum reactivity corresponded to the range of temperature of structure transformation influencing significantly the kinetics of sulfation reactions. The oxygen partial pressures determined the dissociation of Fe^{3+} to Fe^{2+} during reactions. On the other hand, the shrinking core proposed[78] was satisfactory for pure MgO sulfation kinetics and the graph showing temperature dependence of reaction rate constant ($\ln K_2$ versus 1/T) gave linear relationship shown in Figure 2.4.

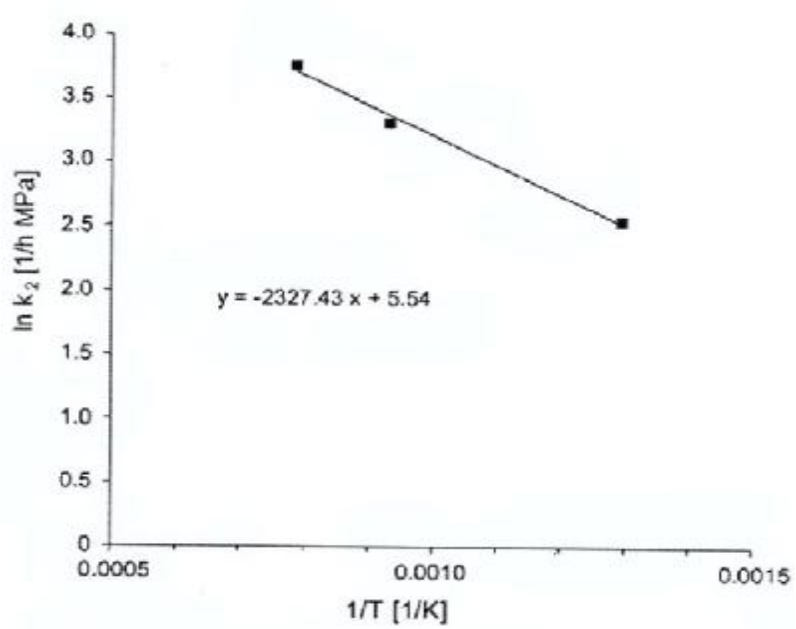


Figure 2.4. Reaction rate constant k_2 of MgO in SO_2-O_2 system between 500°C and 1000°C (Reference Podwórny, Piotrowski and Wojsa[78]).

2.3.3 Structural changes of basic refractory components in sulfur-bearing gases.

The structural features such as phase distribution, grain size, pore size distribution, and crack formation have a significant effect on gas-refractory interactions. In the gas-solid reactions, any mechanism that compromises the refractory structure has a significant influence and possibly initiate sulfate attack on the sites susceptible to reaction[31]. The oxidation-reduction and solution precipitation relationships due to differential diffusion processes at temperatures have been associated with structural changes[28,4–6,55,68,70–71]. In presence of sulfur-bearing gases the basic refractory components have been shown to form sulfate compounds[22,30–13,78], in reaction mechanisms suggested to being due to structural changes influenced by diffusion processes and temperatures[34,36,78]. Several studies[22,30–38] have attributed the refractory failure to secondary product components formed in chemical reactions with different gaseous phases. Massengale ***et al.***[28] showed that diffusion processes, altered phase and pore size distribution, and influenced permeability, which could facilitate diffusion of gases within the refractory structure. Blanco, Davies, and Sridhar[103] demonstrated the tendency of the sulfur-bearing species to infiltrate refractory features through cracks and pores, and decreased of refractory physical properties.

Schumann[21] defined the equilibrium partial pressures of SO_2, S_2, and O_2 in a converter gas phase, at constant temperature and one atmosphere, and established that equilibrium in gas-slag-matte compositions are related, but difficult to achieve due to vented processes used by the reactors. In

the converter, SO_2 formed through dissolution of magnetite (Fe_3O_4) in gas-slag-matte systems, which reacts with the FeS in the slag, resulting in FeO and SO_2. When estimated equilibrium pressures of SO_2 emitted were one atmosphere for conversion processes, the oxygen partial pressures were between $2.7x10^{-8}$ to $3.4x10^{-6}$ atm. Therefore, in practice reactions occur until the SO_2 in the different phases was in equilibrium with that of the off-gases, suggested to be one atmosphere. Changing the composition in the reacting system could change the gas phase and possibly result in phase changes in the refractory components and consequently the microstructure, as suggested in other studies[13,47–52,78].

Hugget[30] investigated used basic refractories and found that the products formed due to sulfation resulted structural disintegration and temperature gradient and physical features were important factors affecting the reactions. Refractory components formed sulfates with CaO and K_2O, as calcium sulfate ($CaSO_4$), potassium sulfate (K_2SO_4), and double sulfate of $CaSO_4{\cdot}K_2SO_4$. A lamellar twining structural feature characterized the double sulfate of $CaSO_4{\cdot}K_2SO_4$ formed. The CaO and K_2O suggested to form sulfates were components found in silicate phases, suggesting that silicate compounds contained the reactive components. The different structural polymorphs of β and γ-$2CaO{\cdot}SiO_2$ reported suggested that the mechanism of sulfation in silicates occurred through structural dissociation, which resulted in CaO crystallization and subsequent sulfation. Therefore, the CaO determined $CaSO_4$ availability in silicate compound and when in excess continued reaction with silicates occurred, however, K_2SO_4 did not reactive with silicates. Decomposition temperatures suggested for $CaSO_4$ were between 1300° and 1500°C, and an immiscible liquid sulfate of K_2SO_4, which enhanced infiltration within the refractory formed. Thermodynamic analyses of liquid-refractory interactions conducted by Mäkipää and Taskinen[13–14] indicated that sulfur and oxygen in the melts, were active elements, which lowered the interfacial energies of solid components upon reactions[13], in chemical equilibriums determined in terms of capillary mechanics[14]. Therefore, further sulfation could possibly occur with refractory oxides. Brisbane and Segnit[31] confirmed the results of Hugget[30], and changes in mineralogical compositions due to sulfate attack occurred in used magnesite-chrome refractories examined. In different parts of the refractories evaluated substantial amounts of complex alkali silicate and alkali-lime sulfates occurred.

Several investigations conducted on used refractories indicated formation of $MgSO_4$[31–38] that occurred mainly at the imperfections, and hampered the physical properties that possibly resulted in failure of the refractory structures[29]. Clark and McDowell[33] also reported the formations of

magnesium sulfate in used basic refractories, where the sulfate attack promoted dissolution of the refractory phases through weakening of the bond structure and resulted in crack formation and corrosion. Olbrich and Rostani[31] investigated the chemical reactions and the physical factors on the behaviour of magnesium aluminate spinels in sodium sulfate. The sulfates formed were compounds of $MgSO_4$ and $Na_2Mg_2(SO_4)_3$, and sulfate mixtures of melilithic glass ($MxCaAlSi_2O_7$) containing silicates and secondary spinels occurred. Therefore, the suggested diffusion processes occurring with the refractory components could possibly result in complex sulfate mixtures. The sulfates structures observed suggested that reaction mechanisms occurred by gases infiltration through the grain boundaries and MgO and CaO contained in silicates of $MgSiO_4$ and $CaMgSiO_4$ formed sulfates. The presence of spinels within the sulfate mixtures observed, suggested dissolution of spinel, which have been indicated to form sulfate in sulfur-bearing gases in other studies[34,36,71]. Podwórny *et al.*[78] confirmed the chemical reactivity of the spinels and mechanism of spinel reactions proposed are presented in the reaction Equation 2.9, 2.11, and 2.13.

Rigby[34] and Trojer[36] reported that sulfation could occur with both iron oxide and magnesia present in magnesioferrite spinel ($MgFe_2O_4$), in chemical reactions that depended upon oxygen pressures and temperature. Large amounts of soluble magnesium sulfate found occurred in all the regions of the refractory in magnesite refractories, whereas in magnesite-chrome and chrome-magnesite refractories $MgSO_4$ compound was found mainly in the cold regions. In sulfated regions, the physical refractory structure had disintegrated forming a porous material, and this effectively reduced the length of the brick, through dissolution and erosion. This was due to the expansion and volume changes associated with sulfate products formed. The suggested decrease in material properties were investigated by examining the reactivity of magnesia formed from decomposed magnesium sulfate. The decomposed material analyzed showed high slag infiltrations, and high reactivity with silicates, and promoted dissolution of the other refractory components. Sulfation reactions lowered the melting point of magnesia from 2800°C (estimated for the unreacted magnesia) to 1124°C, in the decomposed compound. Although there were several factors reported to be contributing to the refractory wear, sulfation was considered as the prevailing mechanism promoting dissolution of the refractory.

Trojer[36] indicated that sulfates did not only form through direct sulfation of calcium or magnesium; indirect sulfation also occurred and this was promoted by dissolution and dependent on the chemical composition of the refractory. The reaction mechanism proposed, occurred

through a series of sulfate decompositions, which liberated SO_3 that reacted with oxides. The silicate phases found along the grain boundaries such as tricalcium silicate, dicalcium silicate, forsterite but mainly monticellite, dissolved and CaO or MgO formed sulfates. Trojer[36] suggested that the reactions that occurred in a molten phase most likely in silicates hindered the re-crystallization of MgO. The silicate phases indicated to being carriers of the reactive oxide components in which silica took no participation in the reactions, but facilitated sulfation. The decomposition of low melting secondary sulfate intermediate phases (from oxides of K_2O, Na_2O and FeO) resulted in $MgSO_4$ at high temperatures, thus a stoicheometric relation between these oxides and total sulfur found in refractories was unlikely. Sulfation could only be associated only with magnesia and calcium oxide being the major end oxides formed at high temperature of about 1000°C.

Treffner[29]discussed the principal mechanisms of refractory deterioration resulting from sulfates and sulfides in basic refractories. The microstructural observations and examined material properties suggested that reactions depended on the reaction thermodynamics of the sulfur-bearing gases and the stability of the oxides involved. Treffner[29] concluded that the amount of sulfate present in the refractories was not related to the weakening of refractory structure as reported in previous studies[30–36]. However, the changes in conditions from a reducing to an oxidizing environment were required for the sulfation reactions, leading to refractory failure in connection with sulfate attack. These conclusions drawn from observations were from parts of the refractories with low sulfate (SO_3) demonstrated physical disintegration, whereas in regions high in sulfides (S), no physical disintegration was demonstrated. The studies[29] suggested that sulfides formed at high temperatures could be oxidized at low temperatures depending on the sulfur-bearing gas pressures. Significant volume changes occurred with sulfates and no changes occurred with sulfides, thus oxidation led to disintegration of the refractory components and corresponding wear of the refractory.

McPherson[37] investigated used basic refractories and similar structural findings with other author's [30–29] were observed. Schumann[21] equilibrium conditions were used to determine equilibrium temperatures of $MgSO_4$ formed, where differential temperature and partial pressure gradient of the SO_2 and O_2 gases across the refractory were the factors affecting the sulfation reactions. The partial pressure of SO_2 and oxygen reported in contact with the refractory affected magnesium sulfate stability, and in gas partial pressures reported[21], $MgSO_4$ formed stable up to 850°C in converter linings. However, due to lack of equilibrium in the reactors, this

temperature was not definite, and based on the changes in log $\{P_{SO2}\ P_{O2}^{½}\}$ reaction equilibrium, when partial pressures of SO_2 were 0.01 atm and O_2 0.01 atm or less the equilibrium temperature range for magnesium sulfate occurred between 929°C and 930°C. In furnaces, these partial pressures vary greatly between the hot surface of the refractory and the cooler regions creating pressure gradient, and temperature influences this variation, with the microstructure (porosity, voids) promoting chemical reactions. Permeability suggested was another factor that enhanced the sulfation through increased gas diffusion, and $MgSO_4$ occurred along the grain boundaries and as pore-space filling products. McPherson[29] proposed the following reaction mechanism:

$$MgO + SO_2 + ½O_2 = MgSO_4 \qquad (2.15)$$

Liouw, Tsikiris and Gray[22] determined the compositional variations of refractory elements and characterized the refractory components from the hot surface to the cooler regions. They indicated that dissolution resulted from migration of elements, which changed phase distribution and structural morphology of the grain size and grain boundaries. Wet analysis method was used to determine formation of sulfates and calcium sulfate and magnesium sulfate occurred, and suggested to being the prevailing mechanism. The structural changes were attributed to the volume expansion that occurred which was reported to be 400 times with $MgSO_4$. The morphology of the $CaSO_4$ formed was a needle structure, which is the crystal structure that can be considered similar to that reported for potassium sulfate in Hugget's[30] studies. The findings agreed with McPherson[37] and a similar reaction mechanism for magnesium sulfate formed was proposed. The dependence of magnesium sulfate on temperature and partial pressure predicted in SO_2 and O_2 gas partial pressures and sulfate relationships could be seen in a predominance area diagram presented in Figure 2.5[22]. The magnesium sulfate predicted was a thermodynamically stable phase at varying temperature ranges and high oxygen partial pressures. Within the suggested SO_2 and O_2 gas partial pressures in Figure 2.5 $MgSO_4$ is a stable product phase for temperatures up to 1000°C, above which MgS forms at high SO_2 pressures and low oxygen pressures.

Gregurek and Majcenovic[37] found significant disintegration of magnesia grains into single grains when MgO of the refractory formed $MgSO_4$ in used basic refractories from different non-ferrous industries. Sulfate formed within the grain boundaries, and the structures suggested that disintegration might have influenced sulfation. They attributed the disintegration to the volume expansion and changes in chemical composition. The sulfates formed within and along the grain

boundary and the mechanism in which the phases formed demonstrated that silicate formed in conjunction with sulfate phase within the grain boundaries. They indicated that oxidation-reduction reactions of the sulfide phases resulted in sulfation, and this corresponded with Trojer[36] and Treffner[29]. The proposed equilibrium temperatures of reaction at 1050°C corresponded with those predicted in the predominance area diagram presented in Figure 2.5[22], which related to studies by Trojer[36], but slightly higher than those calculated for by McPherson[37] and equilibrium temperature proposed for magnesium sulfate was. The physical characteristics of the refractory determine the relative permeability of the gases through the refractory structure[22,28]. The enclosed gas bubbles formed by gases may affect the physical structure thereby generating localized high temperatures and exert destructive pressures on the structure[14]. Detrimental effects resulting in increased the rate of refractory infiltration by gases and crack formations due to volume expansion enhanced further sulfation.

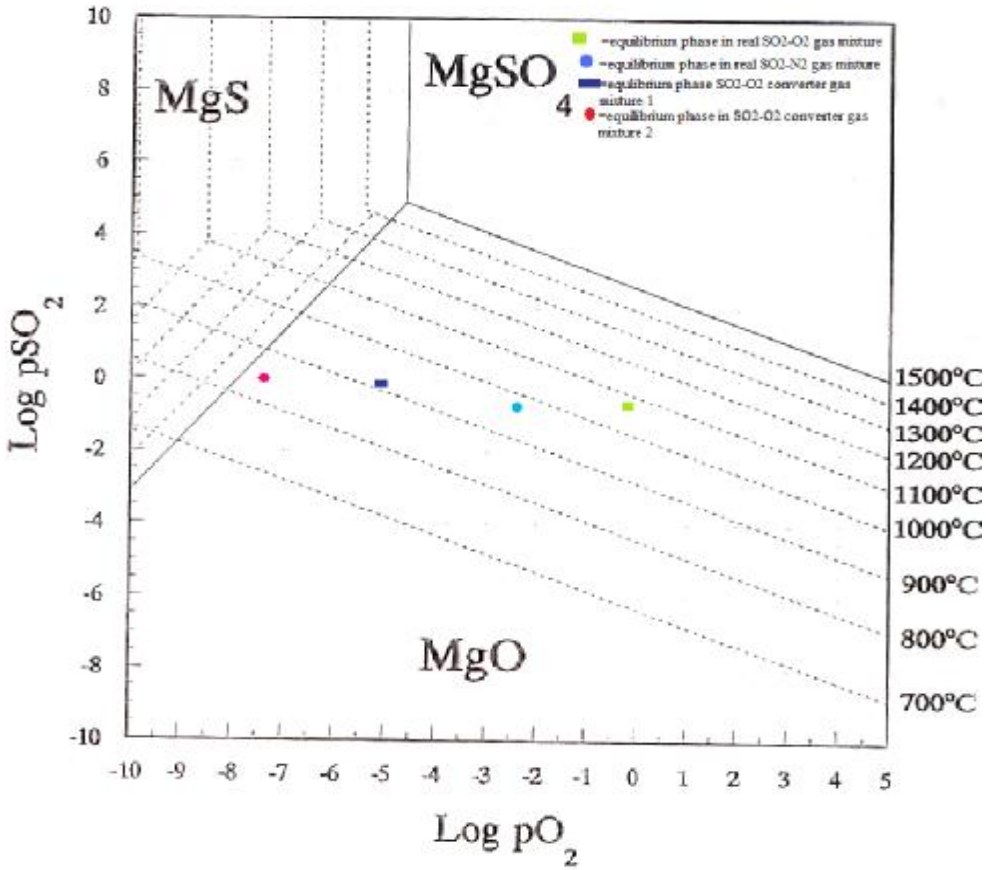


Figure 2.5. Predominance area diagram of magnesium, sulfur and oxygen at varying temperatures, and partial pressure of oxygen and sulfur dioxide (reference, Liouw, Tsikiris and Gray[22]).

2.3.4 Reactions of basic oxides with sulfur-bearing gases.

Gas-solid reaction studies[39–43,83–85], of basic oxides with sulfur-bearing gases have focused on the reaction kinetics of MgO and CaO as absorbents of sulfur dioxide. The behaviour of carbonates when exposed to sulfur-bearing gases in various studies[86–88]. Physical factors of the solid compounds characterized the crystallite size distribution and pore distribution of the raw carbonate during reactions at different temperatures. Clum[86] and Turkdogan, Olsson, Wreidt and Darken[87] showed that pore structure (pore surface area, pore volume, pore size, and distribution) was the primary feature affecting reactivity. Sulfation described related to the surface area exposed and the formation of a dense sulfated product layer around the calcined (CaO) particles, and the calcined product. The factors relating to physical characteristics that have significant effect on the reactivity of the carbonates are the amount of surface area, the impurities, and the crystal structure, which is usually defected during calcination processes. Particles having lager surface area resulted in high sulfation rates while for particles having smaller surface area sulfation was lower[86].

Hartman and Coughlin[39] believed that impurities such as oxides, alumina, silica, and iron oxides indicated in calcites, influenced the kinetic behaviour of the particles, but did not participate in the reactions, and were not subject to the volume changes. However, Clum[86] believed that these impurities formed liquid phases, resulting in decreased sulfation of the oxides. At different temperatures, the transitions from carbonate to oxide involved a metastable condition in which ions (Ca^{2+} and O^{2-}) remained in their original lattices resulting in a high defect oxide structure. The pore structure of CaO found to be uniform and the effect related to the pore surface area and pore volume, which decreased with increasing time and temperature. The changes resulted in incorporation of sulfur-based anions within the structure[86]. Marier and Dibbs[89] and Yang, Shen, and Steinberg[90] studies agreed with the authors[86] in that catalytic reaction were favored in the presence of Fe_2O_3 as an impurity, and the rate of reaction of both the CaO and MgO increased by catalytic conversion of SO_2 to SO_3 in oxygen atmospheres. Wreidt and Darken[91] investigated chemical equilibrium between various gas mixtures within 600°C and 1300°C at total pressures of 1atm. The studies showed that temperatures and partial pressures of SO_2 and O_2 affected the formation of CaS, $CaSO_4$ and FeS found in carbonates. Several reaction mechanisms proposed for $CaSO_4$ showed that in presence of carbonates SO_2 pressures were important in sulfate formation.

Hartman and Coughlin[39] and Georgakis, Chang and Szekely[40] used a simple structural model and grain size model to describe the gas-solid reactions of calcitic and dolomitic carbonates in sulfur bearing. The proposed grain model described a porous particle as comprising spherical grains of uniform size, separated by pores through which the gases diffused. During reaction, a layer of a reaction product was formed on the surface at the surface of each grain, and both porosity and sulfation decreased and diffusion resistance was the limiting factor. The studies[39–40] agreed that pore structure, surface area and grain size of the oxides were related to the original parent material properties and had a significant effect on the conversion rates. Borgwardt and Harvey[43] studied the effects of sulfation on the structural properties of the carbonate rocks and provided understanding on the changes occurring during reactions. Similar findings of principal physical characteristics of the original parent carbonate and the pore structure, surface area and grain size found in other studies[39–40] were observed. The studies showed no relationship between chemical composition and the SO_2 reactivity, but a good relationship between structural features (pore size, pore volume and imperfections) and SO_2 reactivity was demonstrated. Borgwardt[42] demonstrated that temperature had an influence on the initial rate of reaction between 540° and 1100°C. The conversion rates of the calcites increased with increasing temperature and as the reactions progressed. In small particles, chemical reaction was the limiting factor in the sulfation of calcites (CaO) and the initial reaction stages followed a first-order chemical reaction. Internal diffusion resistance was found to be a limiting factor at oxide conversion of about 20% for CaO.

Crnkovic, Milioli and Pagliuso[92] conducted similar studies and agreed with Borgwardt and Harvey[43] in that the physical characteristics affected the reactivity of the oxides with SO_2. They attributed the changes to the different structures forms suggested for MgO and CaO, at different temperatures. They indicated that heterogeneity developed at different temperatures and balance between kinetic and diffusion resistance were limiting factors rather than one factor controlling at different reaction stages, as suggested by Borgwardt[42]. The $MgSO_4$ was confirmed, and suggested to have occurred in presence O_2 present in gases. Studies by Fuertes, Velasco, Alvarez and Fernandez[93] agreed with Crnkovic *et al.*[92] on the temperature effect on physical structure but disagreed on the type oxide material that was affected by the changes. Calcium carbonate was reported to be the only oxide affected by temperature and no changes occurred in magnesium carbonate. Murthi, Harrison and Chan[94] proposed that in gas-solid reactions of carbonates with SO_2, magnesia created a diffusion path for the sulfur dioxide, thus acted as a catalyst transferring sulfur-bearing species to the active calcium oxide sites. Chang and Thodos[95] and Thibault, Steward and Ruthven[96] determined the overall rate of conversion of

calcium and magnesium oxide, and agreed with Borgwardt and Harvey[43] in that chemical reaction was the sole limiting factor in the initial stages of reaction. There was no relationship was found between the chemical composition and SO_2 reactivity, and the conversion of calcium and magnesium oxides correlated with the grain model proposed by Georgakis *et al.*[40] Fan and Satja[97] proposed a volume reaction model that accounted for both diffusion and chemical resistance of the heterogeneous reactions, which occurred in sulfation reactions of calcium and magnesium carbonates. The analyses demonstrated a linear relationship between the particle size and the amount of the material converted and the changes in volume were attributed to product loss from the sulfated outer layer of the particles.

Hsia, Pierre, Raghunathan and Fan[98], Hsia, Pierre and Fan[99] and Borgwardt Bruce and Blake[100] studied the ionic diffusion of cations and anions through $CaSO_4$ layer formed, and proposed sulfation mechanisms. Studies[98–99] showed that ionic diffusion from unreacted CaO core, through $CaSO_4$ layer formed occurred in CaO reaction in SO_2/air gas mixtures between 1300°C and 1400°C. The proposed ionic diffusion occurred by mechanisms of outward diffusion of Ca^{2+} ions and oxygen ions through the complex tetrahedral structure lattice of $CaSO_4$ crystal structures. This created vacancy in the tetrahedron, which consequently induced diffusion of oxygen, possibly due to volume changes, the $CaSO_4$ formed at the $CaSO_4$/gas interface[98–99]. The ionic size difference in $CaSO_4$ crystal was an important factor, in which the SO_4^{2-} = 4.5 Å compared to 1.8 Å for Ca^{2+} ions, increased mobility of Ca^{2+} ions through the structure. At the $CaSO_4$/gas interface outward growth of $CaSO_4$ occurred. Borgwardt *et al.*[100] , proposed sulfation mechanism occurring through ionic diffusion of gas species from the $CaSO_4$/gas interface through the $CaSO_4$ layer formed to the CaO/$CaSO_4$ interface to react with the unreacted CaO. The mechanism suggested that the pore structure had a significant effect on the inward material transport process of O_2^{2-} and SO_4^{2-} through the $CaSO_4$ product layer formed. Therefore, the ionic size could not be considered as the prevailing limiting factor affecting the reactions, and sulfation could occur in reactions that are supported by physical factors instead. They indicated that the inward growth mechanism at CaO/$CaSO_4$ interface by inward transport diffusion facilitated by the energy required for distributing and creating free volume when the expanded $CaSO_4$ formed. This was likely to be affected by the distribution of free volume through the through the crystal boundaries of the $CaSO_4$ product formed, where the product detached from the solid creating volume for further diffusion. Sulfation reaction can be described by two reaction mechanisms, the gas diffusion and ionic diffusion.

2.4 The thermodynamics and equilibrium involving sulfur-bearing compounds.

Studies[101−104] have showed that sulfur-bearing gas species are products of all the reactions occurring during smelting and converting processes. The thermodynamics[23–27,105] of the reactions involved in the reaction processes occurring in smelting and converting processes and the interaction of the refractories with the different chemical phases have been reported in literature[13–20]. Philip[102] reported that the chemical potential of the sulfur-bearing gas species was determined by amount of oxygen utilized in the metallurgical processes during service. Gawel and Wycezesany[106] found that the prediction of the formation of a reaction product in gas-solid reactions was inappropriate by comparing the dissociation pressure with the partial pressure of the gas components in reactions that involved sulfur-bearing species. This was due to problems found in reactions when the solid component was exposed to more than one oxidizing agent, taking into consideration the impurities. They suggested that calculating the gas compositions under thermodynamic equilibrium with assumptions that equilibrium was reached through the reactions was the best approximate method used for predicting the formation of the product on the solid.

The equilibrium concentration of the gases can be deduced from the known equilibrium constants. Thermodynamic data of the gases, oxides, sulfates, and other sulfur compounds are readily available, and exists in compilations such as the Thermo-chemical Properties of Inorganic Substances[107], JANAF Tables[108], and the book by Kubaschewski and Alcock[109]. The thermodynamic properties of the gases are of fundamental interest and a number of equilibrium reactions containing gaseous sulfur compounds have been critically re-evaluated and derived by Evans and Wagman[110], Rosenqvist[111], Richardson and Jeffes[112–113], St. Pierre and Chipman[114–115], Dewing and Richardson[116–117], Marchal[118], Kellogg[79] and Wreidt and Darken[91]. The equilibrium calculations were by:

- extraction of the reliable reaction equilibrium as a function of temperature from many independent investigators, or
- the use of thermodynamic constants at 298°K, such as enthalpy, entropy, and heat capacities ($\Delta H°_f$, $\Delta S°_f$, and C_p) as a function of temperature (°C).

Richardson and Jeffes[112–113] and St. Pierre and Chipman[114–115]derived equations for the standard free energy changes for oxides and sulfur species reactions, and these were based on the spectroscopic measurements of the relevant equilibrium reactions. Richardson and Jeffes[113–113]

derived free energy equations from constructed free-energy diagrams using equilibrium and thermal data of gaseous sulfides in terms of oxygen potentials for steelmaking processes. The oxygen potentials for the reactions were derived from the ratios of CO/CO_2 gas pressures at different temperatures, and oxygen potentials were related to the changes in Gibbs' Free Energy ($\Delta G°$). Pure liquid and solid phases under 1atm pressure were used[112]. Free energies and heats of formation for sulfur species such as S, S_2, SO, SO_2, SO_3, COS, CS, CS_2, HS, and H_2S were obtained from ratios of H_2S/H_2 gas pressures[112] and from lime-iron oxide slags systems equilibrated in different sulfur bearing atmospheres[115]. There were differences in the calculated free energy changed for sulfur species by the data provided by Richardson and Jeffes[112] and St. Pierre and Chipman[114–115]. The reactions for sulfur compounds that formed in the sulfur containing gas mixtures are given in Table 2.3. The equilibrium constants for sulfur-bearing gases at different temperatures are presented in Table 2.4.

St. Pierre and Chipman[115] , Turkdogan and Darken[119] and Dewing and Richardson[117] determined the sulfates from different melts under different gases and determined the gases evolved. St. Peirre and Chipman[115] studied the equilibrium between sulfur and sulfates from CaO-FeO slags equilibrated at 1550 C under SO_2-CO_2 gas mixtures. Sulfur was present as a sulfide at oxygen pressures below 3 $x10^{-5}$ atm, while sulfate was found as $CaSO_4$ at high oxygen partial pressures above 3 $x10^{-4}$ atm. The iron oxide and calcium oxide both promoted an increase in sulfate formation, while the SiO_2 and MgO decreased the formation of sulfide in the slags. This was attributed to the bond strength of Si-O, reported to be stronger than Si-S bond. The MgO decreased the concentration of sulfur in slags thereby increasing the activity coefficient of sulfide ion. Dewing and Richardson[116]determined the sulfur and sulfate amounts from equilibrated silver beads in controlled gas mixtures of SO_2, N_2 and S_2, and from calcium silicate melts in SO_2 and O_2 gas mixtures. The investigations agreed with St. Peirre and Chipman[115] on the sulfate contents of the melts but disagreed on the heats of formation ($\Delta H°_0$) of sulfur species, and the differences were attributed to the changes in oxygen pressures in SO_2/CO gas mixtures used by St. Peirre and Chipman[115].

Turkdogan and Darken[119] equilibrated calcium ferrite melts with SO_2 and O_2, air, CO_2 and CO_2-COgas mixtures between 1290° to 1620°C. The studies agreed with St. Peirre and Chipma[115] in that the transition partial pressures from sulfide to sulfate that were determined by the oxygen partial pressures, and CaO promoted $CaSO_4$ formation. The oxygen partial pressures below 10^{-4} atm favored the sulfide reaction and at higher partial pressures sulfate was formed[119]. It was

shown that pyrosulafte (K_2SO_4 to $K_2S_2O_7$) and potassium sulfate (K_2SO_4) were formed at high SO_2 and O_2 partial pressures, and below 1500°C pyrosulfate, K_2SO_4 to $K_2S_2O_7$ was the main phase in the reaction. The change from potassium sulfate to potassium pyrosulafte was gradual when the product of $P_{SO_2} P_{O_2}^{1/2} > 1$. Turkdogan and Grieveson[120] investigated the transfer of oxygen and sulfur ions between ionic melts of Mn-MnS-MnO and Fe-S-O systems under sulfur and oxygen bearing gases. Sulfur was transferred from a low to a high potential through S-O reactions, and occurred when oxygen was transferred from a high to a low chemical potential and vice versa. The counter diffusion of the sulfide and oxide ions was the rate controlling process.

2.4.1 Reaction equilibrium of sulfur-bearing solids

Marchal[118], Dewing and Richardson[117], Kellogg[79] and Wreidt and Darken[91] determined the gases evolved from sulfate compounds ($CaSO_4$ and $MgSO_4$), and free energy equations for the reactions were derived. Thermodynamic data for the various groups of solid phases (CaO, $CaCO_3$, CaS, and $CaSO_4$) were derived[91] for sulfation reactions of calcium carbonates in reaction mechanism given in Table 2.5. In reactions, sulfates suggested formed for the partial pressure of sulfur dioxide above 10^{-3} atm, between 800°C and 1300°C. The equilibrium values for $MgSO_4$ the gases given by Kellogg[79] were determined for decomposition reactions represented by:

$$CaO + SO_2 + \tfrac{1}{2} O_2 = CaSO_4 \qquad (2.17)$$

$$MgO + SO_2 + \tfrac{1}{2} O_2 = MgSO_4 \qquad (2.18)$$

Wreidt and Darken[91] suggested that at different temperatures, various sulfur compounds such as SO_2, SO_3, S_2, SO and S_2O formed. Marier and Dibbs[89] showed that the reaction between gaseous sulfur dioxide (SO_2) and oxygen (O_2) may proceed through different routes, and this was dependent on the reaction temperature, concentration of the gases and reaction time. Therefore, sulfation in reducing compounds could be presented by:

$$CaO + SO_2 = CaS + \tfrac{3}{2} O_2 \qquad (2.19)$$

$$MgO + SO_2 = MgS + \tfrac{3}{2} O_2 \qquad (2.20)$$

Dewing and Richardson[117] used differential thermal analyses method to determine the thermodynamic data of sulfates from the decomposition pressures of $CaSO_4$ and $MgSO_4$ in controlled gas mixtures of SO_2, N_2 and O_2 between 900°C and 1365°C. Differential thermal analyses method determined the changes in thermal effect and was preferred rather than measuring the total static pressure developed, which was satisfactory only at lower temperatures.

Crystallographic changes (α to β) occurred and neither calcium nor magnesium formed stable basic sulfates. The changes occurred at 1210°C for $CaSO_4$, and a eutectic between $CaSO_4$ and CaO was found at 1365°C, above which melting began before decomposition was complete. For $MgSO_4$ the changes occurred at 1010°C. The ΔH_{298} values of -343000 calories and 94800 calories were obtained for $CaSO_4$ and $MgSO_4$, respectively. Richardson and Jeffes[113], and Rosenquvist[111] data were used to determine the free energy equation for $CaSO_4$ from CaS and SO_2 gases.

Kellogg[79] reviewed the equilibrium decomposition of sulfate compounds and determined the thermodynamic data of the total pressure and known equilibrium constant were utilized to determine the decomposition data. Equilibrium gas mixtures SO_2-O_2-SO_3 were used and the. Kellogg[79] data disagreed with Dewing and Richardson[117], and Marchal[118] on the heats of formations for $MgSO_4$, but agreed with Kubaschewski and Alcock's[109]. The ΔH_{298} values of -311050 calories and -343690 calories were obtained for $MgSO_4$ and $CaSO_4$, respectively. Kellog[79] believed that equilibrium for SO_2-O_2-SO_3 reactions was not attained by Dewing and Richardson[117] and an error may have occurred. The failure of SO_2-O_2-SO_3 gas mixture to achieve equilibrium resulted in decomposition at low temperatures. The difference values obtained by Marchal[118] and Dewing and Richardson[117] demonstrated lack of experimental accuracy in Marchals[118] temperature measurements. The standard free energy equations for the sulfates were derived using the σ-function method represented by:

$$\Delta G = a + bT \log T + cT \text{ cal.} \qquad (2.21)$$

Equations for the standard free energy for the reactions derived by Dewing and Richardson[117], Kellogg[79], and Wreidt and Darken[91] are given in Table 2.7.

Table 2.3. Comparison of free energy data

Reaction	**Richardson and Jeffes[113] Free Energy Equation (cal.)**	**St. Peirre and Chipman[115] Free Energy Equation (cal.)**
$2S(g) = S_2(g)$	$\Delta G^\circ_{(298\text{-}2200K)} = 77250 - 29.70T$	$\Delta G^\circ = -86500 + 29.20T$
$S_2(g) + O_2(g) = 2SO(g)$	$\Delta G^\circ_{(298\text{-}2000K)} = -49000 - 1.25T$	$\Delta G^\circ = 2(-18300 - 1.26T)$
$S_2(g) + 2O_2(g) = 2SO_2(g)$	$\Delta G^\circ_{(318\text{-}1800K)} = -173240 + 34.62T$	$\Delta G^\circ = 2(-86200 + 17.26T)$
$SO_2(g) + ½\ O_2(g) = SO_3(g)$	$\Delta G^\circ_{(318\text{-}1800K)} = -45200 + 42.72T$	$\Delta G^\circ = -19800 + 19.76T$
$2SO(g) + O_2(g) = 2SO_2(g)$	—	$\Delta G^\circ = 2(-67900 + 18.50T)$

Table 2.4: Calculated free energy data of sulphur-bearing gases at different temperatures.

Reaction	**Richardson and Jeffes[113]**									
	ΔG°_{973K} (cal.)	K_{973K}	ΔG°_{1073K} (cal.)	K_{1073K}	ΔG°_{1173K} (cal.)	K_{1173K}	ΔG°_{1273K} (cal.)	K_{1273K}	ΔG°_{1623K} (cal.)	K_{1623K}
$2S(g) = S_2(g)$	48351.9	1.385×10^{-11}	45381.9	5.731×10^{-10}	42411.9	1.257×10^{-8}	39441.9	1.694×10^{-7}	29046.9	1.228×10^{-4}
$S_2(g) + O_2(g) = 2SO(g)$	-51432.5	3.551×10^{-11}	-51682.5	3.349×10^{-10}	-51932.5	4.722×10^{-9}	-52182.5	9.06×10^{-8}	-53057.5	1.391×10^{-7}
$S_2(g) + 2O_2(g) = 2SO_2(g)$	-138812.04	2.19×10^{31}	-136092.74	5.182×10^{27}	-132630.74	5.092×10^{24}	-129168.74	1.485×10^{22}	-117051.74	5.743×10^{15}
$SO_2(g) + ½\ O_2(g) = SO_3(g)$	-1816.72	2.559	319.28	0.861	2455.28	0.349	4591.28	0.163	12067.28	0.024

Table 2.5: Free Energy Data for Decomposition of Sulfates

Reaction	**Kellogg[79] Free Energy Equation (cal.)**	**Dewing and Richardson[117] Free Energy Equation (cal.)**	**Wreidt and Darken[91] Free Energy Equation (cal.)**
$CaSO_4 = CaO + SO_2 + ½ O_2$	$\Delta G°_{(1100\text{-}1638\ K)} = 136830 + 41.61T \log T - 206.73T$	$\Delta G°_{(1210\text{-}1365\ C)} = 111000 - 56.62T$	$\Delta G°_{(1180\text{-}1373\ C)} = 110320 - 56.8T$
$MgSO_4 = MgO + SO_2 + ½ O_2$	$\Delta G°_{(1000\text{-}1428\ K)} = +78560 + 16.58T \log T - 100.69T$	$\Delta G°_{(900\text{-}1150\ C)} = 87180 - 60.2T$	–
$SO_3 = SO_2 + ½ O_2$	$\Delta G° = 25010 + 5.562T \log T - 40.52T$	–	–

Table 2.6: Comparison of Free Energy Data for Formation of Sulfates

Reaction	**Dewing and Richardson[117]**					
	$\Delta G°_{1173K}$ (cal.)	K_{1173K}	$\Delta G°_{1273K}$ (cal.)	K_{1273K}	$\Delta G°_{1623K}$ (cal.)	K_{1623K}
$CaO + SO_2 + ½ O_2 = CaSO_4$	-	-	-38922.74	4.798×10^6	-19105.74	373.487
$MgO + SO_2 + ½ O_2 = MgSO_4$	-16565.4	1218.593	-10545.4	64.583	-	-

Table 2.7: Comparison of Free Energy Data for Formation of Sulfates

Reaction	**Wreidt and Darken[91]**									
	$\Delta G°_{973K}$ (cal.)	K_{973K}	$\Delta G°_{1073K}$ (cal.)	K_{1073K}	$\Delta G°_{1173K}$ (cal.)	K_{1173K}	$\Delta G°_{1273K}$ (cal.)	K_{1273K}	$\Delta G°_{1623K}$ (cal.)	K_{1623K}
$CaO + SO_2 + ½ O_2 = CaSO_4$	-	-	-	-	-	-	-	-	-18133.6	276.308
Reaction	**Kellogg[79]**									
	$\Delta G°_{973K}$ (cal.)	K_{973K}	$\Delta G°_{1073K}$ (cal.)	K_{1073K}	$\Delta G°_{1173K}$ (cal.)	K_{1173K}	$\Delta G°_{1273K}$ (cal.)	K_{1273K}	$\Delta G°_{1623K}$ (cal.)	K_{1623K}
$CaO + SO_2 + ½ O_2 = CaSO_4$	-	-	-50317.502	1.766×10^{10}	-44143.634	1.672×10^8	-38124.011	3.4993×10^6	-18109.747	247.272
$MgO + SO_2 + ½ O_2 = MgSO_4$	-28793.8823	2.926540×10^6	-24435.095	94635.96	-20143.38	5654.28	-15913.194	538.889	-	-
$SO_2 + ½ O_2 = SO_3$	-1755.187	2.478	381.262	0.836	2495.166	0.343	4588.45	0.163	11774.01	0.026

CHAPTER 3
EXPERIMENTAL PROCEDURES

3.1 Overview

The purpose of the present study was to demonstrate the effect of sulfur-bearing gases on physical characteristics of basic refractories used as linings of furnaces in smelting and converting processes in non-ferrous industries. The aim of the research was to determine those principal physical characteristic factors of the refractories relating to sulfur absorption that in turn lead to mineralogical and microstructural changes and deterioration of the refractory. Different methods used to determine the effect of the factors on the progress of sulfation reaction as well as on the characteristic of the product. Experimental procedures involved generating gas composition relevant to industrial converting processes for Platinum Group Metals (PGM) processes. The refractories chosen were three magnesite-chrome refractories, two chrome-magnesite refractories and a magnesite. The refractories exposed to sulfur-bearing gases and their reactivity with sulfur species was determined.

The diffusion phenomena occurring during heating of refractories in O_2, SO_2-N_2, SO_2-O_2, and SO_2 gas mixtures was analysed. The temperature related to changes in physical characteristics, which lead to crystal distribution and pore distribution in the refractories. The experimental set-up consisted of a vertical tube furnace, a quartz reactor tube, a bed of silica wool and alumina bubbles used for separation and to place the refractories, rubber cone stoppers with openings, a Swagelok® vinyl in-let tube, and flow meters. The separation of the refractories during reactions achieved with use of silica wool and alumina bubbles, which allowed conversion of each refractory related to the changes due to physical characteristics.

For each experimental run, the furnace was set up to a predetermined temperature profile and a constant temperature hot-zone. The gas mixture was released into the reactor tube through the bottom entrance through a silica bed and alumina bubbles containing refractories and into the atmosphere. After each experiment, the tube was removed from the furnace and the refractories were cooled to room temperature, weighed, and analyzed for phase composition and microstructure using Scanning Electron Microscopy (SEM). From the analyses, the reaction mechanisms were proposed for the gas-refractory interactions in sulfur-bearing gases.

The Scanning Electron Microscopy (SEM), X-ray diffraction and the weighing methods were chosen to examine the occurring phenomena in sulfation of basic refractories. The Scanning Electron Microscopy (SEM) method was used for characterization of the microstructure and the physical characteristics. The X-ray diffraction method was used for phase composition analysis of the reaction products. Weighing method was used to measure the reaction progress and was determined from the change in weight.

3.2 Materials

The refractory materials used were selected from a wide range of chrome-magnesite, magnesite-chrome, and magnesia refractories, based on the manufacturing route and the chemical composition. The specified application area of the refractory according to the specifications provided in manufacture's manual was taken into consideration. All the selected basic refractories are used for the lining of the converter furnaces by the PGM industries. The magnesia chrome and chrome magnesite refractories were selected from the direct bonded refractories, the reconstituted fused grain refractories, and 100% fused grain chromite-enriched reconstituted refractories. The properties and chemical composition of the refractories are given in Table 3.1.

Table 3.1. Chemical compositions and properties of refractory materials

Refractory	CaO/SiO_2 ratio	Composition (wt%)							Bulk Density	Apparent
		Al_2O_3	CaO	Cr_2O_3	Fe_2O_3	MgO	SiO_2	TiO2	(kg/m^3)	Porosity (%)
Magnesite-Chrome D60/100 MC1	0.6	7.64	1.19	20.3	8.97	51.9	2.03	0.18	3225	16
Magnesite-Chrome brick 1 MC2	0.6	3.45	0.81	14.7	4.57	62.5	1.43		3120	15
Magnesite-Chrome brick 2 MC3	0.7	5.27	0.88	16.6	16.6	63.8	1.3	0.052	3300	12
Chrome-Magnesite A CM1	0.3	8.65	0.94	22.5	9.49	47.3	3.01	0.22	3180	17
Chrome-Magnesite D50-C5 CM2	0.7	5.96	1.22	19.2	6.65	49.5	1.66	0.14	3250	16.5
Magnesite M	3.6	0.14	1.88	0.31	0.21	92.1	0.52	<0.008	2920	17

The magnesite refractory (M) was made up of naturally occurring high quality magnesia, and used for lining electric arc furnace walls and slag line. The magnesite–chrome refractories selected composed of high purity fused mixtures of magnesia and chrome ores. The magnesite–

chrome D60/100 (MC1) and magnesite–chrome brick 1 (MC2) refractories comprised re-constituted fused grain refractory material. The magnesite–chrome brick 2 (MC3) composed of 100% fused magnesia-chrome co-clinker. The chrome-magnesite D50-C5 (CM2) brick composed of fused chrome-enriched minerals, and chrome-magnesite A (CM1) was a direct bonded brick.

Vereeniging Refractories of South Africa supplied the refractories used in the study. The refractory brick pellets supplied had a total weight of 17-19 kg each and 230 x 114 x 76 mm was the dimension of each brick. The bulk chemical analysis of the six selected commercial refractories was determined using an Inductive Coupled Plasma atomic emission spectroscopy (ICP-AES), provided by the Analytical Services Division at Mintek. The basic oxides were supplied as laboratory reagent powders, their purity and sources are given in Table 3.2. All gases used were commercially supplied by Afrox Pty. Ltd. as compressed gases in cylinders, and their purity is given in Table 3.3.

Table 3.2. Materials.

Chemical	Purity	Source
Magnesium Oxide	95% MgO	Chemical Enterprises Pty. Ltd.
Chrome Oxide	97% Cr_2O_3	LABCHEM Pty. Ltd

Table 3.3. Gas Specification as provided by the manufacturer.

	SO_2 Gas	**N_2 Gas**		**O_2 Gas**	
Minimum Purity	**99.9%**	**99.5%**		**99.5%**	
Maximum Impurities %		**Maximum Impurities %**		**Maximum Impurities %**	
Oil	100ppm (m/m)	O_2	4500 vpm	N_2	200 vpm
Residue on evaporation	100ppm (m/m)	H_2O	50 vpm	H_2O	Not specified
Sulfuric acid	100ppm (m/m)	CO_2	Not specified	CO_2	Not specified
Arsenic	3ppm (m/m)	CO	Not specified	CO	Not specified
Lead	10ppm (m/m)	HC	Not specified	HC (methane)	30
Zinc	25ppm (m/m)	–	–	Ar	0.3%
Copper and Zinc	50ppm (m/m)	–	–	H_2	Not specified
Selenium	10ppm (m/m)	–	–	-	-

3.2.1 Sample Preparation

The size of the refractories used in the experimental investigation was reduced by cutting the 230 x 114 x 76 mm pellets into rectangular pieces having dimensions of 10x10x15mm (h x b x l). The low speed Accutom cutting equipment from Struers, Germany (at a speed of 7 rpm) was used to cut the refractories and acetone was used as a lubricant. The refractories were dried for 1hour in an oven at 120°C to allow evaporation of acetone. The small pellets were weighed after cooling to room temperature. The commercial powdered oxide materials used were weighed and pressed into pellets of 20 mm in diameter and 10 mm in height under 20MPa pressure. The powdered refractory materials of magnesite and chrome- magnesite were pressed into pellets of 20 mm in diameter and 10 mm in height under the same pressure. The process employed for pressed pellets used a uniaxially pressing method that uses a steel die at 20MPa with a Hydraulic Power Unit. The mass of the refractories reacted ranged between 14g to 18g, while that of the oxides was in a range of 3g-4g. The mass of the samples was recorded before and after they were reacted each experimental investigation.

3.3 Apparatus

The apparatus consisted of vertical tube furnaces, a quartz reactor tube, a bed of silica wool and alumina bubbles, a thermocouple, a temperature controller, a Swagelok® vinyl inlet tube, a cone rubber stopper with opening and flow meters. The apparatus set-up used is shown in Figure 3.1. The quartz reactor tubes were 100 cm long with 3.2cm diameter in dimensions. The reactor tube was inserted into the vertical tube furnace with the inlet tube and the cone rubber stopper connected at the bottom end. A bed of silica wool and alternating layers of alumina bubbles separating the refractory samples were placed inside the quartz tube and positioned with the hot-zone. A thermocouple used to monitor the temperature inside the tube was positioned within the hot-zone from the top end of the quartz tube. The flow meters were used to monitor the gas flow-rates through the inlet tube.

3.4 Gas Preparation and Flow Regulation

Fischer & Porter Variable-Area (VA) type flow meters were used to regulate the flow-rates of all the gases used in the experiments. These flow meters were controlled on the principle of pressure transfer by sensing the change in pressure along the gas tube line where the change in pressure was directly proportional to the gas flow. The flow-rates for each flow meter setting

were calibrated against air, as given in the calibration charts in Fischer & Porter handbook. However, when calibrating for heavier gases the flow-rate of the gas was calibrated using Equation 3.1:

$$Q_2 = \frac{Q_1 \sqrt{\rho_2}}{\sqrt{\rho_1}} \qquad (3.1)$$

where Q_2 is the volumetric flowrate of the heavier gas, suggested to be SO_2 in this case, Q_1 = volumetric flowrate of air (as calibrated in Fischer and Porter handbook) and ρ_x = density of the gas. The soap bubble solution burette meter method was employed for gas calibrations and measuring of flow-rates. Gas flow rates were measured by timing a soap bubble rising through the burette and a calibration chart was recorded for each gas before mixing. The required flow rates were monitored using both the calibration charts and were determined with the soap bubble flow meter. Gas flow-rate for the gas mixture through the delivery gas line was monitored using the soap bubble flow meter, where the bottom of a 50cm burette was fitted with the 'U' tube filled with bubble soap solution water. The in-let delivery gas tubes from the gas mixtures was connected to the in-let side of the burette meter, and the time it took for the bubble to flow out in specified times. The gas flow chart is shown schematically in Figure 3.2. The moisture from the sulphur dioxide gas was removed by passing it through a cylindrical vessel containing a drying agent mixture of phosphorus pentoxide and dry silica gel.

3.4.1 Mixing of Gases

In experiments using O_2, the gas was led into the quartz tube inside the furnace through the inlet tube. Before entering the quartz tube the gas flow-rates were set at the flow metres using calibration charts, and were accurately determined and monitored using the soap bubble flow meter. In O_2 gas system the gas flow-rate at the flow meter was set to 100mL/min (for O_2). The gas flow rate for the pure gas was 99.5mL/min. In a system having a total pressure of 1atm, this corresponds to equilibrium oxygen partial pressure of 0.995 atm. when equilibrium is achieved. The gas flowed from the bottom end of the reactor tube through the porous alumina bubbles and silica wool packing the refractory samples inside the reactor tube. The porous alumina bubbles and silica wool ensured easy exit of the gas through the top of the reactor tube. For experiments using SO_2 gas, pure sulfur dioxide gas was led into the quartz tube through the inlet tube from the gas mixer chamber. Gas flow-rates were calculated using Equation 3.1 and accurately determined and monitored using the soap bubble flow meter before entering the quartz tube. The gas flow-rate entering the reactor tube was set to 40mL/min. In a system having a total pressure

of 1atm, this corresponds to equilibrium SO_2 partial pressure of 0.999 atm when equilibrium is achieved. The gas flowed as described above for O_2 system.

For experiments using SO_2 and O_2 gas mixtures, the two gases were led into the gas mixer in which the delivery inlet tube into the quartz reactor was connected. The SO_2 gas flow-rate was calculated using Equation 3.1 and SO_2 was fed into the gas mixing chamber at a rate of 20mL/min was set. The O_2 was fed to the mixing chamber at the flow rate of 80 mL/min, giving a total gas volume of 100mL/min in the gas mixer, with the SO_2-O_2 volume ratio of 0.25. Before entering the quartz tube, gas flow-rates led through each flow metre were determined using calibration charts and monitored using the soap bubble flow meter. The total flow rate entering the reactor through the delivery inlet tube was kept constant at 100mL/min, and the flow-rate of the gas mixture due to mixing was set as 19.98 mL/min of SO_2 and 79.6 mL/min oxygen. In a system having a total pressure of 1atm when equilibrium is achieved, this corresponded to equilibrium oxygen and sulfur dioxide partial pressures of 0.796 atm and 0.1998atm, respectively.

In experiments using SO_2 and N_2 gas, a similar set-up was used. The flow-rates of SO_2 were kept constant at 20mL/min and nitrogen flow-rate was set to 80mL/min, giving a total gas mixture flow-rate of 100mL/min. The total gas mixture flow-rate was 19.98mL/min of SO_2 and 79.6mL/min nitrogen. The impurity content of oxygen and water contained in nitrogen gas presented in Table 3.3 gave $3.6x10^{-2}$mL/min of oxygen and $4x10^{-3}$mL/min of water. At total pressure of 1atm when system attains equilibrium, this corresponded to equilibrium pressures of 0.1998 atm., 0.796 atm, 0.003 6atm. and 0.00004 atm. for SO_2, N_2, O_2 and H_2O vapour gas mixtures, respectively.

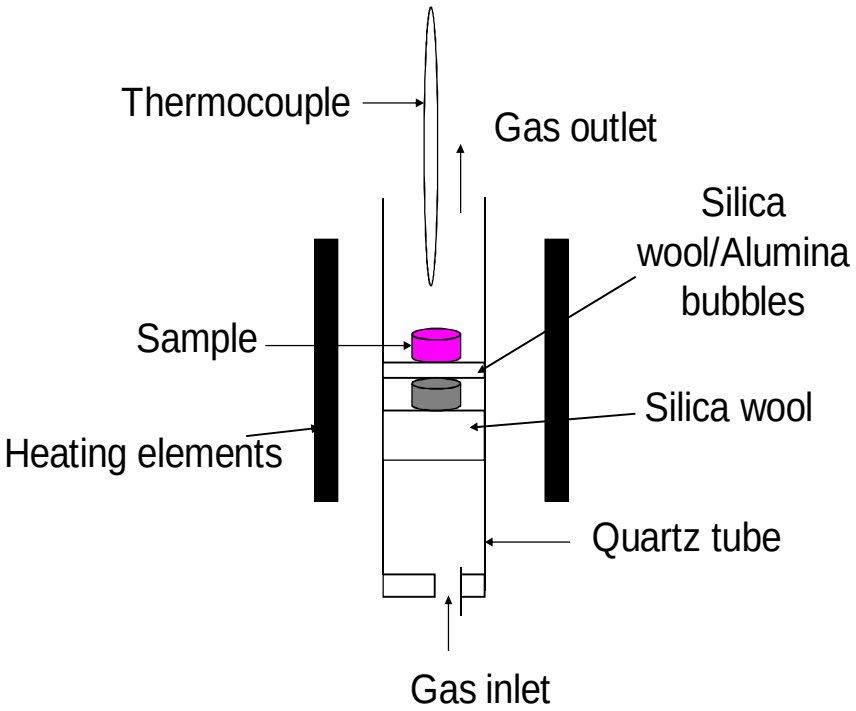




Figure 3.1. Schematic diagram of the apparatus and photograph of the furnace.

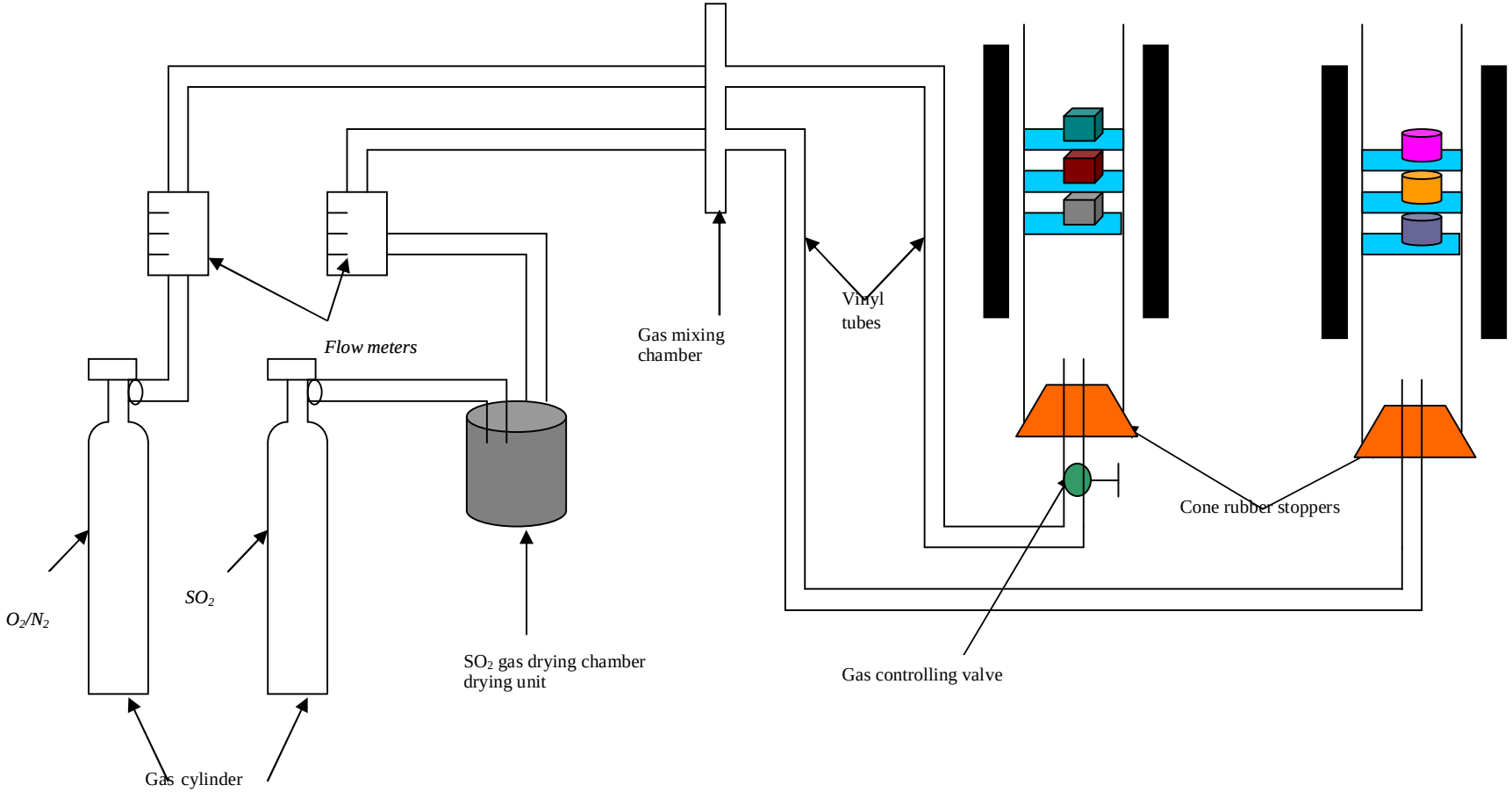


Figure 3.2. Schematic gas flow chart of the gas systems and furnace

.

3.4.1.1 Procedure for O_2 Experiments

For experiments in O_2, the apparatus and set-up was as described above. The refractories were allowed to reach thermal equilibrium monitored by using a thermocouple inside the reactor and temperature controller for the furnace temperatures. When the required temperatures are achieved within the hot-zone, the oxygen gas entered the quartz reactor tube through the one channel inlet tube fitted into stainless steel pipe that was connected to a cone rubber stopper at the bottom of the quartz reactor. The oxygen gas was allowed to come into chemical and thermal equilibrium as it passes through the refractory samples positioned in the constant temperature hot-zone of the furnace. The reaction time of between the oxygen gas and refractories was seven days. The oxygen gas was allowed to exit through the top of the reactor into the gas extractor before releasing to the atmosphere.

3.4.1.2 Procedure for SO_2-O_2 Experiments

This set of experiments was performed at different temperatures and reaction times. In SO_2-O_2 experiments, the apparatus was the same as described above except that two vertical furnaces were used for reactions at different temperatures and a gas flow supplying both furnaces was constructed. This set-up was achieved by fitting the gas mixer chamber with two-way channels of Swagelok® vinyl inlet tubes that lead to the reactor tubes inside the vertical furnaces as shown schematically in Figure 3.2. Gas flow-rates entering the inlet tubes were kept constant at 100mL/min gas mixture by doubling the of the total volume gas mixture entering the gas mixer chamber. Therefore, for SO_2, the gas flow-rate was set to 40mL/min and oxygen was set at 160mL/min resulting in 200mL/min in volume total gas mixture entering the gas mixer chamber.

On exiting the gas mixer, chamber two channels connecting two vinyl inlet tubes that lead to the two reactor tubes inside the horizontal were constructed. A gas regulating system was incorporated into the inlet tubes and flow-rates exiting the two inlet tubes and entering the reactor tubes were determined. This set-up was accomplished by connecting the cone rubber stopper to a stainless steel pipe fitted with a gas-regulating valve. In this way, the gas flowrates entering the reactor tubes were regulated such that 100mL/min entered the reactor tubes. The gas mixture came into chemical and thermal equilibrium as they pass through the refractory samples positioned in the constant temperature hot-zone of the furnace.

3.4.1.3 Procedure for SO_2-N_2 Experiments

For SO_2-N_2 experiments, the apparatus was the same as described above except that nitrogen was used instead of oxygen and the experiments were conducted at different temperatures. The reactors were supplied with gas flow-rate of 100mL/min gas mixture of SO_2 and N_2. The gas flow-rate of SO_2 at the flow meter was set to 40mL/min while that of N_2 was set to 160mL/min, and the flow-rates of the total gas mixture were regulated to achieve 100mL/min mixture entering each reactor. The reactor tubes and refractory samples were allowed to reach thermal equilibrium in the constant temperature hot-zone inside the furnace before the gases were introduced.

3.4.1.4 Procedure for SO_2 Experiments

In experiments using pure SO_2 gas, the apparatus was as described in SO_2-O_2 experiments. Gas regulation ensured that 40mL/min entered each rector tube. The SO_2 gas flowrate was set to 80mL/min in the gas flow meter and total gas mixture entering the gas mixer chamber was 80mL/min. On exiting the gas mixer chamber through two separated tubes the gas was regulated to achieve 40mL/min of the gas entering each reactor.

3.5 Furnaces, Reactors and Temperatures

All the experiments were carried out in vertical tube furnaces, fitted with silicon carbide heating elements as shown in Figure 3.1. One furnace tube was approximately 68 cm long with an inside diameter of 45 mm and outside diameter of 50mm**.** The other furnace tube was 75 cm long with an inside diameter of 40 mm and outside diameter of 44 mm. The temperature limit of both furnaces when calibrated was 1850°C. On each furnace, the temperature was controlled by the second thermocouple inserted close to the heating elements and connected to the controller. The temperature profiles of the furnaces were calibrated and the controller set temperatures that were required to give the desired temperature for the investigations were established. The experiments were carried out in constant temperature hot-zones at 700°, 800°, 900°, 1000° and 1350°C.

Temperatures were measured before each experimental run and two thermocouples for high and low temperatures were used. At high temperatures, the temperature profiles were measured with a B-type thermocouple consisting of 10% Rhodium and 90% platinum and 30% Rhodium and

70% platinum wires. At low temperatures, the K-type thermocouple was used for temperatures up to 1000°C. The supplier verified the uncertainty within ±5°C. Temperature readings were taken after every five minutes from each position. The temperature profiles at the hot zone for all the reactions were constant within ±5°C over a length of 40mm to 50mm inside the furnace.

The experiments were conducted in quartz tube reactors filled with removable bed of alternating porous silica wool and alumina bubbles separating the refractories. The quartz reactor tubes were 1000mm long with outside diameter of 29 mm and outside diameter of 33 mm. These materials provided mechanical support and served as a reaction bed for the specimens. However, due the crystallographic transition that occur with silica at different temperatures, the silica wool was used at temperatures, which did not change the physical structure.

3.6 Experimental Procedures

3.6.1 O_2 Experiments

The oxidation experiments carried out at 700° and 1350°C at oxygen gas flowrate of 99.5mL/min having equilibrium partial pressures of 0.995atm. The refractories reacted in O_2 were treated as blank material from which any microstructural changes and effects of temperature or that of sulfurous gases could be observed and determined. The different refractories were exposed in the oxidizing atmosphere for two weeks, and after the reactor was taken out of furnace, refractories removed and cooled to room temperature. The changes in molecular weight before and after the reaction were recorded by weighing the refractories.

3.6.2 SO_2-O_2 Experiments

The sulfation experiments at 700°, 800°, 1000° and 1350°C, were carried out in a similar way as already described. The composition of the gas mixtures in the investigation were designed such that they reflect the composition of the gases produced from the converting processes. The SO_2-O_2 gas mixture had gas partial pressures of 0.1998atm and 0.796atm for SO_2 and O_2 gases. The microstructure was examined for all the refractories exposed at temperatures of 700° and 1350°C for a period of two weeks. The kinetic measurements to determine the amount converted to sulfate were performed for temperatures between 700° and 1000°C for all the refractories. Changes in weight related to the amount of conversion to sulfate were related to progress of reaction also and these were determined by weighing the samples. These changes in molecular

weight and sulfate absorption in refractories were determined at 700°, 800°, 1000°, and 1350°C for all refractories exposed for period of seven days. The refractories were also taken out of the furnace after 14, 28, 42, 56, 70, and 84hrs and weighed after cooling to room temperature. Weighing was done with high precision, especially for low weight changes in samples. At 1200°C only two refractories were studied, the chrome-magnesite A (CM1) and magnesite-chrome D60/100 (MC1). The conversion ratio was calculated for key component MgO.

3.6.3 SO_2-N_2 Experiments

The refractories that gave high conversion rates in SO_2-O_2 experiments with sulfurous gases were selected for the experiments. The refractories selected for the reactions were chrome-magnesite D50-C5 (CM2), magnesite-chrome brick 1(MC2), magnesite-chrome brick 2(MC3) and for comparison magnesite (M). After the furnace was heated to the required constant temperature hot-zone, a gas mixture of SO_2-N_2 with gas partial pressures of 0.1998atm and 0.796atm for SO_2 and N_2 gases was passed through the refractories. Changes in molecular weight and sulfate absorption were determined for different temperatures, while mineralogy and microstructure were examined in all the refractories exposed at 1350°C for two weeks. Reaction profiles were established at 800° and 1000°C.

3.6.4 SO_2 Experiments

The experiments by suing pure sulfur dioxide were carried out at 800°°C and 1000°C. As in the other experiments, the samples were allowed to reach thermal equilibrium after being inserted into the furnace. SO_2 was at a partial pressure of 0.3996 atm. After 14, 28, 42, 56, and 84 hours the samples taken out of the furnace and removed from the reactor to cool at room temperature. The amount of the refractory converted was determined from the changes in weight of the samples.

3.7 Metallographic Preparation

The samples were prepared for microscopic evaluation in a Scanning Electron microscopy (SEM) by coating them with carbon to avoid charging and no etching used. The mounted cross sections were polished on SiC paper. Scanning Electron microscopy (SEM) method was used for investigation of microstructural changes. The X-ray diffraction method for determining

phase composition of reaction products was employed. The microstructure resulting from phase changes to the development of secondary sulfate phases were studied.

3.8 Scanning Electron Microscopy

Back-scattered electron imaging (BSE) and Energy Dispersive X-ray spectrometer (EDX) with Scanning Electron Microscope (SEM) were the techniques used for characterization of the microstructures contained in the reacted samples. The morphology and texture of the refractories and the degree of reaction of the refractories to sulfation were characterized using the techniques. The mechanisms responsible for refractory sulfation were discussed on the bases of the SEM-EDX analyses in which physical characteristics such as voids, porosity, particle size, cracks and phase mineralogy determined the phenomenological effects of sulfation. In other cases, Energy Dispersive X-ray analysis was used to examine the reaction mechanisms. Back-scattered electron imaging was a valuable technique used to show textural features of the different phases by contrasting image reflecting the average atomic number of the phase, for example, metals tend to be brighter while oxides give darker images. When two materials react together, the resulting product can form by two categories and that was by replacement and/or co-precipitation and this technique revealed the textural features resulting from either of the two reaction mechanisms. In this investigation, textural features of the virgin refractories were compared to the features of the reacted material attained during reactions of the refractories with the gases. The Energy Dispersive X-ray spectrometer was a quantitative analysis that showed the relative abundance of the different elements making up the different phases or compounds in the material.

3.9 X-Ray Diffraction

The identification and characterization of the minerals and crystalline phases of the refractories was carried out by X-ray powder diffraction technique using nickel-filtered Cu K_α radiation with a scanning speed of 2sec/step within step size = 0.02° over 2 hours, carried out on a Siemens D500 diffractometor equipped with an atomic emission technique. The X-ray diffraction patterns were obtained within the range of 2θ= 5-80°. This study was conducted on refractory material before and after the reaction to observe any changes on the different phases existing before and after the reaction. XRD was conducted as means of obtaining additional information

on the mineralogy of the refractory by determining the proportion of the different phases present in each refractory.

3.10 Methods used in Determination of Reaction Products

3.10.1 Conversion Method

For all the reacted refractory material, the percentage fraction converted obtained, was calculated for MgO component converted to sulfate using molecular fractions as

$$X = \frac{\Delta m M_{MgO}}{m_0 (W_{MgO} M_{MgSO_4} + M_{MgO} (W_b - 1))} \qquad (3.2)$$

where Δm is the change in mass of the sample, also taken as added mass after reaction, M_{MgO} is the molar mass of MgO, m_0 is the initial mass of the sample. M_{MgSO4} is the molar mass of $MgSO_4$ calculated for 100% conversion of MgO in the refractory, W_{MgO} is the mass fraction of the magnesium oxide determined in the refractories, W_b is the mass fraction of the other components contained in the refractory. In refractories, the reactivity of the CaO is dependent mainly gas atmospheres and its diffusional release by refractory components. The pore volume, cracks, and voids play an important role in permeability of the gas into the refractory structure. The total weight of the refractory reacted taken into account the percentage weight of different minerals existing in the refractory was determined by bulk analysis.

3.10.2 Product Determining Methods

The refractory samples reacted at 700°C in SO_2-O_2 experiments for two weeks described in Sections 3.6.2 were investigated for the total sulfur added by the reactions. The analysis of total sulfur was conducted by weighing a 1g portion of the sample residue, homogeneously crushed, using Leco IR232 analyser technique. The total sulfur represented the sum of the sulfur ignited plus the elemental sulfur contained in the sample. The refractories reacted at 700°C, 800°C, 1000°C and 1350°C in SO_2-O_2 and SO_2-N_2 gas mixtures for seven days were investigated for sulfate content (SO_4^{2-}). For determination of sulfate precipitate gravimetric analysis method was employed, where $BaCO_3$ was used to quantitatively precipitate out sulfate as $BaSO_4$ as shown in equation (3.5). This method relies on chemical precipitation of the sulfate analyte and the results obtained represent the final determination of weight as a means of quantifying an analyte.

$$Ba^{+2} + SO_4^{-2} = BaSO_4 \qquad (3.3)$$

A thermochemical software and database program, Fact Sage[121–122], was used as part of the experimental procedures to establish the predominance area diagrams for magnesium, sulfur and oxygen, and calcium, sulfur and oxygen components systems. The Predom module[122] software generates predominance area diagrams that have phase boundaries for single or multicomponent systems, and utilizes the Gibbs free energy principle of the related stable compounds. The predominance area diagrams developed were based on the Mg-S-O components systems showed in Liouw *et al.*[22] studies. Kellog[79], and Richardson and Jeffes[113] thermodynamic data were used to generate predominance area diagrams that illustrated the phase boundaries in magnesium, or calcium, sulfur dioxide and oxygen reactions, at varying temperatures and varying partial pressures of sulfur dioxide and oxygen. In their[22] studies, the temperatures varied from 700°C to 1500°C, and the partial pressures ranged from 10^{-10} atm to 10^{10}atm, for $\log P_{SO_2}$ (atm) and $\log P_{O_2}$ (atm). In the present study, the software was allowed to generate predominance area diagrams that show the phase boundaries for both Mg-S-O and Ca-S-O components systems between 700°C to 1350°C, at partial pressures ranging from 10^{-10} atm to 10^{10}atm for $\log P_{SO_2}$ (atm), and 10^{-10} to 10^{5} for $\log P_{O_2}$ (atm). The generated predominance area diagrams were used to predict the phases present in the reaction compounds of MgO and CaO, suggested to being reactive in refractories, when reacted in SO_2-O_2 and SO_2-N_2 gas mixtures.

CHAPTER 4
RESULTS

4.1 Microstructural and physical characteristics of basic Refractories

Figure 4.1 presents the microstructure of the original (as-delivered) magnesite refractory. The microstructure showed large magnesia grains held together by a mass of magnesia aggregate. Between the large magnesia grains, small magnesia aggregates formed a refractory matrix. The magnesia aggregates formed an open periclase structure. The large grains in Figure 4.1b showed relatively fine crystalline magnesia grains connected to each other by an intermediate silicate phase occurring along the grain boundaries. The grains showed a marked variation in magnesia crystalline size, resulting in roughened grain texture. The grains were orientated such that subhedral and small dihedral angles related to the wetting behaviour of silicate matrix obtained were between the magnesia grains. These are the typical structures resulting, as the components were moving towards minimum surface energy for periclase grains and silicate composition to attain equilibrium particularly in relatively impure magnesite[70]. The EDX (Energy Dispersive X-Ray) analyses of the intermediate phases between the magnesia crystals showed tricalcium silicate phase the main silicate matrix between the grains with CaO and SiO_2. Direct contacts were seen occasionally between the magnesia-magnesia grains, while closed pores were observed mostly at the grain boundaries.

The chromite phases in Figures 4.2 to 4.4, resulted in the primary chromite (C1) which was the remnant-unchanged raw material, and three types of secondary chromites. The first types of secondary chromites were the coarse chromite intragranular precipitates found within the magnesia grains (C2). The second types were the continuous chromite precipitates found along the magnesia grain boundaries and formed by intergranular precipitation (C4). These types of secondary chromites possibly precipitated out of magnesia or re-crystallized from spinel-rich liquid upon cooling[2]. The third types occurred along the magnesia grain boundaries as the blocky chromite precipitates, which often extended to the adjacent silicates resulting in angular crystals (C3). The continuous magnesia matrix formed between the chromite-rich magnesia spinels with no precipitation has been reported form through volume diffusion, where the chromite diffused into the magnesia grains resulting in grain growth[4,7,72]. The continuous nature

of the matrix observed suggested that chromite diffused into the magnesia matrix and precipitated out, during cooling, as the coarse and blocky chromite precipitates.

Figure 4.2 presents the microstructure of the original (as-delivered) magnesite-chrome brick 1 refractory. The refractory structure showed a mass of magnesia aggregates, small chromites, and magnesia grains. The most notable feature of this refractory was the highly porous structure and secondary spinel precipitants of iron oxide and secondary chromites within the magnesia grains. The secondary chromites varied in size and occurred as fine precipitates in other grains and being blocky and relatively large in other grains. Continuous chromite precipitates were occasionally observed within magnesia grains as intragranular precipitates. The center of some magnesia grains (top left 'P') were mostly contained iron oxide, showing even diffusion of iron oxide and chromic oxide from the chromite grains to the magnesia grains. The open pore structure indicated incomplete diffusion processes, which suggested that, at firing temperatures, the oxidation of chromite grains and diffusion of sesquioxides possibly did not achieve the elimination of the open pores.

Figure 4.3 presents the microstructure of the original (as-delivered) chrome-magnesite. The chrome-magnesite type refractories consisted of periclase (MgO) that was developed together with precipitants of iron oxide, primary and secondary chromite spinels, calcite-magnesia-silicates and magnesia-silicates (forsterite and monticellite). The microstructure of the chrome-magnesite A type refractory was characterized by direct-bonded structures between periclase, and between periclase and chromite (primary and secondary) phases. Direct bonding structure was described as the direct attachment between phases without any intermediate silicate phase forming connection. The distinct phase characteristics in micrograph (a) are the primary and secondary chromite spinels distinguished with respect to their mechanism of formation and relative diffusivity concentrations. The primary chromite ('C1' in Fig.4.1a) had an irregularly-shaped structure around the edge of the grains. The first types of the secondary spinels are the intragranular chromites ('C2' in Fig.4.1a) that formed on cooling during firing and arise from precipitation on periclase grains and form within the grains. The second types of secondary spinels are the intergranular chromites ('C3' and 'C4' in Fig.4.1a) that are formed by intergranular precipitation of chromite from silicate liquid upon cooling on completion of firing[1]. The intergranular chromites occurred between the magnesia spinels as blocky chromite structures having angular shapes and continuous structures that were elongated. The silicate

matrix (‘S in Fig.4.1a) observed was associated with the primary chromites between magnesia and chromite grains and along the edge of the chromites, having an angular structure close to magnesia. The microstructure showed isolated pores and open pores, which were the black areas. Small chromite grains were present at the periclase grain boundaries

In Figure 4.3b, chrome-magnesite D50-C5 refractory resulted in porous structure and no evidence of direct bonding between the grains. The microstructure showed smaller magnesia aggregates, large coarse chromite grains, and pores. The variously sized periclase aggregates were compacted and distributed unevenly. There was no evidence of magnesia spinels, as precipitants were not observed within the grains. However, fine solid solution phases between iron oxide, chromite, and magnesia phases were observed, and precipitants were observed mostly within the magnesia grains. The magnesia grains interiors (‘P’ in Fig.4.3b) appeared darker than the edge of the grains possible due to the suggested differential diffusion of iron oxide and chromic oxide into the edge of the grains[5,56]. The surface texture of large chromite grains (‘C1’ in Fig.4.3b) appeared to be discontinuous with the pockets of dark magnesia spinels (‘MA’ in Fig.4.3b) phases occurring within and at the edges of the discontinuous chromite. From the observation, these possibly formed because of diffusion of sesquioxides from the chromite spinel[5]. The open pores attributed to the underdeveloped spinel phases, resulting during cooling, from partial precipitation of newly formed sesquioxides observed around the magnesia grains. Some pores formed continuous gaps around the structures, while others appeared to be isolated within the chromite spinel grains.

Figure 4.4 present the microstructure of the original (as-delivered) magnesite-chrome refractories. The microstructure of periclase (MgO) was developed together with solid solutions of iron oxide, primary and secondary chromite spinels, and magnesia-silicate (forsterite) compounds. In Figure 4.4a MC1 the secondary spinels resulted in a large number of blocky intergranular precipitates (C3) and no continuous precipitates (C4), indicating that during cooling, precipitation of chromite might have resulted from the spinel-rich liquid, which then formed small grains. The intragranular chromite spinels (‘C2’ in Fig. 4.4a) formed by precipitation within the periclase grains was the dominant direct bonded structure in the refractory. The chromite precipitates formed chromite-rich clusters of magnesia spinels surrounded by magnesia matrix. The intergranular the blocky chromites within the magnesia matrix (‘C3’ in Fig. 4.4a) had angular crystallographic edges and surrounded the intragranular

spinels. Figure 4.4b presents the microstructure of magnesite-chrome brick 2 refractory. The microstructure showed intragranular chromite precipitates ('C2' in Fig. 4.4b) and continuous chromites within the magnesia grains. Silicate phases were observed within the magnesia matrix surrounding the magnesia spinels and occasionally they formed continuous elongated phases. The intragranular chromite precipitates shown in the refractory were relatively fine assuming precipitation occurred at low firing temperatures during production[68,70]. At low magnification, primary chromite exits within the refractory and was in contact with magnesia with or without the intermediate silicate matrix. The silicate structures observed ('S' in Figure 4.4b) within the refractory contained magnesium, silicon and calcium, or magnesium and silicon. The silicate found throughout the refractory structure was forsterite and less monticellite matrices.

Figure 4.5 shows the quantitative SEM analysis results using EDS to determine the different phases. The silicate matrix showed non-uniformity and the composition of magnesia and calcium varied markedly within the refractory matrices. The composition of forsterite silicate matrix analyzed contained between 30 wt% and 43 wt% SiO_2 content and MgO content is higher between 50 and 60 wt%. In monticellite matrix the composition of silicate components range from 26 to 36 wt% MgO, 20 to 32 wt% CaO and 35 to 40 wt% SiO_2. The compositions of the minerals analyzed are given in Table 4.1. The silicates were found as irregularly shaped elongated matrices within the magnesia matrix surround the magnesia-chromite structures. They also formed intermediate phases between some magnesia-magnesia contacts and between magnesia and chromite grains. The intergranular chromite spinels are seen and are shown as precipitates within the magnesia and as irregularly shaped chromite intergrowths along the magnesia grains.

Table 4.1. Compositions of the forsterite, monticellite and chromite minerals.

Phase	**Compound wt%**					
	MgO	CaO	Fe_2O_3	SiO_2	Cr_2O_3	Al_2O_3
Forsterite (Mg_2SiO_4)	56.96	1.21	–	41.28	0.55	–
Monticellite ($CaMgSiO_4$)	26.25	35.94	–	31.81	–	–
Chromite Spinel	21.95	–	–	–	48.59	17.27

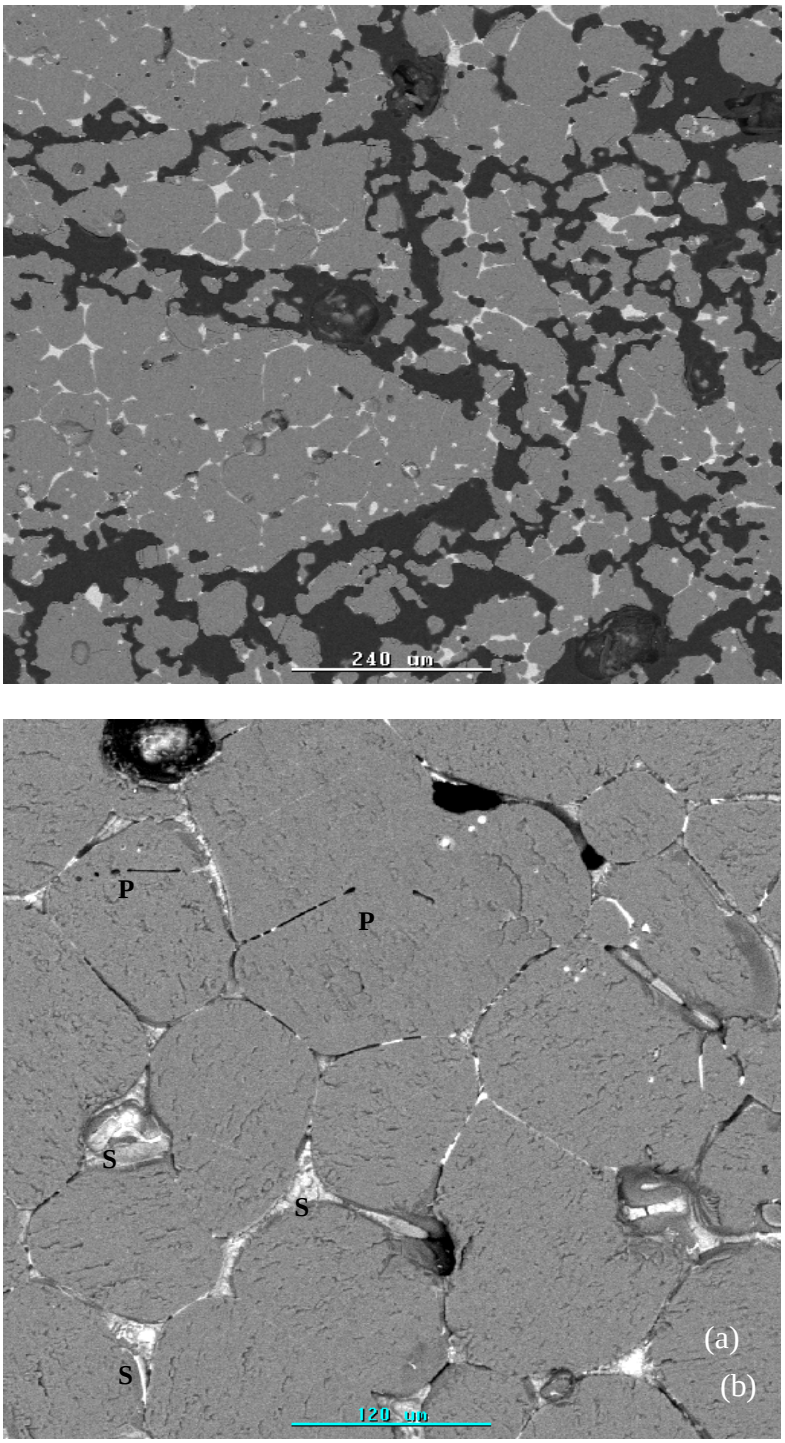


Figure 4.1. SEM-BSE micrographs of Magnesite refractory (a) microstructure at high magnification, gray phase = magnesia (periclase P), light-gray phase = silicate (S) and black= pores, and (b) microstructure at high magnification showing subhedral magnesia grains with spheroidized grain boundaries and dihedral contact angles between the grains**.**

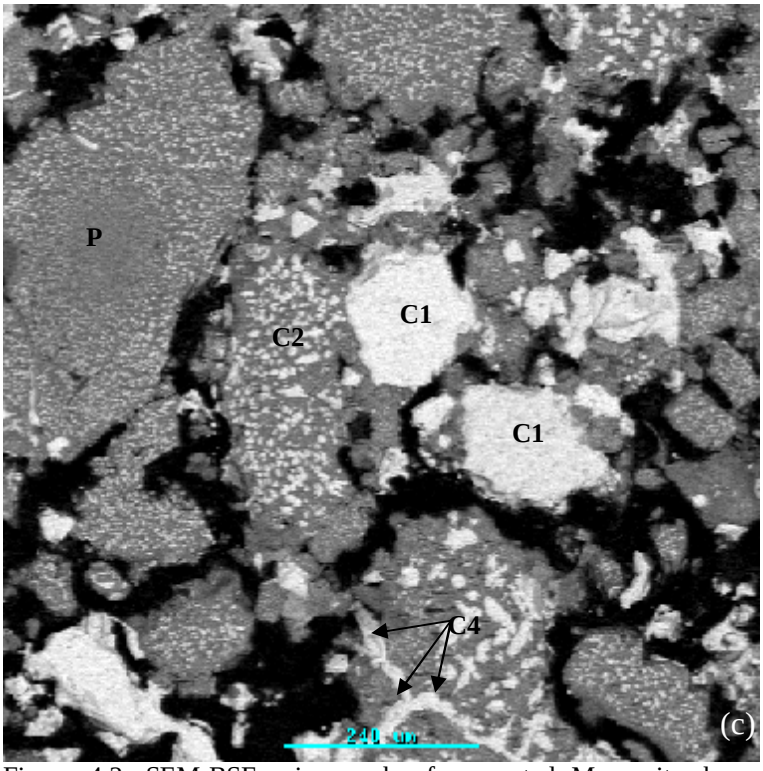


Figure 4.2. SEM-BSE micrograph of unreacted Magnesite-chrome brick 1 showing bright phase= chromite (C1), gray phase = magnesia (periclase P), black= pores. Intragranular precipitate chromites =C2 and precipitate continuous chromites =C4.

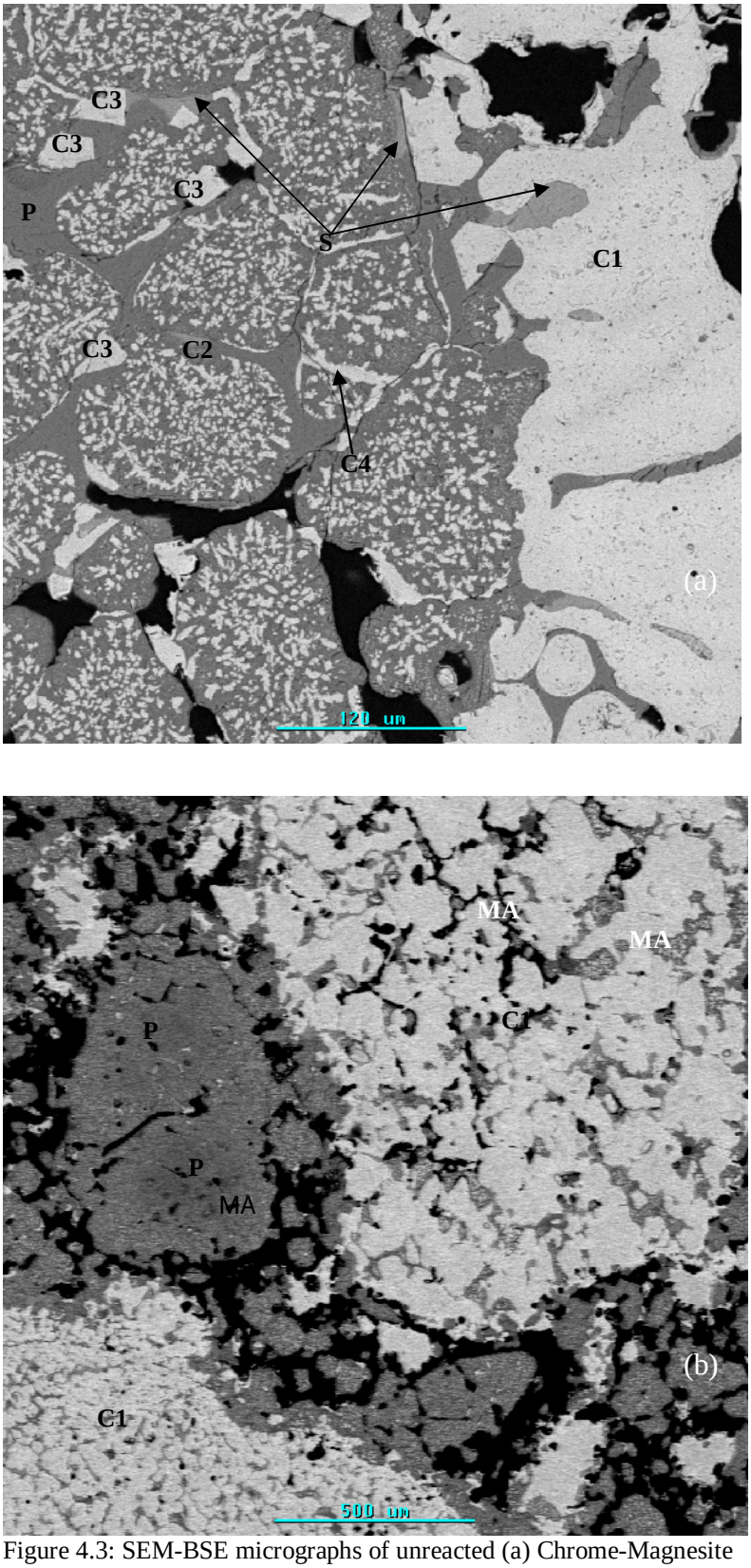


Figure 4.3: SEM-BSE micrographs of unreacted (a) Chrome-Magnesite A showing bright phase= chromite (C1), gray phase = magnesia (periclase P), light-gray phase = silicate (S), black= pores. Intragranular precipitate chromites =C2 and intergranular precipitate chromites = C3 and C4. (b) Chrome-magnesite D50-C5 showing bright phase= chromite (C1), gray phase = magnesia (periclase P), and black= pores.

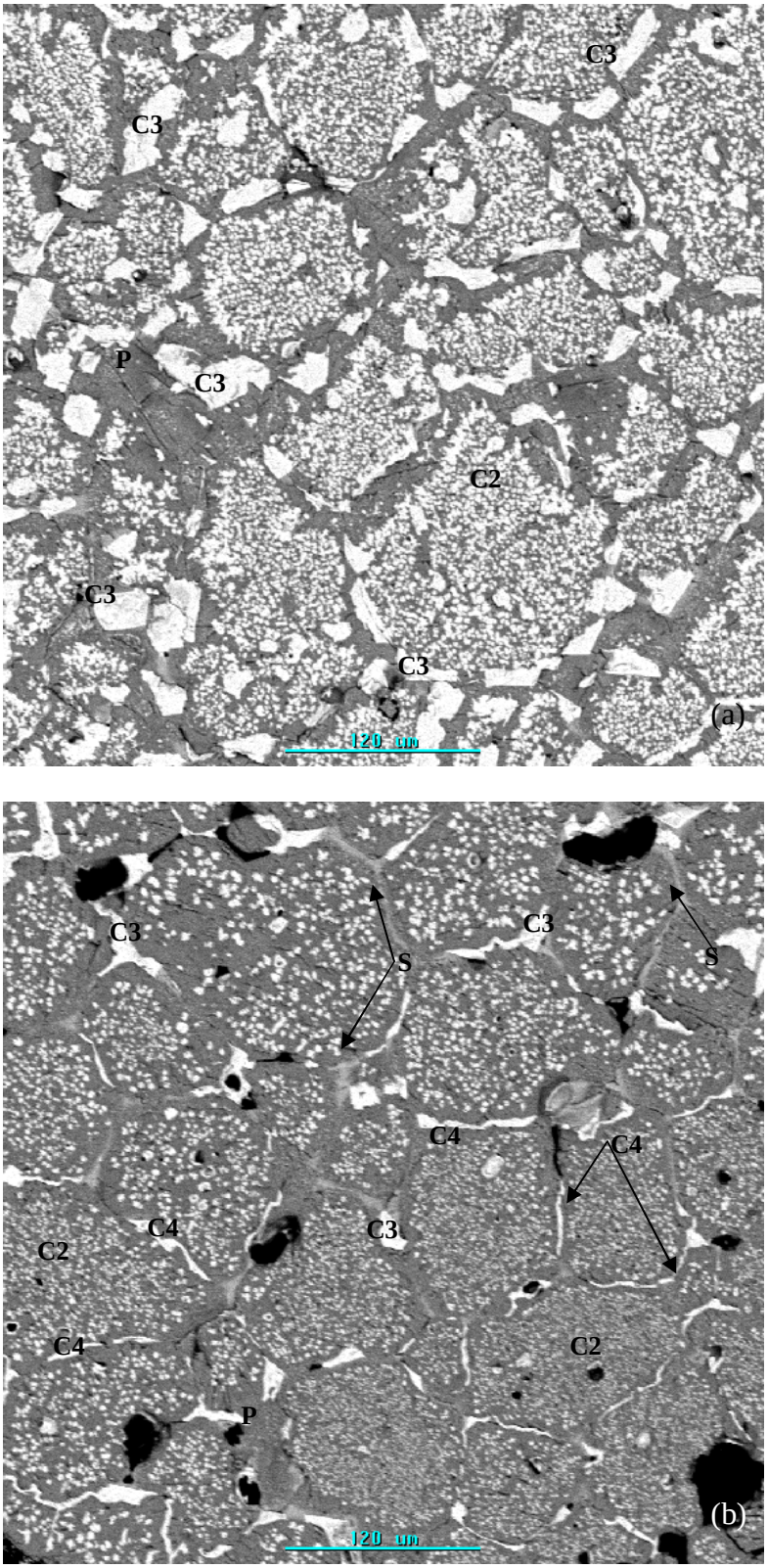


Figure 4.4. SEM-BSE micrographs of unreacted (a) Magnesite-chrome D60/100 showing gray phase = magnesia (periclase P), intragranular precipitate chromites =C2 and intergranular precipitate, blocky chromites = C3 and continuous chromites C4. (b) Magnesite-chrome brick 2 showing gray phase = magnesia (periclase P), black= pores, light-gray phase = silicate (S) and intragranular precipitate chromites =C2 and intergranular precipitate continuous chromites =C4.

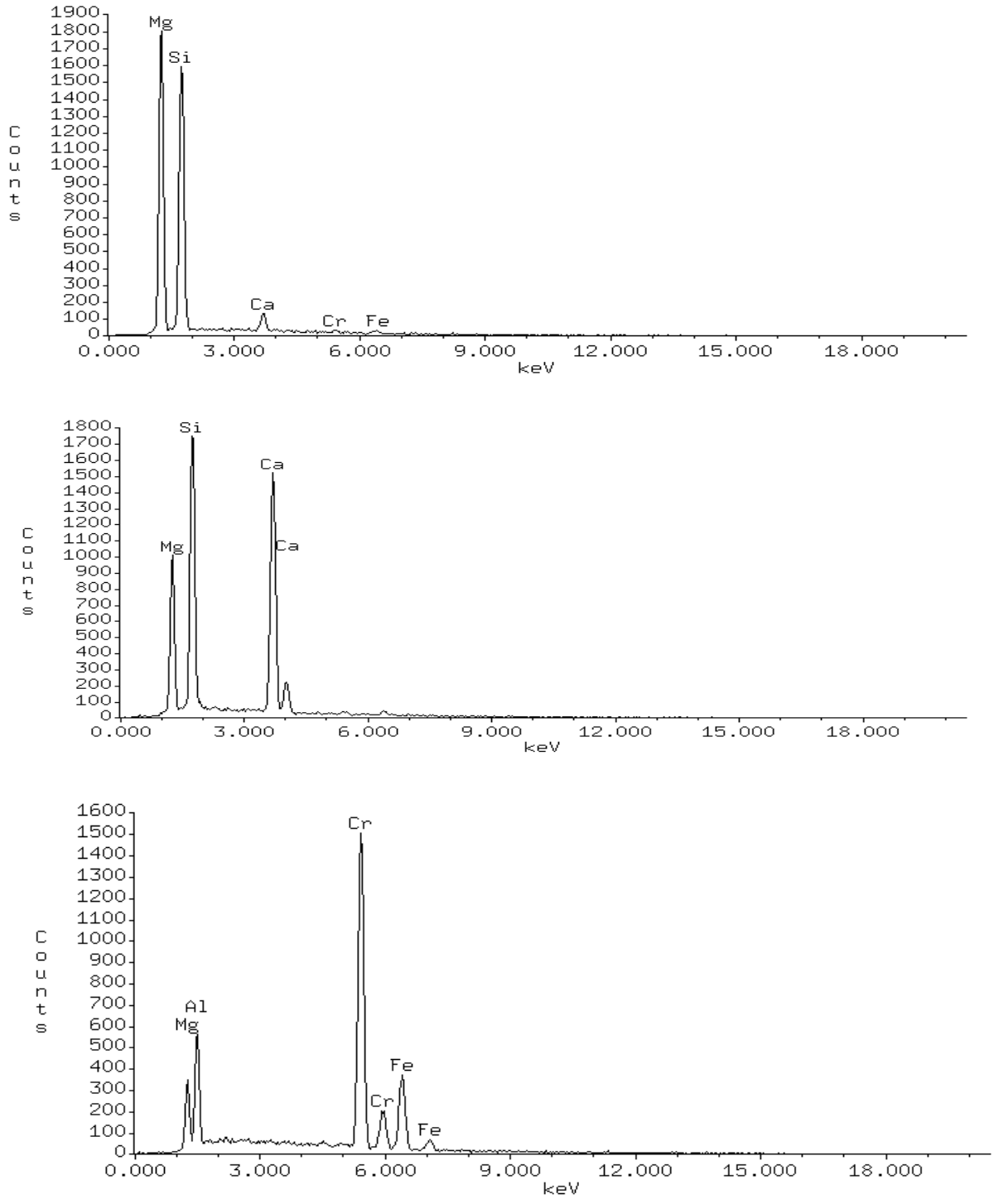


Figure 4.5. EDX spectra of forsterite (a), monticellite (b) and chromite (c) phase showing the elements contained in the minerals.

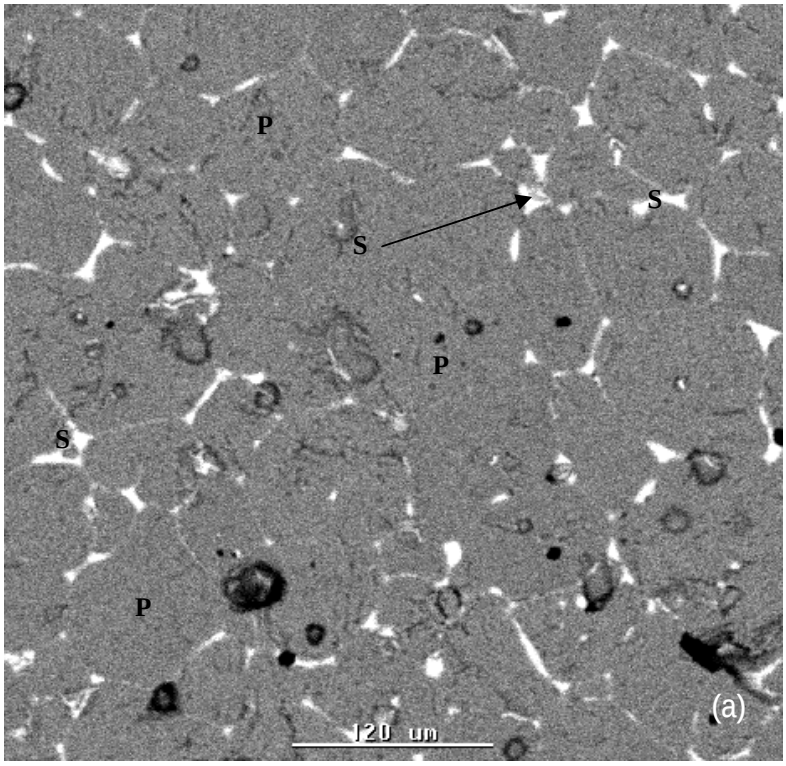
4.2 Microstructural and Physical Characteristics in Oxygen Atmosphere

Figure 4.6 shows micrographs of magnesite refractory reacted at 700°C and 1350°C. The observed marked difference was the distribution of the silicate phases and the orientation of the magnesia grains. At 700°C, the microstructure shown in Figure 4.6a was characterized by uneven texture within the magnesia grains, which were less rounded with dihedral angles at the grain boundaries. The silicates identified as tricalcium silicate were distributed as intermediate phases between the magnesia grains. Figure 4.6b presents microstructure reacted at 1350°C, in which the magnesia grains had a smooth texture and were more rounded with dihedral angles at the grain boundaries, especially at the triple points. The spheroidization of the magnesia grains associated with minimum surface energy was illustrated[70]. The silicates had migrated towards the grain boundaries, leaving well-developed magnesia grains with periclase-periclase bonded structure at the centre of grains. Porosity occurred mainly at the grain boundaries as intergranular porosity. Figure 4.7 shows the microstructure of magnesite-chrome D60/100 (MC1) reheated at 1350°C. It was characterized by the changes in distribution of secondary chromite precipitates and the size of the spinels. Progressive development of secondary chromite spinels from the dissolution and redistribution of the chromites are demonstrated. Figure 4.7a shows the microstructure at low magnification and the volume of the magnesia spinel phases appeared to have increased. Figure.4.7b shows the development of secondary chromite precipitates and the density increased markedly within the grains. The blocky intergranular chromite precipitates developed angular to subhedral structures, while the continuous chromite precipitates were bulky and appeared to have occurred at the expense of blocky intergranular chromite precipitates that surrounded the magnesia spinels (seen as C3 in Fig.4.2a). The crystal size and distribution of the secondary chromites varied between grains and along the grain boundaries as small chromite crystals and precipitates. The direct bonding between the magnesia and chromite increased and the manner in which the chromite crystallites occurred around the spinel solid solutions suggested dissolution effects. Porosity was distributed evenly around the magnesia-chromite spinel structures and appeared to be affected by phase distribution developed.

Figure 4.8 presents the microstructure of the chrome-magnesite A refractory exposed to oxidizing atmospheres at 1350°C. The main feature was the development of magnesia separately from the solid solutions and aggregation of chromites. Figure 4.8a showed dissolution of magnesia-chrome spinels and development of coarse chromite grains. The magnesia grains appeared large with fine intragranular chromite precipitates along the grains boundaries, while

the interior showed fine iron oxide solid solutions. The semi-quantitative EDX analysis method demonstrated isolation of secondary chromites from the interior of the magnesia grains leaving them with 86.13 wt% MgO, 11.14 wt% Fe_2O_3, 0.56 wt% Al_2O_3 and 2.17 wt% Cr_2O_3. The composition around the grain boundaries was different from the interior of the grains and gave 61.25 wt% MgO, 16.84 wt% Fe_2O_3, 4.18 wt% Al_2O_3, 11.29 wt% Cr_2O_3, 5.11 wt% SiO_2, 1.33 wt% CaO. On the other hand the chromite grains contained 17.84 wt% MgO, 9.69 wt% Fe_2O_3, 14.33 wt% Al_2O_3 and 58.13 wt% Cr_2O_3. Figure 4.8b showed that migration of secondary chromites to the grain boundaries led to uneven distribution of the phases.

The silicates and secondary chromites migrated to the grains boundaries, and the chromite grains appeared more rounded and soft. Crack propagation and a large number of pores were observed within the magnesia grains. The composition of the chromite grains was similar to those observed in unreacted CM2 refractory (see Fig. 4.1b) with discontinuous magnesia spinel pockets within the grains, changing both the texture and colour of the grain. However, in CM1 the grains appeared fine and friable. The distribution of the magnesium spinel pockets on the surface of the grain suggested that occurred possibly from diffusion from the magnesia spinels during restructuring of chromite. The microstructure showed a definite trend in dissolution of magnesia-chrome spinels seen in the unreacted refractory (Fig.4.1a) and redistribution of chromites grains in diffusion-controlled processes. Figure 4.8a shows the occurrence of gaps along the grain boundaries surrounding the secondary chromites. The microstructure revealed low silica refractory, with occasional magnesia silicates distributed unevenly within the chromite grains. Figure 4.9 shows the microstructure of chrome-magnesite D50-C5 reheated at 1350°C. Figure 4.9a showed the dissolution of the primary chromite grains. The chromite grains were altered and the magnesia aluminate spinels were reorganized. The magnesia rims at the chromite grain boundaries in unreacted refractory (see Fig. 4.1b) disappeared with formation of coarse chromite grains. The discontinuous magnesia aluminate spinel pockets formed spinel structures. The iron oxide and chromic oxide from the primary chromite diffused into magnesia grains forming magnesia spinels. The magnesia spinels are presented in Figure 4.7b where magnesia is developed together with iron oxide and chromite precipitates surrounded by silicates. Small blocky secondary chromite precipitates and continuous chromite precipitates were observed. EDX analysis of silicate indicated CaO/SiO_2 ratio of about 1 at about 36wt% for each component with magnesia being 26 wt%. The magnesia spinels were rearranged into subhedral grains and the surrounding silicate interface was monticellite.



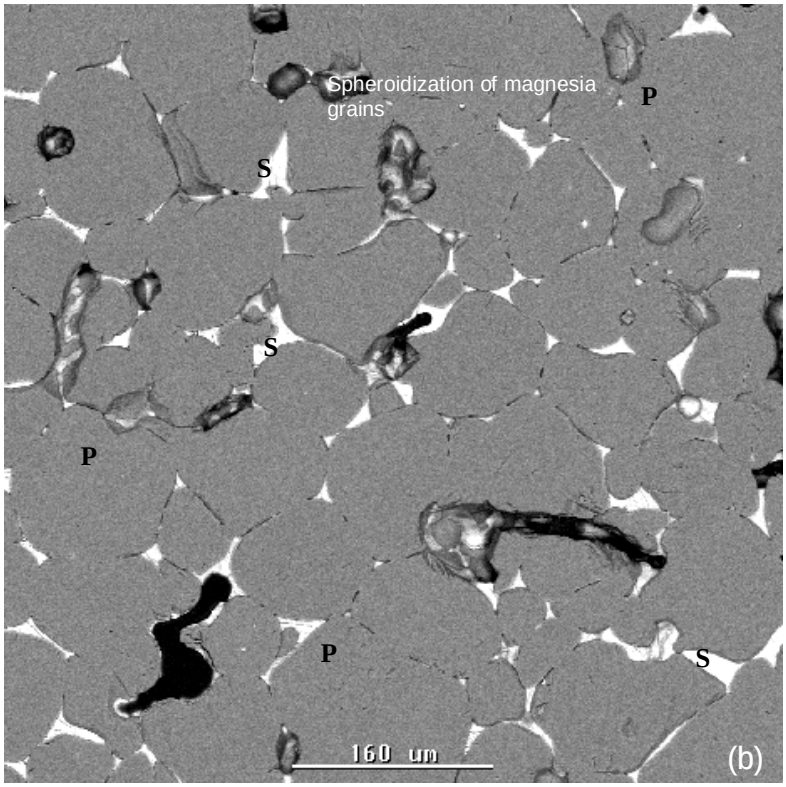


Figure 4.6. SEM-BSE micrographs of (a) Magnesite reacted at 700°C showing uneven texture of magnesia grains with dihedral contact angles. (b) Magnesite reacted at 1350 showing smooth texture of magnesia grains and spheroidization achieved by the magnesia grains at the triple points. The gray phase = magnesia (periclase, P), bright phase = silicate (S) and black= pores.

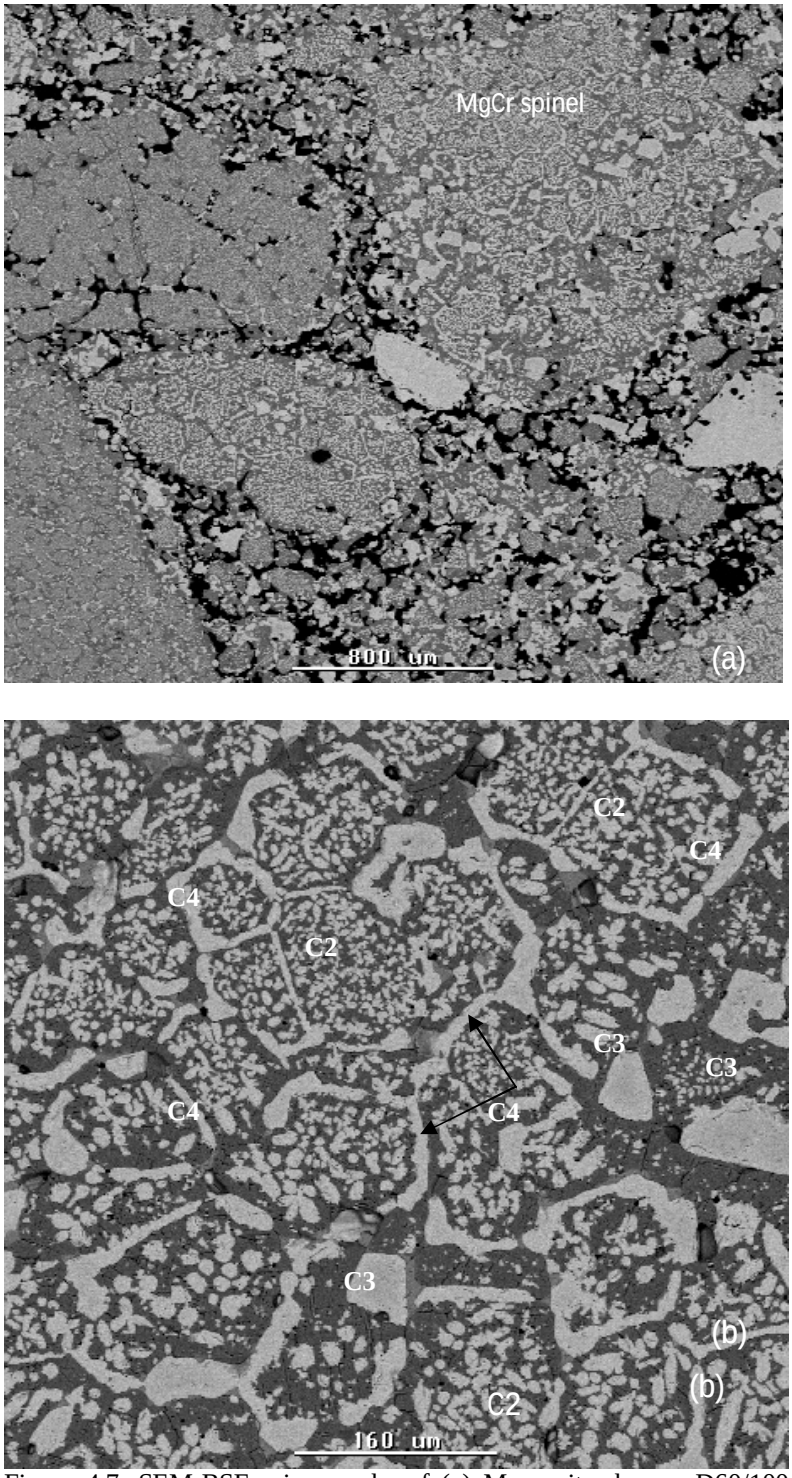


Figure 4.7. SEM-BSE micrographs of (a) Magnesite-chrome D60/100 reacted in O_2 gas at 1350°C, showing distribution of chromite grains and increasing volume of magnesia-chromite spinel at low magnification (b) Magnesite-chrome D60/100 at high magnification, showing angular to subherdal blocky intergranular chromites, continuous intergranular chromites and intragranular chromites. The gray phase = magnesia (periclase P), black= pores, bright phase = intragranular chromites precipitate =C2 and intergranular precipitate chromites = C3 and C4.

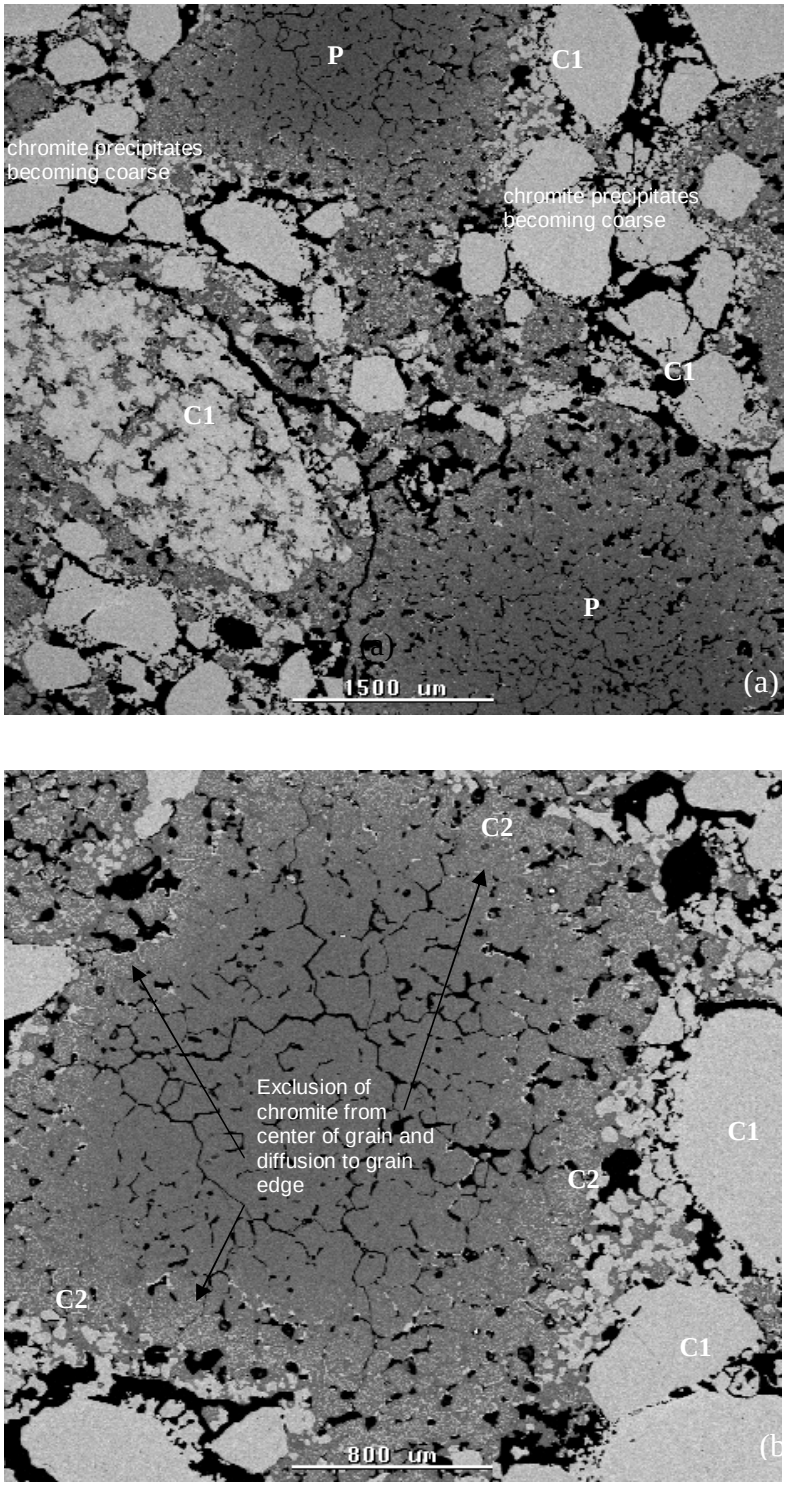


Figure 4.8. SEM-BSE micrographs of (a) Chrome-magnesite A reacted in O_2 gas at 1350°C, showing development and migration of secondary chromites at low magnification (b) Chrome-magnesite A showing magnesia grain with intragranular secondary chromites along the grain boundaries, cracks and high purity interior. Coarse secondary chromites are shown as bright phase= chromite (C1). The gray phase = magnesia (periclase P), black= pores, within magnesia grains borders the bright phase = intragranular chromites precipitate =C2.

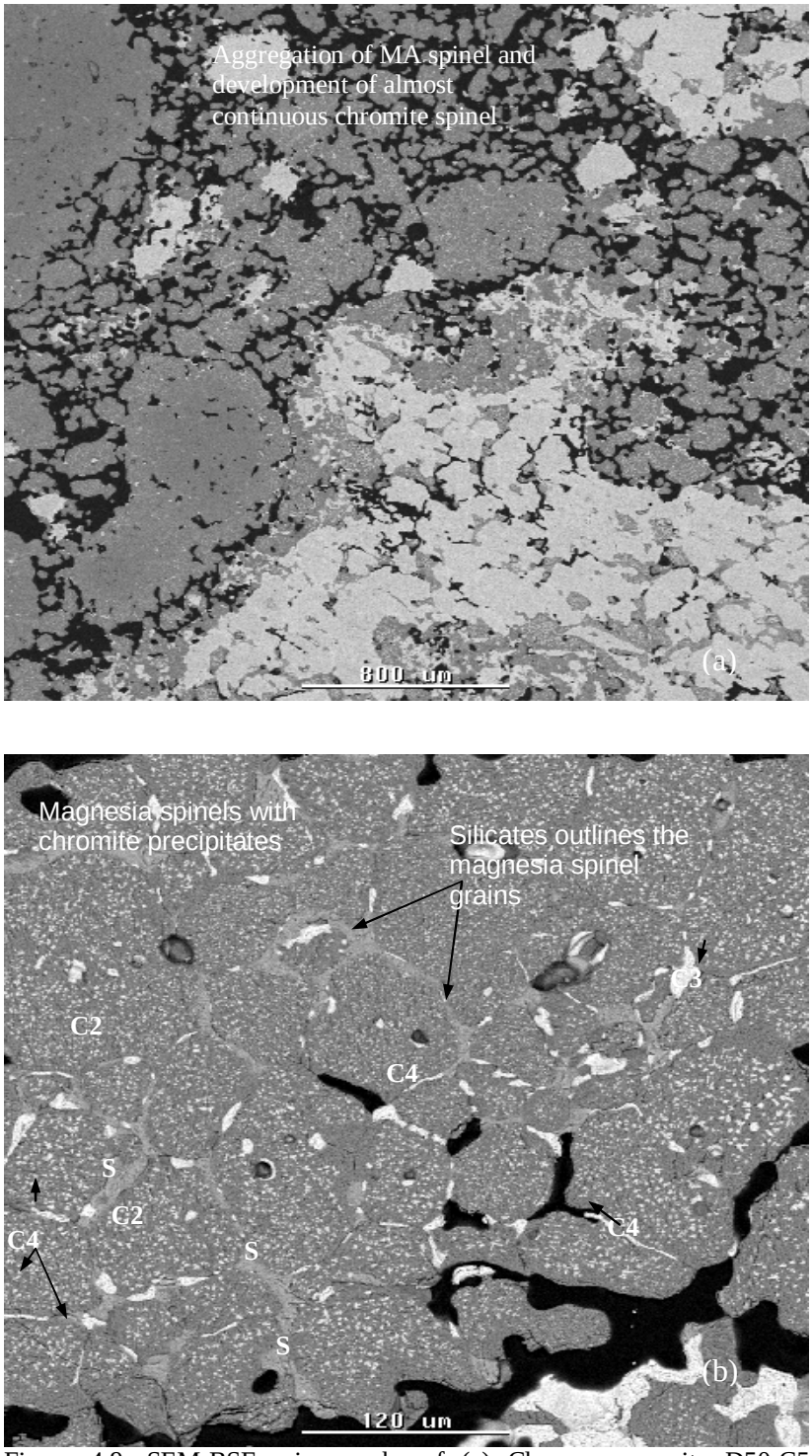


Figure 4.9. SEM-BSE micrographs of (a) Chrome-magnesite D50-C5 reacted in O_2 gas at 1350°C, showing dissolution of primary chromite grains and aggregation of magnesium aluminates spinels. (b) Chrome-magnesite D50-C5 showing intragranular secondary chromite precipitates and intergranular silicates between magnesia-chrome spinels. The gray phase = magnesia (periclase P), light-gray phase = silicate (S), black= pores, bright phase = intragranular chromites precipitate =C2 and intergranular precipitate chromites = C3 and C4.

4.3 Thermodynamic analysis of basic refractories in sulfur-bearing gases

Thermodynamic analyses of reactions that form sulfate phases in refractory-interactions with sulfur-bearing gases were conducted and predominance area diagrams of different phases shown in Figure 4.10 to 4.13 were generated. The reactions of basic refractories were investigated within 700°C to 1350°C temperature range at combination gas mixtures of oxygen and sulfur dioxide, at varying partial pressures. The combination partial pressures of oxygen and sulfur dioxide gases used in the experiments were consistent at low temperature and high temperatures in both SO_2-O_2 and SO_2-N_2 gas mixtures. The formation of sulfate phases were predicted from the predominance area diagrams generated using Kellog[79], Dewing and Richardson[117], Liouw *et al.*[22], Ricahrdson and Jeffes[113] thermodynamic data, and the FactSage software programme. The diagrams generated provided an important support in predicting the reaction products formed in the basic refractories, when MgO and CaO were considered the reactive oxides.

In SO_2-N_2 gas mixtures, at the total pressure of 1 atm the corresponding equilibrium pressures of SO_2, N_2, O_2 in the system were 0.1998 atm., 0.796 atm, and 0.0036 atm, respectively. In Figure 4.10, the predominance area diagram for Ca-S-O compound system generated from Kellog[79] and Ricahrdson and Jeffes[113] data predicts that at the combination partial pressures of oxygen, P_{O_2} =0.0036($\log P_{O_2}$ =-2.4437), and sulfur dioxide, P_{SO_2} = 0.1998($\log P_{S_{O_2}}$ =-0.6994) marked in the diagram, maximum temperatures for calcium sulfate formation are above 1350°C. Figure 4.11, generated from the FactSage software, indicated that under similar combination partial pressures of oxygen and sulfur dioxide, calcium sulfate stability would occur at maximum temperatures above 1350°C, corresponding with Figure 4.10 as indicated. In SO_2-O_2 gas mixtures, at the total pressure of 1 atm, the corresponding equilibrium pressures of SO_2 and O_2 in the system were P_{SO_2} = 0.1998 atm and P_{O_2} = 0.796 atm. The generated predominance area diagrams shown in Figure 4.10 and 4.11, showed similar findings and that in combination gas pressures of oxygen, P_{O_2} =0.796($\log P_{O_2}$ =-9.9087x10^{-2}), and sulfur dioxide, P_{SO_2} =0.1998($\log P_{S_{O_2}}$ =-0.6994), maximum temperatures for $CaSO_4$ are above 1350°C. Therefore, $CaSO_4$ would be formed for all gas mixtures used in the experiments between 700°C and 1350°C, at varying oxygen and sulfur dioxide pressures considered.

Predominance area diagram in Figure 4.12 and 4.13 indicated different favourable conditions for $MgSO_4$ formation under equilibrium partial pressures of oxygen and sulfur dioxide used in SO_2-

N_2 and SO_2-O_2 gas mixtures. In Figure 4.12, results from Kellog's[79] data indicated that maximum temperatures for $MgSO_4$ stability would occur up to 1110°C for the combination gas pressures of P_{O_2}=0.796($\log P_{O_2}$=-9.9087x10^{-2}) and P_{SO_2}=0.1998($\log P_{S_{O_2}}$=-0.6994). In addition, for the combination gas pressures of P_{O_2}=0.0036($\log P_{O_2}$=-2.4437) and P_{SO_2}=0.1998($\log P_{S_{O_2}}$=-0.6994) maximum temperatures would increase and $MgSO_4$ would be formed up to 1290°C. At 1350°C, MgO would be the favourable compound in the combination gas pressures of P_{O_2}=0.796($\log P_{O_2}$=-9.9087x10^{-2}) and P_{SO_2}=0.1998($\log P_{S_{O_2}}$=-0.6994). while MgS would be formed for combination pressures of P_{O_2}=0.0036($\log P_{O_2}$=-2.4437) and P_{SO_2}=0.1998($\log P_{S_{O_2}}$=-0.6994) as indicated in the diagram.

In the temperature range and gas partial pressures combination employed in the study, the data[79] indicated that $MgSO_4$ stability occurred for maximum temperatures up to 1000°C. However, Factsage software results in Figure 4.11 indicated that $MgSO_4$ stability would be formed for maximum temperatures up to 890°C in the gas partial pressures combination of P_{O_2}=0.0036($\log P_{O_2}$=-2.4437) and P_{SO_2}=0.1998($\log P_{S_{O_2}}$=-0.6994) marked in the diagram. In addition, in the combination partial pressures of P_{O_2}=0.796($\log P_{O_2}$=-9.9087x10^{-2}) and P_{SO_2}=0.1998($\log P_{S_{O_2}}$=-0.6994) in Figure 4.11, maximum temperatures for $MgSO_4$ formation are up to 990°C as indicated to be the stable phase. Liouw *et al.*[22] generated the predominance area diagram in Figure 2.5 using Dewing and Richardson[117] data for temperatures between 700°C to 1500°C. From the results, the diagram indicated that at combinations pressures of P_{O_2}=0.0036($\log P_{O_2}$=-2.4437) and P_{SO_2}=0.1998($\log P_{S_{O_2}}$=-0.6994) considered in the experiments, $MgSO_4$ formation would occur at maximum temperatures up to 990°C as marked in the diagram. However, for combination gas pressures of P_{O_2}=0.796($\log P_{O_2}$=-9.9087x10^{-2}) and P_{SO_2}=0.1998($\log P_{S_{O_2}}$=-0.6994) maximum temperatures for $MgSO_4$ formation increased up to 1090°C, suggesting that in the temperature range and gas partial pressures combination employed in the study, $MgSO_4$ would be formed at 1000, corresponding to Kellog's[79] data.

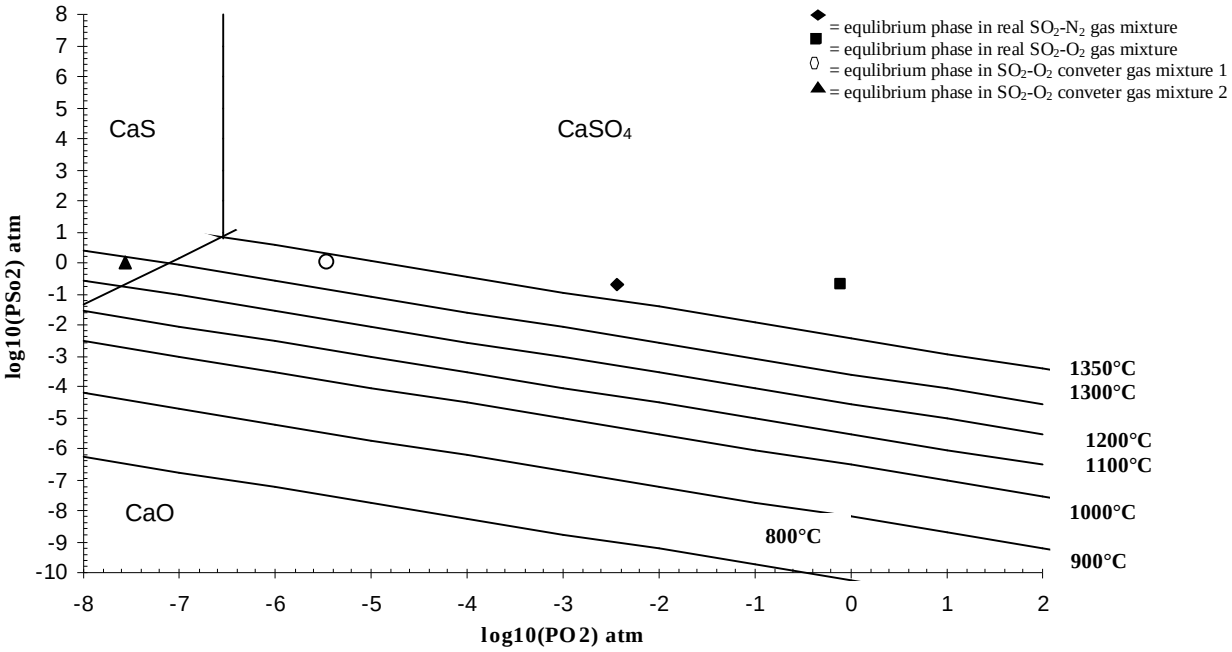


Figure 4.10: Predominance area diagrams for Ca-S-O at 1350°C, and varying partial pressures of oxygen and sulfur dioxide using Kellog[79] and Richardson and Jeffes[113] data.

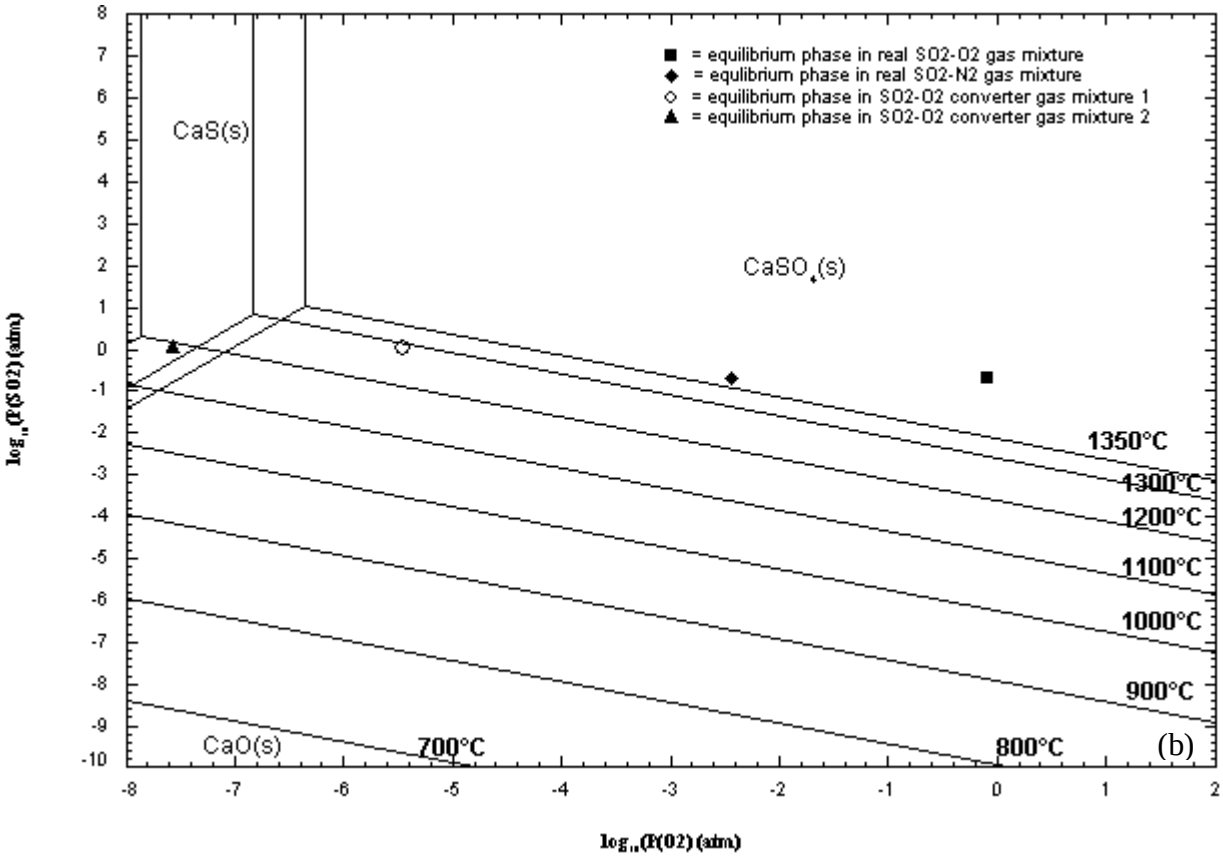


Figure 4.11: Predominance area diagrams for Ca-S-O at 700°C to 1350°C, and varying partial pressures of oxygen and sulfur dioxide using FactSage software programme[121–122].

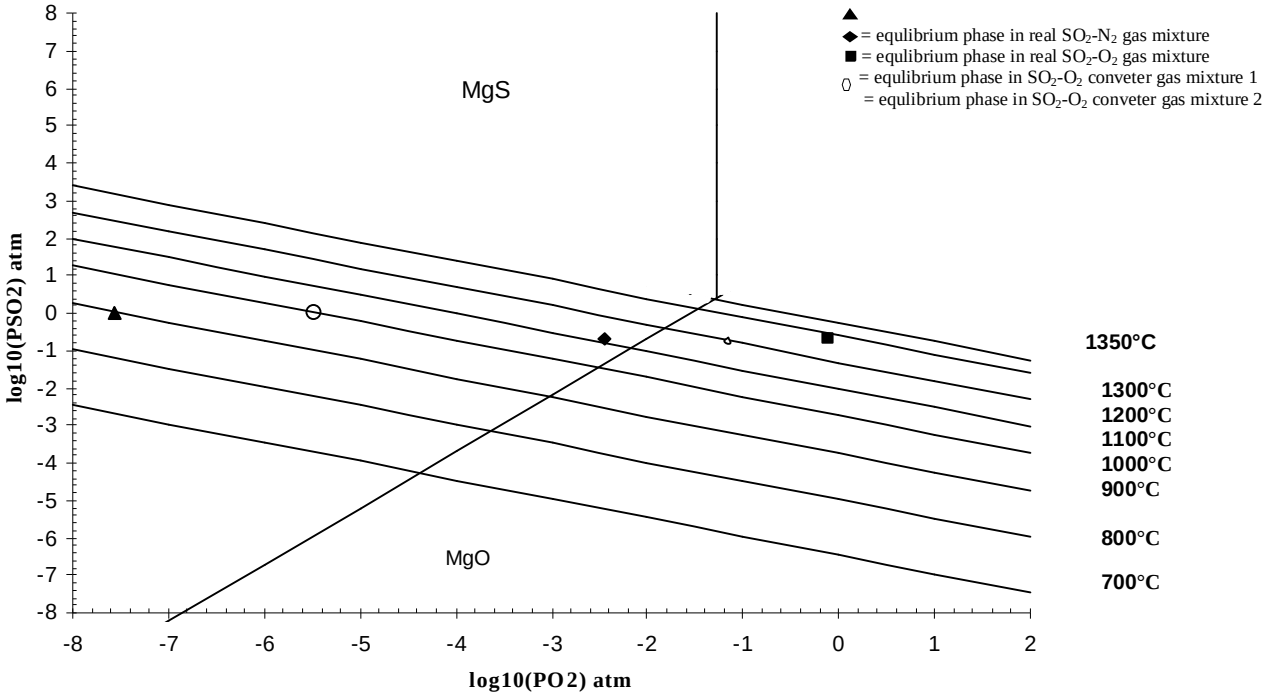


Figure 4.12: Predominance area diagram of Mg-S-O between 700°C to 1000°C, and varying partial pressures of oxygen and sulfur dioxide, using Kellog's data[79].

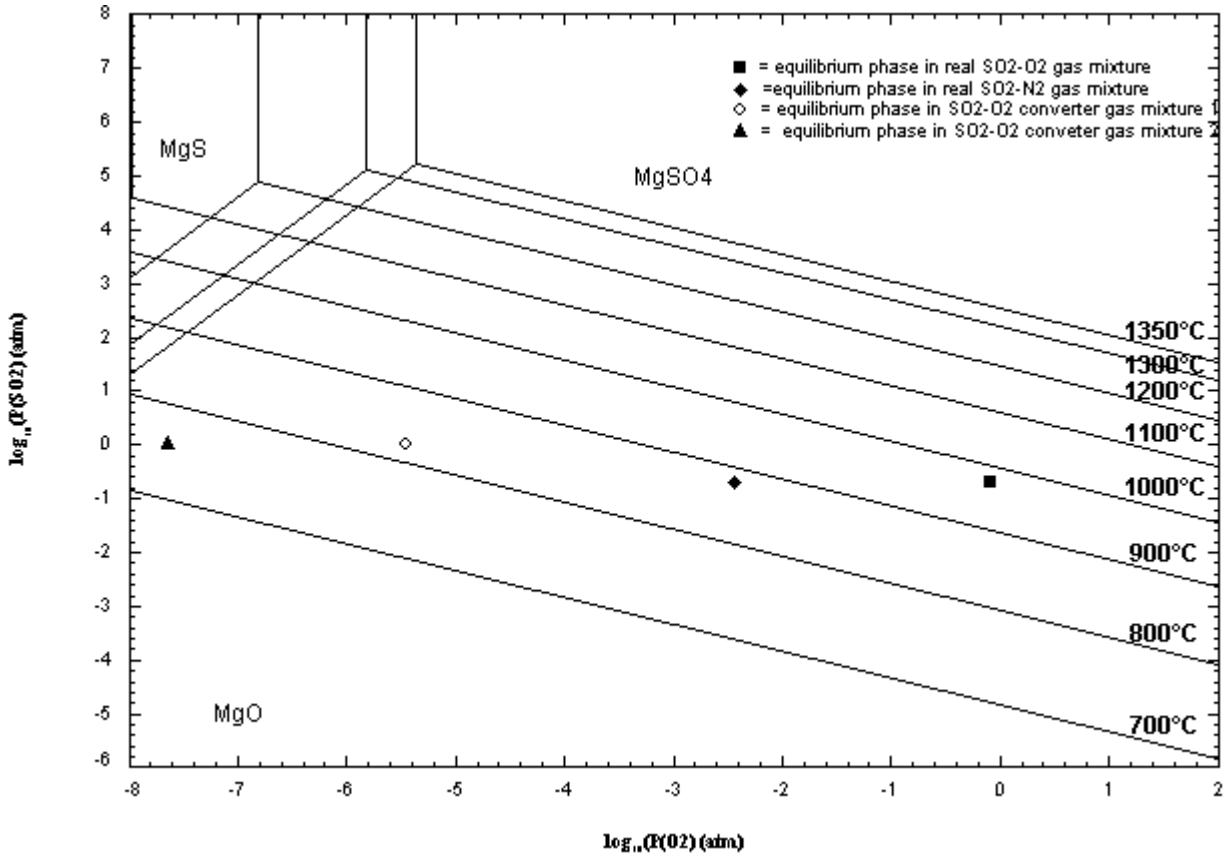


Figure 4.13: Predominance area diagrams of Mg-S-O between 700°C to 1350°, and varying partial pressures of oxygen and sulfur dioxide, using FactSage software[121–122].

4.3.1 Microstructural changes in high temperature SO_2-N_2 Gas mixtures

The phase compositions, microstructure and the development of new phases were examined using the X-ray diffraction and scanning electron microscopy (SEM) and the results are presented in Figures 4.14 to 4.17. Figure 4.14a shows the microstructure of magnesite refractory having magnesia grains, silicates and sulfate phases. Calcium sulfate formed as an intermediate phase between and around the small and the large magnesia grains, while silicates tended to form between the magnesia grains and sulfate phase. Calcium sulfate formed indicated to have occurred from reaction between CaO contained in silicate phase in the refractory and the sulfur-bearing gases. The formation of $CaSO_4$ from the CaO found in the refractory confirmed the results suggested in the predominance area diagram for Ca-S-O system (Figure 4.10 and 4.11). The structural analysis showed large magnesia grains with well-developed direct-bonded structure that had intragranular porosity suggesting that the silicates migrated to the boundaries during diffusion. The calcium sulfate phase formed at the grain boundaries as an interface separating the small magnesia grains. There was no observed chemical reaction between the magnesia grains and the sulfur-bearing gases, which related to the suggestion shown by the predominance area diagram for Mg-S-O system (Figure 2.5, 4.12 to 4.13) at 1350°C. The texture and shape of the grains seen in as-delivered microstructure of magnesite refractory (Fig. 4.14b) changed from rounded subhedral grains with dihedral angles to irregular shaped magnesia grains.

The observed calcium sulfate microstructure in Figure 4.14b appeared two-phased, but actually had minor porosity with considerable intragranular porosity within. Since the microstructure of the as-delivered magnesite refractory showed calcium oxide present only in tricalcium silicate ($CaO_3[SiO_4]$), the formation of calcium sulfate at grain boundaries (Figure 4.14a) suggested diffusion of calcium oxide from the silicate to react with the sulfur-bearing gases. This indicated possible structural disintegration promoted by diffusion processes, and sulfation reactions that resulted in pores and crack formation. New silicate phases formed were identified as forsterite (Mg_2SiO_4), indicating reaction between SiO_2 (from the tricalcium silicate) and magnesia. The silicates occurred between the magnesia grains and calcium sulfate, and had a lighter contrast than the magnesia in the grains. Figure 4.15 present the microstructures of refractory powdered pellet and laboratory magnesium oxide, exposed to SO_2-N_2 gas mixtures. The laboratory magnesium oxide in Figure 4.15a, showed indicated development of powdered material into magnesia grains suggesting sintering effects. There were magnesia-magnesia contacts, but interconnected pores formed a highly porous structure, with few developed magnesia grains.

The observed color change from white powered material to dark grey solid conformed to magnesia found in the refractories. There was no formation of sulfate with the magnesium oxide indicating the lack of reactivity of laboratory suggested in Figure 2.5, 4.12 to 4.13 at 1350°C. In the microstructure of magnesite refractory powdered pellet shown in Figure 4.15b sintering effects resulted in similar development magnesia particles, forming irregularly shaped continuous magnesia grains and high porous structure of discontinuous pores that were open and interconnected. No apparent silicate phases were observed, only randomly distributed small bright inherent impurity silicates. There was no sulfate phase formed, indicating the unreactivity magnesia with sulfur-bearing gases at 1350°C, in any form of structure. The microstructure of chrome-magnesite refractory powdered pellet shown in Figure 4.16, showed similar microstructural features of open pores and voids, which are typical microstructure of the unbounded refractory formed from mixture of magnesite and chromite minerals, due to volume changes attributed to diffusion processes. A distinct microstructure of fine intragranular chromite precipitates around and within the magnesia grains occurred. Magnesia-chromite direct bonding developed within the material suggested reactions that involved diffusion and precipitation.

Silicates were distributed randomly throughout the structure, and were frequently found in close proximity with chromite grains. The newly formed structure showed no formation of sulfate phases suggesting unreactivity of chromite and magnesia refractory with sulfur-bearing gases at 1350°C. Figure 4.17 shows the microstructure of magnesite-chrome and chrome-magnesite refractories that have been reheated in SO_2-N_2 gas mixture at 1350°C. There were no apparent changes demonstrated in the microstructure of magnesite-chrome D60/100 shown in Figure 4.17a. The direct bonding structure between the chromite and periclase grains and the magnesia matrix between the magnesia spinels and intergranular blocky secondary chromites were preserved. Figure 4.17b presents the microstructure of chrome-magnesite A refractory that had similar characteristics to the original structure (Figure 4.3a). Direct bonding between the magnesia and primary chromites, primary and secondary chromite spinels (Mg, Fe) (Cr, Al, $Fe)_2O_4$ were seen. The silicates were randomly distributed between the magnesia spinels and formed between primary chromites and magnesia. There were two types of silicates, with forsterite being the predominant silicate, with less monticellite found. No new phases were formed showing that there was no reaction with sulfur-bearing gases.

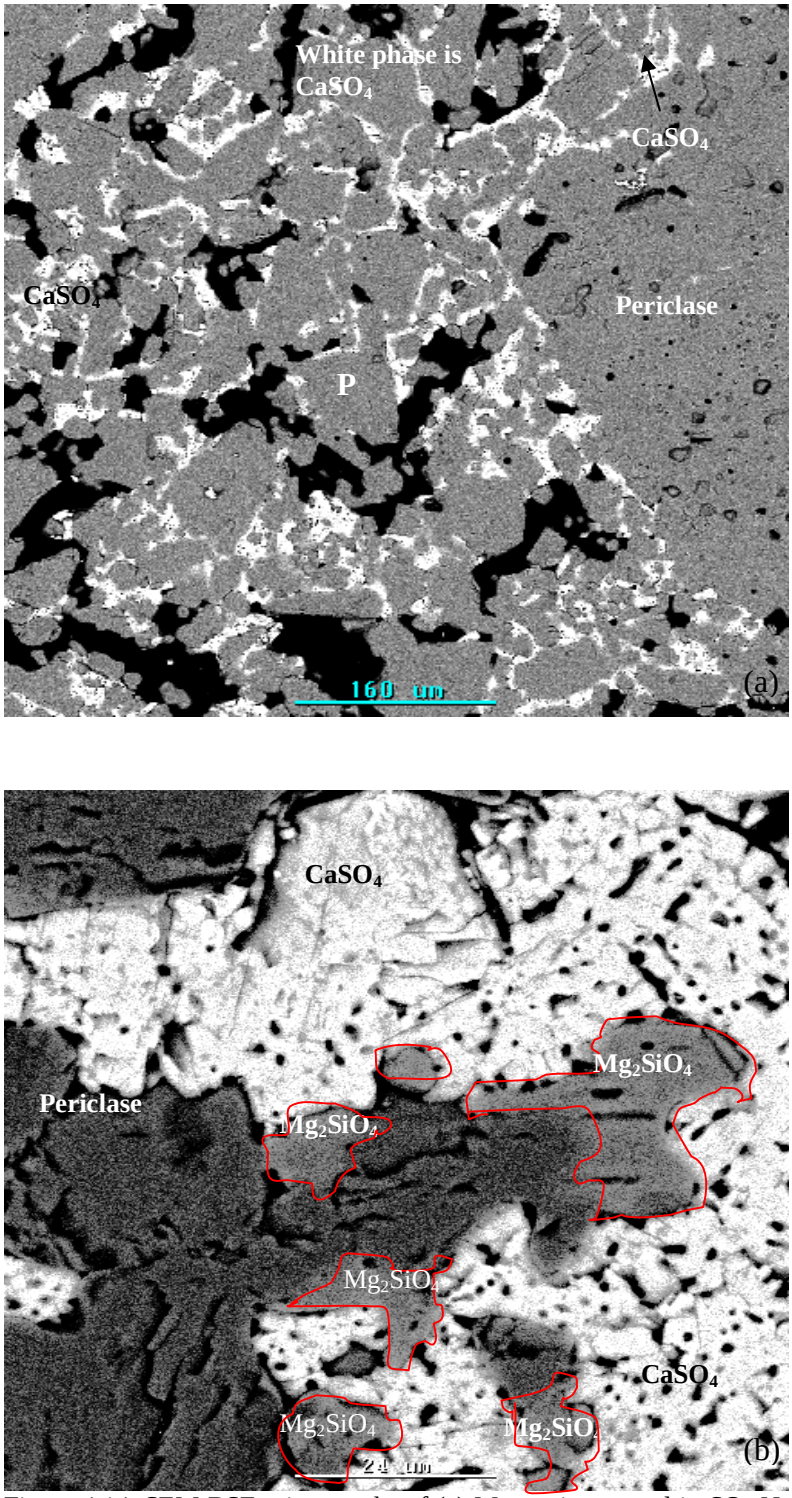


Figure 4.14. SEM-BSE micrographs of (a) Magnesite reacted in SO_2-N_2 gas mixture at 1350°C, showing formation of calcium sulfate at grain boundaries. (b) Magnesite showing formation of silicate and intragranular porosity. The gray phase = magnesia (periclase P), light-gray phase = silicate (S), black= pores and white phase = $CaSO_4$

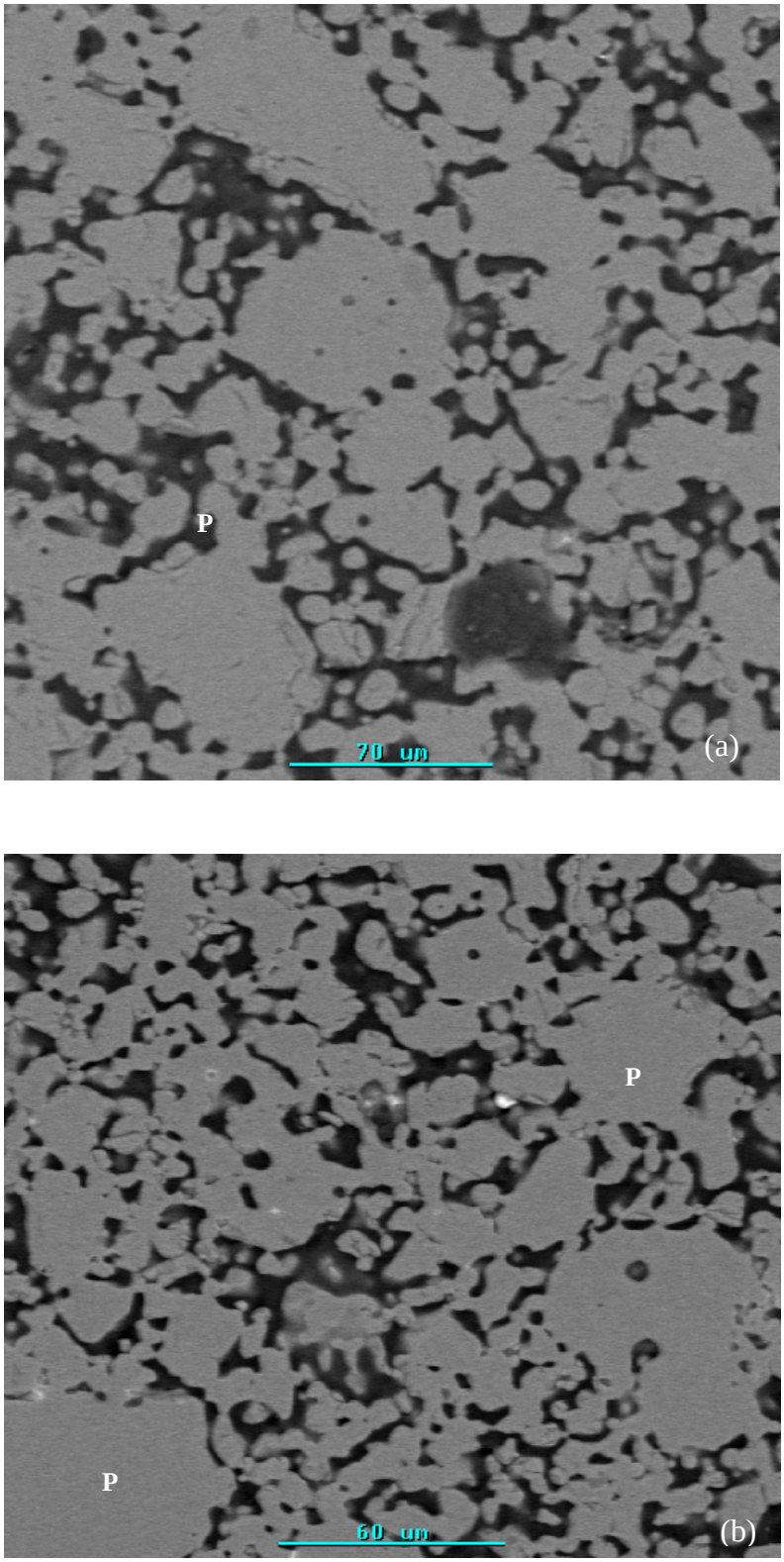


Figure 4.15. SEM-BSE micrographs of (a) laboratory magnesium oxide powdered pellets, reacted in SO_2-N_2 gas mixtures at 1350°C, showing formation of magnesia grains with some direct bonding between grains. (b) Refractory powdered pellet of magnesite showing magnesia grains with a skeletal structure. The gray phase = magnesia (periclase P), black= pores.

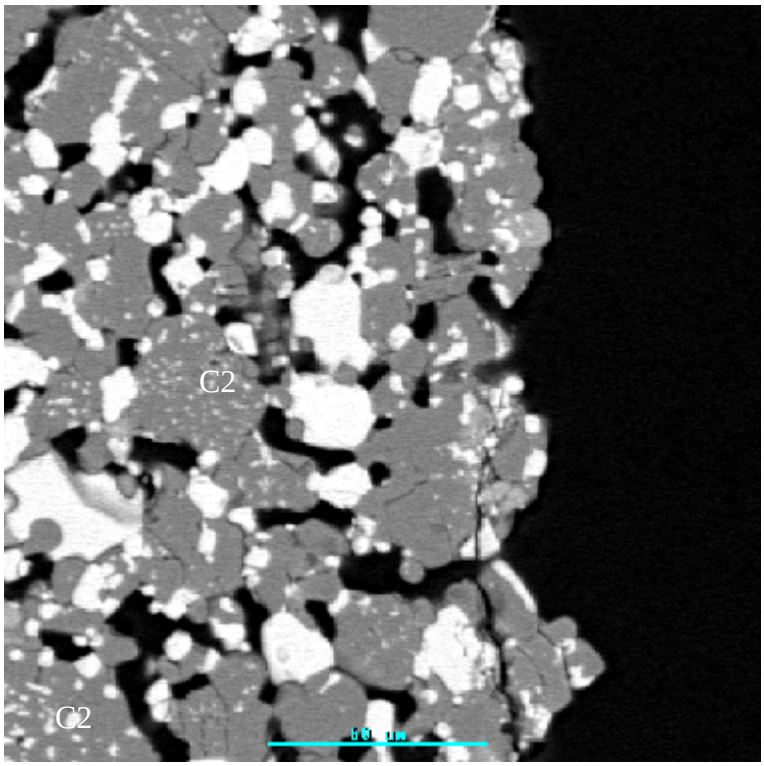


Figure 4.16. SEM-BSE micrograph of a refractory powdered pellet of magnesite-chrome reacted in SO_2-N_2 gas mixtures at 1350°C, showing magnesia-chromite contacts and magnesia spinels. The gray phase = magnesia (periclase P), black= pores, bright phase = chromite and intragranular chromites precipitate =C2.

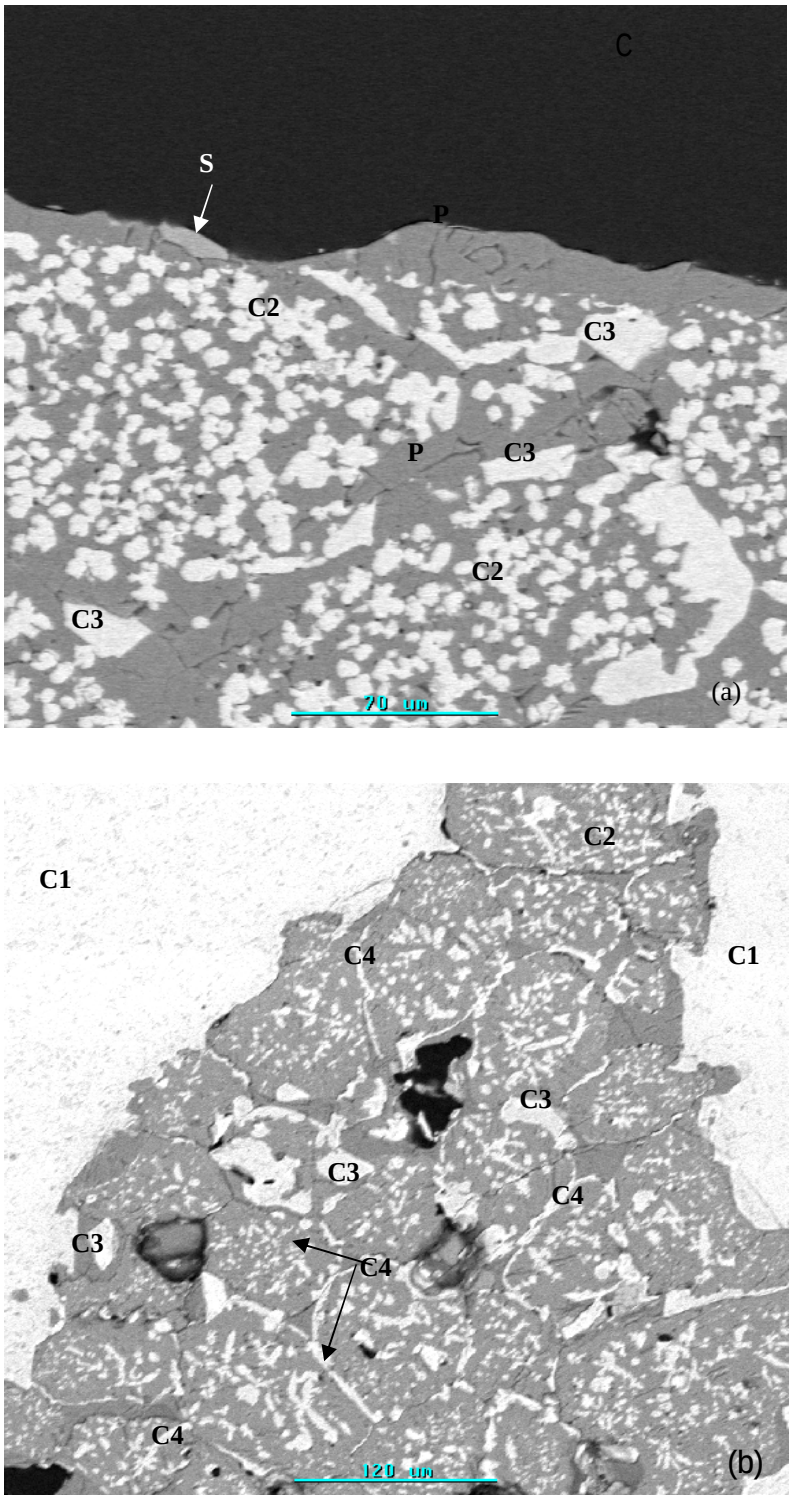


Figure 4.17. SEM-BSE micrographs of (a) Magnesite-chrome D60/100 reacted in SO_2-N_2 gas mixture at 1350, showing gray phase = magnesia (periclase P), light-gray phase = silicate (S), black= pores. Intragranular precipitate chromites =C2 and intergranular precipitate chromites = C3. (b) Chrome-magnesite A showing bright phase= chromite (C1), intragranular chromites precipitate =C2 and intergranular precipitate chromites = C3 and C4, gray phase = magnesia (periclase P), black= pores.

4.3.2 Microstructural Changes in high temperature SO_2-O_2 Gas mixtures

In refractories exposed to SO_2-O_2 gas mixtures the phase compositions, microstructures developed are demonstrated in Figures 4.18 to 4.21. The microstructure of the chrome-magnesite A (Figure 4.18a) and chrome-magnesite D50-C5 (Figure 4.18b) refractories showed formation of calcium sulfate in reaction conducted for two weeks, at 1350°C. In Figure 4.18a observed similar characteristics to the structure heated in oxygen atmospheres at 1350°C (Figure 4.8) were shown. The reactions involved dissolution, reorganization and redistribution of the components and these changed the microstructure of the refractory. The dissolution of magnesia spinels caused separation of the chromite and magnesia minerals, and promoted porosity within and around the grains. The separated secondary chromite migrated to the grain boundaries, aggregated, and formed coarse chromite grains. The aggregation of secondary chromites within magnesia spinels resulted in fine chromite grains surrounded by magnesia matrix, indicating diffusion promoted precipitation. The altered chromite grains and magnesia spinel with fine iron oxide precipitates appeared weakened with high intergranular porosity within the grains, and interconnected porosity and voids within the structure. However, no sulfate phases were observed in both refractories in observations that were consistent with the predominance area diagrams in Figure 2.5, and 4.12 to 4.13, for $MgSO_4$ formation at 1350°C within the oxygen and sulfur dioxide pressures used in the experiments, as indicated in the diagrams. In Figure 4.18b, the dissolution of phases that resulted in altered chromite grains with frail structure occurred, but structural characteristics similar to the original structure (Figure 4.3b) showing varying crystal size of magnesia grains and primary chromite grains was maintained. However, at high magnification, the magnesia-aluminate spinels found within the chromite grains diffused and chromite precipitates within the small magnesia grain aggregates occurred. There was no sulfate phase observed, indicating unreactivity of chrome-magnesite D50-C5 with sulfur-bearing gases as in other refractories.

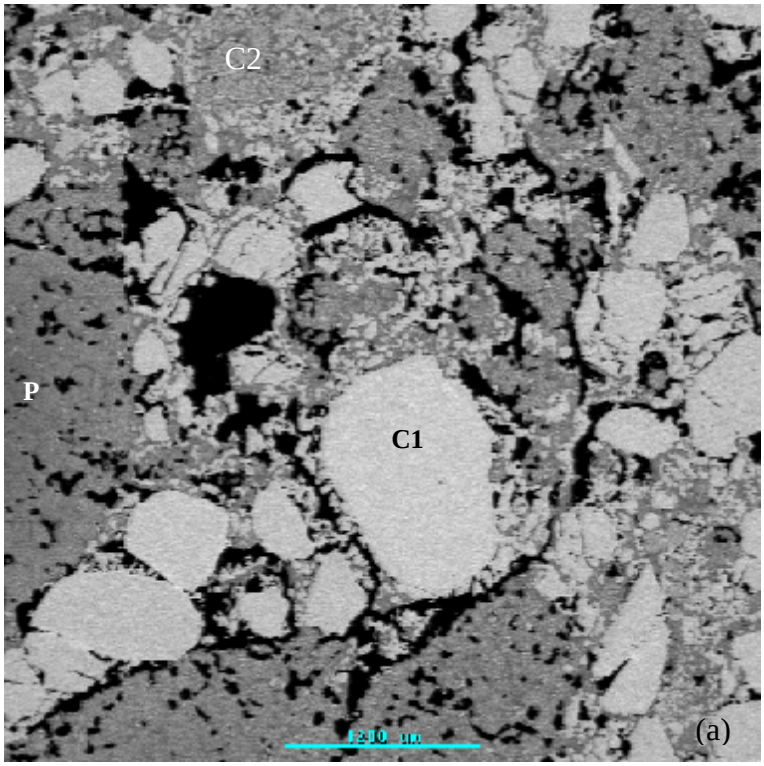
Figure 4.19 showed the microstructure of magnesite refractory and the structure developed corresponded to the structure (Figure 4.13) reacted in SO_2-N_2 gas mixtures at 1350°C. The calcium sulfate formed around the large magnesia grains and along grain, boundaries between the small magnesia grains, and no magnesium sulfate occurred, agreeing with the combination gas pressures marked in the predominance area diagrams of Ca-S-O and Mg-S-O compound systems, in Figure 2.5, 4.10 to 4.13. The tricalcium silicate found within the magnesia grains (Figure 4.1) migrated to the grain boundaries, and in presence of sulfur-bearing gases, it reacted and formed two new phases, illustrated as the $CaSO_4$ and Mg_2SiO_4. The observed CaSO4

occurred at the expense of the CaO contained in the silicate phases, while silica suggested to have combined with magnesia. The analysis of the calcium sulfate gave 58.17 wt% CaO and 41.83 wt% SO_3. Porosity occurred as both isolated intragranular porosity and large interconnected voids resulting in structure that showed large magnesia grains surrounded by fine magnesia aggregates with minor magnesia-magnesia contacts. Figure 4.20 shows the microstructure of magnesite-chrome brick 1, where the dissolution of chromite grains, development of secondary spinels and an open porous structure with even pore distribution were evident. In this structure, considerable intergranular porosity resulted in a structure that showed a collective mass of aggregated grains, with few magnesia spinels developed found within the mass. In some magnesia grains chromite secondary spinels developed resulted fine precipitates, while in smaller magnesia grains chromite precipitates indicated was restricted only to the grain boundaries, indicating differences in diffusion mechanisms within the grains in a processes that resulted in cracks and pores formation. The developed magnesia spinels showed uniform distribution of secondary chromite precipitates. The secondary iron oxide precipitates occurred mainly within the small magnesia grain aggregates and within the cracked grains. At high magnification, chromite grains had angular structures associated with silicate phases that were identified as monticellite. The composition of the chromite grains was similar to magnesite-chrome D50-C5 chromite grains with MgO, Fe_2O_3, Al_2O_3 and Cr_2O_3 having 24.4 wt%, 5.9 wt%, 22 wt% and 47.71 wt%.

In Figure 4.21a, magnesite-chrome D60/100, the major changes observed were the redistribution and reorganization of chromite precipitates within the magnesia spinels, and the increase in grain size. The secondary chromite grains between the large magnesia spinels occurred as fine aggregates, but large grains occasionally occurred. The diffusion processes indicated by the secondary chromite precipitates from the dissolved magnesia spinels and magnesia spinels resulted in crack propagation within the developed phases and pore structure appeared to have increased. The secondary chromite precipitates occurred mainly as intragranular precipitates and very few intergranular continuous precipitates. The structure developed by the secondary spinel aggregates around the large grains resembled that of magnesite-brick 1 (Figure 20b), with considerable intergranular porosity and fine secondary chromite grains. There were no observable blocky intergranular precipitates as observed in original structure (C3 in Figure 4.4a), indicating structures possibly due to dissolution and redistribution due to diffusion processes, which promoted direct-bonding but caused increased pore structure and crack formation. Voids occurred between the neighboring spinel phases, indicating possibly effects of diffusion and

volume changes. Formation of isolated pores within the magnesia spinels demonstrated the migration of chromite and caused volume changes. The observed crack formation and micro-fissures within the refractory were most likely due to the volume changes indicating differences in mass transfer at the interfaces between solid solutions, which occurs on cooling. Silicates formed as forsterite occurred mainly at the grain boundaries in magnesia-chromite solid solutions and were associated with growing chromite spinel structures.

In Figure 4.21b, the microstructure of magnesite-chrome brick 2 indicated that redistribution and reorganization of chromite precipitates within the magnesia spinels resulted in major structural changes. The magnesia spinels and the secondary chromite precipitates observed in original structure appeared to have increased pore structure observed as micro-fissures and crack propagation developed. The diffusion processes indicated frail, weakened structures even with the large chromite grains with magnesia resulting in increased intragranular porosity. Large magnesia grains with inherent iron oxide solid solutions around the grain boundaries showed developed cracks within the grains, while the interior of the grains appeared to have high magnesite content. The results indicated major structural changes that occurred by dissolution of secondary chromites and disintegration of the primary chromites. Cracks and micro-fissures formed indicated volume changes in chromite grains, where a considerable amount of porosity occurred. The observed unreactive nature of forsterite (Mg_2SiO_4) and monticellite ($CaMgSiO_4$) silicate phases suggested differences in structural form, which affected the release of reactive oxides (CaO and MgO), as seen in tricalcium silicate in magnesite. In general, in all the examined magnesite-chrome and chrome-magnesite refractories the high temperatures result in redistribution of the chromite within the magnesia. The chromites reunite into secondary crystals followed by a grain growth. This facilitates diffusion promoting appreciable dissociation of the components, forming energy stable phase compositions with minimum surface energy acquired at equilibrium. The phase composition formed, the type, the structure, and the development of the new phases vary greatly with the composition of the original state of the refractory components. The technological factors experienced during production, especially temperature, determine the resulting structures.



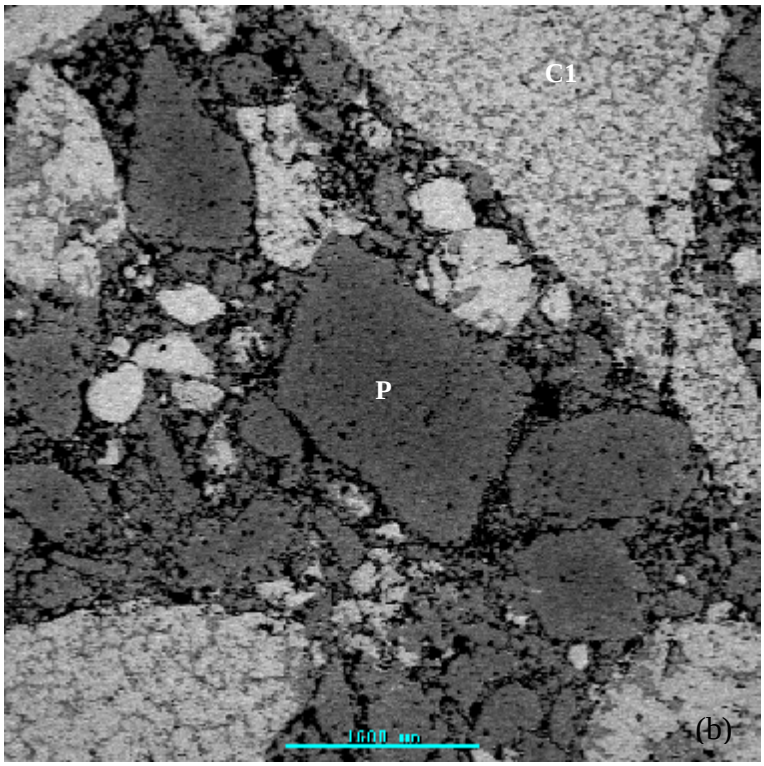


Figure 4.18. SEM-BSE micrographs of (a) Chrome-magnesite A reacted in SO_2-O_2 gas mixture at 1350C, showing gray phase = magnesia (periclase P), black= pores. Intragranular precipitate chromites =C2. (b) Chrome-magnesite D50-C5 showing bright phase= chromite (C1) with discontinuous magnesium spinel pockets, gray phase = magnesia (periclase P), black= pores.

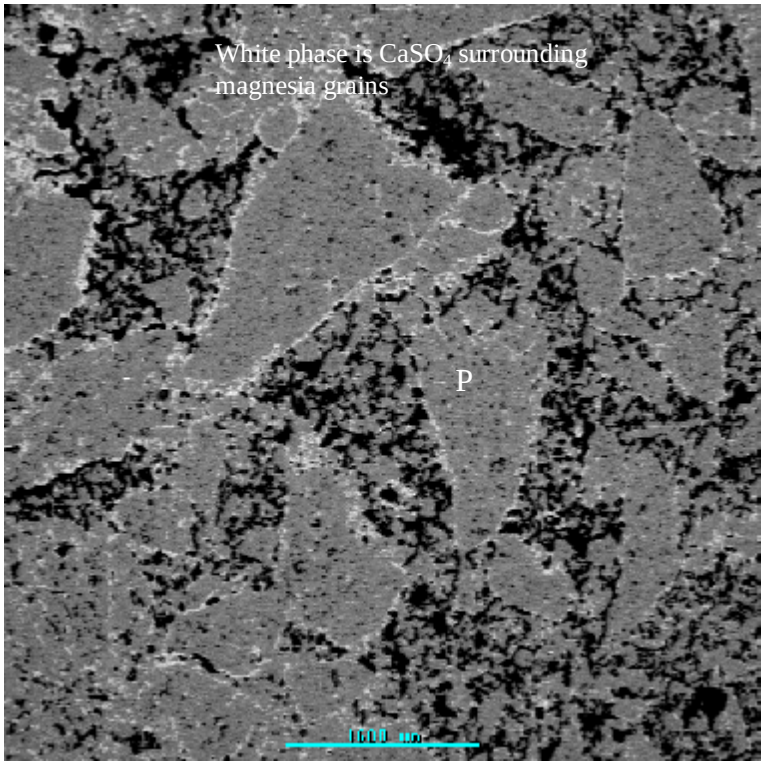


Figure 4.19. SEM-BSE micrograph of the (a) magnesite reacted in SO_2-O_2 gas mixture at 1350C, showing calcium sulfate forming at the grain boundaries. The gray phase = magnesia (periclase P), black= pores and white phase = $CaSO_4$.

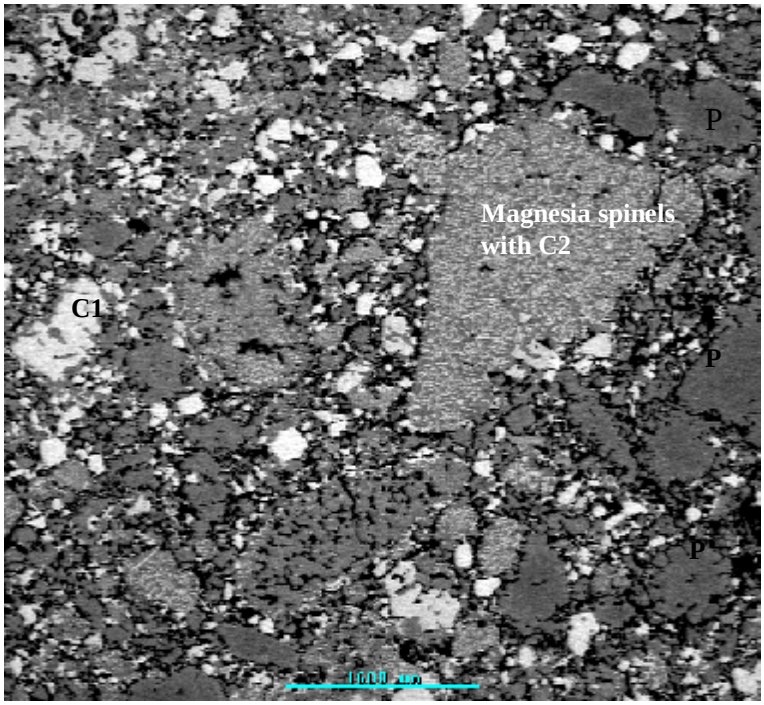


Figure 4.20. SEM-BSE micrograph of Magnesite-chrome brick 1 reacted in SO_2-O_2 gas mixture at 1350C, showing bright phase= chromite (C1), intragranular precipitate chromites =C2, gray phase = magnesia (periclase P), black= pores. .

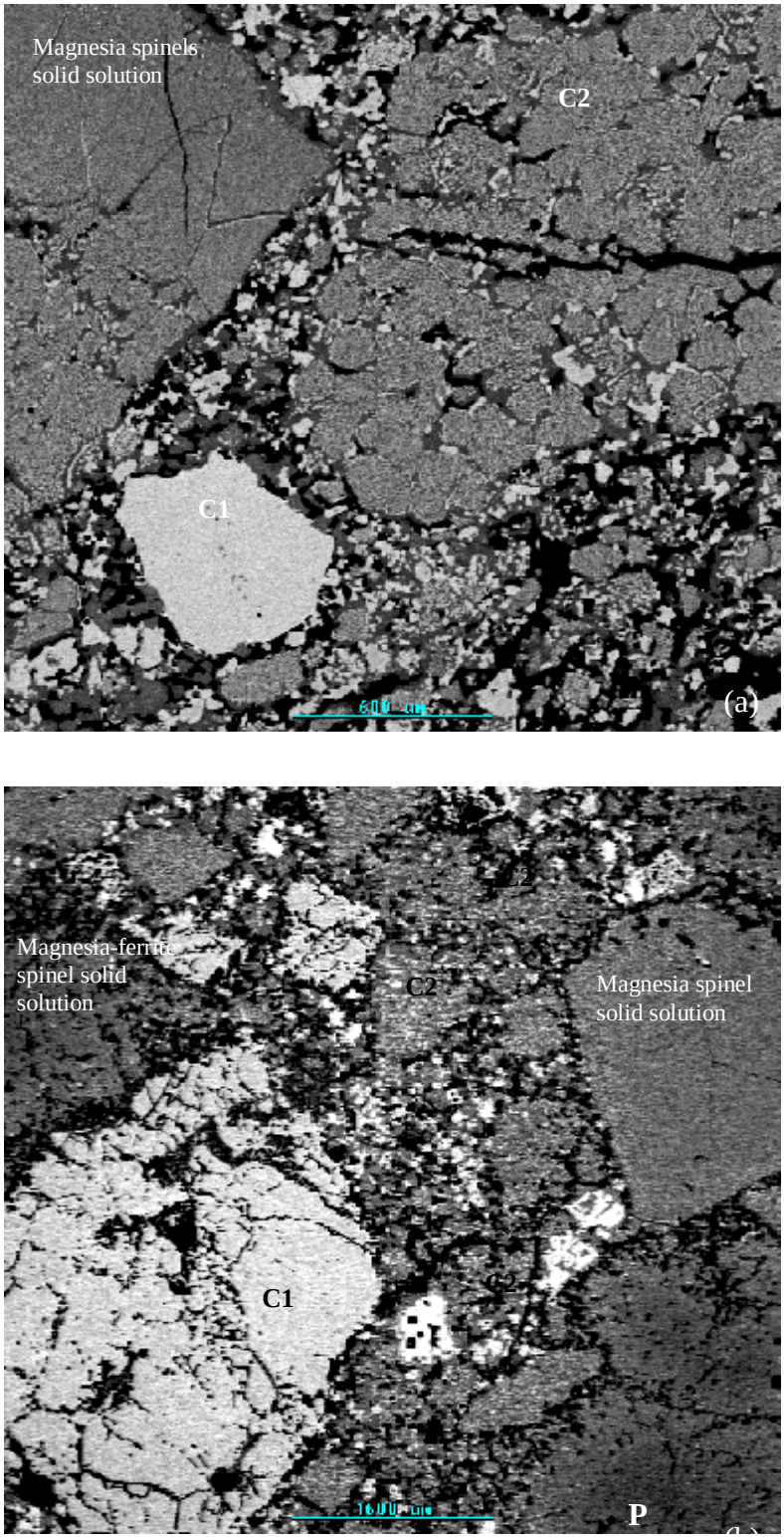


Figure 4.21. SEM-BSE micrographs of (a) magnesite-chrome D60/100 reacted in SO_2-O_2 gas mixture at 1350C, showing formation of magnesia-chromite solid solutions. The gray phase = magnesia (periclase P), bright phase = chromite (C1), (C1), intragranular precipitate chromites = C2, black= pores. (b) magnesite-chrome brick 2 showing disintegration of chromite grains and dissolution of chromite precipitates. The bright phase= chromite (C1), gray phase = magnesia (periclase P), black= pores.

4.3.3 Microstructural changes in low temperature SO_2-N_2 gas mixtures

At low temperatures reactions were conducted at 700°C and the microstructural results are shown in Figure 4.22 to 4.25. The microstructure of the magnesite refractory shown in Figure 4.22a indicated formation of $CaSO_4$ along the grain boundaries. The calcium sulfate formed resulted in irregular and discontinuous crevices at the surface of the grains. The sulfate phases formed comprised of magnesium sulfate ($MgSO_4$) and calcium magnesium sulfate ($CaMg_3(SO_4)_4$). The formation of $MgSO_4$ at 700°C, at the combination of oxygen and sulfur dioxide used in the experiments was consistent with predominance area diagram as indicated in Figure 2.5, 4.12 to 4.13. The $MgSO_4$ formed occurred as collective masses of particles of a spongy form, while the $CaMg_3(SO_4)_4$ formed plate-like structures identified to be concentrated with sulfate (SO_3). The surfaces of the grain boundaries showed ridged structures that had shallow grooves and voids forming crevices between them that were filled by thin layers of sulfate products not shown to have penetrated through the grains. Figure 4.22b shows the microstructure of the refractory powdered pellet of magnesite where the $MgSO_4$ formed occurred as continuous spongy form having grainy structures, which appeared two phased, but actually had minor porosity. The $CaMg_3(SO_4)_4$ plate-like structures identified had varying amounts of calcium oxide and were elongated and occasionally found within the spongy form material. The large magnesia grains showed no chemical reaction with the gases indicating unreactivity of dense magnesite, even at low temperatures as shown in the refractory structure in Figure 4.22a. The structures indicated that reaction occurred mainly at the surface of the grains possibly through infiltration within the porosity that indicated open voids on the surface of the grains and along the grain boundaries.

Figure 4.23 presents the microstructure of laboratory magnesium oxide powdered which the structure indicated was saturated and transformed to $MgSO_4$. The magnesium sulfate formed as a collective mass of particles of a spongy structure and irregularly shaped and plate-like structures. The spongy material showed solid solution with minute white precipitates of unreacted MgO distributed evenly. The occasional spongy dark grey phase and plate-like structures had high concentration of sulfur trioxide (SO_3) resulting in non-uniform sulfate distributions. The microstructure of refractory powdered pellet of magnesite-chrome refractory showed in Figure 4.24 indicated formations of $MgSO_4$ and $CaMg_3(SO_4)_4$ that occurred randomly. Magnesia grains with secondary chromite precipitates and fine magnesia aggregates with chromite solid solutions were observed. In addition to the spongy $MgSO_4$ and $CaMg_3(SO_4)_4$ plate-like structures observed, sulfate mixtures containing secondary spinels of Cr_2O_3, Al_2O_3 and

Fe_2O_3 products formed. The sulfate mixtures occurred with secondary spinels, and varying amounts of MgO and to a less extent CaO, indicating phases resulting from the balance between the diffusion processes and sulfation reaction with silicates and magnesia spinels. The $CaMg_3(SO_4)_4$ with irregular plate-like structures of non-uniform distributions seen in Figure 4.22a were consistent in this structure. There was no chemical reaction between the secondary chromites and the sulfur-bearing gases indicating that the sulfate reaction occurred mainly with the magnesia.

Figure 4.25 shows microstructures of magnesite-chrome and chrome-magnesite, resulted in sulfation reactions that occurred mainly along the grain boundaries Chrome-magnesite (Figure 4.25a) spongy form of $MgSO_4$ and $CaMg_3(SO_4)_4$ plate-like structures and sulfate mixtures containing secondary chromites as reaction products formed. The chemical reaction along the grain boundaries occurred with silicate phases and magnesia matrix, and resulted in the formation of ridges and shallow grooves having voids between them, as shown at the grain boundary surfaces. These discontinuities were similar to those seen in magnesite (Figure 4.22a) and occurred on the surface grain boundaries of the large chromite and some magnesia spinel grains. The chemical reaction with the magnesia spinels was restricted to the magnesia matrix surrounding the magnesia spinels. The $CaMg_3(SO_4)_4$ plate-like structures formed at the grain boundaries and dissolution resulted in combined mixtures of sulfate with secondary spinels that were difficult to characterize as they consisted of a mixture of sulfate phases with different Mg: Si: Ca: Al and occasionally Cr ratios. The mechanism of formation observed in sulfate structures suggested that diffusion processes occurred, and consequently sulfation with the phases formed for equilibrium conditions that are determined by temperature as indicated in the predominance area diagrams. In the microstructure of magnesite-chrome (Figure 4.25b) the results of dissolution of the magnesia spinels, caused aggregation of secondary chromites and fine magnesia-chromite solid solutions that surrounded magnesia spinels with secondary chromites precipitates. The sulfation products were formed along the grain boundaries with magnesia matrix that surrounded the magnesia spinel. The chemical attack occurred mainly along the grain boundaries with magnesia matrix forming $MgSO_4$ and sulfate mixtures. The results suggest that sulfate penetrates preferentially into the refractory along the grain boundaries and accumulates at magnesia/sulfate interface forming a magnesia/gas interface that becomes saturated with sulfates having varying amounts of SO_3 composition.

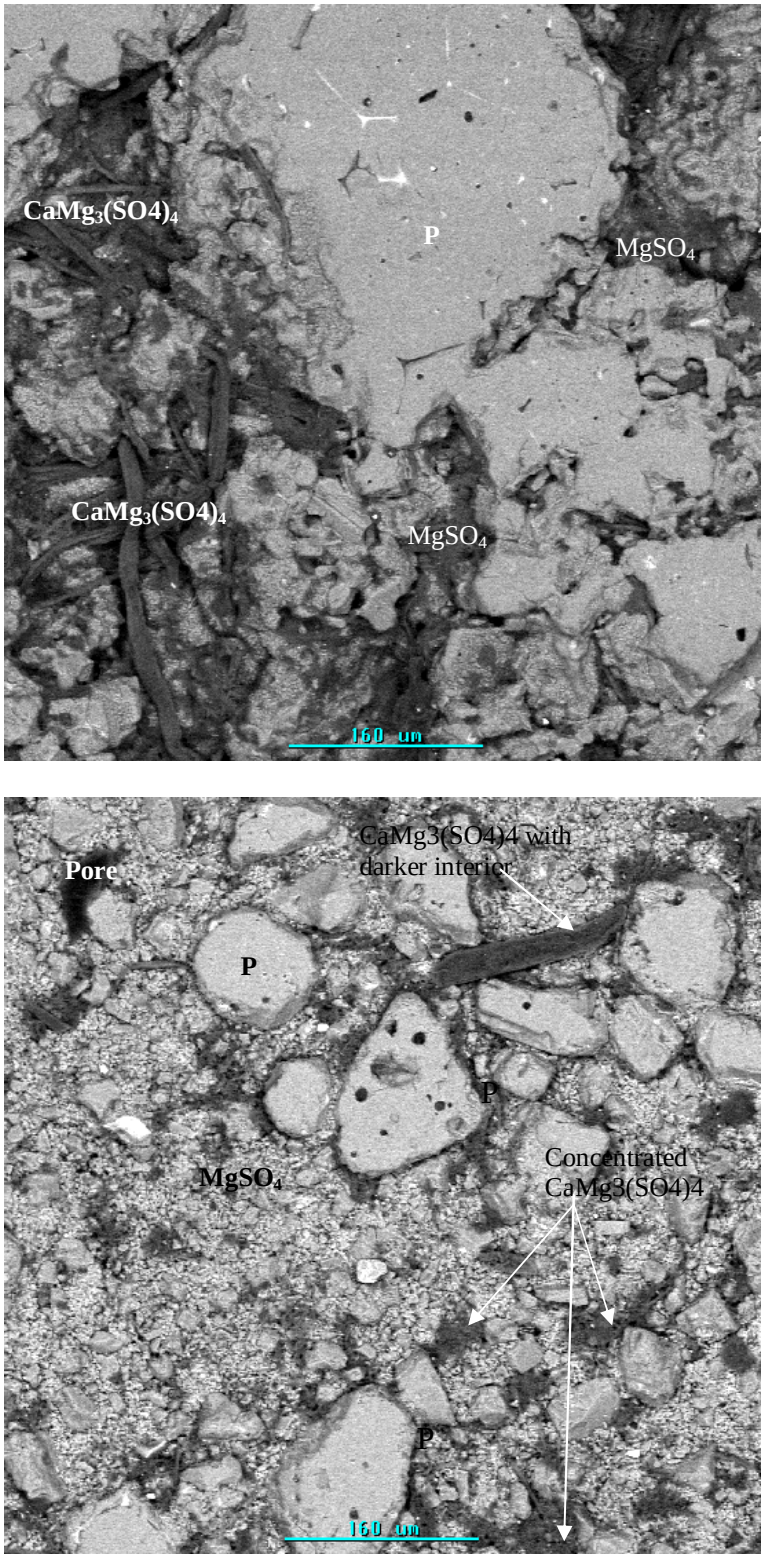


Figure 4.22. SEM-BSE micrographs of (a) magnesite refractory reacted in SO_2-N_2 gas mixture at 700°C, showing magnesium sulfate forming along the grain boundaries. (b) Refractory powdered pellet of magnesite showing heterogeneous reaction of magnesia. The grey phase = magnesium sulfate, light grey phase = magnesia (periclase P), black= pores and bright phase = silicate.

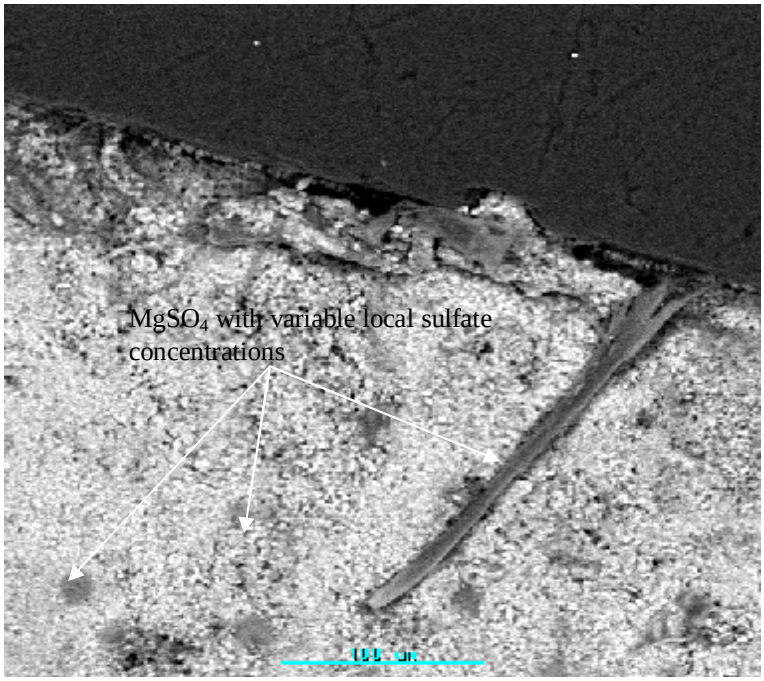


Figure 4.23. SEM-BSE micrographs of (a) laboratory magnesium oxide powdered pellet reacted in SO_2-N_2 gas mixtures at 700°C, showing a collective mass of particles of a continuous spongy sulfate structure. The dark grey phase = magnesium sulfate high in SO_3 concentration, light grey phase = magnesia sulfate, white precipitates = MgO, black= pores.

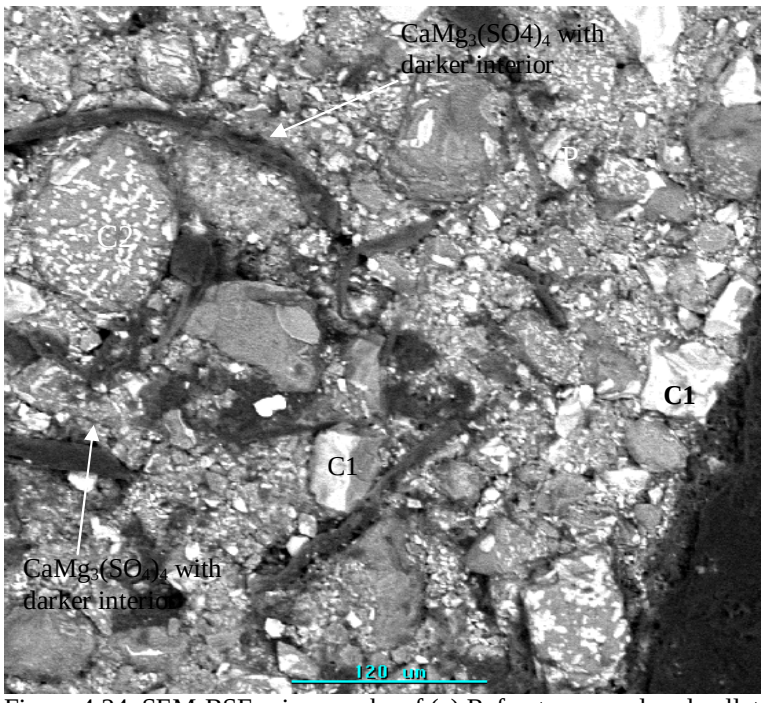


Figure 4.24. SEM-BSE micrographs of (a) Refractory powdered pellet of magnesite-chrome refractory reacted in SO_2-N_2 gas mixtures at 700°C, showing the sulfate phase. The dark grey phase (needles) = calcium magnesium sulfate, black= pores, bright phase = chromite (C1), intragranular precipitate chromites = C2, grey phase = magnesia.

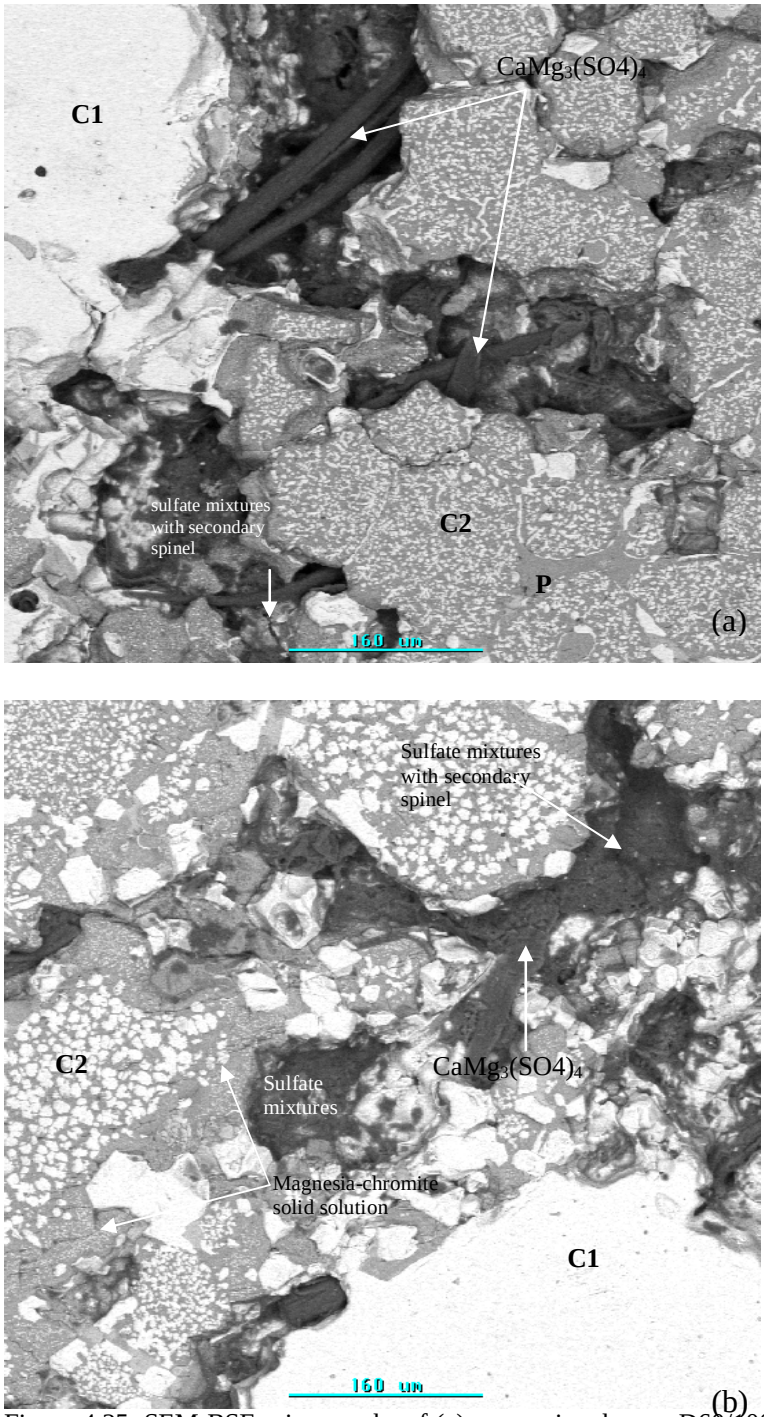


Figure 4.25. SEM-BSE micrographs of (a) magnesite-chrome D60/100 reacted in SO_2-N_2 gas mixture at 700°C, showing reaction of magnesia matrix with sulfur-bearing gases. The gray phase = magnesia (periclase P), bright phase = chromite (C1), intragranular precipitate chromites = C2, black= pores. (b) magnesite-chrome D60/100 showing development of sulfate mixtures with secondary spinels along the magnesia spinel grain boundaries. The bright phase= chromite (C1), gray phase = magnesia (periclase P), black= pores.

4.3.4 Microstructural changes in low temperature SO_2-O_2 gas mixtures

At 700°C, in SO_2-O_2 gas mixtures reaction time was varied to establish the extent of reactions, and the effect of sulfur-bearing gases on the grain boundary reactions. The main purpose of the experiments was to draw attention to the structural differences encountered rather than to compare the grain sizes or particle sizes of the phases formed. Therefore, it would be noted from the examinations that the scale of some micrographs is different. The chemical reaction of the refractory components was observed in all the basic refractories examined and it occurred in the matrices. The grain boundary phases such as Mg-Ca-Si, Mg-Si, and MgO were the main reactants in the reactions between sulfur-bearing gases. Figure 4.26 presents the microstructures of the magnesite refractory, that resulted in complete infiltration by the sulfates products of $MgSO_4$ and $CaMg_3(SO_4)_4$, indicating severe reaction of the grain boundary components and crack formation. During the early stages of reaction at fourteen hours (Figure 4.26a), the microstructure showed sulfate mixtures of different Mg: Si: Ca ratios as sulfation products. The $MgSO_4$ and $CaMg_3(SO_4)_4$ formed collective masses of spongy material. Some of the sulfate phases appeared to have developed radially with structures opening outwardly. The refractory showed less reaction with the sulfur-bearing gases as some characteristics similar to the original refractory (Figure 4.1b) were for the most part preserved. At high magnification, the $MgSO_4$ plate-like structures (Figure 4.26b) formed occurred within the concentrated spongy material, and within $CaMg_3(SO_4)_4$ white minute phases were observed. After reaction for seven days, the result in Figure 4.27a showed the sulfation reactions have progressed in the refractory and the corroded surfaces of the magnesia grains had discontinuities forming shallow grooves and voids with varying sulfate layers.

Figure 4.27b presents the microstructure of magnesite after reaction for two weeks, showing an advanced sulfation reaction resulting in structural destruction of the magnesia grains along the grain boundaries and crack formation. The reactions resulted in volume expansion and the refractory showed numerous fissures and spalling of the magnesia grains. The microstructure resulted in small magnesia grains disintegrated into fine magnesia particles, which reacted to form $MgSO_4$ and mixed with $CaMg_3(SO_4)_4$. The combined mixture of $MgSO_4$, $CaMg_3(SO_4)_4$, MgO and silica showed a collective mass of spongy material occurring within the refractory grain boundaries. The grain boundary surfaces of the observed large magnesia grains showed ridged structures that were reduced in size, corroded by the resulting sulfation that took with it

some magnesia and incorporating it into the sulfate as a mixture found along the grain boundaries. The products resulted in sulfate mixtures of spongy material that surrounded the large magnesia grains. The chemical reaction with the magnesia grains and grain boundary silicates was highly developed and the elongated $CaMg_3(SO_4)_4$ plate-like structures were developed within the sulfates. For the detected $CaMg_3(SO_4)_4$ plate-like structures, the analyses gave 35.47 wt% MgO, 53.49 wt% SO_3 and 10.64 wt% CaO, and the sulfate mixtures of different Mg: Si: Ca ratios formed, indicated 16.35 wt% MgO, 13.30 wt% SO_3 and 40.76 wt% CaO and 29.59 wt% SiO_2. Crack propagation occurred across the magnesia grains (shown by arrows). The elongated sulfate structures that precipitated from the liquid sulfate (i.e. did not result form gas-solid reaction at low temperatures) were mixed with the spongy material. The refractory showed loosening of the bond structure as components reacted with sulfur-bearing gases.

Figure 4.28 shows the microstructure of chrome-magnesite A refractory at different reaction times and magnifications. There were no significant changes observed in the microstructure of the refractory after fourteen hours of reaction time. The $MgSO_4$ formed occurred mainly within the grain boundaries and filled up the open pores, cracks, and fissures. In Figure 4.28a, the reaction of the magnesia matrix surrounding magnesia spinels resulted. In the crevices shown at surface of the chromite and magnesia spinel grains, thin layers of sulfate and few sulfate concentrated areas formed. Sulfate formation occurred without any observable corrosion of the refractory components. The grain boundaries of magnesia spinel near the magnesia matrix dissolved and the suggested chemical reaction with magnesia resulted in sulfate mixtures containing secondary spinels having different composition of dissolved iron oxide, chromite, and alumina. Magnesium sulfate formed as a spongy form material. The structural changes observed in the refractory were due to the rearrangement and redistribution of the chromite precipitates within the magnesia-chromite spinels.

In Figure 4.28b, after reaction for two weeks, the resulting dissolution of the magnesia spinels and resulting sulfation reaction with magnesia, and silicate along the grain boundaries advanced. Sulfate mixtures containing different Mg: Si: Ca: Cr: Al ratios formed. Towards the grain boundaries, small chromite grains having angular structures surrounded by silicates occurred. The dissolution of the magnesia spinels grains at the boundaries was more noticeable with some of the dissolved chromite secondary spinels occurring within the sulfate mixtures. This suggested that magnesia spinel grains loosened and the sulfate mixture of $MgSO_4$ and secondary

chromites formed. The resulting surface boundaries of the dissolved magnesia spinels show disengagement resulting in ridged structures that appeared to have different layers which indicated dissolution towards the grain boundaries (as indicated with arrows at the bottom left of micrograph in Figure 4.28b). The analyses gave 13.75 wt% Cr_2O_3, 42.43 wt% SO_3 and 33.82 wt% MgO, 5.67 wt% CaO and 4.33 wt% SiO_2 for the sulfate mixtures formed directly between magnesia-chromite spinels. Between chromite and magnesia, spinel grains presence of Fe_2O_3 and Al_2O_3 were demonstrated and the compositions of sulfate mixtures varied. Analyses indicated a significant decrease in MgO content to between 14 and 18 wt%, while CaO and SO_3 were shown to be consistent. In parts where the reactions occurred between the chromite and magnesia grains, discontinuities of non-uniform sulfate were evident. The chromite grains and magnesia contained in the magnesia-chrome spinels showed no chemical reaction with the sulfur-bearing gases. Therefore, the sulfate reaction with the spinels was confined to the grain boundaries and the products occurred as sulfates with fine sesquioxides solid particles.

In the microstructure of chrome-magnesite D50-C5 in Figure 4.29, sulfation reactions led to major secondary products forming, while diffusion processes resulted in dissolutions and major structural changes. The sulfation reactions concerned mainly the magnesia spinels of $MgFe_2O_4$, $MgAl_2O_4$, and a considerable amount of sulfate mixtures with secondary spinel mixtures could be observed. After fourteen hours (Figure 4.29a), the reactions resulted in sulfation and spinel dissolution that occurred mainly towards the surface edge of the sample formed layer around the sample, and mixtures of magnesium-aluminum-sulfate and calcium-magnesium-aluminium-sulfate formed with Cr_2O_3, Fe_2O_3, and SiO_2 but to a less extent formed. The magnesium-aluminum sulfate mixtures suggested formed with the magnesia aluminate spinels from the discontinuous pockets of chromite grains, while calcium-magnesium-aluminum sulfates observed could be formed with dissolved phases from chromite grains.

Surrounded by the sulfate mixture chromite and magnesia spinel (mainly $MgFe_2O_4$) grains showed in the original structure (Figure 4.3) were conserved, indicating a possibly low gas infiltration as reactions were confined to the outer edge of the sample. However, porosity, fissures, and crack formation resulted within the grains. After seven days (Figure 4.29b), $MgAl_2O_4$ dissolution from the chromite resulted, but sulfation resulted mainly from $MgFe_2O_4$ reactions and was confined to the grain boundaries. However, there was no indicated disengagement in the magnesia spinels ($MgFe_2O_4$, $MgCr_2O_4$) as indicated in other refractories

(Figure 4.28b), indicating the unreactive nature of magnesia contained in the newly formed spinels. In the experiments conducted for two weeks (Figure 4.29c), the reactions with the refractory samples advanced, resulting in corroded chromite grains. The plate-like structures observed within the sulfate mixtures were prominent. The irregular and discontinuous crevices at the grain boundary surfaces of the chromite grains filled with non-uniform sulfate mixtures were more evident, where the open structure of the altered grains opened path for diffusion route of the gases and promoted sulfation of the magnesia spinels within the pockets.

Figure 4.30 shows the microstructure of the magnesite-chrome D60/100, which resulted in less sulfation products and some dissolution of spinels after long reaction periods was preserved. After fourteen hours (Figure 4.30a), the direct bonded structure of the original refractory was conserved and sulfate phases formed within the pores indicating relatively low infiltration of the gases. Contrary to the other refractories, sulfate formation in the refractory occurred randomly rather than at the grain boundaries, but mainly within the pores as pore space fillings. The sulfates formed were magnesium sulfate and some sulfate mixtures with few secondary spinels could be observed. Although some spinels occurred as sulfate mixtures, the results indicated dissolution occurred to a less extent and mainly the $MgFe_2O_4$ and less Cr_2O_4 or Al_2O_4 could be observed in the mixtures. The magnesium sulfate formed within the pores as pores space filling was the spongy form of collective mass of sulfate that indicated nucleation development of sulfate as magnesia possibly diffused from the surrounding grains to the pores. There were no observable silicates formed between the magnesia-chromite structures.

After seven days (Figure 4.30b), dissolution of the magnesia spinels resulted in disruption of the grains and displacement of the blocky secondary chromites (C3 in Figure 4.4a), and the aggregation of secondary chromite precipitates coming together to form small chromite grains could be observed. The displaced blocky secondary chromites (C3) appeared with angular surface boundaries that were usually associated with silicates, and those found along grain boundaries sulfate mixtures with silica were found. Sulfation reactions occurred with the magnesia exposed to the pore areas and some magnesia grains found within the refractory. After two weeks (Figure 4.30c), the exposed chromites precipitates formed irregularly large grains and the developed chromite structures associated with silicates were evident giving them angular structures. The interesting features of the sulfates formed was that even though there was over-stoichiometry of SO_3 relative to MgO reacted, in the $MgSO_4$ formed as pore space filling, there

was no observed plate-like structure. However, because there was no $CaMg_3(SO_4)_4$ observed the results of $MgSO_4$ formed indicated effect of CaO to the sulfate and reactions resulted from diffusion of magnesia from the spinels to react in the pores and deposition accrued.

Figure 4.31a presents the microstructure of magnesite-chrome brick 2, that resulted in the sulfation reaction of grain boundary components forming $MgSO_4$ and $CaMg_3(SO_4)_4$ with the magnesia matrix and silicate found surround the magnesia spinels. The reaction of magnesia matrix forming $MgSO_4$ could be observed between the magnesia-chromite spinel structures. The $MgSO_4$ disintegrated into sulfate aggregates that surrounded the spinel grains, but some sulfate mixtures having secondary chromites and silica occurred. The $MgSO_4$ formed resulted in disintegrated granular structure that led to crack formation and porosity. After two weeks (Figure 4.31b), the resulting structures from the dissolved spinels led to aggregation of chromite precipitates within the magnesia grains forming small grains (bottom left). The sulfate phases formed along the grain boundaries showed three different forms, the radial outward growth (seen at the top left of the micrograph),the sulfate mixtures occurring with spinels and the spongy form magnesium sulfate found within the altered and disintegrated chromite grains(top right of the micrograph). The sulfates phases that appeared to have developed radially with structures opening outwardly seen were also consistent in Figure 4.29a, as surfaces protruding a small plate-like structures.

In Figure 4.32a, the magnesite-chrome brick 1 microstructure resulted in spalling of the magnesia spinel grains and sulfates formed along the grain boundaries, after seven days of reaction. The aggregation of secondary chromite precipitates within the magnesia grains seen in Figure 4.31b and the disengagement of the magnesia spinels seen in Figure 4.28b could be observed in this refractory. The disengagement or loosening of the spinels at the grain boundaries resulted in occurrence of spinels as sulfate mixtures, and sulfates formed within cracked developed. After two weeks (Figure 4.32b), sulfates formed as both spongy form and plate-like elongated structures. The magnesia spinel ($MgFe_2O_4$) grains had completely disintegrated and magnesia resulting in reaction that led to spongy magnesium sulfate and sulfate mixtures that had secondary Fe_2O_3 spinels and some Cr_2O_3. The textural appearance of the described microstructure was coarse.

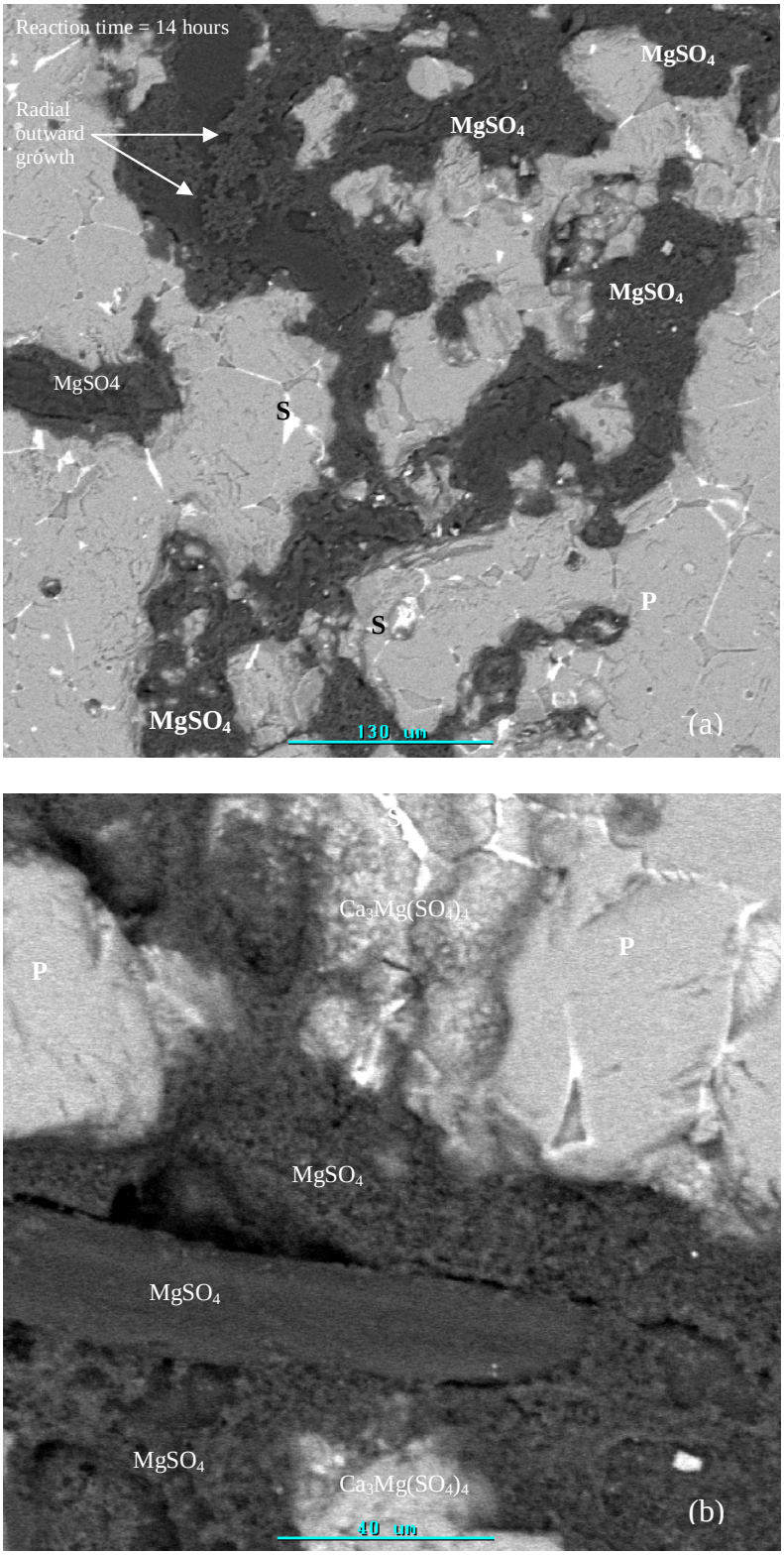


Figure 4.26. SEM-BSE micrographs of (a) magnesite refractory reacted for 14 hours in SO_2-O_2 gas mixture at 700°C. The dark grey porous phase = magnesium sulfate ($MgSO_4$), grey phase = magnesia, bright phase =Silicates (S), (b) magnesite refractory at high magnification, the dark grey phase (needles) = concentrated magnesium sulfate, light grey porous phase= calcium magnesium sulfate ($CaMg_3$ $(SO_4)_4$ and light grey phase =Silicates (S),

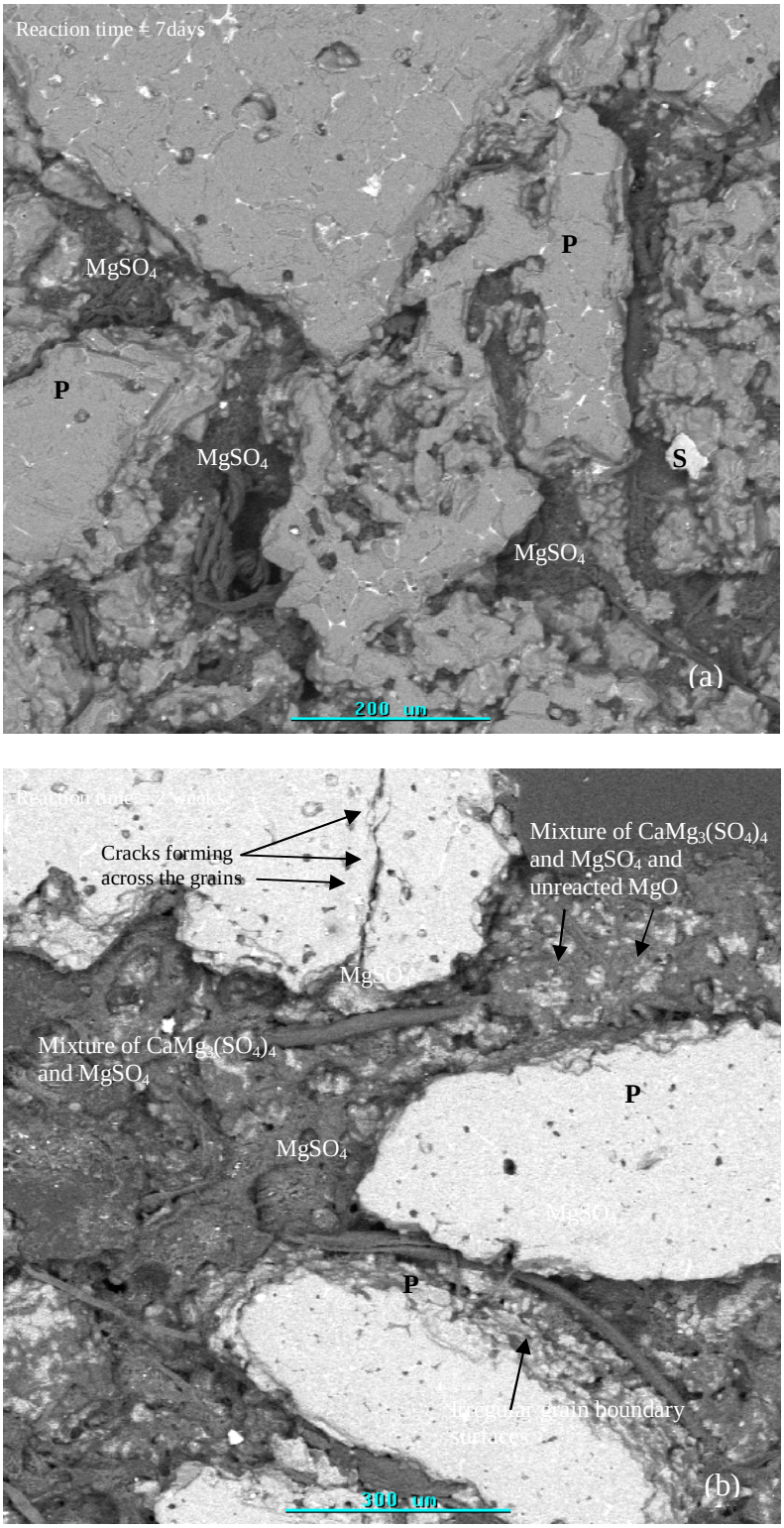


Figure 4.27. SEM-BSE micrographs of magnesite refractory reacted in SO_2-O_2 gas mixture at 700°C where, (a) after 7days, showing chemical reaction with the magnesia grains, The dark grey phase between grains = magnesium sulfate ($MgSO_4$), grey phase = magnesia (P), light grey phase =Silicates (S), (b) shows reaction after 2 weeks, showing crack formation, The dark grey phase along grains (needles) = concentrated magnesium sulfate, dark grey porous phase = magnesium sulfate, light grey porous phase= calcium magnesium sulfate ($CaMg_3$ $(SO_4)_4$.

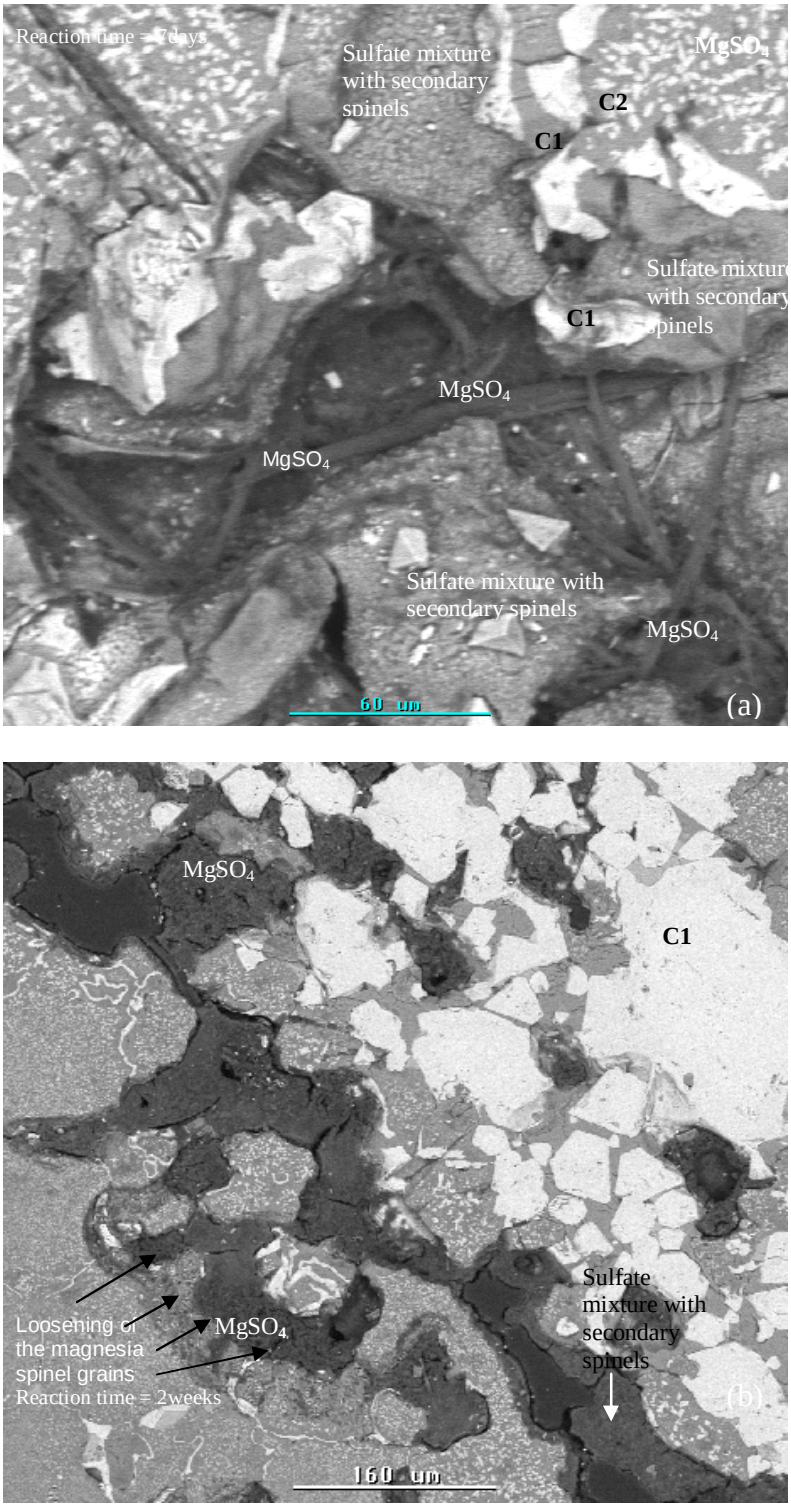


Figure 4.28. SEM-BSE micrographs of chrome-magnesite A refractory reacted in SO_2-O_2 gas mixture at 700°C where, (a) after 7days, showing chemical reaction with the magnesia matrix. The dark gray phase = magnesium sulfate, bright phase = chromite (C1), intragranular precipitate chromites = C2. (b) shows reaction after 2 weeks. The bright phase= chromite (C1), gray phase = magnesia sulfate, grey phase with light precipitates = sulfate mixture with secondary spinels.

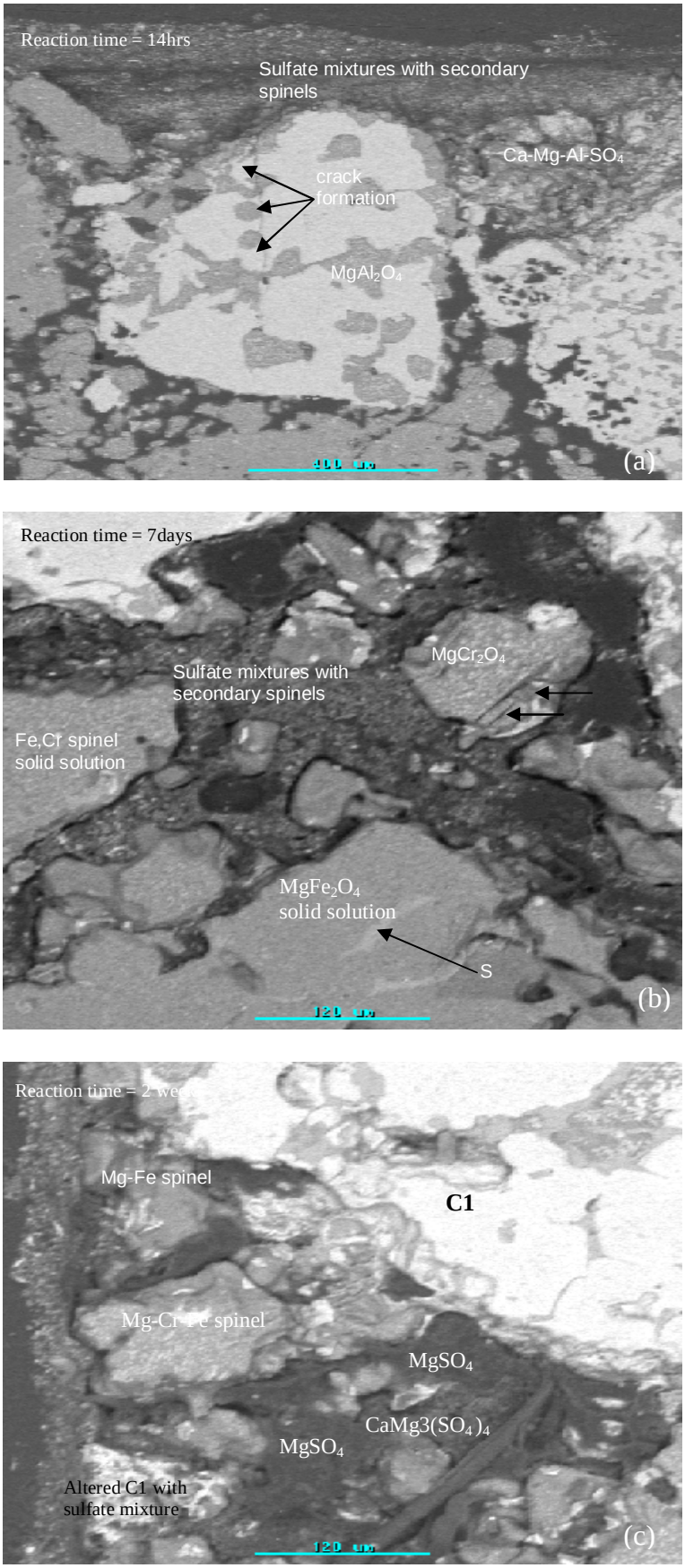


Figure 4.29. SEM-BSE micrographs of chrome-magnesite D50-C5 reacted in SO_2-O_2 gas mixture at 700°C where, (a) after 14 hrs, showing low gas infiltration and reactions forming at the boundaries, (b) after 7days, showing formation of magnesia spinel solid solutions and high gas infiltration. (c) after 2 weeks, showing elongated sulfate structure and spongy sulfate mixtures with secondary spinels.

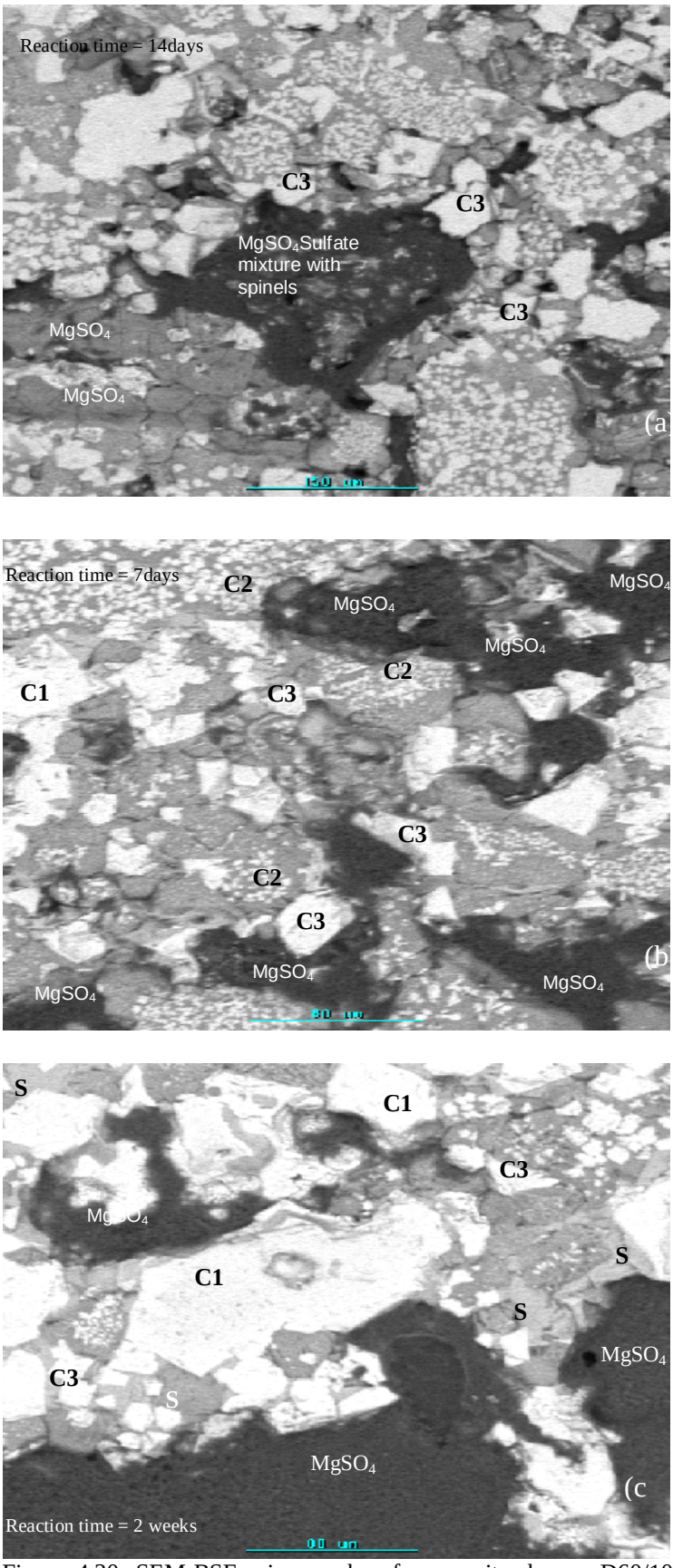


Figure 4.30. SEM-BSE micrographs of magnesite-chrome D60/100 reacted in SO_2-O_2 gas mixture at 700°C, (a) after 14hrs, and showing low gas infiltration reactions forming at the pores. (b) Shows dissolution of spinels, dark gray phase = magnesium sulfate, bright phase = chromite (C1), intragranular precipitate chromites = C2. (c) after 2 weeks, dark grey porous phase = magnesium sulfate, chromite forming large grains (C1), and light grey phase= silicate (S).

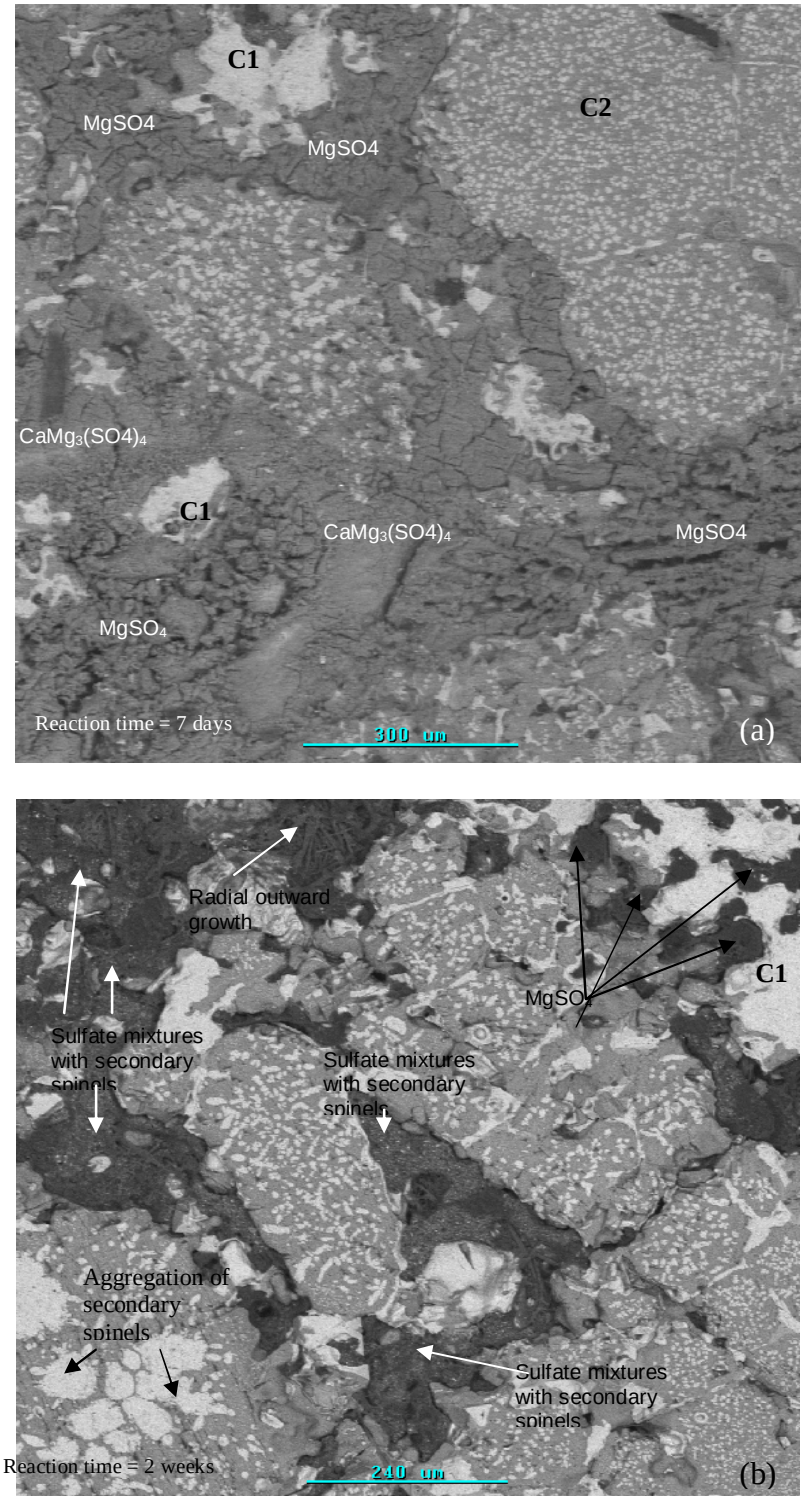


Figure 4.31. SEM-BSE micrographs of magnesite-chrome brick 2 reacted in SO_2-O_2 gas mixture at 700°C, (a) after 7days, showing reaction of magnesia matrix with gases forming sulfates. The disintegrated dark gray phase = magnesia sulfate, bright phase = chromite (C1), intragranular precipitate chromites = C2, black= pores, (b) after 2 weeks, showing dissolution of magnesia-chromite spinels and crack formation, development of sulfate mixtures with secondary spinels along the magnesia spinel grain boundaries. The bright phase= chromite (C1), gray phase = magnesia sulfate, grey phase with light precipitates = sulfate mixture with secondary spinels, and black = pores.

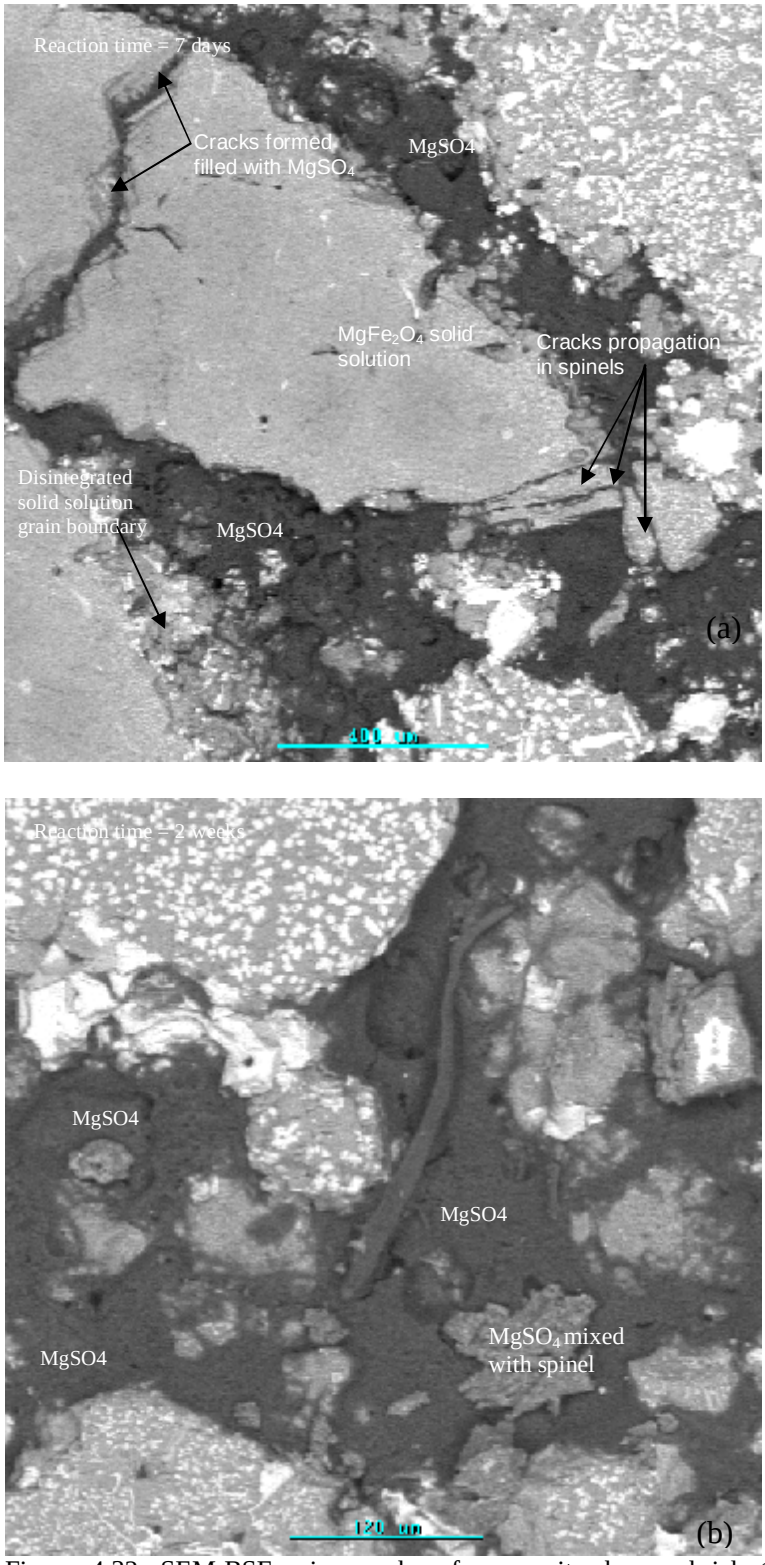


Figure 4.32. SEM-BSE micrographs of magnesite-chrome brick 1 reacted in SO_2-O_2 gas mixture at 700°C where, (a) after 7days, showing crack formation and dissolution of spinels. (b) after 2 weeks, showing disintegration and sulfation $MgFe_2O_4$ spinels.

4.4 Kinetic Effects- basic refractories as absorbents of sulfur-bearing gases.

For each refractory sample, the experimental results were converted to the ultimate conversion of the solid oxide (calculated for MgO as explained in section 3.10.1) and the effect of time and temperature was investigated. The conversions of the six different refractories exposed in SO_2-O_2 gas mixture at 700°C over a reaction time of eighty four hours is shown in Figure 4.33. The observed reaction profiles initially were high, but decreased with time. Magnesite-chrome brick 1 gave highest initial reaction conversions and chrome-magnesite A gave lowest, while other refractories gave equal reaction conversions initially. Chrome-magnesite A and magnesite-chrome D60/100 reactions profiles indicated lower conversions suggesting being less reactive than the other refractory types, based on the calculated MgO conversion to $MgSO_4$. The refractories were analysed for total sulfur and the increasing conversions with increasing time are shown in Figure 4.34 as percentage sulfur. The determined total sulfur increased over the reaction time and magnesite-chrome brick 1 and chrome-magnesite A gave highest and lowest total sulfur percentages, respectively.

The effect of temperature between 700°C and 1200°C on the sulfation reaction of different refractories was determined. The proportions converted to sulfate are plotted against time in Figures 4.35 to 4.40 for all basic refractories. The reaction extents increased with temperature, indicating that the conversion of the oxide within refractories increased within the studied temperature range. The reaction conversion profiles showed sigmoid relationships, and some linear behaviour that frequently occurred in disordered arrangement indicating complex processes. Based on the reaction profiles, the reaction behaviour in the basic refractories could be divided into three periods: the initial period in which conversion reaction occurred spontaneously at the oxide surface, followed by an intermediate period of adaptation to reaction conditions and transformations as the product was formed, and a final period in which the conversion reactions decreased gradually.

The changes in the reaction extents attributed to the intermediated period showed the effect of temperature on the refractory microstructure. This occurred most likely due to transformation of the oxide surface as a developed layer of product was formed. The reaction extents between 700 and 1000°C were highest at 900°C and lowest at 700°C, for the chrome-magnesite type refractories. Within the same temperature range, the reaction extents for the magnesite and magnesite-chrome type refractories were highest at 1000°C and lowest at 700°C. However, the

magnesite-chrome brick 2 was the exception with highest reaction conversions at 900°C. Chrome-magnesite A and magnesite-chrome D60/100 type refractories were also reacted at 1200°C and the reaction conversions were lower compared to all other temperatures of reaction examined.

Variations in gas mixtures were studied between 800°C and 1000°C, for the refractories that showed high reaction conversions when reacted in SO_2-O_2 gas mixtures at 700°C. The four refractories reacted in SO_2-N_2 gas mixtures were magnesite, CrMg D50-C5, MgCr brick 1 and MgCr brick 2 refractory and the reaction conversions are plotted against time in Figures 4.41 and 4.42. In the SO_2-N_2 gas mixture at total pressure of 1atm, the SO_2 and O_2 equilibrium partial pressures corresponded to 0.1998atm and 0.0036atm, respectively. The reaction extents showed a behaviour that is determined by the oxide conversion response of the refractories to sulphur-bearing gases in which the oxide converted to sulfate suggested to increase with time. At 800°C, MgCr brick 2 showed an accelerated conversion response in presence of sulfur-bearing gases indicated by high conversion reaction profiles, while in other refractories reaction profiles increased gradually. The variations of the refractory fraction converted with time in pure SO_2 atmosphere that had equilibrium pressure of 0.999atm are shown Figure 4.43 and 4.44. The conversion reaction extent showed a behaviour described by the gradual increase in sulfate formed and suggested to be dependent on temperature. At 800°C magnesite and MgCr brick 1 refractories presented a conversion behaviour, where the final period of the reaction was contrary to the normal behaviour (stationary decrease), was described by an increased conversion to sulfate. The inverted sigmoid behaviour was consistent with MgCr brick 1 at 1000°C.

The reaction extents showed the highest conversion for gas mixtures containing oxygen. The reaction extents indicated an increased conversion in relation to the sulfur-bearing gases and temperature over time, and were observed higher in pure SO_2 atmosphere. The effect of gas changes on the reaction conversion to sulfate showed a less pronounced effect than temperature. However, at 1000°C the conversion reaction extents in pure SO_2 were comparable to those observed in systems containing oxygen. It must be noted that it is impractical to determine the influence of individual gas species (SO_2, O_2, SO_3) in gas mixtures, because the changes in initial SO_2/O_2 ratio change the pressures of all three gas species. The kinetic relationships indicated that the reactions of the basic refractories with sulfur-bearing gases are quite complex.

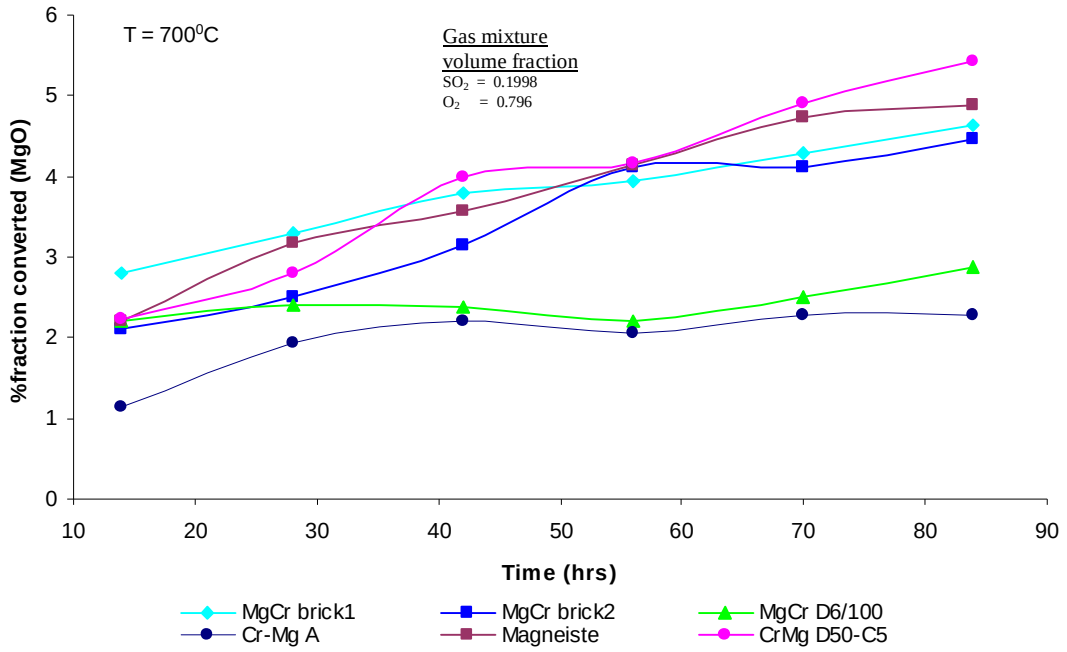


Figure 4.33. Effect of time on sulfation conversions of MgO in basic refractories in SO_2-O_2 mixture at 700°C.

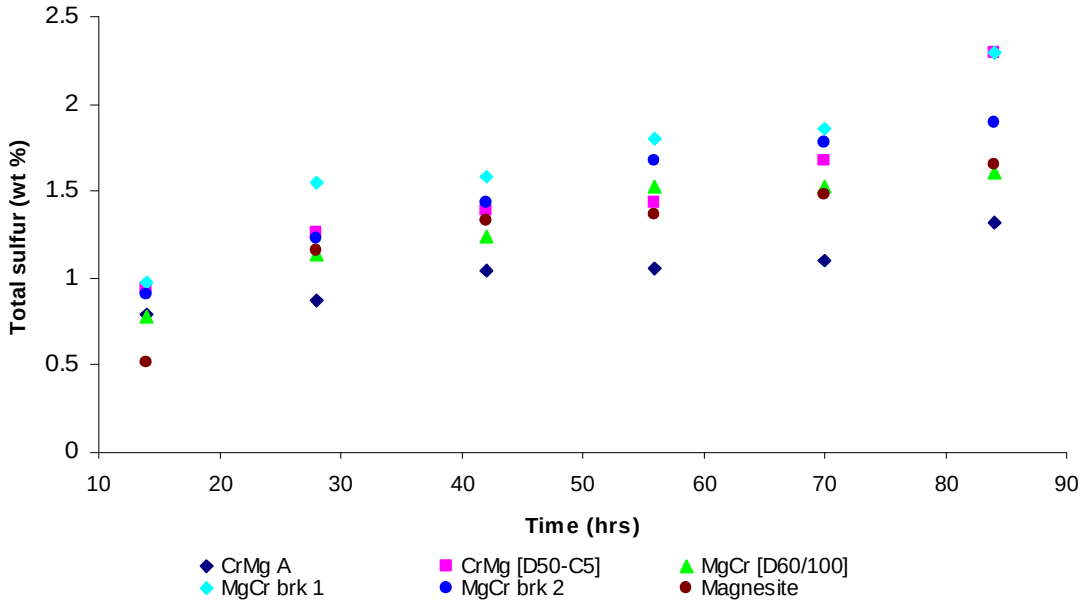


Figure 4.34. Total sulfur (wt %) in basic refractories as a function of time in SO_2-O_2 mixture at 700°C.

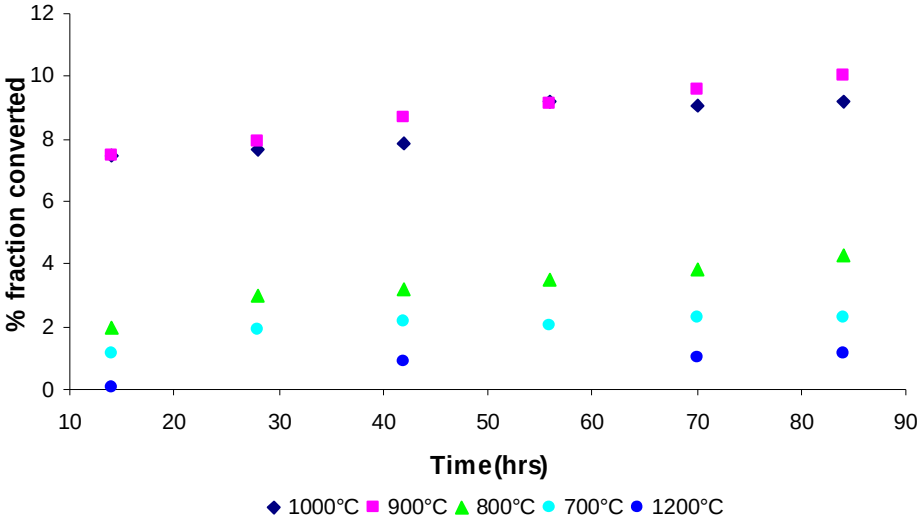


Figure 4.35. Chrome-magnesite A conversion fractions in SO_2-O_2 gas mixtures at different temperatures as a function of time.

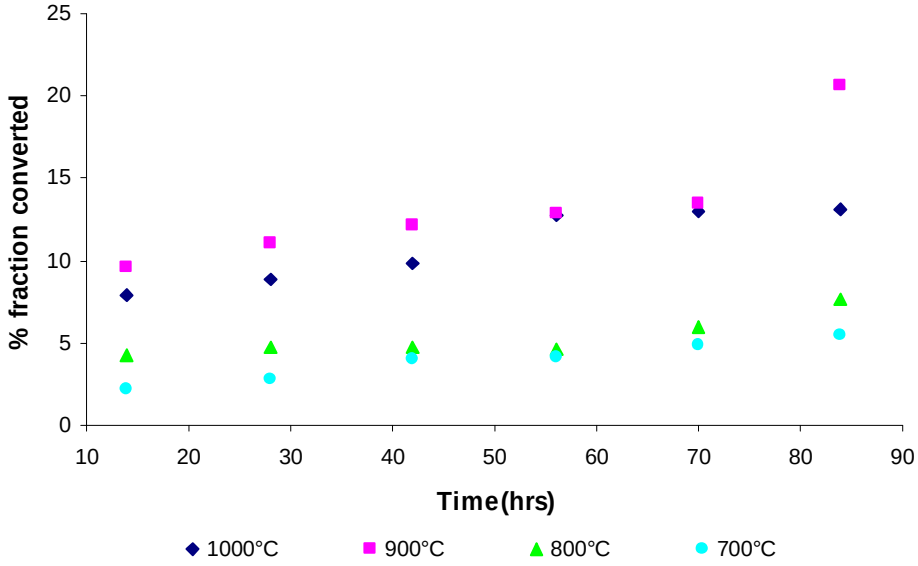


Figure 4.36. Chrome-magnesite D50-C5 conversion fractions in SO_2-O_2 gas mixtures at different temperatures as a function of time.

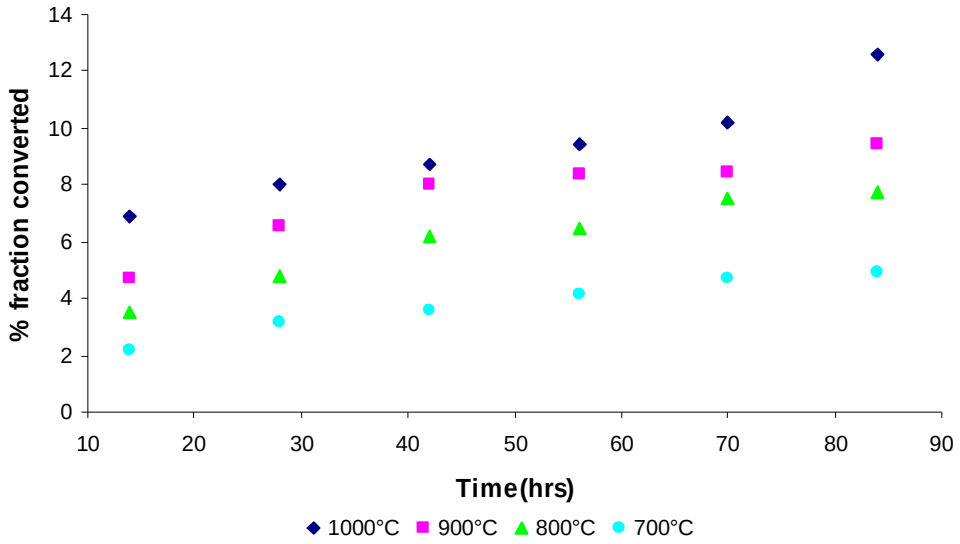


Figure 4.37. Magnesite conversion fractions in SO_2-O_2 gas mixtures at different temperatures as a function of time.

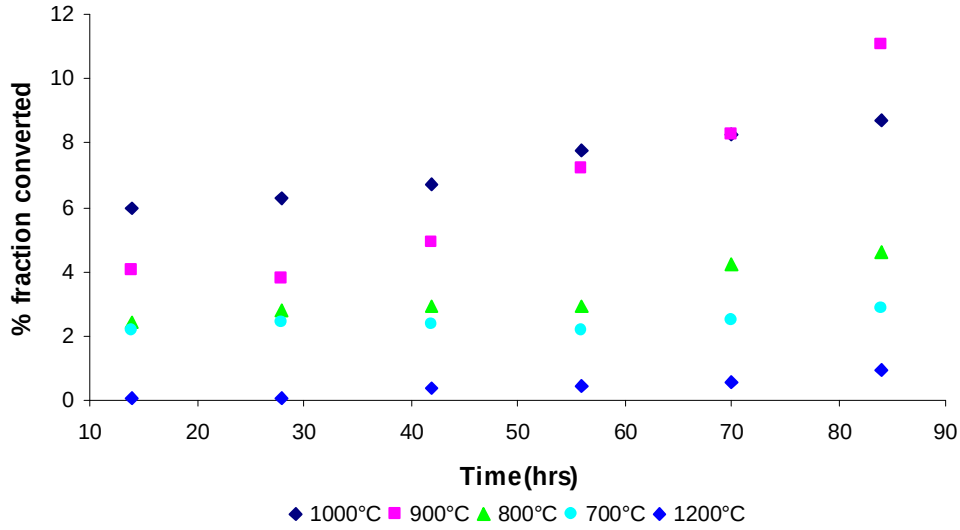


Figure 4.38. Magnesite-chrome D60/100 conversion fractions in SO_2-O_2 gas mixtures at different temperatures as a function of time.

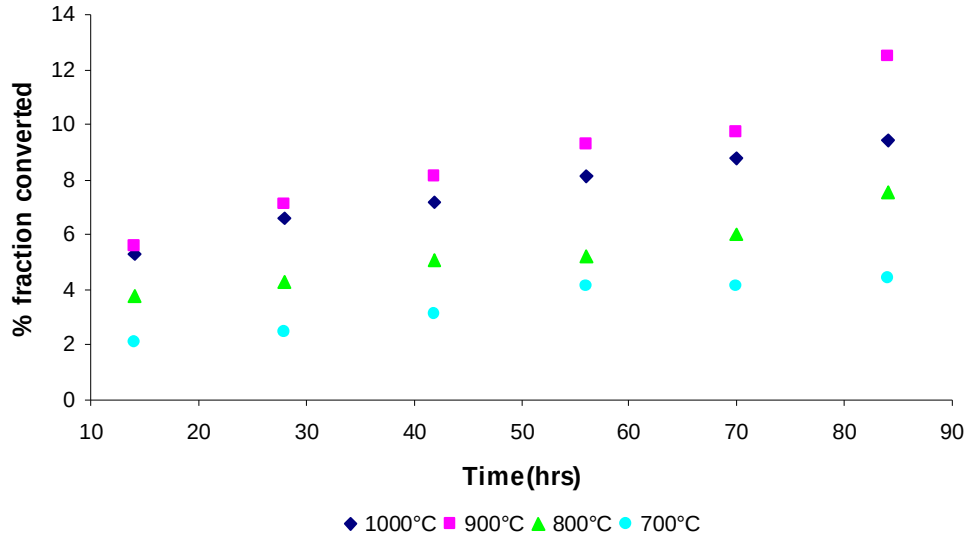


Figure 4.39. Magnesite-chrome brick 2 conversion fractions in SO_2-O_2 gas mixtures at different temperatures as a function of time.

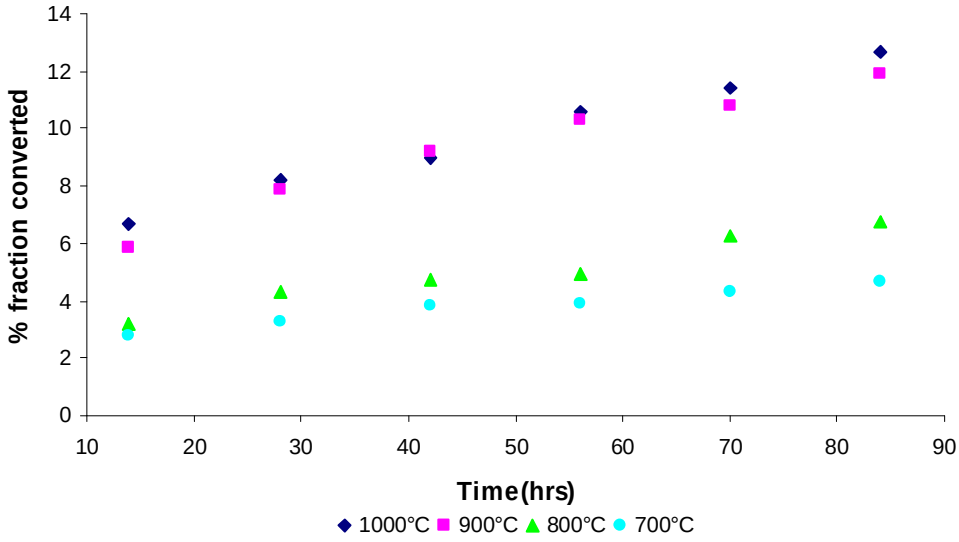


Figure 4.40. Magnesite-chrome brick 1 conversion fractions in SO_2-O_2 gas mixtures at different temperatures as a function of time.

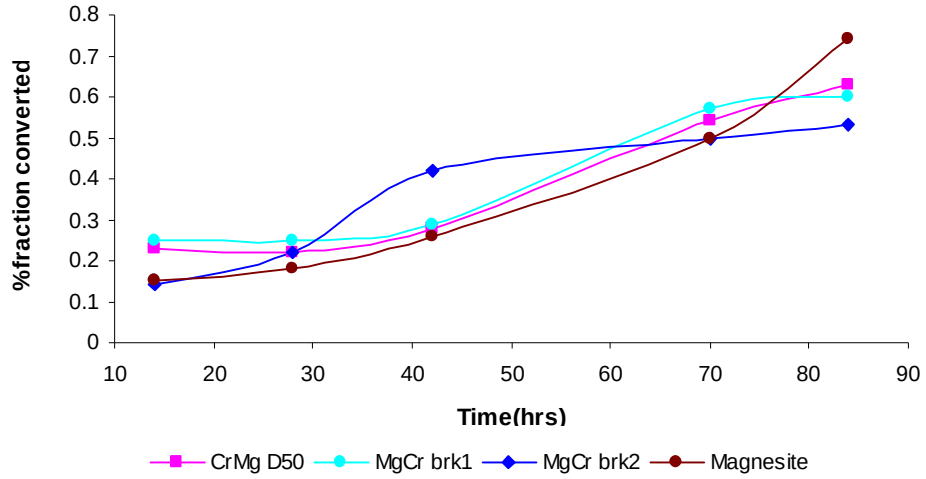


Figure 4.41. Comparison of conversion fractions of basic refractories in SO_2-N_2 gas mixtures at 800°C as a function of time.

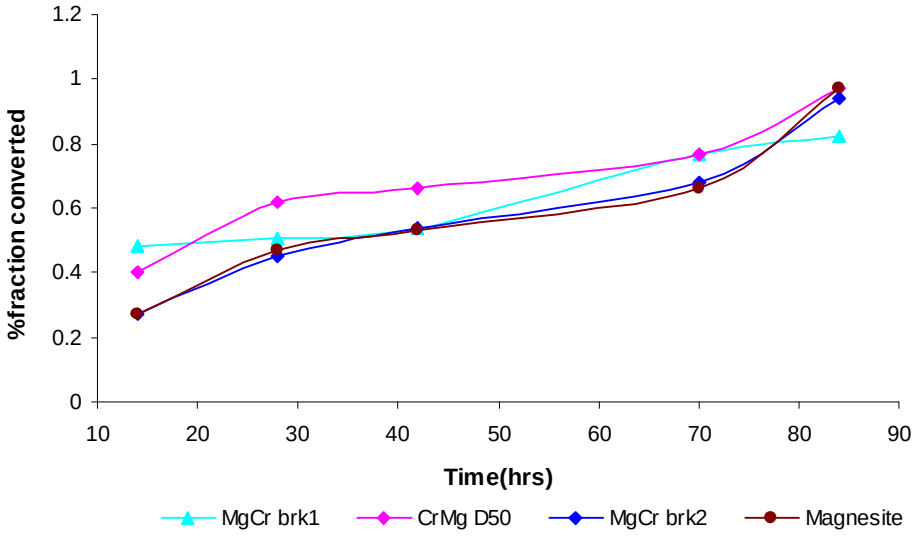


Figure 4.42. Comparison of conversion fractions of basic refractories in SO_2-N_2 gas mixtures at 1000°C as the function time.

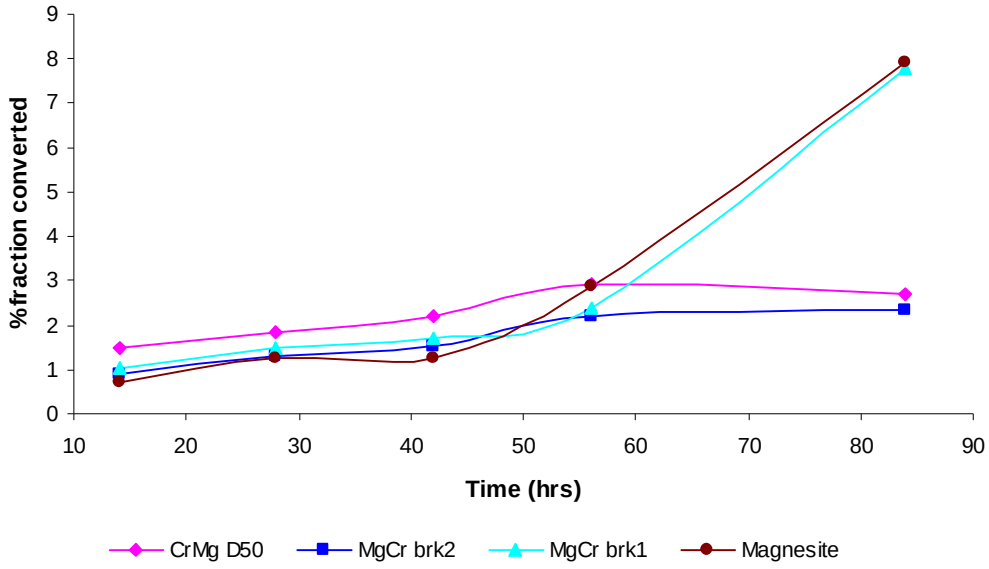


Figure 4.43. Comparison of conversion fractions of basic refractories in SO_2 gas atmosphere at 800°C as the function time.

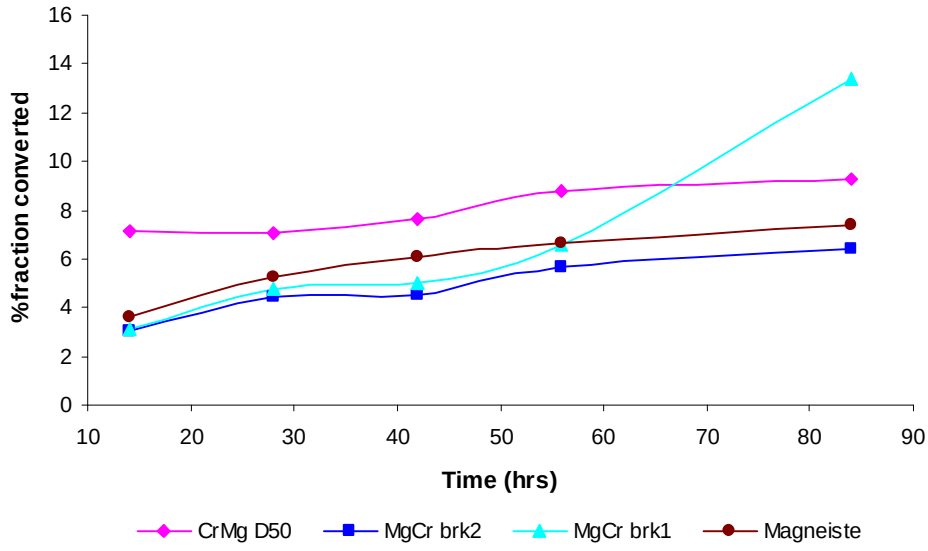


Figure 4.44. Comparison of conversion fractions of basic refractories in SO_2 gas atmosphere at 1000°C as the function time.

In order to compare the effect of changing gas compositions, the refractories were reacted for seven days in SO_2-N_2 and SO_2-O_2 gas mixtures, and the weight gained and sulfate proportions were determined. For SO_2-O_2 gas mixtures the weight gained is plotted as a function of the reciprocal absolute temperature as shown in Figure 4.45. The sulfate proportions in the refractory samples are plotted as a function of temperature in Figure 4.46. In SO_2-O_2 gas mixtures, the reaction displayed different reaction behaviour in relation to the temperature. Between 1350°C and 1000°C, the determined weight of the samples increased, indicating that extent of reaction increased most likely due to increased conversion of the oxide to sulfate, suggested to be affected by reaction thermodynamics[79] and structural changes[78]. Below 1000°C, the weight decreased indicating that the extent of reaction decreased, which might be attributed to the influence of temperature on the structural changes observed in refractories, as suggested previously[78]. Chrome-magnesite D50-C5 and magnesite-chrome D60/100 gave linear reaction pro extents in relation to temperature between 700°C and 1000°C, indicating that reactions sulfate conversion of the oxide involved increased weight. CrMg A and MgCr brick 1 gave conversion reaction extents that decreased with decreasing temperature, indicating structural influences possibly during material adaptation to reaction conditions. For all the basic refractories examined, the reaction extents were highest at 1000°C and lowest at 1350°C. All the examined chrome-magnesite and magnesite-chrome refractories in previous studies[7] also showed weight loss at 1350°C, behaviour suggested being due to structural changes. In reaction processes suggested to be controlled by chemical reactions of MgO to $MgSO_4$, the converted sulfate percentages obtained increased with increasing temperature between 700 and 1000°C, and decreased significantly at 1350°C indicating that reaction extents decreased probably due to the decomposition of sulfates suggested previously[30–38,78–81].

For SO_2-N_2 gas mixtures the weight gained is plotted as a function of the reciprocal absolute temperature as shown in Figure 4.47. Within 700°C to 1350°C, the reaction extents decreased with increasing temperature indicating that conversion to sulfate increased, possible due to increased gas infiltration within the refractories, resulting in increased reaction surface contact with the oxide. The deviations in conversion reaction observed in SO_2-O_2 and SO_2-N_2 gas mixtures, showed complex reaction profiles in relation to the gas-refractory interaction with temperature and gas compositions. In MgCr brick 1 and magnesite refractory the reaction extents indicated increased conversion possible due to increased gas infiltration suggested by the increased open pore structure (Figure 4.2a and Figure 4.3) , as temperature increases. For

other refractories, the reaction extents indicated followed gradual increased reactions at 1000°C, which decreased at 1350°C. The reaction extents between 1000°C and 1350°C decreased for all the refractories, with the exception of the magnesite refractory that indicated increased conversion reaction suggesting continued reaction processes, probably due to other reactive oxide such as CaO above 1000°C. The results suggested that structural changes in basic refractories effected reactions and composition was not vital during sulfation.

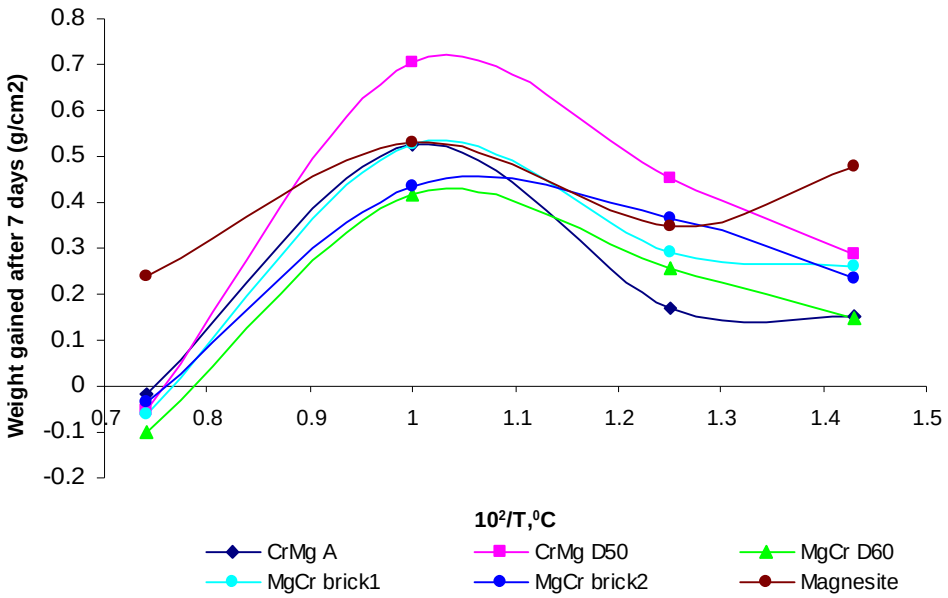


Figure 4.45: The weight gain after 7 days of reaction as a function of the reciprocal absolute temperature at 1atm of SO_2-O_2 gas mixture.

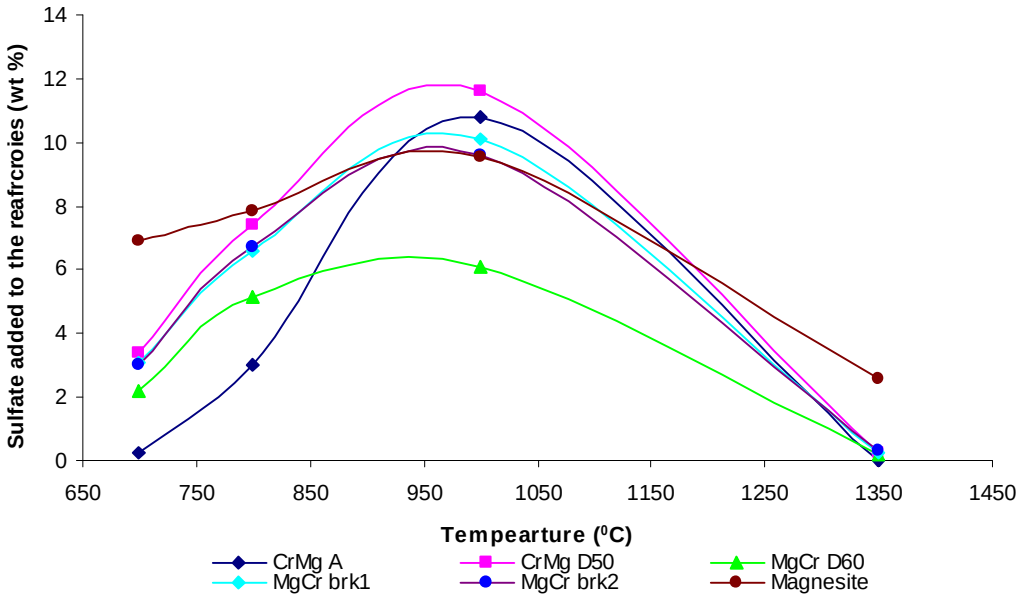


Figure 4.46: Sulfate (wt %) added after 7 days of reaction as a function of temperature at 1atm of SO_2-O_2 gas mixture

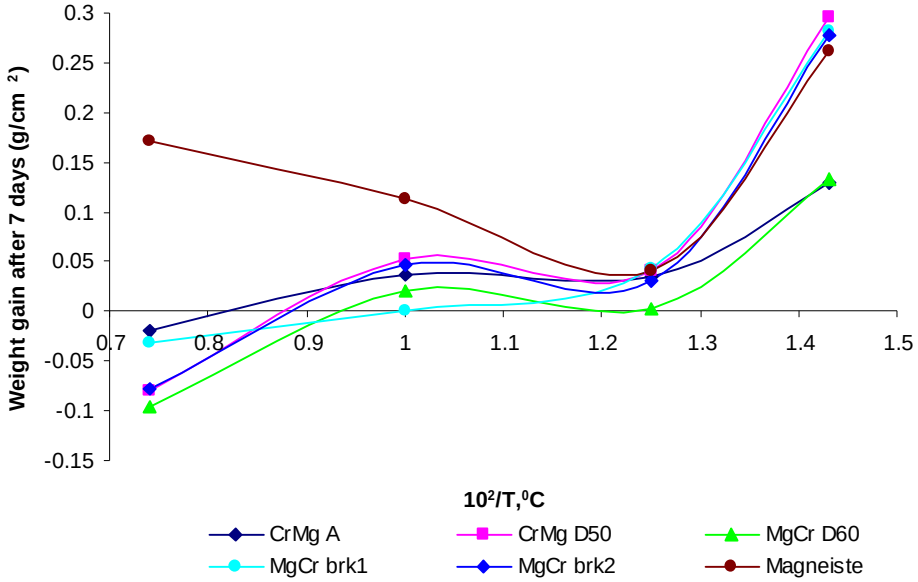


Figure 4.47: The weight gain after 7 days of reaction as a function of the reciprocal absolute temperature at 1atm of SO_2-N_2 gas mixture.

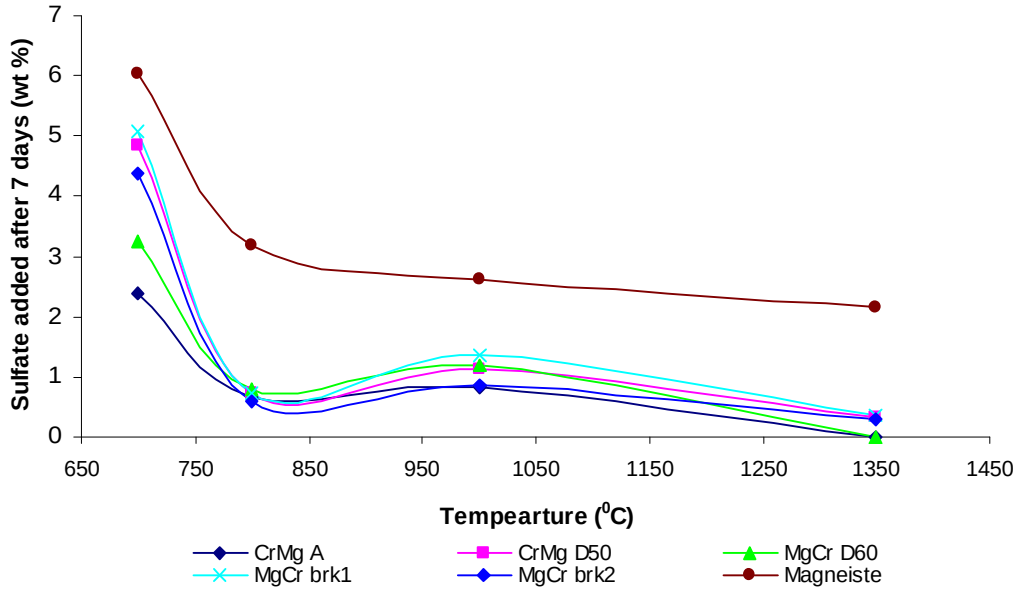


Figure 4.48: Sulfate (wt %) added after 7 days of reaction as a function of temperature at 1atm of SO_2-N_2 gas mixture.

4.5 X-Ray Diffraction Analysis

The refractories exposed SO_2-O_2 and SO_2-N_2 gas mixtures for seven days at 700°C, 800°C, 1000°C, and 1350°C were used in the mineral phase analysis. Both the reacted material and unreacted refractories were examined for phase analysis. Since the detection limit in X-ray diffraction is approximately 7% by volume, any phase that is below that is unlikely to be detected. The X-ray diffraction results for the phase analysis are given in Table 4.1, which confirmed formation of the sulfate secondary phases observed in SEM analysis results. XRD analysis confirmed sulfate formation at low temperatures of 700°C. For the reacted laboratory chromium oxide powdered pellets, no sulfate was detected in all reaction temperatures indicating resistance to sulfate attack. However, in the laboratory magnesium oxide pellets, sulfate ($MgSO_4$) was detected only at 700°C. For chrome-magnesite and magnesite-chrome refractories, XRD analysis showed periclase as a major phase in refractories and silicate was the minor phase. The magnesiochromite spinel phase constituted approximately 5 to 10wt % of the refractory phase composition. However, due to the overlapping of the spinel peaks, the different spinels ($MgCr_2O_4$, $MgAl_2O_4$, $MgFe_2O_4$, Fe_3O_4, and $FeCr_2O_4$) could not be distinguished. The silicates detected showed olivine group minerals, but it was difficult to distinguish between forsterite and monticellite, due to the related crystal structures. Calcium magnesium sulfate was detected in chrome-magnesite D50-C5 and magnesia-chrome brick 1 unreacted sample.

In SO_2-O_2 gas mixtures three types of sulfate compounds were detected in refractories within 700°C and 1000°C temperature range. The sulfate compounds formed by the reactions were $CaMg_3(SO_4)_4$, $CaSO_4$ and $MgSO_4$. At 1350°C, no sulfates were formed in chrome-magnesite and magnesia-chrome refractories. However, in magnesite refractory calcium sulfate, $CaSO_4$ was detected. In samples reacted at low temperatures, dicalcium silicates (Ca_2SiO_4) and olivine group ((Ca, Mg) SiO_4) were detected indicating transformation of the silicate phases. However, at high temperatures olivine group ((Mg, Ca,) SiO_4) that showed increased Mg-end member was detected. The main phases contained in the refractories exposed to SO_2-N_2 gas mixture and the approximate proportions of the new phase were detected. Sulfate formation in all refractories was confirmed at 700°C. Between 800°C and 1000°C, there were low proportions of sulfate, which could not be determined with the X-ray analysis method. At 1350°C, calcium sulfate and calcium magnesium sulfate were detected in magnesite, MgCr brick 1 and CrMg D50-C5 refractories.

Table 4.2. Sulfate phases found after reaction of the different refractories in SO_2-O_2 and SO_2-N_2 atmospheres.

Refractory Type	Before Reaction	SO_2/O_2 Gas Mixture				SO_2/N_2 Gas Mixture	
		Temperature				Temperature	
		700°C	800°C	1000°C	1350°C	700°C	1350°C
Cr-Mg A	–	$CaMg_3(SO_4)_4$, $CaSO_4$, $MgSO_4$	$CaMg_3(SO_4)_4$, $CaSO_4$,$MgSO_4$	$CaMg_3(SO_4)_4$, $CaSO_4$, $MgSO_4$	–	$CaMg_3(SO_4)_4$, $CaSO_4$, $MgSO_4$	–
Cr-Mg D50/C5	$CaMg_3(SO_4)_4$	$CaMg_3(SO_4)_4$, $CaSO_4$, $MgSO_4$	$CaMg_3(SO_4)_4$, $CaSO_4$	$CaMg_3(SO_4)_4$, $CaSO_4$, $MgSO_4$	$CaSO_4$	CaMg3(SO4)4, CaSO4, MgSO4	$CaSO_4$
MgCr D60/100	–	$CaMg_3(SO_4)_4$, $CaSO_4$, $MgSO_4$	$MgSO_4$, $CaSO_4$	$MgSO_4$	–	$CaMg_3(SO4)_4$, $CaSO_4$, $MgSO_4$	–
MgCr brick 1	$CaMg_3(SO_4)_4$	$CaSO_4$	$CaMg_3(SO_4)_4$, $CaSO_4$,$MgSO_4$	$CaMg_3(SO_4)_4$, $MgSO_4$	$CaSO_4$	$CaMg_3(SO_4)_4$, $CaSO_4$,$MgSO_4$	$CaSO_4$
Magnesite	–	$CaMg_3(SO_4)_4$, $MgSO_4$,$MgSO_4.HO_2$	$CaMg_3(SO_4)_4$	$CaMg_3(SO_4)_4$, $CaSO_4$	$CaMg_3(SO_4)_4$, $CaSO_4$	$CaSO_4$	$CaSO_4$
MgO	–	$MgSO_4$	–	–	–	$MgSO_4$	–
Cr_2O_3	–	–	–	–	–	–	–

CHAPTER 5
DISCUSSIONS

5.1 Introduction

Before interpreting and drawing conclusions on the SEM analysis results, it is important to note that a major difference was the chemical composition of the refractory components. The manufacturers did not supply the specifications in manufacturing route and the firing temperatures. The mineralogy of basic refractories[1–7], the mineralogical changes which occur in oxidizing and reducing atmospheres[46–50] and the mechanism of diffusion of the refractory constituents[5,3–6,58–57] have been considered by various investigators.

The original microstructure of magnesite refractory (Figure 4.1) contained magnesia grains surrounded by silicate phases that resulted in rounded magnesia grain surfaces along the grain boundaries, with small dihedral contact angles at the triple points between the grains. The distribution of different phases that occurs during firing, allowed the penetration of silicates between the magnesia grains promoted by temperature and solid-state diffusion. Treffner[70] showed that silicates had a significant influence in changing the orientation of grain boundary surfaces of magnesia. The contact angles between the grains attributed to the wetting between the magnesia and the silicate, achieved for minimum surface energy. During firing, the interfacial energy between the magnesia grains was likely higher than that between magnesia and silicate. Therefore, at high temperatures, silicates most likely achieved equilibrium (possibly through liquid formation) and they penetrated, during cooling, between the magnesia.

In chrome-magnesite and magnesite-chrome refractories, the main phases were periclase, magnesia spinels, chromite spinels, and silicates. The phase distribution and phase relationships of Cr, Fe, Mg, Al, Ca,Si, and O determined in the original structures (Figures 4.2 to 4.4) gave the non-stoicheometric compositions recognized in previous studies[48–50,53,56]. The homogeneous distribution of the iron oxide and alumina within the grains, and the presence of chromite and magnesia in both the periclase and chromite in different concentrations characterized different structures. The diffusion of magnesia into the chromite grains have been shown to be the determining factor in spinel formation[4,56]. The diffusion of sesquioxides into the magnesia grains determined the relative solubility and the ionic radii is the limiting factor[5–6]. There were four primary mineral phases observed; the remnant chromite grains of different compositions

from the original chromite, several forms of secondary chromite spinels, magnesia spinels and silicate phases of different compositions. The suggested solid-state diffusion processes[56] resulted in development of direct bonding between chromite and magnesia, detemined by oxidation and solution precipitation relationships occurring in differential diffusion processes of phases. The concentration of the precipitated secondary spinels upon magnesia grains differed from refractory to refractory, indicating the effects of firing temperatures on reactions that took place. The silicate phases often occurred at the grain boundaries and the pore distribution developed contributed to the observed microstructural characteristics. The factors affecting the phase compositions and mechanisms during heating have been found to affect the kinetics of the diffusion processes and reactions of spinels, as discussed in previous studies[1,3–7,46–53]. The reactions occurring in different systems of Cr, Fe, Mg, Al, and O and Cr, Fe, Mg, Al, Ca, Si, and O can be predicted from the phase diagrams[48–52,54]. The degree of completion of the reactions, and the structure developed are determined by firing temperatures[53].

In Figure 4.2, the observed intragranular and intergranular secondary spinels in MC2 indicated non-stoicheometric compositions that could be presented by $(Mg^{2+}, Fe^{2+})(Fe^{3+}, Cr^{3+}, Al^{3+})_2O_4$ formula, showing incomplete diffusion processes[4,7,48], as suggested in previous studies[48–50]. The pore structure could have been important because the driving force of pore size development during firing temperatures has been known to being high enough to achieve elimination of open pores during solid-state diffusion[55]. Therefore, kinetics during solid-state diffusion could have been the factor in structural development in this refractory and suggested low temperatures could have affected kinetics of diffusion processes[5,47,51]. Richardson and White[48], and Woodhouse and White[49–50] have shown that the dissociation of the sesquioxides to spinels determined the kinetics in diffusion processes. In Figure 4.3a and 4.4b, the effect of pore structure and temperature indicated grain growth and pore volume, as the increased large numbers of closed pores occurred in well-developed direct bonded structures. In Figure 4.3b, there was no observable development of solution precipitates in CM2 suggesting phases presented by $(Mg^{2+}, Fe^{2+})(Fe^{3+}, Cr^{3+}, Al^{3+})_2O_4$ formula[48–50], and the remnant unchanged raw materials of magnesia and chromite were major phases. From structural features, CM2 resulted from coarse-grained compacted material, and MC1 and MC3 resulted from fine-grained material, in which the development of solution precipitates enhanced direct bonding and pore structure. In Figure 4.4a, the observations seen in CM1 structure indicated that diffusion processes enhanced the displacement of silicates to the pore surfaces, and possibly reduced the wetting between the magnesia spinels and silicates, as reported by El-Shahat and White[51].

This indicated that interfacial energies suggested by Treffner[70] might have been higher between chromite and silicate phases, but lower between chromite and magnesia grains promoting direct bonding. The fact that the silicates were distributed randomly suggested that the probably formation of low melting phases with other refractory phases was decreased[3]. Therefore, during firing at high temperatures, formation of large amounts of silicates was prevented[70] while direct bonding between magnesia was increased. The refractory structures suggested that, diffusion processes promoted growth of closed pores, which possibly increased at the expense of smaller ones by pore coalescence[4]. The previous studies[4,56] attributed the pore formation and grain growth to the differential mechanism caused by Kirkendall effect.

In MC1, the noticeable grain growth of the spinel precipitates (C3) indicated progressive diffusion processes that suggested completion of spinel reactions presented by (Mg^{2+}) (Fe^{3+}, Cr^{3+}, Al^{3+})$_2O_4$. The spinel structures developed for minimum surface energy, and on cooling, precipitation was promoted[72], indicating cooling rates as another factors contributing to the extent of solution precipitation[1–2,68,70], where slow cooling promotes precipitation while rapid cooling (quenching) showed structures at the suggested heating temperatures. Similar structures seen in CM1 and MC1 have been observed in low silicate magnesia structures during development of magnesia spinels[70,72]. The reactions in the original structures were characterized by differential diffusion processes detemined by oxidation of the ferrous iron in the chromite grains[4–5,56] and solution phase relationships[48–52,54,71,72]. Therefore, in practice, the original phase composition of the refractory determined the resulting modification of the microstructure.

5.2 Microstructural changes in reheated basic refractories

In practice, the performance of basic refractories is limited by structural disintegration, due to changes that occur in microstructures. A number of other factors that affect the gas-solid reactions, which add to the effects of temperature, composition and the reacting gas partial pressure exist. The technological factors experienced during production determine the principal characteristics of the actual refractory structure, the crystalline size distribution, grain size and the pore size distribution all contribute to gas-solid reactions.

5.2.1 Microstructural changes in oxygen atmospheres

Figures 4.6 to 4.9 show un-used basic refractories reheated in oxygen atmosphere at 1350°C. The oxidizing atmosphere and temperatures affected the structural characteristics of the original

refractories, thereby altering the phase distribution, pore structure, and grain size. The pore distribution, grain size and phase distribution have been shown to be the main factors determining the microstructure[4–5,46–51,56]. The microstructure of magnesite refractory, in Figure 4.6, showed the effect of temperature on diffusion kinetics, which was described by changes in distribution of silicate, phases in the original structure (Figure 4.1). The open structure observed in original structure (Figure 4.1a) was maintained suggesting that changes occurred with the silicate phases and the subhedral grains with dihedral angles at the triple points were determined by the surface energy associated with interaction of silicates with magnesia grains at 700°C. At 1350°C (Figure 4.6b), minimum surface energy was attained for different structural features, and silicates migrated to the grain boundaries and rounded magnesia grain surfaces with subhedral angles were obtained. This suggested that in the interior of the magnesia grains interfacial energy decreased, while at the grain boundaries the wetting behaviour by silicates increased affecting the grain surface boundary angles[70]. The closed pores observed in the interior of the magnesia grain increased due to migration and diffusion processes, suggesting increased diffusion kinetics[4]. At the grains boundaries the increased tendency of liquid silicate most likely resulted in pore coalescence.

The observation were similar to the studies of Gordon *et al.*[58], Kapadia and Leipold[59] and Treffner[70], who showed that diffusion in reheated magnesia resulted in grain growth and the increased amounts of closed pores resulted from grain boundaries passing over the pores, leaving them trapped inside. Studies[56] have suggested that solid-sate diffusion was the main form of diffusion in reactions of spinels with magnesia, and that diffusion processes involved migration of cations through an oxygen lattice by bulk diffusion moving as a front through MgO. Rigby[4], and Homer and Richardson[56] attributed the increased porosity to differential diffusion by Kirkendall effect, due to iron oxide and magnesia. In the present study, established suggestions were that the consequence of the diffusion of the components led to differential solution precipitation in spinels and migration of silicates to the grain boundaries, which influenced the structure at the heating temperature. Figure 4.6b suggested that at 1350°C silicates migrated to the magnesia grain surfaces, while the magnesia grain growth promoted direct bonding. The changes in phase distribution and pore structure during reheating affected the magnesite-chrome and chrome-magnesite refractory structures, as shown in Figures 4.7 to 4.9. The observed structures suggested that temperatures altered the original structures and could possibly be the contributing factor on the structural characteristics[6,70–71]. Reheated MC1 in Figure 4.7 showed elongated continuous secondary spinels (C4) that were not apparent in original structure (Figure

4.4a), which indicated to have occurred possibly by precipitation of chromite from surrounded magnesia spinels, in a reaction progress that has been suggested by Treffner[71], and Scheerer *et al.*[68]. The dissolution of iron oxide in spinels have been reported in previous studies[48–50], and the observed effect in Figure 4.7 resulted in increased concentration of secondary precipitate structures within magnesia in a diffusion phenomenon described by Rigby[4]. This also explained the grain growth observed for magnesia spinels and the accompanying increase in porosity attributed to the unequal diffusion that might have occurred[4,54–71].

Reheating chrome-magnesite mixtures (Figure 4.8) showed continued development in diffusion processes driven by suggested dissolution of spinels. The effects resulted in physical separation of the mineral phases, where magnesia spinels dissociated such that secondary chromite precipitates migrated to the grain boundaries in a manner that resembled the described silicate behaviour in magnesite refractory (Figure 4.6b). At the grain boundaries partial precipitation of secondary chromite occurred, possibly during cooling, leaving magnesioferrite within the grains. The suggested effect of grain growth and unequal diffusion resulting in crack formation was shown by cleavage cracks that occurred on the magnesia grains. The structural features suggested that the diffused secondary chromites combined in trying to achieve minimum surface energy and obtained chromite grains that tended to be rounded, and had mineral composition similar to that observed in remnant primary chromite grains tabulated in Table 4.2 and seen in Figure 4.5. The altered phase redistribution was associated with disruption of the direct bonding in magnesia spinels and led to uneven distribution of the sesquioxides between the mineral phases suggested by increased pore structure and crack formations as reported by Lovell[46]. This has been suggested in previous studies[1–2,51,55–56], when refractories are heated at different temperatures. Previous studies[71–69] showed that continued reactions that occurred by reheating magnesia-chromite mixtures altered the chromite structure resulting in separation of the grains. Treffner[71] suggested that formation of the altered structures occurred by re-crystallization mechanism in chromite phases. Hayhurst and Laming[2], and Treffner[71] demonstrated similar observations of compositional variation in spinel structures of reheated magnesia-chromite mixtures, illustrated by re-crystallization of the chromite and magnesia.

The silicates found suggested that their migration was associated with that of secondary chromite precipitates and possibly contributed to the grain growth and the resulting crack propagation and increased porosity. The explanation was that the increased diffusion kinetics at high temperatures, increased grain growth of closed pores so that, during cooling, effects of unequal

diffusion promoted crack propagation. The effect of silicates on the direct bonding and microstructure were not resolved and conclusions in previous studies[2,68] were contradictory. Hayhurst and Laming[2] concluded that re-crystallization of spinels from the spinel-rich silicate liquid promoted direct bonding. However, Scheerer *et al.*[68] disagreed with the authors[2], suggesting that presence of silicates between the spinel grains caused disruption of direct bonding, rather than promoting it. In the present study, it has been inferred that, occurrence of silicates appeared to have been associated with secondary chromites, thus silicates probably had an influence on the diffusion of secondary spinels and the resulting pore structure altering the structural features of the refractory.

In Figure 4.9b, the suggested dissociation of spinels[48–49] and the accompanying diffusion processes indicated formation of magnesia spinels and aggregation of silicate phases along the grain boundaries. These structural characteristics of spinel formations were not observed in the original microstructure (Figure 4.3). The observed alteration of chromite grains resulted in reduction of discontinuity, indicating that magnesia spinel pockets diffused and aggregated suggesting increased grain growth. The changes in phase distribution shown in Figure 4.9b are characterized by the secondary spinel formations that occurred as fine chromite precipitates and intergranular precipitates in magnesia grains. This suggested diffusion processes continued and the newly formed spinels diffused and precipitated in the original magnesioferrite spinel. Silicate phases found along the grain boundaries within the newly formed magnesia spinel grains, showed similar structural characteristics observed in fired magnesia-chromite mixture, and have been shown by De Menezes[5], Scheerer *et al.* [68], Treffner[70] and Ford *et al.*[72].

Correlations between silica and calcium compositions were established in silicates surrounding the newly formed spinels, suggesting uniform distribution of Ca-Si-Mg ratio[70], indicating monticellite as a predominant silicate phases within spinels. However, in the silicate phases found among developed magnesia aluminate spinels pockets, silica and calcium compositions showed no correlations indicating non-uniform distribution of the phases. The findings agreed with those demonstrated by De Menezes[5] who showed that heterogeneity occurred for reheated magnesia-chrome mixtures at 1300°C. In the present study, silicates occurred as interfaces between the magnesia spinels, which was a structural effect attributed to disruption of the direct bonding by Scheerer *et al.*[68] These suggestions appeared to disagree with Hayhurst and Laming[1–2] who illustrated that in reheated refractories silicates promoted direct bonding through re-crystallization of diffused components. The silicate phases observed in the refractory (Figure

4.9) suggested reactions that did not lead to liquid formations, which is a structural characteristic that appeared to disagree with Hayhurst and Laming[2], as they illustrated that liquid started to form at 1350°C in silicates phases of reheated structures.

There were major fundamental differences demonstrated in these studies[1–2,68], which could have suggested the different findings. Hayhurst and Laming studies[2] original structures were obtained from developed refractory bricks that had been previously heated above 1600°C during manufacture. The original structures demonstrated well-developed mineral phases having secondary spinels and intergranular precipitates (which were associated with silicates). Scheerer *et al.*[68] original structures were developed by heating compacted powdered raw refractory materials at 1650°C to 2200°C in oxidizing atmosphere. Based on different original nature of the materials used in the studies[2,68], this suggested that the conclusions and correlations made by Scheerer *et al.*[68] in relation to Hayhurst and Laming[2] work were unfounded. The findings suggested that the thorough distribution of mineral phases during manufacture[2] led to more stable structures and on reheating precipitation prevailed, rather that diffusion. In the present study, the original structures obtained were from developed refractory bricks, but the reheated structures indicated that diffusion processes continued as phases tended towards stable structures with minimum surface energies (Figure 4.3b).

Therefore, in view of the observations in the present study, the basis of the findings did not necessarily disagree with Hayhurst and Laming [1-2], rather it indicated that the temperatures, and extent of reactions during production of the refractory bricks used were important and different. Therefore, direct bonding described in Figure 9b as precipitation of the secondary spinels upon magnesia in this case, was not necessarily determined by the silicates, infact the silicates separated from phases of the refractory and formed around the newly formed magnesia spinels. The structures suggested limited distribution of the mineral phases during manufacture and the developed direct bonding resulted from continuation of diffusion processes in trying to form stable phases. Based on the structural differences observed between Hayhurst and Laming[1–2], Scheerer *et al.*[68], and in the present studies, the suggested fundamental factors were original structures and effects of first heating temperatures. The composition of the silicate depends mainly on the temperature encountered, the amount of calcium, and melting point in that part of the refractory are correlated[71].

5.2.2 Microstructural changes in sulfur-bearing gases at high temperatures

Based on the structural features observed in basic refractories when reacted with sulfur-bearing gases, mechanisms of reactions were established in SO_2-N_2 (Figures 4.10 to 4.13), SO_2-O_2 (Figures 4.14 to 4.17) gas mixtures. Detailed thermodynamic analysis at temperature range employed was determined for the different phases. In magnesite refractory shown in Figure 4.11a, changes observed in pore structure, grain sizes, and mineral compositions at 1350°C, were similar to the structure illustrated in oxygen atmosphere (Figure 4.6a), the silicates were displaced to the grains boundaries, and they reacted with the sulfur-bearing gases and formed calcium sulfate ($CaSO_4$). The suggested migration of ionic components through diffusion processes[60–67] allowed sulfation reactions in the presence of sulfur-bearing gases and reactive oxides. Since no free CaO was observed in the original structure, the phase analyses (Table 4.2) suggested that the observed $CaSO_4$ formed occurred through reaction of CaO contained in tricalcium silicate, Ca_3SiO_5, boundary interface (Figure 4.1b). The calcium sulfate formed comprised of a large number of intergranular porosity, suggesting a reaction mechanism that involved dissolution of the silicate structure, which resulted in large CaO surface area and a sufficient pore volume for the diffusion of sulfur-bearing gases, and complete conversion to $CaSO_4$.

It has been shown previously[28,97–98] that the inherent refractory features (such pores, cracks and grain boundaries) influenced permeability of gases and overall sulfation of the oxide components. The observations in the present study related to the studies[28] as the presence of grain boundaries and pores appeared to have contributed to the pore volume, permeability, and reactivity of the refractory components. The temperature could possibly have promoted structural disintegration of silicates through diffusion processes. The newly formed magnesia silicate (Mg_2SiO_4, forsterite) suggested reactions of silica from the altered Ca_3SiO_5 structure and magnesia, and occurred often between the calcium sulfate and magnesia grains. The structural features indicated that CaO crystallized independently from the Ca_3SiO_5, suggesting that Ca^{2+} ions and O^{-2} ions dissociated from the bound silicate structure as the bond strengths between calcium ions and sulfate ions (Ca-SO_4) bonds prevailed, as reported in previous studies[115]. St Peirre *et al.*[115] indicated that Si-S bonds are weaker than the tetrahedral bond strength, which play an important role in preventing the Si^{2+} ion diffusion, and changes in lattice possibly allowed Ca^{2+} ion diffusion. Trojer[36] has illustrated similar mechanism where at the grain boundaries of refractories, CaO crystallized from silicate phase that had disintergrated into different product layers of dicalcium silicate, tricalcium silicate phase, and formed the $CaSO_4$.

The mechanism that leads to structural disintergration of Ca_3SiO_5 and recrystallization of CaO has not been determined in the present studies.

Studies[60–66] have suggested that calcium cation diffusion through silicate phases was controlled by distribution of free volume, which could possibly be determined by the ionic size. In the present study, a mechanism of CaO crystallization from Ca_3SiO_5 was proposed based on the ionic size and a schematic illustration of Ca_3SiO_5 given in literature[124], as shown in Figure5.1. The structure is characterized by silicate tetrahedrons (SiO_4), and isolated oxygen ions that are arranged octahedral by the calcium ions. Although the Si^{2+} ion have the least ionic radius, with Si^{2+} (0.34 Å), Ca^{2+} (1.08 Å) and O_2^{2-} (1.32 Å)[123] its diffusion would have been limited by the suggested tetrahedral bond strength[115], and the difference in ionic radius of oxygen and calcium suggested that calcium ions are most likely to diffuse easily within the silicate structure. The changes occurring with the octahedrally arranged oxygen ions would have distorted the lattice structure, which might have changed the lattice parameters[64] resulting in an increased amount and distribution of free volume as reported in previous studies[60–66]. Diffusion of Ca^{2+} ions was promoted and oxygen ions diffused to balance the ionic charge and CaO was formed.

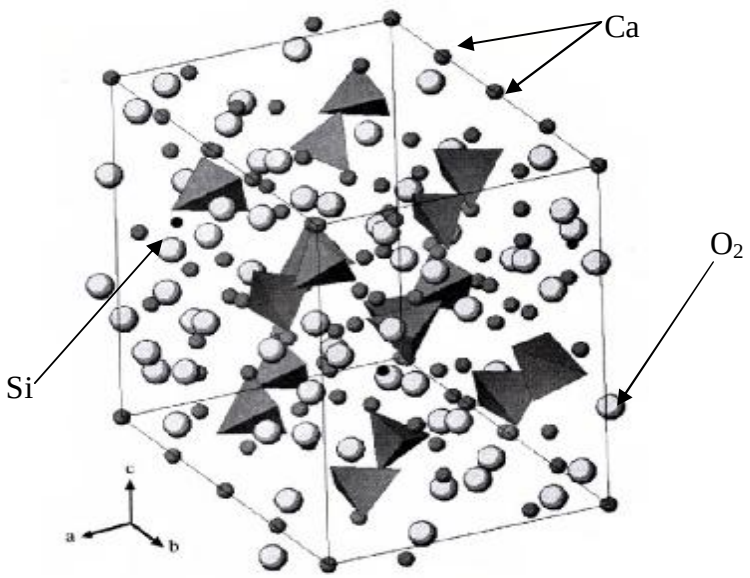


Figure 5.1. The schematic illustration of Ca_3SiO_5, showing [SiO_4] tetrahedral in dark grey. The Ca, O and Si atoms are presented by the rounded spheres in dark grey, light grey and black, respectively. (Reference: Mori *et al.*[124]).

The diffusion of oxygen ions was attributed to the distributed amount of volume created in the structure, this proposed ionic diffusion in tricalcium silicate was supported by diffusion process suggested by Watson[60] for silicate melts at temperatures above 1300°C. In the present study, the proposed mechanism for the formation of CaO described, suggested the following reaction:

$$Ca^{2+} + O^{2-} = CaO \qquad (5.1)$$

The dissociated or crystallized CaO indicated reaction with sulfur-bearing gases and possibly formed $CaSO_4$ according to the following reactions:

$$CaO + ½\ O_2 + SO_2 = CaSO_4 \qquad (5.2)$$

$$Ca^{2+} + O^{2-} + ½\ O_2 + SO_2 = CaSO_4 \qquad (5.3)$$

Hsia, Pierre, and Raghunathan[98–99] proposed that CaO reaction with SO_2 and O_2 gas mixtures occurred in two consecutive stages through Equation 5.2 and Equation 5.3. The suggested reaction mechanism through Equation 5.2 occurred at the surface of the CaO and resulted to an unreacted CaO core with $CaSO_4$ forming a permeable layer. The difference in ionic radius of Ca^{2+} (1.08 Å) and SO_4^{2-} (4.5 Å) in $CaSO_4$ formed played an important role in allowing diffusion of calcium and oxygen ions [98–99] from the unreacted core, and this enhanced reactions by Equation 5.3. Hsia *et al.*[98–99] gave a schematic illustration of $CaSO_4$ given in Figure 5.2, and suggested that sulfation occurred at the $CaSO_4$/ gas interface through outward diffusion and material transport of the Ca^{2+} and O^{2-} ionic species enhanced by difference in ionic radius. In the $CaSO_4$ crystal structure the arrangement of sulfate tetrahedrons (SO_4^{2-}) occupying the interstitial sites and Ca^{2+} ions occupying the lattice and interstitial sites, promote high mobility of Ca^{2+} ions between the SO_4^{2-} tetrahedrons and creat vacancies.

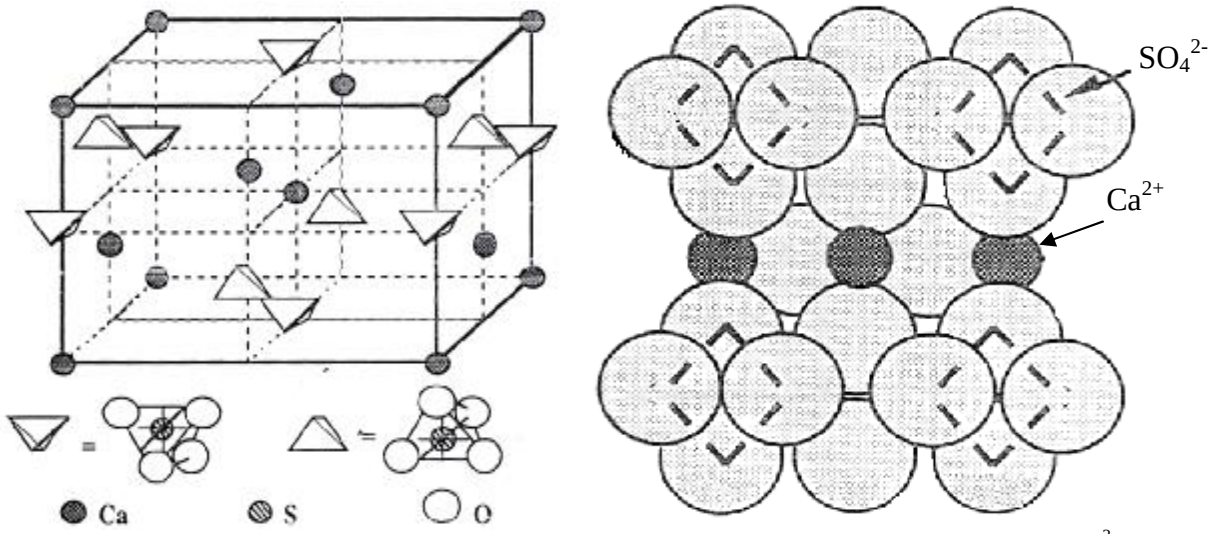


Figure 5.2. The schematic illustration of $CaSO_4$ crystal structure (a), and $CaSO_4$ lattice showing the [SO_4^{2-}] tetrahedra in light grey and dark grey Ca^{2+} cations in-between (Reference, Hasi, Pierre and Raghunathan[98–99]).

This change in distribution of volume and vacancies created enhanced mobility of O^{2-} ions through the sulfate tetrahedrons and formed CaO at the $CaSO_4$/gas interface. Therefore, sulfate reactions with CaO results in outward growth of $CaSO_4$ at the CaO/$CaSO_4$ interface, as suggested in the previous studies[98–99]. However, the structural observations were contrary with

those indicated in Figure 4.1, as a total conversion to $CaSO_4$ occurred. In all the studies[36,60–66,98–99], the reaction mechanisms that led to sulfation were related in that the diffusion and material transport of Ca^{2+} and O^{2-} ionic species was determined by distribution of free volume in silicate and sulfate structure. The complete conversion of CaO to $CaSO_4$ having lager intergranular pores observed in the present study, suggested to have occurred through a series of reaction mechanisms, which most likely involved increased pore volume during material transport. Borgwardt *et al.*[100] proposed a reaction mechanism, which suggested that sulfation could possibly have occurred at the inner surface of the $CaO/CaSO_4$ interface through inward transport diffusion of O_2^{2-} and SO_4^{2-}, if enough volume was created during diffusion and $CaSO_4$ formed was permeable, as suggested by Hsia *et al.*[98–99]. The structural observation suggested that for a complete conversion of sulfate in Figure 4.10b and according to Borgwardt *et al.*[100] mechanism, the pore structure of the $CaSO_4$ formed had a relatively open pore structure that allowed diffusion of O_2^{2-} and SO_4^{2}. The minor porosity and significant amount of intragranular porosity observed in the $CaSO_4$ formed in Figure 4.14 and 4.19, suggested that significant increased pore volume was created, and sulfation reaction may have been facilitated within and through the voids, cracks and micro fractures.

In the present study, the proposed mechanisms suggested that reactions were initiated by the dissociation of Ca_3SiO_5 structure, which possibly involved increased pore volume during diffusion processes, and the porous $CaSO_4$ formed promoted O_2^{2-} and SO_4^{-2} transport through the pores. The microstructural observations suggested that sulfation most likely proceeded at both the $CaO/CaSO_4$[100], and $CaSO_4$/gas[98–99] interface. This mechanism suggested that the ionic size may not have been the controlling factor determining the diffusivity, but physical characteristics seen as pores, cracks and micro fractures on the $CaSO_4$ structure and spalled areas on the magnesia grains were critical in the reactions. The thermodynamic stability and accessibility were the determining factors, but not chemical reaction and diffusivity of the gases. This agreed with previous studies[36,60–66,98–100]. The mechanism of diffusion of the ionic species and relative diffusivity were not investigated in the present study, therefore no conclusions were based on that.

Laboratory magnesium oxide, refractory magnesite and chrome-magnesite powdered pellets in Figures 4.12 and 4.13 were found to be unreactive in SO_2-N_2 mixtures at 1350°C. The temperatures effect on the microstructure caused particles to sinter together, in diffusion processes determined by minimization of surface energy[70] and grain growth[4]. This behaviour

was explained as an effect of pore distribution where pores diffused to the grain boundaries to minimize surface energy[70,71]. Increased purity in magnesite-powdered pellet resulted in uniform silicate distribution, and no apparent reaction with gases. In chrome-magnesite, powdered pellet the phase distribution developed allowed secondary solution precipitates and direct bonding between chromite and magnesia grains, and no sulfate products formed in all gas mixtures. The minor structural changes observed indicated that the kinetics of diffusion processes involved were extremely slow.

Structural dissolution of secondary solution precipitates resulted in softening and spheroidization of chromite grains in CM1 (Figure 4.15a), resulting in a weakened and loosening of magnesia structure, which were structural characteristics similar to those observed in oxidizing atmosphere (Figure 4.6 to 4.9). The phase distribution developed in MC1 (Figure 4.18a) was characterized by large magnesia solid solution grains that had cleavage cracks, but indicated that the cracks did not act as the gas diffusion route that led to sulfation. The transition in pore structure and phase distribution in MC3 (Figure 4.17), resulted in structural disintegration of chromite grains and dissolution of secondary solution precipitates, leaving open magnesia structure. Magnesia solid solutions showed very fine-sized spinel precipitates compared to MC1, and this explained the reduction in cleavage cracks observed. The inhibited crack propagation suggested attributed to the uniformly distributed pore structure and spinel phase features. In MC2 (Figure 4.18b) the transitions in microstructure were characterized by increased closed pores, explained by the development of magnesia spinel and intergranular spinel precipitates that were usually associated with silicate at the pores.

5.2.3 Thermodynamic considerations of $CaSO_4$ formation at high temperatures

The reactions considered for CaSO4 formation occurred at 1350°C, and the results of products analyses in Table 4.2 confirmed the suggested formation of $CaSO_4$ indicated to be temperature depended in Figure 4.10 to 4.11 predominance area diagrams. However, $CaMg_3(SO_4)_4$ was also indicated as another phase formed in SO_2-O_2 gas mixtures although it was not detected in the structures (Figure 4.16) examined. Kellogg[79], Wreidt *et al.*[91]and Dewing *et al.*[117] data were used to calculate the oxygen partial pressures required for $CaSO_4$ formation from the equilibrium reactions derived and the results are tabulated in Table 5.1. The temperature dependency of the equilibrium constants on the reaction can be presented by:

$$\Delta G^\circ = -2.303RT\log K_1, \text{ where } \log K_1 = \frac{\Delta G^\circ}{-2.303RT} \quad (5.4)$$

$$K = \frac{1}{P_{SO_2} P_{O_2}^{1/2}} \quad (5.5)$$

$$\log K_1 = \log\left(\frac{1}{P_{SO_2} P_{O_2}^{1/2}}\right) \quad (5.6)$$

$$-\log P_{O_2} = 2\left(-\log P_{SO_2} + \left(\frac{\Delta G^\circ}{2.303RT}\right)\right) \quad (5.7)$$

The minimum partial pressure of oxygen needed to form $CaSO_4$ in SO_2-N_2 gas mixtures shown in Table 5.1 are within 10^{-20} at 800°C to 10^{-4} at 1350°C, well below P_{O_2} = 0.0036 atm, which was the value of P_{O_2} present in the gas phase, proving that $CaSO_4$ will definitely form. The magnitude of oxygen pressures obtained at 1350°C could be related for all the suggested free energy data given. In SO_2-O_2 gas mixtures the partial pressure of oxygen is much higher at P_{O_2} = 0.796 atm. The findings agreed with previous studies[115–119] that found that in presence of sulfur dioxide at temperatures between 1290°C and 1600°C, $CaSO_4$ formed at oxygen pressures above 10^{-4} and between 800°C and 1300°C[91] $CaSO_4$ formed for sulfur dioxide pressures above 10^{-3}. Therefore, the experiments conducted provided favorable conditions for $CaSO_4$ also seen in the predominance area diagrams in Figure 4.10 and 4.11.

In Figure 4.10, Kellog's[79] data indicated that the favorable conditions for $CaSO_4$ at gas combinations used in SO_2-N_2 and SO_2-O_2 gas mixtures are up to T_{max} above 1350°C. The FactSage results in Figure 4.11 agreed with Kellog's[79], confirming results in Table 4.2, and that $CaSO_4$ was a thermodynamically favorable at 1350°C in the present study. $CaSO_4$ has been found to form in chrome-magnesite and magnesite refractories used as working linings[30–31,36], but Hugget[30] suggested that its reactivity depended on how readily it was released and upon the gas atmosphere. Since silica found was suggested to being ineffective in sulfation reactions as no Si-S phases were detected in all analyses, the mechanism of CaO bound to the SiO_4 (as Ca_3SiO_5) suggested that silica might have promoted sulfation path, thereby by increasing the CaO concentration through increased activity, as reported in previous studies[115–119]. Schumann found that the SO_2 and O_2 pressures in converter furnaces varied with the metallurgical processes being conducted and equilibrium oxygen pressures suggested for converting processes are between 2.7 x10^{-8} atm and 3.4 x10^{-6} atm when a SO_2 pressure is 1 atm.

Table 5.1. The calculated values for equilibrium O_2 partial pressures at different temperatures

Reaction Mechanisms	**Temperature °K**	**Kellog**[79]	**Dewing and Richardson**[117]	**Wreidt and Darken**[91]
A: $CaO + SO_2 + ½\ O_2 = CaSO_4$		$\Delta G°_{(1100\text{-}1638K)} = -136{,}830 - 41.61T \log T + 206.73T$ cal.	$\Delta G°_{(1483\text{-}1638K)} = -111{,}000 + 56.62T$ cal.	$\Delta G°_{(1453\text{-}1646K)} = -110{,}320 + 56.80T$ cal.
		P_{O_2}	P_{O_2}	P_{O_2}
	1073	8.0363×10^{-20}	–	–
	1173	8.961×10^{-16}	–	–
	1273	2.0457×10^{-12}	–	–
	1473	3.44×10^{-7}	–	3.098×10^{-7}
	1573	3.97×10^{-5}	2.015×10^{-5}	3.73×10^{-5}
	1623	3.33×10^{-4}	1.798×10^{-4}	3.281×10^{-4}
Gas mixture partial pressures: $P_{SO_2} = 0.1998$, $P_{O_2} = 0.0036$, $P_{N_2} = 0.796$				

Table 5.2. The calculated values for O_2 equilibrium partial pressures in dissociation. H_2O to H_2 and O_2.

Reaction Mechanisms	**Temperature °K**	**Richardson and Jeffes**[112]	**Kubaschewski and Alcock's**[109]
B: $H_2O = H_2 + ½O_2$		$\Delta G°_{(373-2500°K)} = 59{,}000 - 13.375T$ cal.	$\Delta G°_{(373-2500°K)} = 57{,}250 - 4.48T \log T + 2.21T$ cal.
		P_{O_2}	P_{O_2}
	973	7.62×10^{-11}	6.67×10^{-11}
	1073	5.07×10^{-10}	4.47×10^{-10}
	1173	2.44×10^{-9}	2.18×10^{-9}
	1273	9.20×10^{-9}	8.32×10^{-9}
	1623	1.052×10^{-6}	2.52×10^{-7}

In Figure 4.10[79], the $CaSO_4$ formation was confirmed for the suggested converting gas combination pressures[21], and the maximum temperature indicated occurred at T_{max} = 1340°C at P_{O_2} = 3.4 x10^{-6}, and T_{max} = 1290°C at P_{O_2} = 2.7 x10^{-8} when P_{SO_2} = 1 atm. The indicated results in Figure 4.11[121–122] disagreed with those in Figure 4.10[79], in that maximum temperature for $CaSO_4$ stability occurred at T_{max} = 1290°C for P_{O_2} = 3.4 x10^{-6}, and T_{max} = 1190°C at P_{O_2} = 2.7 x10^{-8} when P_{SO_2} = 1 atm. Since Kellogg[79] data was within the ±20 cal limits of experimental errors for the sulfation potential, the data was more reliable and chosen in the present study. The amount of oxygen introduced by the dissociation of H_2O at different temperatures may have contributed to the equilibrium partial presence of oxygen according to the following reaction:

$$H_2O(g) = H_2(g) + ½O_2(g) \qquad (5.\ 8)$$

and stoicheometry

$$P_{H_2} = \frac{1}{2} P_{O_2} \qquad (5.\ 9)$$

$$\log\left(2P_{O_2}\right) = \frac{2}{3}\left(\log P_{H_2O} - \left(\frac{\Delta G^\circ}{2.303RT}\right)\right) \qquad (5.\ 9)$$

The determined oxygen partial pressures using Richardson and Jeffes[112], and Kubaschewski and Alcock's[109] data in Table 5.2, suggested that the oxygen pressures had no significant effect on the sulfation chemical potential at 1350°C since the pressures were less than 10^{-4} atm

5.2.4 Microstructural changes in sulfur-bearing gases at low temperatures

At low temperatures of 700°C in SO_2-N_2 and SO_2-O_2 gas mixtures, the changes that occurred in basic refractory structures and a through thermodynamic analysis investigated and sulfate formation was confirmed. The observations suggested that the original structure played an important role and influenced resulting reactions. In magnesite refractory (Figure 4.19a, 4.23 and 4.24) it was evident that pore size influenced the gas permeability, and the analyses showed that newly formed phases were $MgSO_4$ and $CaMg_3(SO_4)_4$. Previous investigators[22,30–38] have demonstrated the sulfation of magnesia component in basic refractories below 1000°C. Rigby[34] suggested that in basic refractories $MgSO_4$ was a stable phase for temperatures up to 750°C. In the present study, the important feature of $MgSO_4$ observed was a highly porous structure formed as a collective mass of particles of spongy material. The $CaMg_3(SO_4)_4$ was often formed as an elongated plate-like structure that had irregular shapes. The sulfate structures observed suggested that reactions occurred with the diffused sulfur-bearing gases along grain boundaries,

pores, micro-fractures, and within cracks. The typical original structure showing large magnesia grains (Figure 4.1) indicated that within the imperfections, sulfate phases having different concentrations occurred as pore or boundary space fillings. These observations related to Massengale *et al*[28] studies in that pore size influenced permeability, while diffusion processes affected porosity, and seen to have enhanced the infiltration of sulfur-bearing gases within the refractory structure. The silica observed, occurred often within the sulfate structures formed as a phase mixture. Since it was indicated to being ineffective in sulfation reactions its occurrence as a phase mixture suggested that at low temperatures kinetics of diffusion processes might have been slower, and this had a significant effect on the sulfate compositions.

The highly porous structure of $MgSO_4$ formed as a collective mass of particles of spongy material suggested that initial chemical reactions might not have resulted in an impermeable sulfate product layer, as suggested for gas-solid reactions in previous studies[39−43,38,83−85,94−99]. Therefore, progressive sulfation could possibly occur through the porous structure, which could possibly allowed inward diffusion path for gases, through the porous sulfate product formed to the $MgO/MgSO_4$ interface, as suggested by Borgwardt *et al*[100]. This suggested that, the reaction continued at the $MgO/MgSO_4$ interface until an impermeable layer of product formed eventually, because of 400% expansion volume reported[22] for $MgSO_4$ formation in basic refractories. Gregurek *et al*.[38] showed that the $MgSO_4$ formed along the grain boundaries resulted in disintegration of magnesia grains, and was in association with the silicate phase. The observed ridges, voids and grooves on the surfaces of magnesia grain boundaries possibly resulted in varying partial pressures and non-uniform sulfate structures, and this indicated the effect of product formed on the diffusion processes. The difference in sulfate compositions suggested differences in partial pressures most likely due to local variations in gas concentrations, in which sulfates formed corresponded to the local equilibrium pressures of the gases. Kinetics of diffusion processes have been reported to be higher at the grain boundary surfaces due to suggested increased oxygen activities[59].

Grain boundaries are structural properties resulting from method of manufacture and composition, and it has been shown that it is where the grains change crystal orientation and can act as barriers during diffusion processes[60–67,70]. Since diffusion processes at the grain boundary are affected by the interfacial energy[70], the reaction of MgO with sulfur-bearing gases at the grain surface suggested was influenced by reduced interfacial energies. Mäkipää and Taskinen[13] suggested that, because sulfur and oxygen were active elements, they lowered the surface and

interfacial energies in refractory interactions. This suggest that, as sulfate formed at the ions might not have been activated enough to pass through the grain boundary surfaces, as indicated in a mechanism of outward diffusion[98–99]. Studies[4–5,48–50] have agreed that dissociation in basic refractory components occurred at 700°C, and silicates formed secondary phases with magnesia and spinels[48] in reactions that have suggested to influence pore size due to unequal diffusion of ions[28]. Therefore, the differences in mass transfer across the interfaces and presence of sulfur-bearing gases possibly resulted in non-uniform accumulation, observed to form grooves, voids, and ridges in magnesia grain surfaces (Figure 4.19a and 4.23 to 4.24).

From the observations, suggestions that void formation observed within the grooves related to the pore distribution were established, and this resulted to the discontinuities that occurred at the surfaces. A mechanism proposed for the formation of discontinuities, suggested that, in the initial stages the equilibrium partial pressures of the diffused sulfur-bearing gases at the MgO/gas interface were higher than in the gas phase, and promoted sulfation of MgO. The porous sulfate product formed, increased permeability and gases were transported through the product towards the $MgO/MgSO_4$ interface. At the $MgO/MgSO_4$ interface, the reaction continued with MgO and the equilibrium partial pressures decreased as they approached those of the gas phase, and until the impermeable layer was formed. Gradients both due to the growth effect of $MgSO_4$ formed and the continued formation of sulfates at the outer surface (possibly with the CaO in silicates), made it difficult for sulfate species to diffuse through the gas/$MgSO_4$ interface. From these suggestions, the equilibrium partial pressures that prevailed locally underneath the $MgO/MgSO_4$ interface determined the MgO reactions with sulfur-bearing gases and non-uniform sulfation resulted. Furthermore, deposition of sulfur-bearing gases and chemical reaction that possibly occurred by sulfate precipitation on silicates and at the grain boundaries could possibly occur. At the $MgO/MgSO_4$ interface the suggested reduced concentrations of sulfate species consequently resulted in non-uniform reaction with MgO, in reactions that tended to result in discontinuities on the surface of grain boundaries as seen in Figures 4.18a, 4.22 and 4.23, where the sulfate-rich regions appeared darker. The most important factor in the mechanism was the transport diffusion through the discontinuities.

The presence of silica oxide within the sulfate mixtures, indicated partial disintegration of silicate phases and subsequent reaction of the Ca-Mg oxides with the sulfur-bearing gases forming $CaMg_3(SO_4)_4$, which frequently occurred as elongated plate-like structures. Olbrich ***et al.***[31] Indicated that silicates and spinels formed sulfate mixtures in presence of sulfur-bearing

gases, and formed non-uniform SO_3 concentrations occurred at the grain boundaries with MgO, from the disintegrated secondary spinel. The sulfate mixture identified as $K_2SO_4 \cdot 2CaSO_4$ in basic refractories examined by Hugget[30] was characterized by a lamellar twining structure, instead of $CaMg_3(SO_4)_4$ as in the present study. Therefore, the suggested slow diffusion processes at 700°C had the tendency to increase sulfation, but resulted in entrapment of silica forming sulfate mixtures, whereas in magnesia a build-up of SO_3 non-uniform equilibrium partial pressures resulted in discontinuities filled with varying sulfate concentrations. However, at 1350°C, complete separation of the silicate phase and sulfation of CaO was evident in Figure 4.11 and 4.16, suggesting high diffusion processes. It has been reported that decreasing temperatures reduced the kinetics of diffusion processes and resulted in different microstructures[55,68] Hugget[30], Trojer[36] and Olbricho *et al.*[31] also indicated that silicate phases played a role in transporting the reactive oxides without taking part in reactions[115]. The observed variations in reactivity among the refractories can be explained by considering the structural differences, in which the pore size and phase distribution developed were the important factors, which influenced gas permeability and sulfation.

In laboratory magnesium oxide, refractory magnesite and chrome-magnesite powdered pellets (Figure 4.19b to 4.21) the structures indicated varying sulfate concentrations within the interior of the structure. The structural formations of the precipitates suggested, indicated well-developed rounded particles that could have grown most likely by incorporating small precipitates, and resulted in rough surface observed. The observed elongated plate-like sulfate structures showed sulfate concentration (quantified as SO_3) that was over-stoicheometric with both CaO and MgO at 700°C. These observations suggested that sulfate precipitation, was influenced possibly by gas entrapment within the growing structure, in which the concentration was determined by the partial pressures prevailing inside.

In chrome-magnesite and magnesite-chrome (Figures 4.22 and 4.25 to 4.29) structures, it was evident that sulfate was formed with magnesia and mixtures of silicates and spinels along the grains boundaries. The disengagement of secondary magnesia spinels at the grain boundary surfaces and formation of sulfate mixtures was evident (Figure 4.25b). The weakened structural effect suggested to have taken place as structural changes were induced by diffusion processes and increased open pore structure and crack formation contributed to and sulfation. The presence of Fe_2O_3, Cr_2O_3 and Al_2O_2 secondary spinels as sulfate mixtures was attributed to the slow diffusion kinetics, whereby the sesquioxides and silicates became trapped when the MgO

and CaO exposed formed sulfates. The morphology in which the sulfate mixtures occurred suggested that solid-state diffusion processes and migration promoted gas permeability, and supported reports from previous studies[3,30–31,36,78]. Huggett[30] supported the assumption and reported that reactivity of $CaSO_4$ with alumino-silicates, promoted sulfation and contributed to the presence of Al_2O_3 as a mixture. The diffusing sesquioxides from the chromite grains incorporated within the sulfates so that, on cooling, they will precipitate within the sulfate mixture formed. These factors also contributed to the effectiveness of sesquioxides release within the sulfates, which appeared to have not reacted with the sulfate.

The formation of pyrrhotite, FeS, and ferric sulfate, $Fe_2(SO_4)_3$ were not detected in sulfated areas of the refractories, but are reported in studies of Trojer[36] and Treffner[71] to be intermediate phases that result in sulfation. It was indicated[36] that formation of sulfur compounds (FeS, $Fe_2(SO_4)_3$, K_2SO_4) may lead to sulfation of MgO, and there was no stoicheometric relation between these oxides and total sulfur, thus further investigation is needed. The observed results also disagreed with the studies of Kellogg[79], and Safiullin *et al.*[80], which suggested that iron sulfates were present at 700°C, but agreed with Trojer[36], Rigby[34] and Podwórny *et al.*[78],in that different oxides from disintegrated secondary spinels existed above 600°C, and could be indicating instability of the ferric sulfate, $Fe_2(SO_4)_3$. The reported[39,89] effect of Fe_2O_3 as catalyst that enhances formation of $MgSO_4$ and $CaSO_4$ was not established in the present study, thus correlation were not established.

5.2.5 Thermodynamic considerations of $MgSO_4$ formation at low temperatures

For reactions conducted between 700°C and 1000°C in SO_2-O_2 gas mixtures the results of products analyses in Table 4.2 confirmed the $MgSO_4$, $CaSO_4$ and $CaMg_3(SO_4)_4$ observed in structures. The sulfate formation in SO_2-N_2 gas mixtures could not be determined using X-Ray Diffraction from Table 4.2, but predominance area diagrams in Figure 2.5, 4.10 to 4.13 showed that the conditions were possibly favorable for $MgSO_4$ and $CaSO_4$ formation, and depended on temperature. The temperature dependency of $CaSO_4$ is described in Section 5.2.3, and in predominance area diagram in Figure 4.10 and 4.11 at the combination gas pressures of oxygen and sulfur dioxide used in SO_2-O_2 gas mixtures, $CaSO_4$ stability occurred at both low temperatures and high temperature above 1350°C, as indicated in the diagrams. Kellogg[79], Wreidt *et al.*[91]and Dewing *et al.*[117] data were used to calculate the oxygen partial pressures

required for $MgSO_4$ formation and the favorable conditions predicted in the predominance area diagrams showed that the reaction could be described by the following Equation:

$$MgO_{(s)} + SO_{2\,(g)} + ½\ O_{2\,(g)} = MgSO_{4\,(s)} \qquad 5.10$$

The minimum partial pressure of oxygen needed to form $MgSO_4$ in Table 5.3 increased from 10^{-12} at 700°C to 10^{-5} at 1000°C, which are below P_{O_2} = 0.0036 atm or P_{O_2} = 0.796 atm, the values of P_{O_2} present in the SO_2-O_2 and SO_2-N gas mixtures, confirming that conditions were favourable for $MgSO_4$ formation. The predominance area diagram generated using Kellog's[79] data in Figure 4.11 confirmed the results shown in Table 4.2 and in combination gas pressures used in SO_2-N_2 and SO_2-O_2 gas mixtures the maximum temperatures indicated for $MgSO_4$ stability are up to 1110°C and 1290°C, respectively. However, the studies[79] indicated that the thermodynamic data derived for the reaction was not appropriate outside 726°C to 1155°C (± 20 cal) temperature range. In Figure 2.5, the predominance area diagram generated by Liouw *et al.*[22] agreed with Figure 4.11 confirming the $MgSO_4$ stability, but indicated decreased maximum temperature at the combination gas pressures used in the present study, obtaining T_{max} = 980°C in SO_2-N_2 and T_{max}= 1090°C in SO_2-O_2 mixtures. In Figure 4.13, the indicated maximum temperatures was T_{max} = 990°C in SO_2-O_2 gas combination agreeing more with those shown for combination gas mixture in SO_2-N_2 gas in Figure 2.5.

In converter furnaces large amounts of $MgSO_4$ have been found to form in the basic refractories used as working linings[30–38,78], and the findings in the present study agreed with Rigby[34], Trojer[36], McPherson[37], Gregureck *et al.*[38], Olbrich *et al.*[31] and Podwórny *et al.*[78] , who showed that $MgSO_4$ formed in basic refractories was stable for maximum temperatures up to 1100°C. The SO_2 and O_2 pressures suggested by Schumann[21] for converting processes were determined for $MgSO_4$ stability in the predominance area diagrams. McPherson[37] reported that within these oxygen pressures, suggested equilibrium temperatures for $MgSO_4$ formation increased to 850°C, and in Figure 2.5, gas combinations P_{O_2} = 2.7 x10^{-8} atm and P_{SO_2} = 1 atm, agreed with the findings. The mechanism of $MgSO_4$ formation proposed by Liow *et al.*[22] agreed with McPherson's[37] findings and related to Equation 5.10. McPherson[37] and Liow *et al*[22] calculations were based on Dewing and Richardson[117] data. The favorable conditions for $MgSO_4$ stability indicated were higher at maximum temperature up to 910°C for P_{O_2} = 3.4 x10^{-6} atm and P_{SO_2} = 1 atm gas combination. They[22] explained that $MgSO_4$ formation depended on the temperature gradient across the refractory brick and steep gradients decreased the temperature stability of

$MgSO_4$. This suggested that high temperatures at the material surface decreased $MgSO_4$ stability, but increased diffusion of gases to the cooler regions, which promoted $MgSO_4$ formation at low temperatures.

In Figure 4.12, Kellog's[79] data corresponded with McPherson[37] maximum temperature for $MgSO_4$ stability, at suggested converting gas pressures combinations[21], with T_{max} = 890°C at P_{O_2} = 2.7 x10^{-8}, and $MgSO_4$ would not form at T_{max} =1000°C at P_{O_2} = 3.4 x10^{-6} when P_{SO_2} = 1 atm. The FactSage results in Figure 4.11, disagreed with McPherson[37] and Kellog's[79] data in that in converter gas combinations the maximum temperature T_{max} = 830°C for $MgSO_4$ stability occurred at high oxygen pressures of P_{O_2} = 3.4 x10^{-6} when $P_{S\,O_2}$ = 1 atm, and at P_{O_2} = 2.7 x10^{-8}, Tmax = 760°C. Figure 4.10 indicated that $CaSO_4$ would be formed at low temperatures up to Tmax = 1290°C at P_{O_2} = 2.7 x10^{-8} atm and P_{SO_2} = 1 atm. The higher equilibrium oxygen pressures calculated for $MgSO_4$ (in Table 5.3) than that required for $CaSO_4$ formation (in Table 5.1) between 800°C and 1000°C, suggested that $CaSO_4$ would be formed preferentially in reaction conditions employed in this study.

The previous studies[92–94] supported the suggestions in that CaO is a more basic oxide than MgO and in oxidizing conditions, the oxygen pressures required for $CaSO_4$ formation in sulfur bearing-gases was relatively lower than that of $MgSO_4$. However, in basic refractories investigated in this study, more than 80 wt % was MgO, while CaO was limited only at the silicate phases found within the grain boundaries. This indicated that the CaO sulfation depended on the accessibility and the suggested diffusion from the components[30]. The large amounts of $MgSO_4$ observed in the investigations were due to the readily available MgO found in refractories, and this related to previous studies[22,32–38]. The Fact Sage[121–122] thermo chemical software indicated free energy data that is based on the specific thermo chemical data of the gases, oxides, sulfate compounds, available in compilations of JANAF Tables[108] and Thermochemical Properties of Inorganic Substances[107]. It is worth noting that in the present study, the data considered for sulfation reactions was that of Kellogg[79]due to suggested reduced experimental errors.

Table 5.3. Equilibrium partial pressures in sulfation reactions.

Reaction Mechanisms	**Temperature °K**	**Kellogg[79]**		**Dewing and Richardson[117]**	
A: $MgO + SO_2 + ½\ O_2 = MgSO_4$		$\Delta G°_{(1000\text{-}1428K)} = -78560 - 16.58T \log T + 100.69T$ cal.		$\Delta G°_{(1173\text{-}1423K)} = -87180 + 60.2T$ cal.	
		$\Delta G°$	P_{O_2}	$\Delta G°$	P_{O_2}
	973	-28793.882	2.925×10^{-12}	–	–
	1073	-24435.03	2.787×10^{-9}	–	–
	1173	-20143.38	7.835×10^{-7}	-16565.4	1.687×10^{-5}
	1273	-15913.194	8.626×10^{-5}	-10545.4	6.006×10^{-3}
Gas mixture partial pressures: $P_{SO_2} = 0.1998 atm$ $(\log P_{SO_2} = -0.699404516)$,R = 1.987165 cal/deg/mol					

5.3 Thermodynamic considerations of the sulfur-bearing gases

The SO_2-O_2 gas mixture, P_{SO_2} = 0.1998 atm and P_{O_2} = 0.796 atm, and in SO_2-N_2 gas mixture contained, P_{SO_2} = 0.1998 atm and P_{O_2} = 0.0036 atm. In Section 2.5.1 Richardson and Jeffes[113], St. Pierre and Chipman[115] and Dewing and Richardson's[116] data were considered for SO_2 dissociation and equilibrium reactions considered in the present study are presented by:

$$SO_{2\,(g)} = SO_{(g)} + ½\ O_{2\,(g)} \qquad (5.11)$$

$$SO_{(g)} = ½\ O_{2\,(g)} + ½\ S_{2(g)} \qquad (5.12)$$

$$SO_{2\,(g)} = ½S_{2(g)} + O_{2\,(g)} \qquad (5.13)$$

The values determined using the data[113] are tabulate in Table 2.4, and showed that reactions involved SO_2 dissociation are endothermic at temperatures employed in the investigations. Previous studies[115–119] showed that at oxygen pressures above 10^{-4}, and sulfur dioxide pressures above 10^{-3}, sulfate would form. In the gas mixtures used in the study, the SO_2 and O_2 pressures are well above these indicated pressures for sulfate formation suggesting that sulfate will definitely form. Therefore, the suggested reactions that involved Equation 5.11 to 5.13 possibly occurred to a small extent, and this related to the suggestions made by Evan and Wagman[110], who showed that within mole fractions of 0.01 to 1 the gaseous decomposition of SO_2 to sulfur species were insignificant. The product analyses results (Table 4.2) confirmed the formation of $CaSO_4$ up to 1350°C, while $MgSO_4$ was formed up to 1000°C. The SO_3 equilibrium pressures from the amount of sulfate formed was indicated in the analyses (Figure 4.43 and 4.45). The equilibrium pressures for SO_3 have been investigated in the previous studies[87–88,91,114,116,119–120] for a reaction that can described by the following equation:

$$SO_{2\,(g)} + ½\ O_{2\,(g)} = SO_{3\,(g)} \qquad (5.14)$$

The equilibrium constant for the formation of SO_3 can be presented by:

$$\Delta G^\circ = -2.303RT\log K_1, \text{ where } \log K_1 = \frac{\Delta G^\circ}{-2.303RT} \text{ and} \qquad (5.15)$$

in which

$$\log K_1 = \log P_{SO_3} - \log P_{SO_2} - \tfrac{1}{2}\log P_{O_2} \qquad (5.17)$$

$$\log P_{SO_3} = \frac{(2\log K_1 + 2\log P_{SO_2} + \log P_{O_2})}{2} \qquad (5.18)$$

Kellogg[79], Richardson and Jeffes[113] and St. Pierre and Chipman[115] data were used to calculate the equilibrium SO_3 partial pressures for $MgSO_4$ formed tabulated in Table 5.4. The values obtained from equilibrium oxygen pressure from Equations 5.5, the known SO_2 gas partial pressures of

0.1998 atm, and the equilibrium constant for SO_3 formation given as K_1 in Equation 5.16 were used. From the values, the equilibrium constants were dependent on temperature and an increase in oxygen pressures or sulfur dioxide would increase the product of $P_{SO_2}(P_{O_2})^{1/2}$, which decreased with increasing temperatures. Table 5.4, indicate that SO_3 equilibrium pressure decreases with temperature, but if the required oxygen pressures for $MgSO_4$ formation are available, Table 5.3 suggests that SO_3 will increase (from 10^{-7} at 700°C to 10^{-4} at 1000°C) with increasing oxygen pressures, which increase with temperatures. At 700°C the equilibrium constant were greater than 1 (i.e. K>1) for all the data used indicating that SO_3 formation was favored in the gas phase. This could possibly explained the rapid increase in sulfate shown in Figure 4.42 to 4.45 formed at 700°C, and the suggested over stoicheometry formed for non-uniform sulfate structures observed for the reaction conversions in SO_2-O_2 and SO_2-N_2 gas mixtures. Kellogg[79] and Richardson and Jeffes[113] data gave similar values indicating good correlation, whilst on the contrary St. Pierre and Chipman[115] data resulted in almost half the values obtained for equilibrium constant. In MgO and CaO reactions with sulfur-bearing gas mixtures, temperatures for sulfate formation are determined by the product of log ($P_{SO_2} \cdot P_{O_2}{}^{1/2}$), and increase with increasing product[22,37]. At 1350°C the equilibrium constant decreased to K<1, suggesting that SO_2 and O_2 reactants dominated, but in presence of CaO, $CaSO_4$ was formed. This suggested the decreasing equilibrium constants accounted for a very small degree of dissociation.

The co-existence of CaS and/or $CaSO_4$ at sulfur dioxide partial pressures above 10^{-3}atm [91] has been suggested, but only $CaSO_4$ was confirmed and observed as a dominant sulfate product in magnesite at 1350°C (Figure 4.11 and 4.16). In the predominance area diagrams, shown in Figure 4.10, the values obtained for P_{SO_3} (Table 5.4) in SO_2-O_2 gas mixture with O_2 partial pressures of 0.796 atm, decreased from 10^{-1} at 700°C to 10^{-3} at 1350°C. In SO_2-O_2 gas mixture at O_2 partial pressures of 0.0036 atm. the P_{SO_3} decreased from 10^{-2} at 700°C to 10^{-4} at 1350°C. The dissociation rates were determined by the difference in forward reaction and reverse reaction, in which a small difference would have resulted in increased SO_2 and O_2 products, as the P_{SO_3} calculated decreased significantly. The observations suggested that the sulfate formation did not involve transport of sulfur species from dissociations reactions (S_2, S, and SO). The SO_2 and O_2 gas mixtures transported inward along the grain boundaries and within the cracks reacted to form sulfate, and possibly the cations from solid oxides were transported outward by vacancy diffusion to react with the gas mixture.

Table 5.4. Standard Gibbs-free energies and equilibrium constants for SO_3 formation in different sulfur-bearing gas mixtures.

Reaction Mechanisms	**Temperature °C**	**Kellogg**[79]			**Richardson and Jeffes**[113]			**St. Pierre and Chipman**[114]		
A: $SO_2 + ½\ O_2 = SO_3$	K	$\Delta G° = -25010-5.562T \log T + 40.52T$ cal.			$\Delta G°_{(318\text{-}1800K)} = -22600+ 21.36T$ cal.			$\Delta G° = -19800 + 19.76T$ cal.		
		$\Delta G°$	$K°$	P_{SO_3}	$\Delta G°$	$K°$	P_{SO_3}	$\Delta G°$	$K°$	P_{SO_3}
	973	-1755.187	2.478	4.418×10^{-1}	-1816.72	2.559	4.557×10^{-1}	-573.52	1.345	2.396×10^{-1}
	1073	381.262	0.836	1.49×10^{-1}	319.28	0.861	1.533×10^{-1}	1042.48	0.518	9.228×10^{-2}
	1173	2495.166	0.343	6.112×10^{-2}	2455.28	0.349	6.213×10^{-2}	3378.48	0.235	4.192×10^{-2}
	1273	4588.45	0.163	2.907×10^{-2}	4591.28	0.163	2.971×10^{-2}	5354.48	0.120	2.146×10^{-2}
	1623	11774.01	0.026	4.633×10^{-3}	12067.28	0.024	4.227×10^{-3}	12270.48	0.022	3.959×10^{-3}

Gas mixture partial pressures： $P_{SO_2} = 0.1998atm$ $(\log P_{SO_2} = -0.699404516)$, and $P_{O_2} = 0.796atm\left(\log P_{O_2} = -9.908693226x10^{-2}\right)$; R = 1.987165 cal/deg/mol,

Reaction Mechanisms	**Temperature °C**	**Kellogg**[79]			**Richardson and Jeffes**[113]			**St. Pierre and Chipman**[114]		
A: $SO_2 + ½\ O_2 = SO_3$	K	$\Delta G° = -25010-5.562T \log T + 40.52T$ cal.			$\Delta G°_{(318\text{-}1800K)} = -22600+ 21.36T$ cal.			$\Delta G° = -19800 + 19.76T$ cal.		
		$\Delta G°$	$K°$	P_{SO_3}	$\Delta G°$	$K°$	P_{SO_3}	$\Delta G°$	$K°$	P_{SO_3}
	973	-1755.187	2.478	2.971×10^{-2}	-1816.72	2.559	3.067×10^{-2}	-573.52	1.345	1.613×10^{-2}
	1073	381.262	0.836	1.003×10^{-2}	319.28	0.861	1.067×10^{-2}	1042.48	0.518	8.629×10^{-3}
	1173	2495.166	0.343	4.111×10^{-3}	2455.28	0.349	4.182×10^{-3}	3378.48	0.235	2.814×10^{-3}
	1273	4588.45	0.163	1.955×10^{-3}	4591.28	0.163	1.953×10^{-3}	5354.48	0.120	1.444×10^{-3}
	1623	11774.01	0.026	3.116×10^{-4}	12067.28	0.024	2.845×10^{-3}	12270.48	0.022	2.671×10^{-4}

Gas mixture partial pressures: $P_{SO_2} = 0.1998atm$ $(\log P_{SO_2} = -0.699404516)$, and $P_{O_2} = 0.0036atm\left(\log P_{O_2} = -2.443697499\right)$; R = 1.987165 cal/deg/mol,

5.4 Sulfation kinetics of basic refractories in sulfur-bearing gases

It must be noted that the relative reactivity of the basic refractories shown in the present study only served as a guide and does not necessarily predict accurately the behavior of the refractories under the dynamic and complex conditions of the converter furnace. In the converter furnace, the temperature of the gases varies with the type of reactions occurring and the thermochemical reaction time is long, possibly months. Furthermore, the prevailing partial pressures of SO_2, S_2 and O_2 varies with the amount of oxygen or air used during blowing, and above all, the furnaces are open reactors and thus equilibrium is not attained in reaction systems. The off-gases contain other volatile gases, moisture, and compounds (particularly SiO_2 and CaO) from the flue gases, which might influence the SO_2 oxidations and reaction kinetics. Therefore, it is difficult to predict the amount of oxides necessary to cause erosion due to sulfation. In the reaction conditions (temperature, type of refractory and gas composition), the absorption of sulfur-bearing gases was influenced by permeability and pores size, and varied with time. In kinetics of the reactions, diffusion processes and crystallization of the reactive oxide species accounts for all the reactions. Solid-state diffusion within the particles (either external or intraparticle), pore diffusion, and product layer diffusion were factors affecting reactions. The effect of time, temperature, and changing gas composition were investigated.

5.4.1 Effect of Time.

The kinetic conversion profiles for the sulfation of refractories in different sulfur-bearing gases as the function of time are illustrated in Figures 4.33 at 700°C and Figures 4.33 to 4.44 for reactions at different temperatures. For all the refractories reacted over 84 hours, the reaction extents increased with increasing reaction processes giving profiles that conformed to changing conversion profiles. The conversion profiles suggested that reaction conversion of the oxide (calculated for MgO shown in 3.10.1) to sulfate increased as the reaction progressed. The fraction of the refractory oxide converted to sulfate was found to be between 2 and 14%. For the reaction processes carried out for 14 hours, the amount of the refractory oxide found converted to sulfate were different for all refractories. Sulfation rate versus time plots indicated include the initial period, a period for establishing transformation conditions and a stationary period.

Figure 4.30 showed reaction extents for sulfation conversions at 700°C, and the reaction kinetics suggested increased conversion within 28 hours of the reaction progress. This was possibly due to the spontaneous conversion reactions[85–96], which occurred at the oxide surface with the sulfur-

bearing gases, and has been reported to be the factor in reaction progress in sulfation of various carbonates[39-43,83-86,92-97]. Magnesite-chrome brick 1 suggested reaction conversions that conformed to linear relations, between 14 to 42 hours, suggesting a chemical reaction in which the conversion progress followed a first order reaction and affected the reaction extents, as suggested by Borgwardt[42]. However, for other refractories, reaction extents gave different conversion profiles, suggesting that the chemical reaction might not have been a factor in the conversion progress, but, the microstructural changes such as pore distribution, pore surface area and the structure probably affected the conversions, as reported in previous studies[83–86,93–97]. Hartman[85] showed that sulfur-bearing gases reacted rapidly with the MgO and CaO and conversion reactions increased rapidly at small gas concentrations, but the extent of reaction decreased with reaction progress. From the structural observations (Figure 4.1 to 4.4), the refractories contained porosity, which promoted permeability and suggested increased gas diffusion when exposed at different temperatures. This suggested that pore surface area in contact with reactive oxide might have been the factor in the reaction conversions, rather than the overall pore volume. This was because not in all pores observed, a reactive oxide or sulfate product was found. Other inherent structural features in refractories were the grain boundaries found between different phases, usually occupied by silicates (found along grain boundaries), where the reactive oxide exposures appeared to have a significant effect on the reaction progress.

The conversion extents continued to increase gradually between 28 and 70 hours and plateaus off at 84hours. This behaviour correlated to an intermediate period of adaptation to reaction conditions characterized by structural changes in refractory components[36,78,86] and transformation as the product formed. Clum[86] suggested that structural transitions to oxide involved a metastable condition, which promoted high defect oxide structure and sulfation was promoted. The studies indicated that diffusional transports of sulfur-bearing gases were factors affecting reaction progress. From this understanding, the pore distribution and the sulfate formed determined the extent of reaction conversion, where after a certain fractional conversion to sulfate, the reactions decreased with increasing time[39-43]. The suggested dissolution[48–51] of the magnesia spinels due to changes from Fe_2O_3 to Fe_3O_4, has been shown to cause disengagement and loosening in spinels (shown in Figure 4.28b and 4.32a), which have a major effect on sulfation in chrome-magnesite and magnesite-chrome refractories. The gradual increase of sulfation areas as silicates and spinels loosened, predominantly due to diffusional release of Ca^{2+} ions by silicates and Mg^{2+} ions out of the spinels particularly ($MgFe_2O_4$), increased reaction of the oxides.

The diffusion processes and activity of the oxides, that resulted in appearance of grooves and voids that harbored non-uniform localized gas concentrations at low temperatures, determined the extent of oxide diffusional exposure and influenced the non-linear reaction profiles. The effects of differential diffusion of Fe^{3+} ions found to diffuse rapidly than Mg^{2+} ions[4–5], could have resulted in increased void formation through vacancy coalescence in the phase structures. In this study, the reactions explained based on diffusion effects and void formation. Podworny ***et al.***[78] established similar observations, and demonstrated that structural changes that occurred within the magnesia spinels because of diffusion processes, affected the sulfation rates resulting in non-linear reaction extents. The structural changes due to diffusion processes could have caused formation of micro porosity or voids within affected contact area between the gases and the oxides, most likely through changes in vacancy probability and promoted free volume distribution. This effect caused progressive separation of the phases as time increased. These effects together with structural features (pores, cracks, and fractures) and loosening of the structures resulted in non-uniform reaction and altered reaction profiles.

Since this cannot necessarily be the determining factor when interpreting linear relations as reaction determining factors may differ, a different mechanism was suggested. The linear reaction extents observed within the conversion profiles were related to sulfation that occurred without complex reactions brought about by structural changes due to diffusional effects and subsequently sulfation. The suggested sulfate products from such reaction most likely resulted from precipitation, which was suggested to form the elongated plate-like sulfate structures, and sulfate-rich grooves and voids observed on the surface of grain boundaries. Therefore, in this case, reactions could possibly be limited by the permeability of the sulfate product and diffusion through the surface of the grain boundaries. Additionally, the stress concentration could have risen sufficiently to cause micro fractures on both the sulfate layer formed and on the surface of the grains[97], enhancing sulfation of the exposed reactive sites and resulted possibly in linear extents. Fan and Satja[97] suggested that as sulfation reaction progressed; accompanying the volume expansion was crack formation and micro fissures on the surface that increased the reaction volume exposing the reactive oxide, also seen in Figure 4.27 and 4.32a. Such changes could be related to the indicated different reaction profiles observed in the present study. The over non-stoicheometric sulfate gas concentration may have precipitated and formed plate-like structures within the cracks formed and around the surface of grain boundaries.

Figure 4.35 to 4.40 showed sulfation conversions at different temperatures in which the reaction profiles were similar to those at 700°C, in that they exhibited non-linear behaviour with higher conversions. The present studies considered that if the suggested oxide release from the components was significantly affected by temperature, which promoted dissolution, increased diffusion transport of gas and, or ions would have occurred, and increased the conversion reaction as seen in profiles between 900°C and 1000°C. Comparison of the sulfation profiles at 700°C with 800°C, 900°C and 1000°C, suggested that diffusion at 800°C could be correlated with that at 700°C, in magnesite-chrome and chrome-magnesite refractories. This was because of the similarities in sulfation profiles at these temperatures. Contrary, correlation of diffusion at 900°C and 1000°C with that at 700°C appeared to be distinctly different in that sulfation profiles related to structural changes and extent of reactions with oxides. However, when 900°C and 1000°C were compared good correlation was established.

The observations suggested that between 700°C, 800°C, no major structural instabilities occurred and decreased conversion reactions were caused by pore clogging most likely due to increased SO_3 concentrations. However, between 900°C and 1000°C (Figure 4.31 to 4.36), structural instability influenced the reactivity of the refractories. The time that it would take for cations to arrive at the sulfate/gas interface by diffusion might have been a factor, and probably tend to decrease as the migration distance increased with sulfate layer formed. This would posibly affect the conversion profiles, which decreased gradually. The extent of iron oxide contribution to the sulfation reactions could not be established as there were no iron sulfates or ferric sulfates could be detected in the refractories. This agreed with previous studies[34,36, 79,85] which showed that iron oxide had no effect on sulfation reactions, but was found within the sulfate mixtures. This disagreed with Marier and Dibbs[89], who reported that presence of iron oxide in the oxides had a catalytic effect on the sulfation reactions. The iron oxide and other sesquioxides such as chromic and alumina found as mixtures in sulfates might have limited optimum contact between the reactive oxide surface and gases, thus indirectly affecting conversion reactions.

The sulfation profiles of magnesite (Figure 4.36) showed good correlations within the temperature employed, indicating decreased possibilities of changes in reaction conditions. Therefore, the use of magnesite as a "virgin" refractory was suitable for comparison in the present study, and its reactivity can be understood by examining the structural features. At low temperatures, slow diffusion kinetics resulted in sulfate mixtures attributed to the changes in reaction profiles. Borgwardt and Harvey[43] attributed the variation in reactions rates to the

contribution of impurities present and their effect on structural changes. The suggested increased diffusion at high temperatures and consequent diffusional increase might have significantly decreased the depth of grooves and formation of voids on the grain boundary surfaces. This could have occurred thereby facilitating the ease of cation and anion activity and diffusion, which could have resulted in optimum sulfation of reactive oxide and decreased the non-uniform localized gas concentrations, thus in increased sulfation. On the other hand, if the increased diffusional processes caused surface voids that were probably filled with sulfur-bearing gases within, mass changes due to volume expansion, as sulfate absorption by the reactive oxide would have closed the voids. The stress developed may have caused rupture that could possibly lead to increased conversion, and consequently increased localized gas concentration. The effect of time showed that the reaction of the solid reactants and formation of the new solid phases was not restricted and was effected by the crystallographic changes during diffusion processes.

5.4.2 Effect of Refractory Composition

The interactions of the basic refractories with sulfur-bearing gases were affected by the type of phases particularly those found within the refractory imperfections, in which the gases diffused through. It has been shown in the present study and previous studies[1–2,70,72] that diffusion processes resulted in migration of phases, whereby silicates were displaced to the grain boundaries. According to Watson[60], the transitions and transformations that occurred within the silicates to release the reactive oxide are determined by the amount and distribution of free volume in the structure, and bond strength between the oxide and silica, and that between oxide and sulfate. Therefore, it was inferred that the relative composition (reactive oxides) and structure of the silicate had an effect on the development of sulfate. In presence of gases, the suggested pores formed, through migration and disintegration of components influenced permeability, which affected sulfation. Trojer[36], Olbrich *et al.*[31] and the present study has demonstrated that sulfation attack occurred mainly with the silicates found within the grain boundaries, but some secondary spinels have been shown to loosen and expose reactive oxide. The silica (SiO_2) and the sesquioxides forming spinels (Fe_2O_3, Al_2O_3, and Cr_2O_3) occurred as mixture within the sulfate formed, but have no effect on the sulfation reactions.

In this study, CaO/SiO_2 ratio was categorized into two groups and the considered ratios were that between 0-1 and 1-3.6. The fact that silicates were found in corresponding positions indicated that phases were distributed uniformly within the refractory, most likely due to the effect of

equilibrium[70]. Phase diagram[5,67] of MgO-CaO-SiO_2 showed that uniform distribution between CaO and SiO_4 was obtained for CaO/SiO_2 ratio less than 1. For CaO/SiO_2 ratio, approaching 1 melting occurred at relatively low temperatures, and further increase in ratio promoted dissolution of the components, in which distribution was determined by temperature and components stability. The tendency for the silicates to crystallize into two or more chemically identical forms (but different structures) increased with increasing amount of calcium and silica, while decreased with magnesia indicating increased stability in its presence[67]. Therefore, at increased temperatures diffusion processes changed the silicate structures, which led to reaction of CaO and MgO components to form sulfates. The investigations on the mechanisms of silicates crystallization in presence of sulfur-bearing gases are not included in this study, and further investigation is important. In literature tricalcium silicate Ca_3SiO_5 has been shown to be unstable at temperatures below 1700°C[67], which supported the structural separation observed in the study and that observed by Trojer[36]. The sulfate formed (Figure 4.46 and 4.48) in the magnesite refractory indicated $CaSO_4$ at 1350°C, suggesting the ability of Ca_3SiO_5 to crystallize, and CaO diffused to form $CaSO_4$. This increased with increasing temperature and the amount of silica found within the sulfate mixtures decreased with increasing temperature suggesting faster diffusion rates and decreased possibility of silica and spinel entrapment within sulfate. The diffusional release of CaO in silicates determined the formation of $CaSO_4$.

In chrome-magnesite and magnesite-chrome refractories, the correlation between the effect of CaO/SiO_2 ratio and their reactivity with sulfate was not established. This was attributed to the presence of Mg_2SiO_4 that occurred as a predominant phase in mixed refractories and to the effects of the original microstructure in which silicate phases were randomly distributed within. However, sulfate mixtures that had spinels and silica were occasional observed, thus the random distribution might have affected the silica tendency to be combined sulfates, and promoted direct bonding and decreased sulfation as seen in Figure 4.4a. It was evident that the reactivity of the basic refractories in different atmospheric conditions could not be related to the variation of CaO/SiO_2 ratio, but the microstructure and its distribution appeared to have an effect on the reactivity at temperatures up to 1000°C. The observations in this study agreed with the previous authors[22, 30,34,37–38] on the $MgSO_4$ formation up to 1000°C, and suggested that any formation of sulfate above dependent on the atmosphere. Therefore, the SO_2/O_2 ratios play an important role at high temperatures in presence of silicate compound containing high CaO content. The silicates affected the diffusional rates and pore structures, in reactions where the temperature was the determining factor.

5.4.3 Effect of Temperature.

In this study, two temperature ranges were used to derive the effect of temperature on the reaction kinetics in gas-refractory interactions. Firstly, the temperature range between 700°C and 1000°C, and secondly between 1000°C and 1350°C. The effect of temperature on the conversion reactions was determined based on the compounds that formed in refractories at varying temperatures and predicted in the predominance area diagrams shown in Figure 4.10 to 4.13, and 2.5. The temperature range 700°C and 1000°C suggested the transformation range that resulted in structural changes in refractory mineral phases, which possibly affected the conversion reactions.

Figure 4.44 showed conversion reactions in SO_2-O_2 gas mixtures, which increased with increasing temperatures within 700°C and 1000°C, but decreased within 1000°C and 1350°C. The observed conversion reaction profiles were highest at 1000°C. The results suggested that in presence of MgO indicated for conversion reactions in Section 3.10.1, $MgSO_4$ formed in refractories. The predominance area diagram illustrated in Figure 2.5, 4.12 to 4.13 indicated that in combination gas pressures used in SO_2-O_2 mixtures, $MgSO_4$ would form for temperatures above 1000°C. However, the kinetic conversions indicated between 700°C and 1000°C in the present studies, corresponded to the suggestions made in previous studies[36,37–38,78–79], which were associated with the $MgSO_4$ formation at 1000°C. Under similar conditions, $CaSO_4$ would be formed between 700°C and 1350°C. This indicated that between 700°C and 1000°C, mainly $MgSO_4$ formed in the refractories confirmed in Table 4.2, owing to its availability while CaO was restricted. The reaction profiles decreased significantly between 1000°C and 1350°C possibly due to occurring changes suggested in SO_2-O_2 gas partial pressures, which affected the tendency of conversion to sulfate.

Figures 4.16 to 4.28 illustrated an increase in sulfate conversions for the temperature range from 700°C to 1000°C. The CM2 refractory showed highest conversion with weight increasing by 0.42 wt% from 0.287 wt% at 700°C to 0.706 wt% at 1000°C. This was expected for CrMg D50-C5 due to the effects of structural changes, the permeability that influenced porosity and had an effect on gas diffusion, and temperatures. The MgCr D60/100 showed lower conversion at 1000°C compared to other refractories suggesting that the prominent direct bonding distribution observed contributed to the decreased conversions, and diffusional processes had minor effect on pore distribution. The major differences in these refractories were the spinel phases, in which

$MgFe_2O_4$ spinel found to be reactive in CrMg D50-C5 was not indicated as a mineral phase in MgCr D60/100, instead the Fe_2O_3 occurred as a solution phase within the $MgCr_2O_3$ spinels rather than coarse precipitates on magnesia observed in CrMg D50-C5. Therefore, in MgCr D60/100 conversion reactions that occurred were effected to a very lesser degree by structural changes, and the suggested decreased volume changes within the developed spinels contributed to the decreased contact area between the reactive oxides and sulfur-bearing gases.

Podwórny *et al.*[78] demonstrated that in SO_2-air mixtures, the kinetics and mechanism of MgO-MgR_2O_4 spinels reactions were affected by temperatures between 550°C and 1000°C, and $MgFe_2O_4$ spinel was found to be the reactive spinel and influenced conversion reactions. This was due to the suggested oxidation state of iron oxide from Fe^{3+} to Fe^{2+} during dissociation processes, which caused defected structural components[78], and pore structural changes increased with increasing temperature[4,55,57], exposing the reactive oxide for subsequent sulfation. The CM1 and MC3 showed increasing weight accounted for sulfate formation from 700°C to 1000°C from 24.81 wt% to 49.53 wt%. The weight in MC2 increased by 54.5 wt% from 700°C to 1000°C. This suggested that, conversion to sulfate increased with increasing temperature, and amount of amorphous sulfate mixtures (caused by spinel dissolutions) formed at high temperatures. The decreased kinetic profiles at 700°C could be due to decreased diffusion processes, which would have increased non-uniformity as conversion progresses and caused pore clogging that gradually decreased conversion reactions. On the other hand, the increased kinetic profiles at 700°C indicated for magnesite refractory (M), suggested increased surface area for reactions, because there are no spinels, and increased conversion ratios.

At 1350°C, the suggested diffusional processes increased, but the conversion reactions to $MgSO_4$ are shown to have not occurred, and the findings were confirmed in phase analyses results shown in Table 4.2, and corresponded to the Mg-S-O predominance area diagram (Figure 4.10 and 4.11). The negative decreased weight shown by profiles, corresponded to the effects of volume changes due to dissolution of spinels, in which loss of oxygen by Fe_2O_3 suggested to occur at about 1000°C, resulted in the weight loss in chrome-magnesite and magnesite-chrome refractories[56]. This reduction of ferric oxide to form magnesiowustite (MgO·FeO) spinels, and also the associated increased porosity and grain growth have been shown previously[4–5,46]. The sulfates found shown in Figure 4.43, were attributed to the probable condensation of the sulfur gas vapor species that possibly could be oxidized as the temperature decreased, during cooling. The vapor species may have been trapped within the increasing pore structure or micro fractures

because of grain growth. However, for magnesite refractory different result were observed as the conversion profiles shown were relatively higher, possibly due to $CaSO_4$, as suggested in Ca-S-O predominance area diagram (Figure4.10b) for the partial pressures of oxygen P_{O_2} =0.796 and sulfur dioxide P_{SO_2} =0.1998 employed in the experiments, and confirmed in phase analyses results shown in Table 4.2. The structural observations (Figure 4.19) showed that $CaSO_4$ formed because of structural disintegration in tricalium silicate phase found between the magnesia grains, where conversion corresponded to the CaO diffusing out of the silicate.

In SO_2-N_2 gas mixtures the conversion profiles shown in Figure 4.47 indicated that sulfation decreased with increasing temperatures between 700°C and 1000°C. The conversion profiles showed highest amounts of converted sulfate occurred at 700°C, instead of 1000°C as shown in conversion profiles obtained for SO_2-O_2 gas mixtures. The formation of sulfate in the refractories could not be confirmed by X-Ray diffraction phase analyses technique employed in the studies, due to low proportions obtained from the reacted samples. However, the suggested formation of sulfate in refractories observed in Figure 4.45 at oxygen and sulfur dioxide pressures considered corresponded to the predominance area diagrams shown in Figure 2.5, 4.12 and 4.13. Therefore, the probable oxidation of SO_2 to SO_3 by O_2 to form sulfate might have affected the sulfation potential in the refractories. Treffner[29] reported that in refractories the conversion to sulfate can be described by the SO_3 formation, which was suggested to be determined by the product of log ($P_{SO_2} \cdot P_{O_2}{}^{1/2}$) by McPherson[37]. Therefore, decreasing the oxygen pressures most likely decreased the conversion reactions to form sulfate. This related to Evan and Wagman[110] investigations, which indicated that in SO_2-O_2-SO_3 gas mixtures the equilibrium compositions of SO_3 dominated at low temperatures between 700°C and 1000°C. Marier and Dibbs[89] and Marier and Ingrahm[125] reported that oxidation was necessary for sulfation in SO_2-O_2 gas mixtures and the conversion rate was proportional to the area of the oxide/sulfate interface. They[125] found that the sulfate product layer formed in presence of SO_3 facilitated progressive reaction with oxide, while the product formed in presence of SO_2-O_2 gas mixtures decreased sulfation of the oxide. From this understanding, in SO_2-O_2 gas mixtures the sulfate formed an impermeable layer that did not allow gas diffusion and possible ionic diffusion. This suggests that sulfation proposed by other investigators[98–100]could not be promoted.

In the present studies, the sulfate was found predominantly at the pores and along grain boundaries, therefore it could be suggested that the decreased partial pressures of oxygen possibly minimized the localized gas concentration. This decrease in localized equilibrium concentration decreased subsequent increases in SO3 formation. The surface area for reactions was thus increased, but rapid sulfation in SO_2-O_2 gas mixtures resulted in pore closure (from an impermeable layer formed), which decreased conversion reactions as the product layer was formed. The suggested 400% expansion in volume changes indicated for $MgSO_4$[22], and expansion from $CaSO_4$ could have caused pore closure in the refractory and decreased gas diffusion and subsequently conversion reactions. The results suggested that the depth of the gas diffusion into the refractory structure could have affected the conversion reactions, where the sulfation that prevailed at the outer surface of the refractory possibly resulted in pore closure.

5.4.4 Effect of SO_2/O_2 on Sulfation Reaction.

The MgCr brick 2, MgCr brick 1, Magnesite, and CrMg D50-C5 refractories were investigated for sulfation at 800°C and 1000°C in SO_2-N_2 gas mixtures and pure SO_2 atmosphere. The SO_2/O_2 ratio in SO_2-N_2 gas mixtures was 55.5, at equilibrium partial pressures of SO_2, and O_2 equivalent to P_{SO_2} = 0.1998 atm and P_{O_2} = 0.0036 atm. In pure SO_2 atmosphere the partial in the reaction was equivalent to P_{SO_2} = 1 atm at gas flow rates of 40mL/min. The conversion reactions for sulfation of the refractories in these gas mixtures at different temperatures are illustrated in Figure 4.41 to 4.44. Non-linear relations that were similar to those observed in SO_2-O_2 gas mixtures were observed, and the sulfation increased with increasing time. The conversion reaction profiles showed possibly dependence on the oxidation of SO_2 to SO_3, being an important factor in reactions, as reported by Marier *et al.*[89] and Yang *et al.*[90], and diffusion resistance increased. St. Peirre *et al.*[115] and Turkdogan *et al.*[119] have demonstrated that sulfide was a thermodynamically favorable reaction at low oxygen partial pressures ($<10^{-4}$ atm), while sulfate dominated at higher oxygen partial pressures and low temperatures.

The increased conversion reactions at small gas concentrations suggested by Hartman[85], indicated as the extent of reaction decreased with reaction progress, which could be due to decreasing the tendency for SO_2 oxidation. In Figure 4.41, a significant decrease in a conversion profiles ranged from 0.25 to 0.15 for SO_2-N_2 gas mixtures reacted at 800°C, whereas in pure SO_2 conversion profiles shown in Figure 4.39, the decrease was indicated between at 0.73 to 1.47. The sulfate conversion profiles of magnesite refractory showed good correlations on comparison

in different gas mixtures. This indicated that the open pore structure possibly facilitated diffusivity of gases and reactive sites, while the temperature facilitated diffusional release of oxides and consequently the reactive areas. This was also observed with CrMg D50-C5, which showed correlation with MgCr brick 2 and MgCr brick 1 in pure SO_2 and SO_2-N_2 gas mixtures respectively. Mäkipää and Taskinen[13] indicated that sulfur and oxygen were active elements, which lowered surface and interfacial energies in interaction with chrome-magnesite and magnesite refractory components, suggesting that diffusion into the porous structure was promoted, and sulfation reactions are determined by the oxygen concentrations.

At 1000°C, conversion reaction profiles in pure SO_2 were highly comparable with those obtained in SO_2/O_2 gas mixtures at 700°C, indicating the possibly increasing effect of spinel dissociation, associated with O_2 release as the temperatures increased. The indicated O_2 release from the reduction of Fe_2O_3 mainly in spinels suggested reactions that promoted oxidation of SO_2. Therefore, in SO_2 atmosphere internal diffusion of oxygen form the Fe_2O_3 dissociation and that of SO_2 to reach the reactive areas suggested to affect the oxidation of SO_2 and the sulfation reactions. However, another mechanism, which involved elimination of SO3 as an intermediate in the reaction, was proposed. The sulfates occurred by precipitation of SO_2 molecules as they condensed and deposit on the oxide surfaces in reactions that did not involve facilitated oxidation processes. However, because the reaction involved formation of CaS compound, the XRD studies did not support the proposed mechanism. It appeared that decreasing the flow rates increased the contact time between the SO_2 molecules, which then increased the oxidation mechanism.

Kellogg[79] indicating that Dewing and Richardson data were based on erratic thermodynamic data due to suggested equilibrium conditions that were not achieved in their experiments. Therefore, McPherson[37] and Liow *et al*[22] calculations could not be used as reliable source of data in the present study. Base on the findings, the Mg-S-O predominance area diagrams shown in Figure 2.1[22] and 4.10a do not represent the exact reaction mechanisms, but can be used to predict the reaction products, which must be confirmed by phase analyses (X-ray diffraction in this case) and SEM. The effect of temperature and equilibrium gas mixtures within the refractories can explain the increasing conversion reactions observed for the basic refractories investigated between 700°C and 1000°C. The kinetic data related with the observations by Podwórny *et al.*[78], who demonstrated that sulfate in magnesia spinels increased with temperature, and give non-uniform conversions for magnesia spinels due to structural changes. The dissociation of

refractory phases and oxidizing conditions has been shown to increase sulfation[34–29]. In the present study, the presence of the sulfate mixtures having secondary spinels and sulfate phases in which SO_3 was over-stoicheiometric in relation to CaO and MgO suggested that the sulfates were not in equilibrium with the diffused gas mixtures.

The amount of sulfate (SO_4) determined varied from 0.22 to 3.07 wt% (Figure 4.46 and 4.48) in SO_2-O_2 gas mixtures at 700°C in the magnesite-chrome and chrome- magnesite-chrome refractories reacted for seven days. These were half the amounts of sulfate reported by McPherson[37] for refractories that have been exposed to nonferrous metallurgical processes for unspecified period. The amount of sulfate in magnesite refractory corresponded to 6.93 and 6.05 wt % in SO_2-O_2 and SO_2-N_2 gas mixtures respectively. Sulfate amounts of about 7 w t% and below could not be detected using X-ray diffraction method for SO_2-N_2 gas mixtures. Rigby[34] demonstrated that sulfate content of about 0.7 wt% corresponded to $MgSO_4$ in chrome-magnesite refractories investigated. The CrMg D50-C5 refractory (Figure 4.3b) showed the typical fired refractory structure characterized by high porosity which increased gas permeability and promoted high reaction rates (Figure 4.32 and 4.38 to 4.42) than all the other refractories.

CHAPTER 6
CONCLUSIONS

In this project, the basic refractories investigated, were typical lining materials of furnaces used for smelting and converting processes, in non-ferrous industries, and were selected according to microstructures and chemical composition. The aim of the study was to determine the effects of the principal physical changes of the refractories when reacted with sulfur-bearing gases. The investigations involved thorough analyses of microstructures and detailed thermodynamic analysis of chemical reactions. The mechanisms of reactions when un-used magnesite, chrome-magnesite, magnesite-chrome refractories were exposed to SO_2-O_2, SO_2-N_2, SO_2 and O_2 gas mixtures between 700°C and 1350°C, indicated that phase changes influenced the chemical reactivity. The product analyses and detailed thermodynamic analyses of chemical reactions indicated that $MgSO_4$ and $CaSO_4$ formed as main sulfate phases in basic refractories and shown to be temperature dependent.

The structural examination showed that phase changes altered phase compositions and that temperature had a significant influence on the phase distribution and pore structure developed. The phase changes in different gas atmospheres resulted from the composition and original microstructure and related to the oxidation-reduction and solution precipitation relationships. The phase relation observed in the spinel phases of un-used magnesite, chrome-magnesite and magnesite-chrome refractories were identical and corresponded to those predicted in phase diagrams (Fe-Al-Cr-Mg-O relationship systems) and diffusion processes, that are shown in the microstructures by other authors[1–53]. In oxygen atmospheres, the changes resulted in dissolution of magnesia spinels, which influenced pore structure and grain growth. The microstructures showed that the kinetics of the diffusion in components were different and consistent with the structural phenomena suggested for the diffusion mechanisms controlled by dissociation of components and bulk diffusion, which increased porosity in previous studies[4,54,56]. The phase distribution had a significant influence on the release of reactive compounds such as CaO and the pore structure influenced the permeability of gases. The results demonstrated the formation of secondary sulfates, which occurred as space fillings along the grain boundaries and within pores. The structural characteristics of the different refractories demonstrated that phase changes, pores size distribution, and phase distribution were important factors in the gas-refractory interactions.

The magnesite-chrome (D60/100) refractory, demonstrated the importance of these factors, where the suggested uniform pore size distribution and the observed well-developed magnesia spinels resulted in low conversion reaction profiles, between 700°C and 1000°C. Therefore, developed spinels minimized the effects of structural changes, and decreased sulfation. The coarse-grained chrome-magnesite D50-C5, demonstrated the significant effect of temperature on structural changes, attributed to the oxidation-reduction and solution precipitation relationships, observed to result in magnesia spinels. The development of magnesia spinels by diffusion processes promoted release of free oxide components and increased surface area, which resulted in high conversion profiles. The diffusion processes enhanced pore size structure and influenced permeability. The structural changes resulted in dissolution of the newly formed $MgFe_2O_4$ spinel, and MgO reacted to form sulfates, while Fe_2O_3 occurred as mixture, with Cr_2O_3, and Al_2O_3 from chromite grains. The results demonstrated detailed phase distribution developed, observed in reactions occurring in basic refractories in different oxidizing atmospheres, in previous studies[1–7,46–52]. Conclusions established are that phase distribution, pore size distribution, and structure developed related to sulfate formed. The amount sulfate formed in basic refractories calculated as the fraction converted for MgO, increased to about 12 wt% (g/cm^2) at 1000°C, for all refractories. The suggested permeability depended upon temperature and concentration gradient, if all other things equal. The gas diffusion resistance increased with the sulfate product layer formed, and non-uniform compound mixtures of sulfates formed enhanced sulfate deposition.

The sulfates formed mainly with the silicate phases along grain boundaries and within the pores, cracks, and micro-fractures. In magnesite refractory, the pore size distribution and volume, and type of bonding silicates were important factors, where structural analysis confirmed the instability of Ca_3SiO_5 phase, which disintegrated with crystallization of CaO and formed $CaSO_4$ at 1350°C. Between 700 and 1000°C, compound mixtures of $CaMg_3(SO_4)_3$ and sulfate deposition, in which SO_3 content was not balanced (over-stoichiometry) in relation to MgO and CaO for the proposed reactions, occurred. In chrome-magnesite and magnesite-chrome refractories, $MgSO_4$, $CaSO_4$, $CaMg_3(SO_4)_3$ and compound mixtures of sulfate that contained silica and secondary spinels of Fe_2O_3, Al_2O_3 and Cr_2O_3 in different compositions formed. This agreed with previous studies[30–31,34,36,71], in that in presence of sulfur-bearing gases, pure sulfate compounds and sulfate mixtures resulted from dissolution of magnesia spinel.

REFERENCES

1. Hayhurst, A. and Laming, J., *Trans. Brit. Ceram. Soc*., **1963, 62**, 12, 989-1005.
2. Hayhurst, A. and Laming, J., *Trans. Brit. Ceram. Soc.*, **1963**, **62**, 3, pp. 135-142.
3. Rigby, G. R., Hutton R. F., and Hamilton B.G., *J. Am. Ceram. Soc.*, **1963**, **46**, 7, 332-342
4. Rigby, G.R., *Trans. Brit. Ceram. Soc.*, **1956**, **55**, 22-33.
5. De Menezes, I., Reactions in Magnesia-Chrome Refractories, Masters Thesis, Pennsylovia State University, PA, **1965**.
6. Treffner, W. S., *J. Am. Ceram. Soc.*, **1961**, **44**, 12, 583-591.
7. Richardson, H. M., Fitchett, K., and Lester, M., *Trans. Brit. Ceram. Soc.*, **1960**, **59**, 11, 483-499.
8. Pehlke, R. D., Pyrometallurgy III: Smelting and Converting, Unit Processes of Extractive Metallurgy, New York, American Elsevier Publishing Company, **1973**, pp. 67-98.
9. Jones, R.T., Sou. *Afri. J. Sci.*, **1999, 95**, 11, 525-534.
10. Jones, R.T., An Overview of South African PGM Smeltinng, Nickel and Cobalt 2005: Challenges in Extraction and Production, 44th Annual Conference of Metallurgists, Calgary, Canada, 2005, 147-178.
    http:/www.mintek.co.za?Pyromet/Files/2005JonesPGMsmelting.pdf
11. Itagaki, K., Sohn, H. Y. and Perez-Tello, M., Basic Principles of Sulfide Smelting and Converting with Oxygen –Rich Gas, Sulfide Smelting 2002, Stephens R.L. and Sohn Y. (Eds), TMS, (The Minerals, Metals and Material Society), **2002**, pp. 15-39
12. Nell, J., *J. SAIMM*., **2004**, 8, 1-6.
13. Makipaa, M. and Taskinen, P., *Scand. J. Metall.*, **1980, 9**, pp. 273-281.
14. Makipaa, M and Taskinen, P., *Scand. J. Metall.*, **1993, 22**, 203-212.
15. Crites, M.D., Karakus, M., Schlesinger, M.E., Somerville, M.A. and Sun, S., *Can. Metall. Q.* **2000, 39**, 2, 129-133.
16. Oprea, G., Lo W., Chen M., Troczynski, T., Brothers, M. and Richard, G., Secondary effects of chromium-bearing dissolution in iron rich non-ferrous smelting slags. *Advances in Refractories for the Metallurgical Industries IV*, Edited by Rigaud M. and Allair C., 43rd Annual Conference of Metallurgist of CIM, **2004**, pp. 459-471.
17. Chen Y., Brooks, G., Nightingale, S., Coley, K. and Hamed, M., Marangoni Effect in refractory slag line dissolution., *Advances in Refractories for the Metallurgical Industries*

IV, Edited by Rigaud M. and Allair C., 43rd Annual Conference of Metallurgist of CIM, **2004**, pp. 513-526.

18. Utigard, T., Warczok, A., Plascencia, G., Behnood, N. and Zamalloa, M., Interaction between copper mattes and refrcatories, *Advances in Refractories for the Metallurgical Industries IV*, Edited by Rigaud M. and Allair C., 43rd Annual Conference of Metallurgist of CIM, **2004**, pp. 433-443.
19. Fukuyama, H., Donald, J.R. and Togori, J.M., *J. Am. Ceram. Soc*., **80**, 9, pp. 2229-2236.
20. Santander, N., Grau, P. and Castro, L., Chilean refractory experience in El Teniente copper converters, *Copper91-Cobre91*, **1991**, Vol. IV, pp. 247-258.
21. Schumann, Jr. R., *Trans. AIME*, **1950,** 188, 873-884
22. Liouw, J.L., Tsikiris, P., and Gray, N.B., *Can. Metall. Q.*, **1998**, **37**, 2, 99-117.
23. Simeonov, S.R, Sridahar, R., Toguri, J.M., **1995**, **26B**, pp 325-333
24. Simeonov, S.R, Sridahar, R., Toguri, J. M., *JOM*, **1997**, 48-52.
25. Yazawa, A., *Can. Metall. Q.*, **1974**, **13**, 3, 443-453.
26. Dalvi, A.D and Sridhar, R., *Can. Metall. Q.*, **1976**, **15**, 4, 349-357.
27. Meyer, G.A., Waner, J.S., Rao, Y.K and Kellog, H. H., *Metall. Trans. B*, **1975**, **6B**, 229-235.
28. Massengale, G.B., Mong, L.E. and Heidl, R.A., *J. Am. Ceram. Soc.*, **1953**, **36**, 7, 222-229
29. Treffner, W. S., *Am. Ceramic. Soc. Bull*, **1968, 47**, 634-636
30. Hugget, L.G., *Trans. Brit. Ceram. Soc*., **1957, 56**, 87-109.
31. Olbrich, M. and Rostani, F., *Glastech. Ber*., **1990**, **63**, 7, 204-209.
32. Brisbane, S. M. and Segnit, E. R., *Trans. Brit. Ceram. Soc*., **1957, 56**, 237-252.
33. Clark, B. C and McDowell, S. J., *J. Metals*, **1959**, 119-124.
34. Rigby. G. R., *Trans. Met. Soc.* AIME, **1962**, **224**, 887-892.
35. Mikami H. M and Sidler G., *Trans. Met. Soc.* AIME, **1963**, **227**, 887-892.
36. Trojer, F., *Am. Ceramic. Soc. Bull.,* **1968**, **47**, 630-633.
37. McPherson, R., *Am. Ceramic. Soc. Bull.,* **1969, 48**, 791-793
38. Gregurek, D. and Majcenovic, C., *RHI Bulletin*, **2003**, 1, 17-21.
39. Hartman, M. and Coughlin, R., *AIChE. J*., **1976**, **22,** 3, 490-498.
40. Hartman, M. and Coughlin, R., *Ind. Eng. Chem. Process Des. Dev.*, **1974**, **13**, 3, 248-253.
41. Georgakis, C., Chang, C.W. and Szekely, J., *Chem. Eng. Sci.*, **1979**, **34**, 1072-1075.
42. Borgwardt, R., *Environ. Sci. Technol.*, **1970**, 4, 1, 59-63.
43. Borgwardt, R. and Harvey, D., *Environ. Sci. Technol*, **1972**, **6**, 4, pp. 350-360

44. Hloben P., Refractory Materials, Major industrial applications, Rexxon Corporation, South Africa, 2000,
45. Alper, A. M. (Editor), High Temperature Oxides: Part I, Magnesia, Lime and Chrome Refractories, **1970**, **5**, London: Academic Press.
46. Lovell, G. H. B., *Trans. Brit. Ceram. Soc.*, **1952**, **51**, 369-386.
47. Lovell, G. H. B., Some Factors Influencing The Suitability of South African Raw Materials for the Manufacture of Basic Refractories , PhD. Thesis, University of the Witwatersrand, South Africa, **1957**,
48. Richards, R.G. and White, J., *Trans. Brit. Ceram. Soc.*, **1954**, **53**, 422-459.
49. Woodhouse, D. and White, J., *Trans. Brit. Ceram. Soc.*, **1955**, **54**, 333-366
50. Woodhouse, D. and White, J., *Trans. Brit. Ceram. Soc.*, **1957**, **56**, 569-580.
51. El-Shahat, and White, *Trans. Brit. Ceram. Soc.*, **1964**, **60**, 313-330.
52. Booth, C., *Trans. Brit. Ceram. Soc.*, **1950**, **49**, 58-79.
53. White, J., *Trans. Brit. Ceram. Soc.*, **1957**, **56**, 553-568
54. Harbach, A.J. and Ford, W. F., *Trans. Brit. Ceram. Soc.*, **1964**, **63**, 143-161
55. Brindley, G.W., Schaefer, W.L., *Trans. Brit. Ceram. Soc.*, **1964**, **63**, 31-38
56. Homer, P.N and Richardson, H.M., *Trans. Brit. Ceram. Soc.*, **1964**, **63** , 8, 389-415
57. Stubucan, V.S. and DeMenezes, I., *J. Am. Ceram. Soc.*, **1966**, 49, 10, 535-540.
58. Gordon, R. S., Marchant, D. D., Hollenberg, G.W., *J. Am. Ceram. Soc.*, **1970**, **53**, 7, 399-406.
59. Kapadia, C. M. and Leipold, M. H., *J. Am. Ceram. Soc.*, **1974**, **57**, 1, 41-42.
60. Shannon, R.D. and Prewitt, C.T., *Acta Crystallogr.*, **1970**, **B26**, 1046-1048.
61. Shannon, R.D. and Prewitt, C.T., *Acta Crystallogr.*, **1969**, **B25**, 946-952.
62. Medford, G. A., *Can. J. Earth Sci.*, **1973**, **10**, pp. 394-402
63. Hofmann, A. W. and Magaritz M., *J. Geophys. Res,* **1977**, **82**, 33, 5432-5440
64. Watson, E. B., *Geochim. Cosmochim. Acta.*, **1979a**, **43**, 313-322
65. Marioka, M., *Geochim. Cosmochim. Acta.*, **1981**, **45**, 1573-1580
66. Marioka, M., *Geochim. Cosmochim. Acta*, **1991**, **55**, 751-759.
67. Ricker, R. W. and Osborn, E. F., *J. Am. Ceram. Soc.*, **1954**, **37**, 3, 133-139.
68. Scheerer, P.E., Mikami, H.M. and Tauber, J.A., *J. Am. Ceram. Soc.*, **1964**, **47**, 6, 297-305.
69. Cockbain, A.G. and Johnson, W., *Trans. Brit. Ceram. Soc.*, **1958**, **57**, 511-526.
70. Treffner, W. S., *J. Am. Ceram. Soc.*, **1964**, **47**, 8, 401-409.
71. Treffner, W.S., *J. Am. Ceram. Soc.*, **1962**, **45**, 10, 455-463.

72. Ford, W.F, Hayhurst, A. and White, J., *Trans. Brit. Ceram. Soc*., **1961**, **60**, 582-601.
73. Berry, T.F., Allen, W.C., Snow, R.B., *J. Amer. Chem. Soc*., **1950**, **33**, 4, 121-132
74. Rigby, G.R. and Hamilton, B., *Trans. Brit. Ceram. Soc.*, **1961**, **44**, 5, 201-205.
75. Van Dreser, M.L. and Boyer, W.H., High, *J. Amer. Chem. Soc.*, 1963, 46, 6, 257-264.
76. Davis, W.R. and Rigby, G.R., *Trans. Brit. Ceram. Soc*., **1957**, **56**, 259-276.
77. Buchebner, G., Molinari, T. and Rumpf, D., *JOM*, **200**, 68-72.
78. Podwórny, J., Piotowski, J. and Wojsa, J., *Ceram. Int*., **2007**, doi: 10.1016/j.ceramint.2007.04.019
79. Kellogg, H. H., *Trans. AIME*, **1964**, **230**, 1622-1631
80. Safiullin, N. S., Gitis, E. B., Panasenko, N. M., *Russ. J. Inorg. Chem*. **1968**, **13**, 10, 1493-1494.
81. Gallagher, P.K., Johnson, D.W. and Schrey, F., *J.Americ. Ceram. Soc.*, 1**970**, **53**, 12, 666-670.
82. Hartman, M. and Trinka, O., *Chem. Eng. Sci.*, **1980**, **35**, 1189-1194.
83. Hartman, M, Pata, J. and Coughlin, R., *Ind. Eng. Chem. Process Des. Develop.*, **1978**, **13**, 4, 411-419.
84. Hartman, M. and Trinka, O., *Chem. Eng. Sci.*, **1980**, **35**, 1189-1194.
85. Hartman, M., *Inter. Chem. Eng. J*., **1978**, **18**, 4, 712-717
86. Clum, J. A., *Met. Trans.*, **1975**, **6B**, 343-344
87. Turkdogan, E. T., Olsson, R. G., Wreidt, H. A. and Darken, L. S., *Trans. SME- AIME*, **1973**, **254**, 9-21.
88. Turkdogan, E. T and Rice, B. B., *Trans. SME- AIME*, **1973**, **254**, 28-33.
89. Marier, P. and Dibbs, H. P., *Thermochimica Acta*, **1974**, **8**, 155-165
90. Yang, R. T, Shen, M. and Steinberg, M., *Environ. Sci. Technol*, **1978**, **12**, 915
91. Wreidt, H. A. and Darken, L. S., *Trans. SME- AIME*, **1973**, **254**, 1-9.
92. Crnkovic, P. M., Milioli, F. E. and Pagliuso, .J. D., *Thermochimica Acta*, **2006**, **447**, 161-166
93. Fuertes, A. B., Velasco, T., Alvarez, G. and Fernandez, M. J., *Thermochimica Acta*, **1995**, **254**, 63-78.
94. Murthi, K. S., Harrison, D. and Chan, R. K., *Environ. Sci. Technol*., **1971**, **5**, 9, 776-781.
95. Chang, E. Y. and Thodos, G., *AIChE. J*., **1984**, **30**, 3, 450-457.
96. Thibault, J. D., Steward, F. R. and Ruthven, D. M., *Can. J. Chem. Eng.*, **1982**, **60**, 796-801.
97. Fan, L. and Satija, S., *Chem. Eng. J*., **1984**, **28**, 151-162.

98. Hsia, C., Pierre, G. R., Raghunathan, K. and Fan, L. S., *AIChE J*. **1993**, **39**, 4, 698-700.

99. Hsia C., Pierre G. R.and Fan L. S., *AIChE J*., **1995**, **41**, 10, 2337-2340.

100. Borgwardt, R. H., Bruce, K. R. and Blake, J., *Ind. Eng. Chem. Res.*, **1987**, **26**, 1993-1998.

101. Mostert, J. C., Roberts P.N., *J. SAIMM*., **1973**, 290-299.

102. Philip, T. P., *JOM*, **1969**, 38-45.

103. Bell, M. C., Blanco, J. A., Davies, H. and Sridar, R., *JOM*, **1978**, 9-13.

104. Cramer, L. A., *JOM*, **2001**, 14-18.

105. Bale; C. W. and Toguri; J. M., *Can. Metall. Q.*, **1976**, **15**, 4, 305-317.

106. Gawel, J. and Wycezesany, A., *Corrosion Sc*., **1976**, **28**, 9, 867-872.

107. Knacke, O., Kubaschewski, O. and Hesselmann, K., Thermo-chemical Properties of Inorganic Substances, 1st and 2nd Edition, Suppl. Springer-Verlag, New York,

108. JANAF Thermochemical Tables, 2nd ed. National Bureau of Standards, **1971**

109. Kubaschewski, O. and Alcock, C. B., Metallurgical Thermo-chemistry, 5th ed. Pargamon Press, Oxford and New York, **1977**

110. Evans, W. H. and Wagman, D. D., *J. Res. Nat. Bur Std.*, **1952**, **49**, 141-148

111. Rosenqvist, T., *Trans. AIME*, and *J.Metals*, **1951**, **3**, 535-540

112. Richardson, F. D. and Jeffes, H. E., *J. Iron and Steel Inst*., **1949**, 397-420

113. Richardson, F. D. and Jeffes, H. E., *J. Iron and Steel Inst*., **1952**, **171**,165-174

114. St. Peirre, G. and Chipman, J., *J. Amer. Chem. Soc.*, **1954**, **76**, 4787-4791

115. St. Peirre, G. and Chipman, J., *J. Metals*, **1956**, **8**, 1474-1483

116. Dewing, E. and Richardson, F. D., *Trans. Faraday. Soc*., **1958**, **54**, 679-685

117. Dewing, E. and Richardson, F. D., *Trans. Faraday. Soc*., **1959**, **55**, 611-615

118. Marchal, G., *J. Chim. Phys.*, **1925**, **22**, 493-517

119. Turkdogan, E. T and Darken, L. S., *Trans. AIME*, **1961**, **222**, 464-474.

120. Turkdogan, E. T. and Grieveson, P., *Trans. AIME*, **1962**, **224**, 316-323

121. Bale, C.W., Chartrand, P., Decterov, S.A., Eriksson, G., Hack, K., Mahfoud, R. B., Melançon, J., Pelton, A. D. and Petersen, S., *Calphad Journal*, **2002**, **62**, 189-228.

122. Bale, C. W., Pelton , A. D. and Thompson, W. T., *Can. Met. Quart.*, **1986**, **25**, 107-112 .

[123]. Whittaker, E. J. W. and Muntus, R., *Geochem. Cosmch. Acta.*, **1970**, **34**, 945-956.

[124]. Mori, K., Fukunaga, T., Shiraishi, Y. Iwase, K., Xu, Q., Oishi, K., Yatsuyanagi, K., Yonemura, M., Itoh, K., Sugiyama, M., Ishigaki, T., Kamiyama, T., Kawai, M., *Cement and Concrete Research*, **2006**, **36**, 4, 2033-2038

125. Marier, P. and Ingraham, T. R., *Can. Metall. Q.*, **1972**, **11**, 4, 617-619.